ASSESSMENT OF EQUATION-OF-MOTION COUPLED-CLUSTER METHODS WITH APPROXIMATE TREATMENTS OF HIGHER-ORDER EXCITATIONS AND DEVELOPMENT OF NOVEL SCHEMES FOR ACCURATE CALCULATIONS OF DIRADICAL ELECTRONIC SPECTRA AND BOND BREAKING

By

Adeayo Olayinka Ajala

A DISSERTATION

Submitted to Michigan State University in partial fulfillment of the requirements for the degree of

Chemistry - Doctor of Philosophy

2017

ABSTRACT

ASSESSMENT OF EQUATION-OF-MOTION COUPLED-CLUSTER METHODS WITH APPROXIMATE TREATMENTS OF HIGHER-ORDER EXCITATIONS AND DEVELOPMENT OF NOVEL SCHEMES FOR ACCURATE CALCULATIONS OF DIRADICAL ELECTRONIC SPECTRA AND BOND BREAKING

By

Adeayo Olayinka Ajala

The development and implementation of electronic structure methods based on the exponential wave function ansatz of the single-reference coupled-cluster (CC) theory and its extensions to excited states exploiting the equation-of-motion (EOM) and linear response frameworks have witnessed great success in a wide range of applications, but there are areas of chemistry, especially studies of chemical reaction pathways and photochemistry, where further improvements in the existing CC and EOMCC methodologies are needed. In order to make progress in this area, it is important to evaluate the quality of the results that the existing CC/EOMCC methods provide, particularly in applications involving the interpretation and prediction of photochemical phenomena and electronic excitations spectra involving closed- and open-shell molecules. Thus, in the first part of this PhD project we use a database set of 28 organic molecules ranging from linear polyenes, unsaturated cyclic hydrocarbons, aromatic hydrocarbons, and heterocycles to aldehydes, ketones, amides, and nucleobases to examine the performance of the completely renormalized (CR) EOMCC approaches for excited electronic states, in which the relatively inexpensive non-iterative corrections due to triple excitations are added to the energies obtained with the standard EOMCC approach with singles and doubles, abbreviated as EOMCCSD. We focus on two variants of the approximately size-intensive CR-EOMCC methodology with singles, doubles, and noniterative triples, abbreviated as δ -CR-EOMCCSD(T), and the analogous two variants of the newer, rigorously size-intensive, left-eigenstate δ -CR-EOMCC(2,3) approach based on the biorthogonal formulation of the method of moments of CC equations.

In the second part of this dissertation, we focus on the development of new EOMCC methods that are particularly well-suited for accurate calculations of diradical electronic spectra and single bond breaking. They are the cost-effective variants of the doubly electronattached (DEA) EOMCC methodologies with up to 3-particle-1-hole (3p-1h) or 4-particle-2-hole (4p-2h) excitations, abbreviated as DEA-EOMCC $(3p-1h)\{N_u\}$ and DEA-EOMCC $(3p-1h,4p-2h)\{N_u\}$, respectively, which utilize the idea of applying a linear electron-attaching operator to the correlated CC ground state of an (N-2)-electron closed-shell reference system in order to generate the ground and excited states of the N-electron open-shell species of interest, while using N_u active unoccupied orbitals to select the dominant 3p-1h and 4p-2hterms. We demonstrate that the relatively inexpensive DEA-EOMCC(3p-1h,4p-2h) $\{N_u\}$ method greatly reduces the computational costs of the parent active-space DEA-EOMCC $(4p-2h)\{N_u\}$ and full DEA-EOMCC(4p-2h) approaches, needed to obtain highly accurate results for open-shell systems having two electrons outside the closed-shell cores, with virtually no loss in accuracy of the resulting excitation and dissociation energies. We also show that the active-space DEA-EOMCC(3p-1h) $\{N_u\}$ method accurately reproduces the results of the parent DEA-EOMCC(3p-1h) calculations at the small fraction of the cost. In addition to a series of benchmark examples that illustrate the performance of the DEA-EOMCC(3p-1h) $\{N_u\}$, DEA-EOMCC(3p-1h,4p-2h) $\{N_u\}$, and other DEA-EOMCC approaches with 3p-1h and 4p-2hexcitations, including singlet-triplet gaps in methylene, trimethylenemethane, and several antiaromatic diradicals and bond breaking in the fluorine molecule, we provide the most essential details of DEA-EOMCC equations with an active-space treatment of 3p-1h and 4p-2h terms, as implemented in our codes and interfaced with the GAMESS package.

Copyright by ADEAYO OLAYINKA AJALA 2017

This is dedicated to Oluwatoyin an	d Abayomi (deceas	nielle and my da ed), and my sibli Olanrewaju.	ughter Dara, my s ings Babatunde (d	supportive parents leceased) and

ACKNOWLEDGMENTS

I owe a great deal of gratitude to my PhD advisor, Professor Piotr Piecuch, for his patience and thorough guidance throughout my graduate career. Since my first day in his group he has driven me to be a better scientist in paying attention to details and discovering my potential. I am also indebted to him for his continuous support throughout my academic journey at Michigan State University.

I would like to thank the other members of my committee, Professor Benjamin G. Levine, Professor Robert I. Cukier, and Professor Rémi Beaulac for all their support, advice, and patience in overseeing my graduate study.

It is also important to mention the valuable effort of Dr. Jun Shen from our group. As a result of his guidance and several discussions, I progressed much more quickly than I would have without him, especially in the development work presented in this dissertation. I would also like to thank Dr. Jun Shen for checking some of the equations presented in this work. My sincere appreciation also goes to Dr. Jared Hansen for his great assistance in one of the projects presented in this dissertation. Lastly, I would like to thank other members of the Piecuch group, both past and present, for the help and friendship they provided, including Dr. Nicholas P. Bauman, Mr. Jorge Emiliano Deustua, Mr. Ilias Magoulas, and Mr. Stephen H. Yuwono.

TABLE OF CONTENTS

LIST (OF TA	ABLES		ix
LIST (OF FI	GURES .		xi
Chapt	er 1	Introduc	etion	1
Chapt	er 2	Project	Objectives	9
\mathbf{Chapt}	er 3	Benchma	arking Completely Renormalized Equation-of-Motion	
		Coupled	-Cluster Methods with Triple Excitations	10
3.1	Back	ground Info	ormation and Motivation	10
3.2	Theo	ry		14
3.3	Bench	hmark Mol	ecules and Computational Details	18
3.4	Resu	ts and Dis	cussion	21
	3.4.1	Geometr	ries and their Effect on the Calculated Vertical Excitation En-	
		_		21
	3.4.2		s on the Calculated Vertical Excitation Spectra for Molecules	
			atabase of Ref. [17]	46
		3.4.2.1	Linear Polyenes: Ethene, E-butadiene, all-E-hexatriene, and	
			all-E-octatetraene	49
		3.4.2.2	Unsaturated Cyclic Hydrocarbons: Cyclopropene, Cyclopen-	
			tadiene, and Norbornadiene	50
		3.4.2.3	Aromatic Hydrocarbons: Benzene and Naphthalene	52
		3.4.2.4	Heterocycles: Furan, Pyrrole, Imidazole, Pyridine, Pyrazine,	
			Pyrimidine, Pyridazine, s-Triazine, and s-Tetrazine	53
		3.4.2.5	Aldehydes and Ketones: Formaldehyde, Acetone, and	
			p-Benzoquinone	58
		3.4.2.6	Amides: Formamide, Acetamide, and Propanamide	61
		3.4.2.7	Nucleobases: Cytosine, Uracil, Thymine, and Adenine	64
3.5			Analysis for the Entire Benchmark Set	65
3.6	Conc	lusions		104
\mathbf{Chapt}	er 4	Economi	ical Doubly Electron-Attached Equation-of-Motion	
		_	-Cluster Methods with an Active-Space Treatment of	
		3-particl	e-1-hole and 4-particle-2-hole Excitations	107
4.1		_	ormation and Motivation	108
4.2	Theo		corithmic Details	114
	4.2.1		ements of the DEA-EOMCC Formalism and the Previously	
		_	ed DEA-EOMCC $(3p-1h)$, DEA-	
		EOMCC	$S(4p-2h)$, and DEA-EOMCC $(4p-2h)\{N_u\}$ Approximations	114

	4.2.2	The Active-Space DEA-EOMCC $(3p-1h)\{N_u\}$ and DEA-	
		$EOMCC(3p-1h,4p-2h)\{N_u\}$ Approaches Developed in this Thesis Projec	t119
	4.2.3	Key Details of the Efficient Computer Implementation of the Active-	
		Space DEA-EOMCC(3p-1h) $\{N_u\}$ and DEA-EOMCC	
		$(3p-1h,4p-2h)\{N_u\}$ Methods	122
	4.2.4	The Remaining Algorithmic Details and Illustrative Timings of DEA-	
		$EOMCC(3p-1h)\{N_u\}$ and DEA-EOMCC	
		$(3p-1h, 4p-2h)\{N_u\}$ Calculations	137
4.3	Nume	erical Examples	140
	4.3.1	Adiabatic Energy Gaps Involving Low-Lying Singlet and Triplet States	
		of Methylene	143
	4.3.2	The Complete Basis Set Limit Investigation of Singlet and Triplet	
		States of Methylene	150
	4.3.3	Adiabatic Singlet–Triplet Gap in Trimethylenemethane	154
	4.3.4	Vertical Singlet-Triplet Gaps in Antiaromatic Diradicals	163
	4.3.5	F–F Bond Dissociation in the Fluorine Molecule	171
4.4	Concl	usions	174
Chapte	er 5	Summary and Future Outlook	176
APPE	NDIC	ES	180
API		X A Derivation of the Non-Iterative Energy Correction Defining the	
		nogonal MMCC Theory	181
API		X B Factorized Form of the DEA-EOMCC $(4p-2h)$ Equations Based on	400
	CCSL	Reference Wave Functions	186
BIBLI	OGR A	APHY	189

LIST OF TABLES

Table 3.1:	Symmetry unique Cartesian coordinates of the ground-state geometries for the 28 molecules comprising the benchmark set resulting from the MP2/6-31G* optimizations	23
Table 3.2:	Symmetry unique Cartesian coordinates of the ground-state geometries of the 28 molecules comprising the benchmark set resulting from the CR- $CC(2,3)$,D/TZVP optimizations carried out in this work	29
Table 3.3:	Vertical excitation energies (in eV) for singlet states of all molecules in the test set using the geometries optimized at the MP2/6-31G* level. a,b	36
Table 3.4:	Vertical excitation energies (in eV) for singlet states of all molecules in the test set using, in the case of the EOMCCSD and δ -CR-EOMCC results, the geometries optimized at the CR-CC(2,3),D/TZVP level. ^a	41
Table 3.5:	Statistical error analyses of the various CC/EOMCC data, including EOMCCSD, δ -CR-EOMCCSD(T),IA (δ -CR(T),IA), δ -CR-EOMCCSD(T),ID (δ -CR(T),ID), δ -CR-EOMCC(2,3),A (δ -CR(2,3),A), δ -CR-EOMCC(2,3),D (δ -CR(2,3),D), CC3, and EOMCCSDT-3, from their CASPT2 counterparts.	68
Table 3.6:	Statistical error analyses of the various CC/EOMCC data, including EOMCCSD, δ -CR-EOMCCSD(T),IA (δ -CR(T),IA), δ -CR-EOMCCSD(T),ID (δ -CR(T),ID), δ -CR-EOMCC(2,3),A (δ -CR(2,3),A), δ -CR-EOMCC(2,3),D (δ -CR(2,3),D), CC3, and EOMCCSDT-3, from their TBE-2 counterparts.	68
Table 3.7:	Statistical error analyses of the EOMCCSD, δ -CR-EOMCCSD(T),IA (δ -CR(T),IA), δ -CR-EOMCCSD(T),ID (δ -CR(T),ID), δ -CR-EOMCC(2,3),A (δ -CR(2,3),A), and δ -CR-EOMCC(2,3),D (δ -CR(2,3),D) data from their CC3 counterparts	69
Table 3.8:	Statistical error analyses of the EOMCCSD, δ -CR-EOMCCSD(T),IA (δ -CR(T),IA), δ -CR-EOMCCSD(T),ID (δ -CR(T),ID), δ -CR-EOMCC(2,3),A (δ -CR(2,3),A), and δ -CR-EOMCC(2,3),D (δ -CR(2,3),D) data from their EOMCCSDT-3 counterparts	69
Table 4.1:	Explicit algebraic expressions for the one- and two-body matrix elements of $\bar{H}_{N,\text{open}}^{(\text{CCSD})}$	124

Table 4.2:	The various classes of restricted projections that must be considered when generating the computationally efficient form of the equations defining the DEA-EOMCC($3p$ - $1h$, $4p$ - $2h$) $\{N_u\}$ eigenvalue problem	128
Table 4.3:	A comparison of CPU times required by the various DEA-EOMCC calculations characterizing the X 3A_2 state of TMM, as described by the cc-pVDZ and, in parentheses, cc-pVTZ basis sets, along with the formal scalings of the most expensive steps in the diagonalization of $\bar{H}_{N,\text{open}}$ with n_o, n_u , and N_u .	138
Table 4.4:	A comparison of the full CI and various DEA-EOMCC adiabatic excitation energies, along with the corresponding MaxUE and NPE values relative to full CI, characterizing the low-lying states of methylene, as described by the TZ2P basis set. ^a	145
Table 4.5:	Comparison of the adiabatic excitation energies (in eV) for the low-lying states of CH_2 , as obtained with various DEA-EOMCC approaches using the ACxZ (x =T, Q, and 5) basis sets and (N – 2)-electron RHF orbitals, and extrapolating to the CBS limit, with the corresponding QMC results and experiment. ^a	155
Table 4.6:	The selected DEA-EOMCC results for the adiabatic singlet–triplet separation, $\Delta E_{\rm S-T}=E(B~^1A_1)-E(X~^3A_2'),$ in kcal/mol, in trimethylenemethane (TMM), as described by the cc-pVDZ and, in parentheses, cc-pVTZ basis sets, calculated using the SF-DFT/6-31G(d) geometries. a	158
Table 4.7:	The DEA-EOMCC results for the vertical singlet–triplet gaps, $\Delta E_{\rm S-T} = E({\rm S}) - E({\rm T})$, in kcal/mol, in systems 1–7, as described by the VDZ and mATZ basis sets	166
Table 4.8:	A comparison of the $\Delta E_{\mathrm{S-T}}$ values (in kcal/mol) characterizing systems 1–7 obtained with the DEA-EOMCC[4p-2h] extrapolation in the DEA-EOMCC(4p-2h){ N_u }/VDZ calculations with the UCCSD(T), UBD(T), ROHF-MkCCSD, and CASSCF-MkCCSD results reported by Saito et al.	171
Table 4.9:	A comparison of the full CI and various DEA-EOMCC ground-state energies of F_2 at the equilibrium ($R_e = 2.66816$ bohr) and a few other F-F distances, along with the corresponding MUE and NPE values relative to full CI, obtained with the DZ basis set. ^a	172

LIST OF FIGURES

Figure 3.1:	Benchmark set of molecules considered in this work	19
Figure 3.2:	Correlation plot of the δ -CR-EOMCC(2,3),D/TZVP excitation energies (in eV) computed using the MP2/6-31G* and CR-CC(2,3),D/TZVP geometries	35
Figure 3.3:	Correlation plot for the calculated singlet excited states: EOMCCSD/TZVP vs CASPT2/TZVP vertical excitation energies (in eV) at MP2/6-31G* geometries. The table on the right hand side shows the list of outliers, marked with open circles in the plot.	78
Figure 3.4:	Correlation plot for the calculated singlet excited states: δ -CR- EOM-CCSD(T),IA/TZVP (δ -CR-(T),IA) vs CASPT2/TZVP vertical excitation energies (in eV) at MP2/6-31G* geometries. The table on the right hand side shows the list of outliers, marked with open circles in the plot	79
Figure 3.5:	Correlation plot for the calculated singlet excited states: δ -CR- EOM-CCSD(T),ID/TZVP (δ -CR-(T),ID) vs CASPT2/TZVP vertical excitation energies (in eV) at MP2/6-31G* geometries. The table on the right hand side shows the list of outliers, marked with open circles in the plot	80
Figure 3.6:	Correlation plot for the calculated singlet excited states: δ -CR-EOM CC(2,3),A/TZVP (δ -CR-(2,3),A) vs CASPT2/TZVP vertical excitation energies (in eV) at MP2/6-31G* geometries. The absence of the table on the right hand side indicates that there are no outliers	81
Figure 3.7:	Correlation plot for the calculated singlet excited states: δ -CR-EOM CC(2,3),D/TZVP (δ -CR-(2,3),D) vs CASPT2/TZVP vertical excitation energies (in eV) at MP2/6-31G* geometries. The absence of the table on the right hand side indicates that there are no outliers	82
Figure 3.8:	Correlation plot for the calculated singlet excited states: EOMCCSD/TZVP vertical excitation energies (in eV) at MP2/6-31G* geometries vs TBE-2 data. The table on the right hand side shows the list of outliers, marked with open circles in the plot.	83
Figure 3.9:	Correlation plot for the calculated singlet excited states: δ -CR-EOM CCSD(T),IA/TZVP vertical excitation energies (in eV) at MP2/6-31G* geometries (δ -CR-(T),IA) vs TBE-2 data. The table on the right hand side shows the list of outliers, marked with open circles in the plot	84

Figure 3.10:	Correlation plot for the calculated singlet excited states: δ -CR-EOM CCSD(T),ID/TZVP vertical excitation energies (in eV) at MP2/6-31G* geometries (δ -CR-(T),ID) vs TBE-2 data. The table on the right hand side shows the list of outliers, marked with open circles in the plot	85
Figure 3.11:	Correlation plot for the calculated singlet excited states: δ -CR-EOM CC(2,3),A/TZVP vertical excitation energies (in eV) at MP2/6-31G* geometries (δ -CR-(2,3),A) vs TBE-2 data. The absence of the table on the right hand side indicates that there are no outliers	86
Figure 3.12:	Correlation plot for the calculated singlet excited states: δ -CR-EOM CC(2,3),D/TZVP vertical excitation energies (in eV) at MP2/6-31G* geometries (δ -CR-(2,3),D) vs TBE-2 data. The absence of the table on the right hand side indicates that there are no outliers	87
Figure 3.13:	Correlation plot for the calculated singlet excited states: EOMCCSD/TZVP vs CC3/TZVP vertical excitation energies (in eV) at MP2/6-31G* geometries. The table on the right hand side shows the list of outliers, marked with open circles in the plot	88
Figure 3.14:	Correlation plot for the calculated singlet excited states: δ -CR-EOM CCSD(T),IA/TZVP (δ -CR-(T),IA) vs CC3/TZVP vertical excitation energies (in eV) at MP2/6-31G* geometries. The table on the right hand side shows the list of outliers, marked with open circles in the plot	89
Figure 3.15:	Correlation plot for the calculated singlet excited states: δ -CR-EOM CCSD(T),ID/TZVP (δ -CR-(T),ID) vs CC3/TZVP vertical excitation energies (in eV) at MP2/6-31G* geometries. The table on the right hand side shows the list of outliers, marked with open circles in the plot	90
Figure 3.16:	Correlation plot for the calculated singlet excited states: δ -CR-EOM CC(2,3),A/TZVP (δ -CR-(2,3),A) vs CC3/TZVP vertical excitation energies (in eV) at MP2/6-31G* geometries. The absence of the table on the right hand side indicates that there are no outliers	91
Figure 3.17:	Correlation plot for the calculated singlet excited states: δ -CR-EOM CC(2,3),D/TZVP (δ -CR-(2,3),D) vs CC3/TZVP vertical excitation energies (in eV) at MP2/6-31G* geometries. The table on the right hand side shows the list of outliers, marked with open circles in the plot	92
Figure 3.18:	Correlation plot for the calculated singlet excited states: EOMCCSD/TZVP vs EOMCCSDT-3/TZVP vertical excitation energies (in eV) at MP2/6-31G* geometries. The table on the right hand side shows the list of outliers, marked with open circles in the plot.	93

Figure 3.19:	Correlation plot for the calculated singlet excited states: δ -CR-EOM CCSD(T),IA/TZVP (δ -CR-(T),IA) vs EOMCCSDT-3/TZVP vertical excitation energies (in eV) at MP2/6-31G* geometries. The absence of the table on the right hand side indicates that there are no outliers	94
Figure 3.20:	Correlation plot for the calculated singlet excited states: δ -CR-EOM CCSD(T),ID/TZVP (δ -CR-(T),ID) vs EOMCCSDT-3/TZVP vertical excitation energies (in eV) at MP2/6-31G* geometries. The absence of the table on the right hand side indicates that there are no outliers	95
Figure 3.21:	Correlation plot for the calculated singlet excited states: δ -CR-EOM CC(2,3),A/TZVP (δ -CR-(2,3),A) vs EOMCCSDT-3/TZVP vertical excitation energies (in eV) at MP2/6-31G* geometries. The absence of the table on the right hand side indicates that there are no outliers	96
Figure 3.22:	Correlation plot for the calculated singlet excited states: δ -CR-EOM CC(2,3),D/TZVP (δ -CR-(2,3),D) vs EOMCCSDT-3/TZVP vertical excitation energies (in eV) at MP2/6-31G* geometries. The table on the right hand side shows the list of outliers, marked with open circles in the plot.	97
Figure 3.23:	Normal distribution curves for the deviation of the δ -CR-EOMCCSD(T),IA excitation energies at MP2/6-31G* geometries from the CASPT2/TZVP (green), CC3/TZVP (black), EOMCCSDT-3/TZVP (red) and TBE-2 (blue) results	100
Figure 3.24:	Normal distribution curves for the deviation of the δ -CR-EOMCCSD(T),ID excitation energies at MP2/6-31G* geometries from the CASPT2/TZVP (green), CC3/TZVP (black), EOMCCSDT-3/TZVP (red) and TBE-2 (blue) results	101
Figure 3.25:	Normal distribution curves for the deviation of the δ -CR-EOMCC(2,3),A excitation energies at MP2/6-31G* geometries from the CASPT2/TZVP (green), CC3/TZVP (black), EOMCCSDT-3/TZVP (red) and TBE-2 (blue) results	102
Figure 3.26:	Normal distribution curves for the deviation of δ -CR-EOMCC(2,3),D excitation energies at MP2/6-31G* geometries from the CASPT2/TZVP (green), CC3/TZVP (black), EOMCCSDT-3/TZVP (red) and TBE-2 (blue) results.	103
Figure 4.1:	The key elements of the algorithm used to compute $\langle \Phi^{\mathbf{A}bc}_{k} (\bar{H}_{N,\text{open}}^{(\text{CCSD})} R_{\mu}^{(+2)})_{C} \Phi \rangle$ in the efficient implementation of the DEA-EOMCC(3p-1h,4p-2h){ N_{u} } method	136

Figure 4.2:	Diradical systems considered in this work. 1: C_4H_4 , 2: $[C_5H_5]^+$, 3:	
	$C_4H_3NH_2$, 4: C_4H_3CHO , 5: $C_4H_2NH_2CHO$, 6: C_4H_2 -1, 2-(CH_2) ₂ , and	
	7: C_4H_2-1 , $3-(CH_2)_2$	164

Chapter 1

Introduction

Quantum chemistry has become an indispensable part of modern molecular science, providing us with concepts and ideas which play a central role in our understanding of chemical systems and processes. The development of quantum chemistry has also provided us with versatile computational tools, whose application in many areas of physical and biological sciences offer quantitative data and useful insights, helping us to predict, verify, and understand experimental observations and measurements. Given the plethora of electronic structure methods, accompanied by the emergence and development of program suites, it is essential to critically evaluate the performance and accuracy of existing quantum chemistry approximations and to formulate and implement new and improved ideas. Both of these aspects are reflected in this dissertation.

One of the most effective approaches to the critical assessment of the existing methods is by testing these methods on databases that contain larger numbers of well-characterized molecular species. A few examples of the databases that exist for benchmarking a broad range of ground-state properties of *ab initio* and density functional theory (DFT) methodologies are the Gaussian Gn test sets [1–6] for atomization energies, ionization potentials, electron affinities, proton affinities, and enthalpies of formation, the S22 [7], S26 [8], and S66 [9] training sets for non-covalent interactions, the ATcT [10–12] benchmark set for thermochemical data, the DBH24 [13] test set for barrier heights, the W4 [14] training set for

total atomization energies, the 3dBE70 [15] benchmark set for average bond energies of 3d transition-metal-containing compounds, and the "mindless" benchmark set [16], which is a diversity-oriented collection of randomly generated molecules for main group thermochemical properties.

Unfortunately, for the corresponding excited-state properties, where theoretical and computational quantum chemistry methods have great potential to make significant contributions to interpretation and prediction of photochemical phenomena and electronic molecular spectra, only one such comprehensive test set has been proposed so far [17]. As a result, fewer methods for excited states have been systematically tested on large datasets. The test set developed in Ref. [17] consists of 28 organic molecules, 149 singlet vertical excitation energies, and 72 triplet vertical excitation energies, with the majority of excited states being dominated by one-electron transitions and some having more substantial two-electron excitation components. In Refs. [17–25], several quantum chemistry approaches, including the complete-active-space self-consistent field [26, 27] based second-order perturbation theories, such as CASPT2 [28, 29] and NEVPT2 [30–33], a variety of coupled-cluster (CC) [34–37] linear-response [38–47] and equation-of-motion (EOM) [48–54] CC methods, time-dependent DFT [55, 56], and the DFT-based multi-reference configuration interaction (CI) [57] approximation, have been tested using this set [17–25], providing useful information. We should also mention the analogous work from Pal and co-workers [58], which highlights a benchmark investigation of the ionized (IP) EOMCC approach with singles and doubles (IP-EOMCCSD) [59–62] using the geometries and selected spectroscopic properties of a variety of doublet radicals, comparing its performance with experiment and other CC approaches.

All of the above examples illustrate that, benchmarking using larger datasets has become an important procedure in the evaluation and assessment of the quality and validation of ab initio electronic structure methods, including the higher-level methods of CC theory and its extensions to excited and open-shell states. Following on this theme, the first part of this dissertation will focus on using the comprehensive dataset of Ref. [17] to examine the performance of new generations of EOMCC methods developed by our group based on the idea of correcting the excitation energies obtained with EOMCCSD for the effects of triple excitations, abbreviated as δ -CR-EOMCCSD(T) [63] (see, also, Refs. [64–66]) and δ -CR-EOMCC(2,3) [67–69]. In doing this, we will rely on our exhaustive study published in Ref. [70] and the accompanying high-level EOMCC and linear response CC data reported in Refs. [17, 19, 20, 22, 24, 25].

Our effort to benchmark the non-iterative δ -CR-EOMCCSD(T) and δ -CR-EOMCC(2,3) triples corrections to EOMCCSD will show that these approaches are capable of greatly improving the results of EOMCCSD calculations without the need to go all the way to prohibitively expensive EOMCC levels, such as EOMCCSDT [71–73], where triple excitations in the cluster and EOM excitation operators are treated fully, but there are situations, especially the excitation spectra of open-shell species, such as radicals and diradicals, where it is worth considering alternative approaches. The δ -CR-EOMCCSD(T) and δ -CR-EOMCC(2,3) methods are cost efficient and capable of handling excited states dominated by one- as well as two-electron transitions, but like all single-reference particle-conserving CC/EOMCC schemes implemented using the spin-integrated spin-orbital equations they break the spin-symmetry of the non-relativistic Hamiltonian in open-shell systems, even when the reference determinant is of the restricted (e.g., restricted open-shell Hartree-Fock or ROHF) type. The δ -CR-EOMCCSD(T) and δ -CR-EOMCC(2,3) methods, being highly correlated, eliminate much of this problem numerically, offering accurate results for radical [66, 68] and diradical [74] electronic spectra, even when the excited states of interest have a multi-reference character, but the problem of spin contamination in open-shell systems remains.

Within the EOMCC framework that interests us in this thesis, the cleanest approach to electronic spectra of open-shell systems, resulting in a rigorously spin-adapted description, is to consider the electron-attached (EA) [75–81] and IP [59–62, 77, 79–85] EOMCC theories and their extensions to multiple electron-attachment and multiple ionization cases, such as the case of doubly electron-attached (DEA) EOMCC framework and its doubly ionized (DIP) counterpart [53, 86–94]. To appreciate these kinds of methods, we begin our discussion with the EA- and IP-EOMCC methodologies. In the EA- and IP-EOMCC theories, the ground and excited states of an $(N\pm 1)$ -electron system are generated by applying a linear electronattaching or ionizing operator to the correlated CC ground state of the related N-electron closed-shell core. The basic EA-EOMCCSD [75, 76] and IP-EOMCCSD [59–62] approximations, in which the electron-attaching and ionizing operators of EOMCC are truncated at the 2-particle-1-hole (2p-1h) and 2-hole-1-particle (2h-1p) terms, respectively, have difficulties with accurately describing excitation spectra of radicals [75, 79, 80, 95, 96, 96, 97], but, in analogy to particle-conserving EOMCC schemes, where one needs to go beyond doubles, one can resolve this inadequacy through the inclusion of 3p-2h/3h-2p [79, 80] and 4p-3h/4h-3p[85, 96] components of the electron-attaching and ionizing operators of EOMCC. The resulting EA-EOMCCSDT [78], IP-EOMCCSDT [82, 83], EA-EOMCCSD(3p-2h) [79, 80], IP-EOMCCSD(3h-2p) [79, 80], EA-EOMCCSD(4p-3h) [96], IP-EOMCCSD(4h-3p) [96], EA-EOMCCSD(4h-3p) [96], EA-EOMCCSD(4h-3h) [96], EA-EOMCCSD(4EOMCCSDTQ [85], and IP-EOMCCSDTQ [85] schemes greatly improve the EA-EOMCCSD and IP-EOMCCSD results even when the excited states of radicals of interest gain a significant multi-determinantal character, but computer costs associated with such high-level EAand IP-EOMCC methods are quite high. For example, the EA-EOMCCSDT calculations, where the cluster operator is truncated at the three-body terms and the EOM electronattaching operator at 3p-2h excitations, are characterized by the expensive CPU iterative steps which scale as $n_o^3 n_u^5$ in the underlying CCSDT computations for the closed-shell core and $n_o^2 n_u^5$ in the steps related to the diagonalization of the similarity-transformed Hamiltonian (n_o and n_u are the numbers of occupied and unoccupied orbitals used in the post-SCF calculations). These kinds of iterative steps are not computationally affordable for routine chemical applications for larger molecular problems.

In order to address the issue of large costs of high-order EA- and IP-EOMCC calculations, the active-space CC [98–109] and EOMCC [71, 72, 110–114] approaches (see Ref. [115] for a review) have been extended to the EA-EOMCC and IP-EOMCC [79–81, 96] methodologies. The examples of the active-space EA- and IP-EOMCC methods are EA-EOMCCSDt and IP-EOMCCSDt [79–81]. The EA-EOMCCSDt and IP-EOMCCSDt methods are obtained by reducing the numbers of 3p-2h and 3h-2p amplitudes in the parent EA-EOMCCSD(3p-2h) and IP-EOMCCSD(3h-2p) calculations with the help of active orbitals. As shown in Refs. [79–81, 96, 116], this offers major savings in the computational effort compared to the EA-EOMCCSD(3p-2h) and IP-EOMCCSD(3h-2p) approaches and their EA-EOMCCSDT and IP-EOMCCSDT counterparts, which treat 3p-2h and 3h-2p terms fully, with virtually no loss of accuracy in the calculated radical excitation spectra. This is telling us that one should be able to use the idea of active orbitals to select higher-order terms in the DEA-and DIP-EOMCC frameworks, which we discuss next.

In the DEA- and DIP-EOMCC approaches [53, 86–94], which are particularly well-suited to describe systems having two electrons outside the N-electron closed-shell core, such as diradicals, the ground and excited states of (N + 2)- or (N - 2)-electron species are obtained by applying suitably defined operators that attach two electrons to (the DEA case)

or remove two electrons from (the DIP case) the N-electron reference system, while relaxing the remaining electrons. The levels of theory that leads to the desired accuracies in describing electronic spectra of diradicals (errors in the energy gaps of 1 kcal/mol or smaller) are DEA-EOMCC(4p-2h) in the DEA case and DIP-EOMCC(4h-2p) in the DIP case. In the DEA-EOMCC(4p-2h) approach, we truncate the electron-attaching operator of EOMCC at 4p-2h terms. In the DIP-EOMCC(4h-2p) scheme, the corresponding ionizing operator is truncated at 4h-2p component. As demonstrated in Refs. [92–94], the incorporation of 4p-2hand 4h-2p excitations in the DEA- and DIP-EOMCC frameworks greatly improving the accuracy compared to the basic DEA-EOMCC(3p-1h) and DIP-EOMCC(3h-1p) models, where the EOM operators attaching or removing two electrons from the related closed-shell cores are truncated at 3p-1h and 3h-1p levels. Unfortunately, as in all CC/EOMCC methods with higher-than-double excitations, the full implementation of the DEA-EOMCC(4p-2h) and DIP-EOMCC(4h-2p) approaches that give these high accuracies comes at a high price, resulting in schemes that have very expensive iterative $n_o^2 n_u^6$ (the DEA case) and $n_o^4 n_u^4$ (the DIP case) steps. One way to incorporate 4p-2h and 4h-2p excitations without running into the prohibitive costs of the full DEA-EOMCC(4p-2h) and DIP-EOMCC(4h-2p) computations is to employ the previously discussed active-space ideas to select the dominant higher-rank excitation amplitudes [92, 93]. This is particularly true in the DEA-EOMCC(4p-2h) case, where the use of active orbitals to select the dominant 4p-2h components reduces the iterative $n_o^2 n_u^6$ steps of full DEA-EOMCC(4p-2h) to a much more acceptable $N_u^2 n_o^2 n_u^4$ level, where $N_u \ (\ll n_u)$ is the number of active orbitals unoccupied in the N-electron closed-shell reference system. Similar reduction in the computational effort is observed when one selects the dominant 4h-2p terms in the DIP-EOMCC(4h-2p) approach using N_o ($< n_o$) active occupied orbitals. This allows us to replace the original $n_o^4 n_u^4$ scaling of DIP-EOMCC(4h-2p) by much less expensive $N_o^2 n_o^2 n_u^4$. The results reported in Refs. [92, 93] show that the DEA- and DIP-EOMCC methods with an active-space treatment of 4p-2h and 4h-2p excitations accurately reproduce the parent, nearly exact DEA-EOMCC(4p-2h) and DIP-EOMCC(4h-2p) data at the fraction of the computational cost.

The active-space DEA-EOMCC(4p-2h) and DIP-EOMCC(4h-2p) approaches of Refs. [92, 93] have been very successful in accurately describing diradical electronic spectra and single bond breaking, but one issue that prevents such methods from becoming more popular is the high cost of handling the lower-order 3p-1h terms within the active-space DEA-EOMCC(4p-2h) framework. Indeed, the cost of computing 3p-1h terms fully scales as iterative $n_0 n_u^5$, making the full treatment of 3p-1h contributions very expensive when basis sets used in the calculations are larger (so that n_u is large). This issue is addressed in this dissertation by developing the new form of the DEA-EOMCC approach, in which both 3p-1h and 4p-2h terms are treated with the help of active orbitals, allowing us to reduce the scalings of the CPU steps associated with the full treatment of these terms from the original and prohibitively expensive $n_o n_u^5$ and $n_o^2 n_u^6$ levels to $N_u n_o n_u^4$ and $N_u^2 n_o^2 n_u^4$, respectively [94]. As shown in this thesis research and as demonstrated in our recently published studies [94, 117], the DEA-EOMCC calculations with an active-space treatment of 3p-1h and 4p-2h contributions provide highly accurate results for electronic spectra of diradicals and single bond breaking, which can compete with those obtained with the parent full DEA-EOMCC(4p-2h) approach, at the small fraction of the computational cost of the latter method. The byproduct of this work is the implementation of the active-space DEA-EOMCC(3p-1h) scheme, which is not as accurate as its higher-level DEA-EOMCC(4p-2h) counterpart, but still quite useful in diradical applications. The active-space DEA-EOMCC(3p-1h) approach, where 4p-2h correlations are neglected, uses active orbitals to select the dominant 3p-1h contributions, reducing the expensive $n_o n_u^5$ steps of full DEA-EOMCC(3p-1h) to a considerably more practical $N_u n_o n_u^4$ level. As shown in this dissertation, and as demonstrated in our recent work [94, 117], the active-space DEA-EOMCC(3p-1h) method allows us to accurately reproduce the parent DEA-EOMCC(3p-1h) data, where 3p-1h terms are treated fully at the small fraction of the computational costs of full DEA-EOMCC(3p-1h) calculations.

Chapter 2

Project Objectives

The main objectives of this dissertation work are

- A. Benchmark the δ -CR-EOMCCSD(T) and δ -CR-EOMCC(2,3) approaches for vertical excitation energies using a database of 28 small to medium sized organic molecules.
- B. Develop and apply reduced-cost DEA-EOMCC(4p-2h) method with an active-space treatment of 3p-1h as well as 4p-2h excitations and its lower-level counterpart truncated at 3p-1h terms to study the electronic spectra of diradicals and single bond dissociations.
- C. Describe the details of our implementations of the spin- and symmetry-adapted DEA-EOMCC methods based on the CCSD reference wave function with an active-space treatment of 3p-1h and 4p-2h contributions and how the DEA-EOMCC equations were derived, factorized, and translated into FORTRAN code.

Chapter 3

Benchmarking Completely

Renormalized Equation-of-Motion

Coupled-Cluster Methods with Triple

Excitations

3.1 Background Information and Motivation

As mentioned in the Introduction, the first part of this dissertation focuses on using the test set introduced in Ref. [17], with additional information and updates provided in Refs. [19, 21, 24, 25], to examine the performance of the newer generations of the non-iterative triples corrections to the vertical excitation energies obtained in the EOMCCSD [48–50, 118–121] calculations, abbreviated as δ -CR-EOMCCSD(T) [63] and δ -CR-EOMCC(2,3) [69]. These corrections, resulting from the excited-state extensions [67, 122–124] of the method of moments of CC equations (MMCC) [65, 68, 122, 125–129], are the approximately size-intensive [42, 130] (δ -CR-EOMCCSD(T)) or rigorously size-intensive (δ -CR-EOMCC(2,3)) modifications of the CR-EOMCC approaches called CR-EOMCCSD(T) [63, 65, 66] and CR-EOMCC(2,3) [67, 68]. Herein lies our motivation for benchmarking the δ -CR-EOMCCSD(T)

and δ -CR-EOMCC(2,3) methods using the test set of Ref. [17].

It is generally thought that the basic EOMCCSD [48–50] and linear-response CCSD [41, 42] approximations, which construct the desired excited-state information on top of the conventional CCSD [131–134] ground state, and which are characterized by the relatively inexpensive iterative CPU steps that scale as $n_o^2 n_u^4$ or \mathcal{N}^6 , where \mathcal{N} is a measure of the system size, provide an accurate description of excited states dominated by one-electron transitions. However, the EOMCCSD method is often not accurate enough to obtain a quantitative description of such states, especially when larger polyatomic species are examined (cf., e.g., Refs. [69, 135–137]; for a thorough evaluation of a number of EOMCC methods, including EOMCCSD, illustrating the same, see Refs. [17, 19, 20, 22, 24, 25]). It also fails to describe states with significant two-electron excitation contributions [63–68, 70–72, 74, 122].

One can address these shortcomings by including the effects of connected triple excitations, as is done in full EOMCCSDT [71–73]. While the full treatment of triple excitations substantially improves the description of excited electronic states, often providing virtually exact results (see, e.g., Refs. [64, 65, 71–73, 115, 138–141]), it is also accompanied by a steep increase in the CPU times characterizing the EOMCCSDT computations (the iterative $n_o^3 n_u^5$ or \mathcal{N}^8 steps), limiting its applicability to systems with up to a dozen or so correlated electrons and smaller basis sets. Thus, if one is to make use of the EOMCC methodologies in accurate calculations of molecular electronic spectra in medium size and larger systems, including vertical excitation energies that interest us in this work, EOMCC schemes which can account for the effects of triples in an approximate, cost effective, and yet reliable manner need to be employed.

There are several ways of incorporating triple excitations in the EOMCC and linearresponse CC formalisms without running into the prohibitive computational costs of full EOMCCSDT. For example, one can select the dominant triply excited components of the cluster operator T that defines the underlying ground-state CC wave function and three-body components of the linear excitation operator R_{μ} in the EOMCC wave function ansatz through the use of active orbitals, as is done in the active-space EOMCCSDt method [71, 72, 110–112] (see Refs. [115, 129] for reviews; cf., also, Refs. [98–109] for the closely related active-space CC methods for the ground electronic states). While this allows for full-EOMCCSDT-quality results at the cost of EOMCCSD times a prefactor proportional to the numbers of active occupied and active unoccupied orbitals used to select the triples, the approach is no longer strictly speaking black-box as one has to select the active orbitals.

One can also contemplate approaches for identifying the most important triples contributions through the many-body perturbation theory or the aforementioned MMCC analysis. Some examples of these types of non-iterative triples methods are the EOMCC(2)PT(2) approach [142] and its size-intensive EOMCCSD(2)_T modification [143], the linear-response CCSDR(3) method [46, 47], the EOMCCSD(T) [51], EOMCCSD(T) [52], and EOMCCSD(T') [52] hierarchy obtained from the perturbative analysis of the EOMCCSDT equations, the CR-EOMCC family, such as the original CR-EOMCCSD(T) schemes [63, 65, 66], the newer CR-EOMCC(2,3) approaches [67, 68], and their approximately and rigorously size-intensive δ -CR-EOMCC counterparts [63, 69], as well as the related N-EOMCCSD(T) scheme [144], the spin-flip [145–147] extensions of variants A and D of CR-EOMCC(2,3) implemented in Ref. [148] and abbreviated as EOMCCSD(fT) and EOMCCSD(dT), respectively, and the iterative EOMCCSDT-n (n = 1, 2, 3) [51, 52] and CC3 [44–47] methodologies. These various approaches account for the leading triples effects, while replacing the iterative $n_o^3 n_u^5$ (\mathcal{N}^8) CPU steps of full EOMCCSDT by the iterative (EOMCCSDT-n and CC3) or even less expensive non-iterative (EOMCC(2)PT(2), EOMCCSD(2)_T, CCSDR(3), EOMCCSD(T),

EOMCCSD($\tilde{\mathbf{T}}$), EOMCCSD(\mathbf{T}'), CR-EOMCCSD(\mathbf{T}), N-EOMCCSD(\mathbf{T}), CR-EOMCC(2,3)) $n_o^3 n_u^4$ (\mathcal{N}^7) CPU costs. This, combined with their black-box character, makes the above approximate treatment of triple excitations within the EOMCC and linear-response CC frameworks attractive candidates for routine use in photochemistry and other areas where accurate excited-state information is called for. Another promising approach in this category is the similarity-transformed EOMCC (STEOMCC) methodology [24, 53, 54], which incorporates higher-than-double excitations into the EOMCC framework through the suitable transformation of the similarity-transformed Hamiltonian of EOMCCSD.

The performance of many of the above methods is already well established. In particular, the EOMCCSDT-3 and CC3 approaches and their non-iterative EOMCCSD(T), EOMCCSD(T), and CCSDR(3) counterparts have been thoroughly examined in Refs. [17, 19–22, 24, 25] using the database developed in Ref. [17]. The same applies to the STEOMCC approaches, which have been tested against the EOMCCSDT-3 and CC3 data that are generally recognized as accurate, using the singlet and triplet excited states of the 28 molecules constituting the database of Ref. [17]. Although a number of successful applications of the CR-EOMCCSD(T), CR-EOMCC(2,3), δ -CR-EOMCCSD(T), and δ -CR-EOMCC(2,3) methods have been published (see, e.g., Refs. [63–69, 74, 111, 115, 135, 136, 149–186]), showing considerable promise in applications involving singly and more multi-reference doubly excited states, none of the CR-EOMCC approaches have been subjected to a comprehensive statistical evaluation of the type used in Refs. [17–25]. This present work addresses this issue by testing the approximately size-intensive δ -CR-EOMCCSD(T) method and its biorthogonal and strictly size-intensive δ -CR-EOMCC(2,3) counterpart against the previously published EOMCCSDT-3, CC3, CASPT2, and theoretical best estimate (TBE) data using the database of excited states developed in Ref. [17] and the subsequent studies [19–22, 24, 25]. Comparisons with the EOMCCSDT-3 and CC3 results reported in Refs. [17, 19, 21, 22, 24, 25] are particularly useful, since the δ -CR-EOMCCSD(T) and δ -CR-EOMCC(2,3) approaches replace the iterative $n_o^3 n_u^4$ (\mathcal{N}^7) CPU steps and $\sim \mathcal{N}^6$ storage requirements by the much less expensive iterative $n_o^2 n_u^4$ (\mathcal{N}^6) and non-iterative $n_o^3 n_u^4$ (\mathcal{N}^7) steps and $\sim \mathcal{N}^4$ storage requirements. Comparisons with the CASPT2 and TBE data are useful too, since δ -CR-EOMCC methods are computational black boxes and the multi-reference CASPT2 approach is not. Furthermore, the existing TBE data can presently be regarded as some of the best estimates of the excitation energies for the molecules comprising the database of Ref. [17], which one would like to reproduce with a reasonable accuracy.

3.2 Theory

As already alluded to in Section 3.1, in the δ -CR-EOMCCSD(T) and δ -CR-EOMCC(2,3) methods of Refs. [63] and [69], we correct the vertical excitation energies obtained in the EOMCCSD calculations for the leading triples effects extracted from the MMCC considerations. Thus, if $\omega_{\mu} = E_{\mu} - E_0$ represents the vertical excitation energy from the ground state $|\Psi_0\rangle$ to the excited state $|\Psi_{\mu}\rangle$, the δ -CR-EOMCCSD(T) and δ -CR-EOMCC(2,3) values of ω_{μ} can be given the following general form:

$$\omega_{\mu} = \omega_{\mu}^{(CCSD)} + \delta_{\mu}, \tag{3.1}$$

where $\omega_{\mu}^{(\text{CCSD})}$ is the EOMCCSD excitation energy obtained by diagonalizing the similarity-transformed Hamiltonian of CCSD, i.e.,

$$\bar{H}^{(CCSD)} = e^{-T_1 - T_2} H e^{T_1 + T_2},$$
(3.2)

in the space of singly and doubly excited determinants, $|\Phi_i^a\rangle$ and $|\Phi_{ij}^{ab}\rangle$, respectively, and δ_{μ} is the triples correction to $\omega_{\mu}^{(\text{CCSD})}$. As usual, T_1 and T_2 are the singly and doubly excited components of the cluster operator T obtained by solving the ground-state CCSD equations and $i, j, \ldots (a, b, \ldots)$ are the spin-orbitals which are occupied (unoccupied) in the reference determinant $|\Phi\rangle$ (in the case of the δ -CR-EOMCC calculations reported in this dissertation, the restricted Hartree–Fock (RHF) determinant). Both δ -CR-EOMCC approaches use the same general expression for δ_{μ} , namely,

$$\delta_{\mu} = \sum_{\substack{i < j < k \\ a < b < c}} \ell_{\mu,ijk}^{abc} \, \mathfrak{M}_{\mu,abc}^{ijk}, \tag{3.3}$$

and the only difference between the δ -CR-EOMCCSD(T) and δ -CR-EOMCC(2,3) methods is in the explicit formulas for $\ell_{\mu,ijk}^{abc}$ and $\mathfrak{M}_{\mu,abc}^{ijk}$. For a derivation of the formula for δ_{μ} , Eq. (3.3), see Appendix A.

In the δ -CR-EOMCCSD(T) approximation, which is based on the more general CR-EOMCCSD(T) considerations described in Ref. [63], $\mathfrak{M}_{\mu,abc}^{ijk}$'s are the generalized moments of the EOMCCSD equations corresponding to projections of these equations on the triply excited determinants $|\Phi_{ijk}^{abc}\rangle$,

$$\mathfrak{M}_{\mu,abc}^{ijk} = \langle \Phi_{ijk}^{abc} | \bar{H}^{(CCSD)}(R_{\mu,0} + R_{\mu,1} + R_{\mu,2}) | \Phi \rangle, \tag{3.4}$$

where $R_{\mu,0}$, $R_{\mu,1}$, and $R_{\mu,2}$ are the zero-, one-, and two-body components of the linear excitation operator R_{μ} defining the EOMCC wave function ansatz $|\Psi_{\mu}\rangle = R_{\mu}e^{T}|\Phi\rangle$ resulting from the EOMCCSD calculations, in which $T = T_1 + T_2$ and $R_{\mu} = R_{\mu,0} + R_{\mu,1} + R_{\mu,2}$ ($R_{\mu,0}$ is defined as $r_{\mu,0}\mathbf{1}$, where $r_{\mu,0}$ provides the weight of the reference determinant in

the EOMCCSD wave function and $\mathbf{1}$ is the unit operator). The corresponding amplitudes $\ell^{abc}_{\mu,ijk}$ that multiply moments $\mathfrak{M}^{ijk}_{\mu,abc}$ to produce the δ_{μ} correction are calculated using the expression

$$\ell_{\mu,ijk}^{abc} = \langle \tilde{\Psi}_{\mu} | \Phi_{ijk}^{abc} \rangle / \langle \tilde{\Psi}_{\mu} | \Psi_{\mu}^{(CCSD)} \rangle, \tag{3.5}$$

where $|\Psi_{\mu}^{(\text{CCSD})}\rangle = (R_{\mu,0} + R_{\mu,1} + R_{\mu,2})e^{T_1+T_2}|\Phi\rangle$ is the EOMCCSD wave function of excited state μ and $|\tilde{\Psi}_{\mu}\rangle$ is defined as

$$|\tilde{\Psi}_{\mu}\rangle = \{R_{\mu,0} + (R_{\mu,1} + R_{\mu,0}T_1) + [R_{\mu,2} + R_{\mu,1}T_1 + R_{\mu,0}(T_2 + \frac{1}{2}T_1^2)] + [\tilde{R}_{\mu,3} + R_{\mu,2}T_1 + R_{\mu,1}(T_2 + \frac{1}{2}T_1^2) + R_{\mu,0}(T_1T_2 + \frac{1}{6}T_1^3)]\}|\Phi\rangle.$$
(3.6)

Here, $\tilde{R}_{\mu,3}$ represents the approximate form of the three-body component of R_{μ} given by

$$\tilde{R}_{\mu,3} = \sum_{\substack{i < j < k \\ a < b < c}} \tilde{r}_{\mu,abc}^{ijk} a^a a^b a^c a_k a_j a_i, \tag{3.7}$$

where

$$\tilde{r}_{\mu,abc}^{ijk} = \mathfrak{M}_{\mu,abc}^{ijk} / D_{\mu,ijk}^{abc}$$

$$\tag{3.8}$$

are the corresponding triple excitation amplitudes and a^p (a_p) is the creation (annihilation) operator associated with spin-orbital p. In the most complete δ -CR-EOMCCSD(T) treatment, defining variant ID of it and abbreviated, following the naming convention introduced in Ref. [63], as δ -CR-EOMCCSD(T),ID, the $D_{\mu,ijk}^{abc}$ denominator entering Eq. (3.8) is calculated as

$$D_{\mu,ijk}^{abc} = \omega_{\mu}^{(\text{CCSD})} - \sum_{n=1}^{3} \langle \Phi_{ijk}^{abc} | \bar{H}_{n}^{(\text{CCSD})} | \Phi_{ijk}^{abc} \rangle, \tag{3.9}$$

where $\bar{H}_n^{(\text{CCSD})}$ is the *n*-body component of $\bar{H}^{(\text{CCSD})}$. In the simplified IA version of δ -CR-EOMCCSD(T), abbreviated as δ -CR-EOMCCSD(T), IA, we replace the Epstein–Nesbet form of $D_{\mu,ijk}^{abc}$, Eq. (3.9), by the Møller–Plesset-style expression

$$D_{\mu,ijk}^{abc} = \omega_{\mu}^{\text{(CCSD)}} - (\varepsilon_a + \varepsilon_b + \varepsilon_c - \varepsilon_i - \varepsilon_j - \varepsilon_k), \tag{3.10}$$

where ε_p 's are the spin-orbital energies (diagonal elements of the Fock matrix).

The δ -CR-EOMCC(2,3) method proposed in Ref. [69], which is a rigorously size-intensive version of the CR-EOMCC(2,3) methodology of Refs. [67, 68], relies on the same general expressions for ω_{μ} and δ_{μ} as those used in the δ -CR-EOMCCSD(T) considerations, Eqs. (3.1) and (3.3), respectively, but the explicit formulas for $\ell_{\mu,ijk}^{abc}$ and $\mathfrak{M}_{\mu,abc}^{ijk}$ are different. As shown in Refs. [68, 69], the enforcement of strict size intensivity of the δ_{μ} triples correction ($\omega_{\mu}^{\text{(CCSD)}}$ is size intensive [42, 130]) requires that we replace the complete moment $\mathfrak{M}_{\mu,abc}^{ijk}$, Eq. (3.4), in Eq. (3.3) by its truncated analog ignoring the ground-state $r_{\mu,0}\langle\Phi_{ijk}^{abc}|\bar{H}^{\text{(CCSD)}}|\Phi\rangle$ contribution, i.e.,

$$\mathfrak{M}_{\mu,abc}^{ijk} = \langle \Phi_{ijk}^{abc} | \bar{H}^{(CCSD)}(R_{\mu,1} + R_{\mu,2}) | \Phi \rangle. \tag{3.11}$$

At the same time, because of the use of the biorthogonal version of the MMCC formalism in designing the CR-EOMCC(2,3) schemes, we have to replace Eq. (3.5) for $\ell_{\mu,ijk}^{abc}$ in Eq. (3.3) by

$$\ell_{\mu,ijk}^{abc} = \langle \Phi | (L_{\mu,1} + L_{\mu,2}) \,\bar{H}^{(CCSD)} | \Phi_{ijk}^{abc} \rangle / D_{\mu,ijk}^{abc}, \tag{3.12}$$

where $L_{\mu,1}$ and $L_{\mu,2}$ are the one- and two-body components of the linear deexcitation operator L_{μ} defining the bra counterparts of the EOMCCSD excited states, $\langle \Psi_{\mu}^{(\text{CCSD})} | = \langle \Phi | (L_{\mu,1} + L_{\mu,2}) e^{-T_1 - T_2}$ (the zero-body component of L_{μ} , i.e., $L_{\mu,0}$, vanishes when excited

states are considered). Again, if the $D^{abc}_{\mu,ijk}$ denominator entering Eq. (3.12) is given by the Epstein–Nesbet-type expression, Eq. (3.9), we obtain the more complete variant D of δ -CR-EOMCC(2,3), abbreviated as δ -CR-EOMCC(2,3),D. If we replace Eq. (3.9) for $D^{abc}_{\mu,ijk}$ in Eq. (3.12) by the Møller–Plesset-type expression given by Eq. (3.10), we obtain the simplified A variant, abbreviated as δ -CR-EOMCC(2,3),A. As explained in Ref. [69] (cf., also, Ref. [68]), the δ -CR-EOMCC(2,3),A approximation is equivalent to the EOMCCSD(2)_T approach of Ref. [143] and, if we limit ourselves to vertical excitation energies, which is the case in this work, to the EOMCCSD(\tilde{T}) method of Ref. [52].

3.3 Benchmark Molecules and Computational Details

The database set of 28 organic molecules proposed in Ref. [17] is composed of seven unsaturated aliphatic hydrocarbons, eleven aromatic hydrocarbons and heterocycles, six carbonyl compounds, and four nucleobases, all shown in Fig. 3.1. The main Tables I and II of Ref. [17] contain a total of 221 electronically excited states, namely, 149 singlet and 72 triplet excitations. The Supporting Information to Ref. [17] provides data on 22 additional singlet states, but this study, particularly in its statistical error analysis in Section 3.5, focuses on the 149 singlet excitations listed in Table I of Ref. [17]. Our EOMCC calculations have produced 54 additional singlet excited states in the energy range covered by Table I of Ref. [17], including five states that can be found in the Supporting Information to Ref. [17] and 49 states that have not been considered in the earlier benchmark work [17–25]. We provide information about these 54 additional singlet excitations in our tables as well, but we do not include them in our statistical error analyses, since the EOMCCSDT-3 and CC3 reference data are not available for them.

Ethene E-Butadiene all-E-Hexatriene all-E-Octatetraene Cyclopropene Cyclopentadiene Norbornadiene Aromatic Hydrocarbons and Heterocycles Penzene Naphthalene Furan Pyrrole Imidazole Pyridine Pyrazine Pyrimidine Pyridazine Norbornadiene Norbornadiene

Figure 3.1: Benchmark set of molecules considered in this work.

Adenine

Uracil

Thymine

Cytosine

In determining the corresponding vertical excitation energies, we considered the groundstate equilibrium geometries taken from Ref. [17], which were optimized at the Møller–Plesset second-order perturbation theory (MP2) level using the 6-31G* [187] basis. In addition, to examine the effect of geometry on the calculated vertical excitation energies, we also re-optimized the ground-state geometries of the same set of molecules at the higher CR-CC(2,3),D level [127, 128], consistent with the δ -CR-EOMCC(2,3),D approximation, using the TZVP [188] basis, which was used in the vertical excitation energy calculations reported in Refs. [17–20, 22–25] and which is used in the EOMCC computations discussed in this work. These additional CR-CC(2,3),D geometry optimizations were carried out using the parallel coarse-grain finite-difference model available in the CIOpt program suite [189, 190], which we interfaced with the CR-CC(2,3) routines [127, 128, 191] available in the GAMESS package [192, 193]. All of the δ -CR-EOMCCSD(T),IA, δ -CR-EOMCCSD(T),ID, δ -CR-EOMCC(2,3),A, and δ -CR-EOMCC(2,3),D computations reported in this work and the underlying EOMCCSD calculations were performed using the CC/EOMCC routines developed in Refs. [63, 68, 127, 194], available in GAMESS as well. In all of the correlated calculations reported in this work, core electrons were kept frozen and spherical components of d basis functions were employed throughout.

3.4 Results and Discussion

3.4.1 Geometries and their Effect on the Calculated Vertical Excitation Energies

Comparing the MP2/6-31G* and CR-CC(2,3),D/TZVP geometries, Tables 3.1 and 3.2, we see that the corresponding bond lengths and bond angles, which differ by 0.005 Å and 0.2 degrees, respectively, on average, are in excellent agreement with each other. Among the individual molecules, the largest differences in the bond lengths and angles occur in the nucleobases, namely, cytosine (0.019 Å) and adenine (0.6 degrees). For the dihedral angles, the largest difference between the MP2/6-31G* and CR-CC(2,3),D/TZVP results, of 0.3 degrees, occurs for cyclopropene.

Using the above two sets of geometries, we computed the 203 vertical excitation energies for the 28 molecules comprising the database of Ref. [17], which are presented in Table 3.3 for the MP2/6-31G* geometries and Table 3.4 for the CR-CC(2,3),D/TZVP geometries. Comparing the two sets of vertical excitation energies, we can see that they are in very good agreement for each of the EOMCC approaches employed in this work. For example, if we examine the correlation plot for the vertical excitation energies corresponding to the 149 singlet excited states listed in Table I of Ref. [17] and computed at the δ -CR-EOMCC(2,3),D/TZVP level using the MP2/6-31G* and CR-CC(2,3),D/TZVP geometries, shown in Fig. 3.2, we observe that their correlation coefficient is 0.9994 and maximum energy difference (MaxE) is 0.18 eV. The corresponding mean unsigned error (MUE) and mean signed error (MSE) values are 0.05 and 0.04 eV, respectively.

This similarity of the δ -CR-EOMCC(2,3),D excitation energies obtained at the MP2/6-

31G* and CR-CC(2,3),D/TZVP geometries remains virtually the same if we include the entire set of 203 excitations listed in Tables 3.3 and 3.4 in our calculations. Thus, we can safely rely on the MP2/6-31G* geometries in discussing the relative performance of various EOMCC methods in this work. For this reason, much of our assessment of the δ -CR-EOMCC approaches examined in this dissertation is based on the results obtained with the MP2/6-31G* geometries collected in Table 3.1. The same geometries were used in the previous method assessments using the database of Ref. [17], reported in Refs. [17–25], which helps us in making judgments regarding the performance of the δ -CR-EOMCCSD(T) and δ -CREOMCC(2,3) methods, particularly when compared with the previously published EOMCCSDT-3 [22, 24], CC3 [17, 19, 21, 25], and CASPT2 [17, 21] data.

Table 3.1: Symmetry unique Cartesian coordinates of the ground-state geometries for the 28 molecules comprising the benchmark set resulting from the $MP2/6-31G^*$ optimizations.

Molecule (symmetry)	Atom	X	Y	Z
Ethene (D_{2h})	Н	0.000000	0.923274	1.238289
	С	0.000000	0.000000	0.668188
E-Butadiene (C_{2h})	Н	-1.080977	2.558832	0.000000
,,	Η	-2.103773	1.017723	0.000000
	Η	0.973565	1.219040	0.000000
	\mathbf{C}	0.000000	-0.728881	0.000000
	С	-1.117962	1.474815	0.000000
all-E-Hexatriene (C_{2h})	Н	-0.953777	1.207691	0.000000
(210)	Н	2.155816	0.952317	0.000000
	Н	2.125769	3.402692	0.000000
	Н	0.275642	3.397162	0.000000
	\mathbf{C}	0.000000	0.676808	0.000000
	\mathbf{C}	1.204938	1.485654	0.000000
	\mathbf{C}	1.203567	2.831663	0.000000
all-E-Octatetraene (C_{2h})	Η	0.971328	1.220141	0.000000
(216)	Н	-2.098090	0.984719	0.000000
	Н	-0.146884	3.418505	0.000000
	Н	-2.193473	4.766086	0.000000
	Н	-3.225698	3.230501	0.000000
	\mathbf{C}	0.000000	0.721498	0.000000
	\mathbf{C}	1.125020	-1.479523	0.000000
	\mathbf{C}	1.121077	-2.928812	0.000000
	С	2.237388	-3.682282	0.000000
Cyclopropene (C_{2v})	Н	0.912650	0.000000	1.457504
	Η	0.000000	-1.585659	-1.038624
	\mathbf{C}	0.000000	0.000000	0.859492
	С	0.000000	-0.651229	-0.499559
Cyclopentadiene (C_{2v})	Н	-0.879859	0.000000	1.874608
, ,	Н	0.000000	2.211693	0.612518
	Н	0.000000	1.349811	-1.886050
	\mathbf{C}	0.000000	0.000000	1.215652
	\mathbf{C}	0.000000	-1.177731	0.285415
	\mathbf{C}	0.000000	-0.732372	-0.993420
Norbornadiene (C_{2v})	Н	0.901419	0.000000	1.967823
(== /	Н	0.000000	2.156504	0.616597

Table 3.1 (cont'd).

Molecule (symmetry)	Atom	X	Y	Z
	Η	1.924341	1.340999	-1.022814
	\mathbf{C}	0.000000	0.000000	1.346369
	\mathbf{C}	0.000000	1.119526	0.272221
	С	1.235500	0.672374	-0.517602
Benzene (D_{6h})	Н	2.151390	1.242106	0.000000
	С	1.209657	-0.698396	0.000000
Naphthalene (D_{2h})	Н	1.240557	2.492735	0.000000
	\mathbf{H}	3.377213	1.246082	0.000000
	\mathbf{C}	0.000000	0.716253	0.000000
	\mathbf{C}	1.241539	1.403577	0.000000
	С	2.432418	0.707325	0.000000
Furan (C_{2v})	Н	0.000000	2.051058	0.851533
(20)	Η	0.000000	1.371979	-1.821224
	\mathbf{C}	0.000000	1.095840	0.348301
	\mathbf{C}	0.000000	0.714027	-0.963274
	Ο	0.000000	0.000000	1.164881
Pyrrole (C_{2v})	Н	0.000000	2.114611	0.770889
0 (20)	Η	0.000000	1.358585	-1.850224
	Η	0.000000	0.000000	2.130670
	\mathbf{C}	0.000000	1.125828	0.333870
	\mathbf{C}	0.000000	0.709235	-0.984789
	N	0.000000	0.000000	1.119862
Imidazole (C_s)	Η	0.000000	2.119822	0.714354
· · · /	Η	0.000000	1.202262	-1.904898
	\mathbf{H}	0.000000	-2.104815	0.663782
	Η	0.000000	-0.010302	2.116597
	\mathbf{C}	0.000000	1.120107	0.305897
	\mathbf{C}	0.000000	0.635508	-0.983749
	\mathbf{C}	0.000000	-1.091835	0.283881
	N	0.000000	-0.741378	-0.994001
	N	0.000000	0.000000	1.104571
Pyridine (C_{2v})	Н	0.000000	2.061947	1.308539
	H	0.000000	2.156804	-1.184054
	Н	0.000000	0.000000	-2.475074
	\mathbf{C}	0.000000	1.145417	0.721005
	$\dot{\mathrm{C}}$	0.000000	1.197637	-0.673735

Table 3.1 (cont'd).

Molecule (symmetry)	Atom	X	Y	Z
	С	0.000000	0.000000	-1.387901
	N	0.000000	0.000000	1.426610
Pyrazine (D_{2h})	Η	0.000000	2.068464	1.258236
	\mathbf{C}	0.000000	1.135920	0.697884
	N	0.000000	0.000000	1.417402
Pyrimidine (C_{2v})	Н	0.000000	2.156588	1.120200
z_{j} z_{ij} z_{ij}	H	0.000000	0.000000	-2.400385
	Н	0.000000	0.000000	2.440403
	C	0.000000	1.186684	0.626213
	$\overset{\circ}{\mathrm{C}}$	0.000000	0.000000	-1.312625
	$\overset{\circ}{\mathrm{C}}$	0.000000	0.000000	1.354949
	N	0.000000	1.203523	-0.717781
Pyridazine (C_{2v})	Η	0.000000	2.409486	-0.149325
	Η	0.000000	1.271234	2.102647
	\mathbf{C}	0.000000	1.325698	-0.063084
	\mathbf{C}	0.000000	0.693095	1.182948
	N	0.000000	0.674211	-1.238929
s-Triazine (D_{3h})	Н	0.000000	0.000000	2.386083
$\sim 111621110 \; (2.511)$	H	0.000000	2.066408	-1.193041
	C	0.000000	0.000000	1.298345
	$\overset{\circ}{\mathrm{C}}$	0.000000	1.124400	-0.649173
	N	0.000000	0.000000	-1.379450
	N	0.000000	1.194639	0.689726
m · · · (D)	TT	0.000000	0.000000	0.05.450.4
s-Tetrazine (D_{2h})	Н	0.000000	0.000000	-2.354794
	\mathbf{C}	0.000000	0.000000	1.269044
	N	0.000000	1.204572	0.670429
Formaldehyde (C_{2v})	Н	0.000000	0.934473	-0.588078
	\mathbf{C}	0.000000	0.000000	0.000000
	O	0.000000	0.000000	1.221104
Acetone (C_{2v})	Н	0.000000	2.136732	-0.112445
r ($\sim 2v$)	H	-0.881334	1.333733	-1.443842
	С	0.000000	0.000000	0.000000
	C	0.000000	1.287253	-0.795902
	O	0.000000	0.000000	-0.795902 1.227600
	U	0.000000	0.000000	1.221000

Table 3.1 (cont'd).

Molecule (symmetry)	Atom	X	Y	Z
p -Benzoquinone (D_{2h})	Н	0.000000	2.182973	1.259286
1 (210)	\mathbf{C}	0.000000	0.000000	1.441079
	\mathbf{C}	0.000000	1.266644	0.674582
	O	0.000000	0.000000	2.678518
Formamide (C_s)	Η	-0.927427	-0.600301	0.000000
	Η	1.070498	-1.782390	0.000000
	Η	2.024514	-0.325050	0.000000
	\mathbf{C}	0.000000	0.000000	0.000000
	O	0.000000	1.225060	0.000000
	N	1.119392	-0.775069	0.000000
Acetamide (C_s)	Н	1.173209	-1.735763	0.000000
(C_s)	Н	2.035841	-0.226201	0.000000
	Н	-2.121189	-0.156089	0.000000
	Н	-1.310647	-1.472742	0.885504
	C	0.000000	0.000000	0.000000
	$\overset{\circ}{\mathrm{C}}$	-1.267042	-0.831610	0.000000
	Ö	0.000000	1.229439	0.000000
	N	1.158967	-0.727718	0.000000
Propanamide (C_s)	Н	1.171887	-1.734653	0.000000
1 Topanamide (C_s)	H	2.036508	-1.734033 -0.225526	0.000000
	H	-1.256737	-1.492368	0.877197
	H	-3.420939	-0.590421	0.000000
	H	-2.544313	0.678541	-0.880209
	$^{\rm II}$	0.000000	0.000000	0.000000
	C	-1.272727	-0.833216	0.000000
	$\stackrel{ ext{C}}{ ext{C}}$	-2.523376	0.033790	0.000000
	Ö	0.000000	1.230373	0.000000
	N	1.159100	-0.726409	0.000000
Cytosine (C_s)	Η	-2.114860	-1.429678	0.000000
	Η	-0.173973	-2.806186	0.000000
	Η	2.073228	-1.658021	0.000000
	Η	3.175240	0.564335	0.000000
	Η	2.235202	2.033636	0.000000
	\mathbf{C}	-0.060783	-1.726152	0.000000
	\mathbf{C}	1.144884	-1.099470	0.000000
	С	1.107049	0.338190	0.000000
	С	-1.227573	0.430359	0.000000
	O	-2.315109	0.998271	0.000000

Table 3.1 (cont'd).

Molecule (symmetry)	Atom	X	Y	Z
	N	0.000000	1.058130	0.000000
	N	-1.201178	-0.989148	0.000000
	N	2.278974	1.024187	0.000000
Thymine (C_s)	Н	0.217481	-2.676720	0.000000
* (- /	Η	2.052694	0.924773	0.000000
	Н	-1.943101	-1.709021	0.000000
	Н	-3.360610	0.309754	0.000000
	Η	-2.616463	1.665008	0.879105
	\mathbf{C}	1.356951	-0.994496	0.000000
	\mathbf{C}	0.000000	1.121102	0.000000
	\mathbf{C}	-1.214538	0.306431	0.000000
	\mathbf{C}	-1.085764	-1.041812	0.000000
	\mathbf{C}	-2.529824	1.020445	0.000000
	O	2.444132	-1.558490	0.000000
	O	0.023681	2.350992	0.000000
	N	0.145112	-1.666249	0.000000
	N	1.192460	0.382130	0.000000
Uracil (C_s)	Н	-2.025413	-1.517742	0.000000
(-,	Н	-0.021861	1.995767	0.000000
	Η	2.182391	-1.602586	0.000000
	Н	-0.026659	-2.791719	0.000000
	\mathbf{C}	-1.239290	0.359825	0.000000
	\mathbf{C}	1.279718	0.392094	0.000000
	\mathbf{C}	1.243729	-1.064577	0.000000
	\mathbf{C}	0.055755	-1.709579	0.000000
	O	-2.308803	0.954763	0.000000
	O	2.287387	1.092936	0.000000
	N	-1.139515	-1.026364	0.000000
	N	0.000000	0.978951	0.000000
Adenine (C_s)	Н	0.974930	-3.075149	0.000000
	Η	2.134658	2.075802	0.000000
	Н	3.312010	0.776987	0.000000
	Η	-3.052077	-0.334232	0.000000
	Н	-2.711876	2.203052	0.000000
	\mathbf{C}	0.662834	-2.032900	0.000000
	С	1.359313	0.172553	0.000000
	\mathbf{C}	0.000000	0.547434	0.000000
	\mathbf{C}	-0.924835	-0.500714	0.000000
	\mathbf{C}	-1.906806	1.478795	0.000000

Table 3.1 (cont'd).

Molecule (symmetry)	Atom	X	Y	Z
	N	-0.658577	-1.817838	0.000000
	N	1.672594	-1.133202	0.000000
	N	-2.150759	0.128726	0.000000
	N	-0.616118	1.783396	0.000000
	N	2.352763	1.090709	0.000000

Table 3.2: Symmetry unique Cartesian coordinates of the ground-state geometries of the 28 molecules comprising the benchmark set resulting from the CR-CC(2,3),D/TZVP optimizations carried out in this work.

Molecule (symmetry)	Atom	X	Y	
Ethene (D_{2h})	H	0.000000	0.924035	1.236513
$\mathbb{E}^{\text{mene}}(\mathbb{E}_{2n})$	C	0.000000	0.000000	0.668881
	Ü	0.000000	0.00000	0.000001
E-Butadiene (C_{2h})	Н	-2.733502	0.488401	0.000000
(216)	Н	-1.996346	-1.209626	0.000000
	Н	-0.493204	1.480741	0.000000
	\mathbf{C}	0.613255	-0.399134	0.000000
	\mathbf{C}	-1.846790	-0.134268	0.000000
all-E-Hexatriene (C_{2h})	Н	-0.689671	-1.373825	0.000000
, - 107	Η	-1.779265	1.550035	0.000000
	Η	-3.983818	0.481440	0.000000
	Η	-3.188581	-1.190249	0.000000
	\mathbf{C}	-0.611506	-0.287351	0.000000
	\mathbf{C}	-1.860731	0.465059	0.000000
	\mathbf{C}	-3.076386	-0.110589	0.000000
all-E-Octatetraene (C_{2h})	Η	-0.609354	1.435522	0.000000
	Η	-1.864325	-1.371454	0.000000
	Н	-3.082792	1.500066	0.000000
	Η	-5.238862	0.334070	0.000000
	Η	-4.370232	-1.299431	0.000000
	\mathbf{C}	-0.638128	0.346740	0.000000
	\mathbf{C}	1.835457	0.282916	0.000000
	\mathbf{C}	3.116293	-0.412631	0.000000
	\mathbf{C}	4.305668	0.215978	0.000000
Cyclopropene (C_{2v})	Η	0.914476	0.000000	1.478608
	Н	0.000000	-1.579439	-1.022564
	\mathbf{C}	0.000000	0.000000	0.887272
	С	0.000000	-0.650147	-0.480853
Cyclopentadiene (C_{2v})	Н	-0.884693	0.000000	1.884064
	Н	0.000000	2.210781	0.627891
	Н	0.000000	1.348160	-1.876762
	С	0.000000	0.000000	1.235311
	С	0.000000	-1.181911	0.294218
	С	0.000000	-0.737921	-0.982749
Norbornadiene (C_{2v})	Н	0.901246	0.000000	1.976906

Table 3.2 (cont'd).

Molecule (symmetry)	Atom	X	Y	Z
	Н	0.000000	2.156931	0.625501
	Н	1.933914	1.340614	-1.010326
	\mathbf{C}	0.000000	0.000000	1.357782
	\mathbf{C}	0.000000	1.123491	0.279727
	\mathbf{C}	1.244064	0.671585	-0.512920
D (D.)	TT	0.000000	0.400070	0.000000
Benzene (D_{6h})	Н	0.000000	2.482672	0.000000
	С	0.000000	1.397828	0.000000
Naphthalene (D_{2h})	Н	1.241938	2.490352	0.000000
1 (210)	Н	3.377709	1.245631	0.000000
	\mathbf{C}	0.000000	0.712349	0.000000
	\mathbf{C}	1.245787	1.404252	0.000000
	\mathbf{C}	2.434128	0.710577	0.000000
Furan (C_{2v})	Н	0.000000	2.050655	0.816080
Furan (\bigcirc_{2v})	H	0.000000	1.377422	-1.844443
	С	0.000000	1.377422 1.095512	0.318614
	C	0.000000	0.720764	
	0			-0.989032
D		0.000000	0.000000	1.138748
Pyrrole (C_{2v})	H H	0.000000	2.113533	0.765168
		0.000000	1.361742	-1.848823
	Н	0.000000	0.000000	2.129579
	С	0.000000	1.126599	0.330605
	\mathbf{C}	0.000000	0.714934	-0.985073
	N	0.000000	0.000000	1.123459
Imidazole (C_s)	H	-1.619793	1.573819	0.000000
	Η	1.123222	1.935864	0.000000
	Η	0.334319	-2.168241	0.000000
	Η	-1.909946	-0.965998	0.000000
	\mathbf{C}	-0.806312	0.867796	0.000000
	\mathbf{C}	0.557098	1.018433	0.000000
	\mathbf{C}	0.213535	-1.095313	0.000000
	N	1.191626	-0.213966	0.000000
	N	-1.017600	-0.499248	0.000000
Pyridine (C_{2v})	Н	0.000000	2.057742	1.279370
J == (= 270)	Н	0.000000	2.157421	-1.204811
	H	0.000000	0.000000	-2.499000
	$^{\mathrm{n}}$	0.000000	1.142017	0.696089
	$\stackrel{ ext{C}}{ ext{C}}$	0.000000	1.198401	-0.699905

Table 3.2 (cont'd).

Molecule (symmetry)	Atom	X	Y	Z
	С	0.000000	0.000000	-1.414468
	N	0.000000	0.000000	1.403713
Pyrazine (D_{2h})	Н	0.000000	2.064971	1.251200
	\mathbf{C}	0.000000	1.131290	0.698767
	N	0.000000	0.000000	1.419992
Pyrimidine (C_{2v})	Н	0.000000	2.151421	1.143883
	Η	0.000000	0.000000	-2.367202
	Н	0.000000	0.000000	2.465179
	\mathbf{C}	0.000000	1.185180	0.649436
	\mathbf{C}	0.000000	0.000000	-1.282724
	\mathbf{C}	0.000000	0.000000	1.382204
	N	0.000000	1.204114	-0.692499
Pyridazine (C_{2v})	Н	0.000000	2.402231	-0.101371
(20)	Н	0.000000	1.274904	2.147804
	\mathbf{C}	0.000000	1.321686	-0.017415
	\mathbf{C}	0.000000	0.691188	1.234582
	N	0.000000	0.673098	-1.186891
s-Triazine (D_{3h})	Н	0.000000	0.000000	2.379949
(0,17)	Η	0.000000	-2.061096	-1.189974
	\mathbf{C}	0.000000	0.000000	1.295214
	\mathbf{C}	0.000000	1.121689	-0.647607
	N	0.000000	0.000000	-1.379413
	N	0.000000	1.194607	0.689706
s-Tetrazine (D_{2h})	Н	0.000000	0.000000	-2.345244
· •	\mathbf{C}	0.000000	0.000000	1.263568
	N	0.000000	1.201393	0.665348
Formaldehyde (C_{2v})	Н	0.000000	0.936522	-1.194669
v (= v /	\mathbf{C}	0.000000	0.000000	-0.611070
	Ο	0.000000	0.000000	0.601026
Acetone (C_{2v})	Н	0.000000	2.146422	-0.027075
·/	Н	-0.882224	1.327228	-1.347775
	\mathbf{C}	0.000000	0.000000	0.101073
	\mathbf{C}	0.000000	1.290335	-0.700873
	Ο	0.000000	0.000000	1.318967
p-Benzoquinone (D_{2h})	Н	0.000000	2.186299	1.257330

Table 3.2 (cont'd).

Molecule (symmetry)	Atom	X	Y	Z
	С	0.000000	0.000000	1.447657
	\mathbf{C}	0.000000	1.272483	0.672789
	O	0.000000	0.000000	2.672016
Formamide (C_s)	Н	-0.035245	-1.510395	0.000000
(0)	Н	1.985297	-0.387754	0.000000
	Н	1.220829	1.174175	0.000000
	С	-0.086417	-0.408385	0.000000
	O	-1.137024	0.203772	0.000000
	N	1.148803	0.169288	0.000000
Acetamide (C_s)	Н	-0.429500	1.963037	0.000000
110000111140 (03)	H	-1.825424	0.919709	0.000000
	Н	1.968854	-0.768041	0.000000
	H	1.731392	0.760691	0.885868
	C	-0.048142	-0.085394	0.000000
	$\dot{\mathrm{C}}$	1.447136	0.186847	0.000000
	O	-0.530756	-1.207321	0.000000
	N	-0.826744	1.039291	0.000000
Propanamide (C_s)	Н	-1.718718	1.621719	0.000000
1 (0)	Н	-2.558968	0.106405	0.000000
	Н	0.700516	1.446972	0.880124
	Н	2.8946227	0.629339	0.000000
	Н	2.0703450	-0.674316	-0.880899
	\mathbf{C}	-0.5133681	-0.079956	0.000000
	\mathbf{C}	0.7402250	0.793991	0.000000
	\mathbf{C}	2.0241565	-0.031604	0.000000
	O	-0.4793028	-1.300110	0.000000
	N	-1.6935733	0.618024	0.000000
Cytosine (C_s)	Н	2.103205	1.409422	0.000000
	Η	0.192912	2.827585	0.000000
	Η	-2.076127	1.733417	0.000000
	Η	-3.230237	-0.441208	0.000000
	Η	-2.342275	-1.940394	0.000000
	\mathbf{C}	0.057348	1.753262	0.000000
	\mathbf{C}	-1.160876	1.158804	0.000000
	\mathbf{C}	-1.160455	-0.287378	0.000000
	\mathbf{C}	1.168040	-0.430384	0.000000
	O	2.229243	-1.026481	0.000000
	N	-0.075930	-1.033377	0.000000

Table 3.2 (cont'd).

Molecule (symmetry)	Atom	X	Y	Z
	N	1.184394	0.990106	0.000000
	N	-2.355274	-0.933983	0.000000
Thymine (C_s)	Н	-1.808790	1.976164	0.000000
,	Η	-0.960101	-1.978634	0.000000
	Η	0.472725	2.586214	0.000000
	Η	2.845328	1.936434	0.000000
	Н	3.138260	0.420783	0.880445
	\mathbf{C}	-1.629921	-0.052812	0.000000
	\mathbf{C}	0.757392	-0.836268	0.000000
	\mathbf{C}	1.185247	0.572789	0.000000
	\mathbf{C}	0.232776	1.529218	0.000000
	\mathbf{C}	2.660700	0.859484	0.000000
	O	-2.818136	-0.308378	0.000000
	O	1.510510	-1.794389	0.000000
	N	-1.122941	1.236814	0.000000
	N	-0.634602	-1.019928	0.000000
Uracil (C_s)	Н	-2.017408	-1.525923	0.000000
(0)	Н	-0.037071	2.000601	0.000000
	Н	2.186816	-1.597809	0.000000
	Н	-0.017760	-2.789145	0.000000
	\mathbf{C}	-1.239995	0.355737	0.000000
	\mathbf{C}	1.277990	0.401032	0.000000
	\mathbf{C}	1.247659	-1.064625	0.000000
	\mathbf{C}	0.063207	-1.709410	0.000000
	O	-2.304131	0.941040	0.000000
	O	2.276936	1.095016	0.000000
	N	-1.138733	-1.030829	0.000000
	N	-0.005322	0.988101	0.000000
Adenine (C_s)	Н	2.011864	-2.505708	0.000000
· · · /	Η	1.265984	2.708859	0.000000
	Η	2.822411	1.913573	0.000000
	Η	-2.721643	-1.389953	0.000000
	Η	-3.312695	1.099409	0.000000
	\mathbf{C}	1.351251	-1.644974	0.000000
	\mathbf{C}	1.214246	0.657399	0.000000
	\mathbf{C}	-0.188214	0.522517	0.000000
	\mathbf{C}	-0.677566	-0.781382	0.000000
	\mathbf{C}	-2.302961	0.717203	0.000000
	N	0.042556	-1.915431	0.000000

Table 3.2 (cont'd).

Molecule (symmetry)	Atom	X	Y	Z
	N	1.976462	-0.449014	0.000000
	N	-2.048158	-0.639855	0.000000
	N	-1.219795	1.457921	0.000000
	N	1.817944	1.868950	0.000000

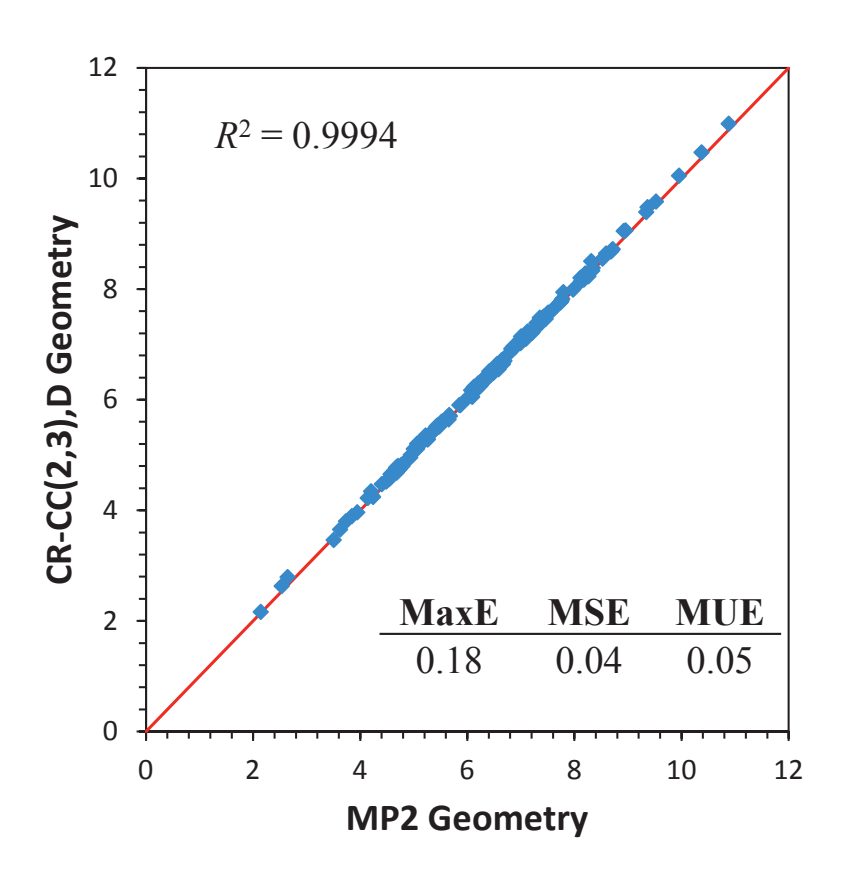


Figure 3.2: Correlation plot of the δ -CR-EOMCC(2,3),D/TZVP excitation energies (in eV) computed using the MP2/6-31G* and CR-CC(2,3),D/TZVP geometries.

Table 3.3: Vertical excitation energies (in eV) for singlet states of all molecules in the test set using the geometries optimized at the MP2/6-31G* level. a,b

Molecule	State	REL^c	SD^d	δ -CR(T),IA e		δ -CR(2,3),A ^f	δ -CR(2,3),D ^f	$CC3^g$	$SDT-3^h$	$CASPT2^{i}$	TBE-1 i	TBE- 2^i
Ethene	$1 {}^{1}B_{1u}(\pi \to \pi^*)$	1.034	8.51	8.26	8.22	8.25	8.18	8.37	8.40	8.54	7.80	7.80
E-Butadiene	$1 ^1B_u(\pi \to \pi^*)$	1.056	6.73	6.44	6.39	6.37	6.31	6.58	6.61	6.47	6.18	6.18
L Buttanione	$2 {}^{1}A_{a}(\pi \rightarrow \pi^{*})$	1.219	7.42	6.92	6.78	6.74	6.61	6.77	6.89	6.62	6.55	6.55
all-E-Hexatriene	$1 {}^{1}B_{u}(\pi \rightarrow \pi^{*})$	1.064	5.72	5.43	5.38	5.31	5.26	5.58	5.61	5.31	5.10	5.10
-II E Oststatus	$2 \stackrel{1}{}_{Ag}(\pi \to \pi^*)$	1.225	6.61	6.03	5.91	5.79	5.67	5.72	5.88	5.42	5.09	5.09
all-E-Octatetraene	$ \begin{array}{ccc} 2 & A_g(\pi \to \pi^*) \\ 1 & B_u(\pi \to \pi^*) \end{array} $	1.211 1.069	5.98 5.08	5.41 4.78	5.32 4.74	5.11 4.63	5.01 4.58	4.97 4.94	5.17 4.97	4.64 4.70	4.47 4.66	4.47 4.66
	,	1.000	0.00	1.10		1.00	1.00	1.01	1.01	1110	1.00	1.00
Cyclopropene	$1 {}^{1}B_{1}(\sigma \rightarrow \pi^{*})$	1.066	6.97	6.76	6.71	6.72	6.67	6.90	6.92	6.76	6.76	6.67
	$1 {}^{1}B_{2}(\pi \to \pi^{*})$	1.048	7.25	7.01	6.96	6.97	6.90	7.10	7.14	7.06	7.06	6.68
Cyclopentadiene	$1 {}^{1}B_{2}(\pi \to \pi^{*})$	1 055	E 07	E E 7	E E0	E E0	E 49	E 79	E 7E	5 51	E E E	E EE
Cyclopentadiene	$\begin{array}{c} 1 B_2(\pi \to \pi) \\ 2 A_1(\pi \to \pi^*)^j \end{array}$	1.055 1.153	5.87 7.05	5.57 6.70	5.52 6.59	5.50 6.52	5.43 6.42	5.73 6.61	5.75 6.71	5.51 6.31	5.55 6.31	5.55 6.28
	$3 {}^{1}A_{1}(\pi \to \pi^{*})^{j}$	1.055	8.96	8.66	8.62	8.60	8.53	8.69	8.76	8.52	0.01	0.20
	${}^{1}B_{2}(\pi \to \pi^{*})^{k}$	1.073	8.94	8.72	8.68	8.64	8.59					
37 1 1	. 1 . / . *\	4 000	F 00		T 10		T 00	= 0.1	F 00	F 0.4	T 0.1	
Norbornadiene	$1 {}^{1}A_{2}(\pi \to \pi^{*})$ $1 {}^{1}B_{2}(\pi \to \pi^{*})$	1.063 1.076	5.80 6.69	5.53 6.43	5.49 6.38	5.41 6.29	5.36 6.24	5.64 6.49	5.68 6.55	5.34 6.11	5.34 6.11	5.37 6.21
	$2 {}^{1}B_{2}(\pi \rightarrow \pi^{*})$	1.061	7.85	7.59	7.55	7.48	7.42	7.64	7.68	7.32	0.11	0.21
	$2 \stackrel{1}{}^{1}A_{2}(\pi \rightarrow \pi^{*})$	1.067	7.86	7.63	7.58	7.51	7.47	7.71	7.74	7.45		
	${}^{1}B_{1}(\pi \to \pi^{*})^{k}$	1.079	8.01	7.80	7.76	7.68	7.65					
	$\underline{2} {}^{1}A_{1}(\pi \to \pi^{*}/\pi \to \sigma^{*})^{k}$	1.062	7.99	7.81	7.79	7.73	7.70			7.97		
Ponzono	1 l P. (-) -*\	1.104	5.10	4.01	1 09	4 7C	4.60	5.07	5.10	5.04	5.00	5.00
Benzene	$1 {}^{1}B_{2u}(\pi \to \pi^{*})$ $1 {}^{1}B_{1u}(\pi \to \pi^{*})$	1.104 1.053	5.19 6.75	4.91 6.47	4.83 6.42	4.76 6.38	4.69 6.32	5.07 6.68	5.10 6.69	5.04 6.42	5.08 6.54	5.08 6.54
	$1 {}^{1}E_{1u}(\pi \to \pi^{*})$	1.069	7.66	7.38	7.33	7.27	7.22	7.45	7.52	7.13	7.13	7.13
	$2 {}^{1}E_{2g}(\pi \to \pi^{*})$	1.166	9.21	8.81	8.63	8.48	8.34	8.43	8.60	8.18	8.41	8.15
27 1 1 1	4 lp / *\	4 400		4.40	4.05	2.00	0.07	4.0=	4.00			4.05
Naphthalene	$1 {}^{1}B_{3u}(\pi \to \pi^{*})$ $1 {}^{1}B_{2u}(\pi \to \pi^{*})$	1.109 1.075	4.41 5.22	4.10 4.91	4.05 4.86	3.90 4.71	3.85 4.65	4.27 5.03	4.30 5.09	4.24 4.77	4.24 4.77	4.25 4.82
	$2 {}^{1}A_{g}(\pi \rightarrow \pi^{*})$	1.117	6.23	5.93	5.87	5.72	5.66	5.98	6.05	5.87	5.87	5.90
	$1 {}^{1}B_{1q}(\pi \to \pi^{*})$	1.109	6.53	6.19	6.12	5.93	5.86	6.07	6.22	5.99	5.99	5.75
	$2 {}^{1}B_{3u}(\pi \to \pi^{*})$	1.080	6.55	6.26	6.22	6.07	6.02	6.33	6.41	6.06	6.06	6.11
	$2 {}^{1}B_{1g}(\pi \to \pi^{*})$	1.077	6.98	6.69	6.64	6.51	6.46	6.79	6.84	6.47	6.47	6.46
	$2 {}^{1}B_{2u}(\pi \to \pi^{*})$ $3 {}^{1}A_{q}(\pi \to \pi^{*})$	1.079 1.154	6.77 7.77	6.49 7.35	6.44 7.25	6.30 6.98	6.25 6.89	6.57 6.90	6.64 7.14	6.33 6.67	6.33 6.67	6.36 6.49
	$3 {}^{1}B_{2u}(\pi \rightarrow \pi^{*})$	1.084	8.78	8.51	8.46	8.32	8.27	8.44	8.56	8.17	0.07	0.43
	$3 {}^{1}B_{3u}(\pi \to \pi^{*})$	1.177	9.03	8.61	8.50	8.23	8.13	8.12	8.33	7.74		
	.15 (*)											
Furan	$1 {}^{1}B_{2}(\pi \to \pi^{*})$ $2 {}^{1}A_{1}(\pi \to \pi^{*})$	1.061	6.80	6.43	6.39	6.37	6.29	6.60	6.64	6.39	6.32	6.32
	$3 {}^{1}A_{1}(\pi \rightarrow \pi)$ $3 {}^{1}A_{1}(\pi \rightarrow \pi^{*})$	1.119 1.078	6.89 8.83	6.58 8.51	6.48 8.46	6.41 8.42	6.33 8.35	6.62 8.53	6.69 8.61	6.50 8.17	6.57 8.13	6.57 8.13
		1.010	0.00	0.01	0.10	0.42	0.55	0.00	0.01	0.11	0.10	0.10
Pyrrole	$^{1}A_{2}(\pi \rightarrow \sigma^{*})^{k}$	1.075	6.30	6.05	6.01	5.98	5.93					
	$2 {}^{1}A_{1}(\pi \to \pi^{*})$	1.108	6.61	6.33	6.24	6.17	6.10	6.40	6.46	6.31	6.37	6.37
	$1 {}^{1}B_{2}(\pi \to \pi^{*})$ ${}^{1}B_{1}(\pi \to \sigma^{*})^{k}$	1.068	6.88 7.00	6.55 6.82	6.51 6.78	6.49	6.42 6.70	6.71	6.75	6.33	6.57	6.57
	$^{1}A_{2}(\pi \rightarrow \sigma^{*})^{k}$	1.077 1.071	7.69	7.47	7.43	6.75 7.40	7.36					
	${}^{1}B_{1}(\pi \rightarrow \sigma^{*})^{k}$	1.066	7.80	7.59	7.56	7.53	7.49					
	${}^{1}A_{2}(\pi \rightarrow \sigma^{*})^{k}$	1.072	8.29	8.07	8.03	8.00	7.96					
	$3 {}^{1}A_{1}(n \to \pi^{*})$	1.084	8.44	8.12	8.07	8.05	7.98	8.17	8.24	8.17	7.91	7.91
	$^{1}B_{1}(\pi \rightarrow \sigma^{*})^{k}$	1.065	8.34	8.14	8.11	8.08	8.04					
Imidazole	$1 {}^{1}A''(n \to \pi^*)$	1.090	7.01	6.79	6.72	6.63	6.57	6.82	6.89	6.81	6.81	6.65
midazoic	$2 {}^{1}A'(\pi \rightarrow \pi^{*})^{l}$	1.094	6.79	6.47	6.39	6.34	6.26	6.58	6.64	6.19	6.19	6.25
	$3 {}^{1}A'(\pi \to \pi^{*})^{m}$	1.082	7.27	6.96	6.90	6.86	6.79	7.10	7.14	6.93	6.93	6.73
	$2 {}^{1}A''(n \rightarrow \pi^{*})$	1.085	8.16	7.93	7.86	7.79	7.73	7.93	8.01	7.90		
	$4^{1}A'(\pi \to \pi^*)$	1.091	8.69	8.41	8.35	8.30	8.23	8.45	8.51	8.16		
Pyridine	$1 {}^{1}B_{2}(\pi \to \pi^{*})$	1.104	5.27	4.98	4.89	4.81	4.74	5.15	5.18	5.02	4.85	4.85
V	$1 {}^{1}B_{1}(n \to \pi^{*})$	1.090	5.26	5.00	4.94	4.86	4.80	5.05	5.12	5.17	4.59	4.59
	$2 {}^{1}A_{2}(n \rightarrow \pi^{*})$	1.096	5.73	5.54	5.46	5.32	5.27	5.50	5.59	5.51	5.11	5.11
	$2 {}^{1}A_{1}(\pi \to \pi^{*})$	1.057	6.94	6.65	6.60	6.55	6.49	6.85	6.87	6.39	6.26	6.26
	$3 {}^{1}A_{1}(\pi \to \pi^{*})$ $2 {}^{1}B_{2}(\pi \to \pi^{*})$	1.073	7.94	7.64	7.59	7.52	7.46	7.70	7.78	7.46	7.18	7.18
	${}^{1}B_{2}(\pi \to \pi^{*})$ ${}^{1}A_{2}(\pi \to \sigma^{*})^{k}$	1.079 1.068	7.81 8.21	7.52 7.99	7.46 7.96	7.40 7.90	7.33 7.86	7.59	7.66	7.27	7.27	7.27
	$^{1}A_{2}(n \rightarrow \sigma)^{k}$	1.079	8.49	8.23	8.17	8.10	8.05					
	${}^{1}B_{1}(n \rightarrow \pi^{*}/\pi \rightarrow \sigma^{*})^{k}$	1.069	8.75	8.54	8.50	8.45	8.41					
	${}^{1}B_{1}(n \rightarrow \pi^{*}/\pi \rightarrow \sigma^{*})^{k}$	1.084	8.85	8.61	8.55	8.48	8.43					
	${}^{1}B_{1}(n \to \pi^{*}/\pi \to \sigma^{*})^{k}$	1.073	9.07	8.85	8.81	8.75	8.71		0			
	$4 {}^{1}A_{1}(\pi \to \pi^{*})$ $3 {}^{1}B_{2}(\pi \to \pi^{*})$	1.140 1.172	9.44 9.64	9.11 9.20	8.98 9.01	8.82 8.84	8.71 8.69	8.68 8.77	8.86 8.97	8.69 8.60		

Table 3.3 (cont'd).

$ \begin{array}{c c c c c c c c c c c c c c c c c c c $	Molecule	State	REL^c	SD^d	δ -CR(T),IA ^e	δ -CR(T),ID ^e	δ -CR(2,3),A ^f	δ -CR(2,3),D ^f	$CC3^g$	$SDT-3^h$	$\mathrm{CASPT2}^i$	TBE-1 ⁱ	$TBE-2^i$
$ \frac{1}{1} B_{0}(\pi - \pi^{+}) 1.02 5.14 4.82 4.73 4.65 4.57 5.02 5.05 4.85 4.64 6.06 6.05 1.18 1.18 1.18 6.02 6.81 6.55 6.55 6.55 6.55 6.55 6.55 6.85 6.41 6.06 6.05 1.18 1.18 6.02 6.81 6.57 6.81 6.56 6.57 6.81 6.05 6.57 6.81 6.05 $	Pyrazine		1.083	4.42	4.14	4.08	4.00	3.95	4.24	4.30	4.12	3.95	4.13
1 1 1 1 1 1 1 1 1		$1 ^1A_u(n \rightarrow \pi^*)$	1.094	5.30	5.06	4.98	4.86	4.80	5.05	5.13	4.70	4.81	4.98
$ 1 B_{00}(r - \pi^*) 1.115 1.14 $		$1 ^{1}B_{2u}(\pi \rightarrow \pi^{*})$	1.102	5.14	4.82	4.73	4.65	4.57	5.02	5.05	4.85	4.64	4.97
$ 1 B_{la}(x = \pi^+) 1.054 7.18 6.87 6.81 6.77 6.70 7.07 7.00 6.89 6.88 6.83 2.79 2.79 7.72 7.85 2.79 2.79 7.84 7.76 7.78 8.05 8.15 7.70 7.70 7.81 7.8$		$1 ^1B_{2g}(n \rightarrow \pi^*)$	1.096	6.03	5.75	5.68	5.59	5.52	5.74	5.83	5.68	5.56	5.65
$ 1 B_{la}(x = \pi^+) 1.054 7.18 6.87 6.81 6.77 6.70 7.07 7.00 6.89 6.88 6.83 2.79 2.79 7.72 7.85 2.79 2.79 7.84 7.76 7.78 8.05 8.15 7.70 7.70 7.81 7.8$		$1 {}^{1}B_{1g}(n \to \pi^{*})$	1.115	7.14	6.92	6.81	6.65	6.56	6.75	6.89	6.41	6.60	6.69
$ \begin{array}{c c c c c c c c c c c c c c c c c c c $		$1 {}^{1}B_{1u}(\pi \to \pi^{*})$	1.054	7.18	6.87	6.81	6.77	6.70	7.07	7.09	6.89	6.58	6.83
$ \begin{array}{c c c c c c c c c c c c c c c c c c c $		$2 {}^{1}B_{1u}(\pi \rightarrow \pi^{*})$	1.075	8.35	8.00	7.94	7.86	7.78	8.06	8.15	7.79	7.72	7.86
$ \begin{array}{c c c c c c c c c c c c c c c c c c c $		$2 {}^{1}B_{2u}(\pi \rightarrow \pi^{*})$	1.082	8.29	7.99	7.92	7.84	7.76	8.05	8.12	7.66	7.60	7.81
$ \begin{array}{c c c c c c c c c c c c c c c c c c c $										9.00			
$ \begin{array}{c} 1 \\ 1 \\ 1 \\ 1 \\ 1 \\ 1 \\ 1 \\ 1 \\ 1 \\ 1 $				9.54	9.09	8.91	8.73	8.60	8.69	8.90	8.61		
$ \begin{array}{c} 1 \\ 1 \\ 1 \\ 1 \\ 1 \\ 1 \\ 1 \\ 1 \\ 1 \\ 1 $	Pyrimidine	$1 {}^{1}B_{1}(n \to \pi^{*})$	1.092	4.70	4.46	4.38	4.28	4.23	4.50	4.57	4.44	4.55	4.43
$ 1 \frac{1}{2} f_{1}(r) = \pi^{+}) 1.105 5.49 5.19 5.19 5.10 5.10 4.04 5.36 5.39 5.24 6.34 6.54 6.52 6.24 6.34 6.35 6.24 6.34 6.35 6.24 6.34 6.35 6.24 6.34 6.34 6.35 6.24 6.34 $		$1 {}^{1}A_{2}(n \to \pi^{*})$											
$ \begin{array}{c} 2^{1}A_{1}(x-\pi^{+}) & 1,002 & 7.17 & 6.86 & 6.81 & 6.75 & 6.09 & 7.09 & 7.09 & 6.31 & 6.82 \\ 3^{1}A_{1}(x-\pi^{+}) & 1,008 & 7.97 & 7.66 & 7.90 & 7.52 & 7.45 & 7.74 & 7.81 & 7.21 & 7.65 \\ 3^{1}A_{1}(x-\pi^{+}) & 1,008 & 7.97 & 7.66 & 7.60 & 7.52 & 7.45 & 7.74 & 7.81 & 7.21 & 7.65 \\ \hline \\ Pyridazine & 1,124(x-\pi^{+}) & 1,007 & 4.12 & 3.85 & 3.78 & 3.68 & 3.63 & 3.63 & 3.62 & 4.90 & 4.31 & 4.31 & 4.41 \\ 2^{1}A_{1}(x-\pi^{+}) & 1,100 & 5.35 & 5.03 & 4.94 & 4.85 & 4.77 & 5.22 & 5.25 & 5.18 & 5.18 & 5.20 \\ 2^{1}A_{2}(x-\pi^{+}) & 1,100 & 5.35 & 5.03 & 4.94 & 4.85 & 4.77 & 5.22 & 5.25 & 5.18 & 5.18 & 5.20 \\ 2^{1}B_{2}(x-\pi^{+}) & 1,100 & 6.70 & 6.46 & 6.37 & 6.25 & 6.18 & 6.41 & 6.51 & 6.52 & 6.57 & 5.66 \\ 2^{1}B_{2}(x-\pi^{+}) & 1,003 & 7.09 & 7.48 & 7.42 & 7.34 & 7.28 & 7.55 & 7.61 & 7.29 & 7.75 & 7.62 \\ 2^{1}B_{2}(x-\pi^{+}) & 1,003 & 7.09 & 7.48 & 7.42 & 7.34 & 7.28 & 7.55 & 7.61 & 7.29 & 7.75 & 7.62 \\ 2^{1}B_{2}(x-\pi^{+}) & 1,009 & 4.96 & 4.78 & 4.68 & 4.54 & 4.49 & 4.78 & 4.85 & 4.40 & 4.70 & 4.70 & 4.75$		$1 {}^{1}B_{2}(\pi \to \pi^{*})$	1.105	5.49	5.19	5.10	5.01	4.94	5.36	5.39	5.24	5.44	5.34
$ \begin{array}{c} 3^{1}A_{1}(x-x^{+}) & 1.086 & 7.97 & 7.66 & 7.60 & 7.52 & 7.45 & 7.74 & 7.81 & 7.21 & 7.65^{+} \\ \\ \text{Pyridazine} & 1^{1}B_{2}(n-x^{+}) & 1.087 & 4.12 & 3.85 & 3.78 & 3.68 & 3.63 & 3.63 & 3.63 & 3.63 & 3.43 & 4.25 \\ 2^{1}A_{2}(n-x^{+}) & 1.109 & 5.35 & 5.63 & 4.44 & 4.81 & 4.25 & 4.49 & 4.9 & 4.31 & 4.31 & 4.44 \\ 2^{1}A_{2}(n-x^{+}) & 1.109 & 5.35 & 5.63 & 5.44 & 4.85 & 4.77 & 5.22 & 5.25 & 5.18 & 5.18 & 5.20 \\ 2^{1}B_{2}(n-x^{+}) & 1.100 & 0.70 & 6.46 & 6.37 & 6.25 & 6.18 & 6.41 & 6.51 & 6.52 \\ 1^{1}B_{2}(n^{+}-x^{+}) & 1.063 & 7.09 & 6.75 & 6.68 & 6.62 & 6.55 & 6.39 & 6.63 \\ 1^{1}B_{2}(n^{+}-x^{+}) & 1.098 & 0.00 & 7.79 & 7.48 & 7.42 & 7.34 & 7.28 & 7.55 & 7.61 & 7.29 \\ 2^{1}B_{2}(n^{+}-x^{+}) & 1.099 & 4.72 & 4.46 & 4.54 & 4.49 & 4.78 & 4.85 & 4.00 & 4.00 & 4.70 \\ 1^{1}A_{2}^{0}(n^{+}-x^{+}) & 1.094 & 4.99 & 4.72 & 4.64 & 4.55 & 4.49 & 4.78 & 4.85 & 4.00 & 4.00 & 4.70 \\ 1^{1}A_{2}^{0}(n^{+}-x^{+}) & 1.094 & 4.99 & 4.72 & 4.64 & 4.55 & 4.49 & 4.78 & 4.81 & 4.89 & 4.00 & 4.70 & 4.75 \\ 1^{1}A_{2}^{0}(n^{+}-x^{+}) & 1.094 & 4.99 & 4.72 & 4.64 & 4.55 & 4.49 & 4.78 & 4.81 & 4.89 & 4.00 & 4.70 & 4.75 \\ 1^{1}A_{2}^{0}(n^{+}-x^{+}) & 1.094 & 5.02 & 4.79 & 4.71 & 4.59 & 4.54 & 4.81 & 4.89 & 4.70 & 4.75 \\ 1^{1}A_{2}^{0}(n^{+}-x^{+}) & 1.097 & 7.51 & 7.19 & 7.13 & 7.07 & 7.00 & 7.41 & 7.44 & 7.25 \\ 1^{1}A_{2}^{0}(n^{+}-x^{+}) & 1.098 & 8.25 & 7.98 & 7.91 & 7.82 & 7.76 & 8.04 & 8.13 & 7.05 & 7.71 \\ 1^{1}A_{2}^{0}(n^{+}-x^{+}) & 1.088 & 8.28 & 7.99 & 7.91 & 7.82 & 7.76 & 8.04 & 8.13 & 7.05 \\ 1^{1}A_{2}^{0}(n^{+}-x^{+}) & 1.084 & 8.28 & 7.99 & 9.91 & 9.09 & 9.32 \\ 1^{1}A_{2}^{0}(n^{+}-x^{+}) & 1.081 & 9.02 & 9.09 & 9.13 & 9.07 \\ 1^{1}A_{2}^{0}(n^{+}-x^{+}) & 1.118 & 1.004 & 9.73 & 9.59 & 9.42 & 9.31 \\ 1^{1}A_{2}^{0}(n^{+}-x^{+}) & 1.118 & 1.004 & 9.73 & 9.59 & 9.42 & 9.31 \\ 1^{1}A_{2}^{0}(n^{+}-x^{+}) & 1.118 & 1.004 & 9.73 & 9.59 & 9.42 & 9.31 \\ 1^{1}B_{2}^{0}(n^{+}-x^{+}) & 1.118 & 1.004 & 9.73 & 9.59 & 9.42 & 9.31 \\ 1^{1}B_{2}^{0}(n^{+}-x^{+}) & 1.109 & 0.33 & 5.01 & 4.92 & 4.81 & 4.73 & 4.97 & 5.11 & 4.73 & 4.79$									7.06	7.09	6.63	6.95	
$ \begin{array}{c} 3^{1}A_{1}(x-x^{+}) & 1.086 & 7.97 & 7.66 & 7.60 & 7.52 & 7.45 & 7.74 & 7.81 & 7.21 & 7.65^{+} \\ \\ \text{Pyridazine} & 1^{1}B_{2}(n-x^{+}) & 1.087 & 4.12 & 3.85 & 3.78 & 3.68 & 3.63 & 3.63 & 3.63 & 3.63 & 3.43 & 4.25 \\ 2^{1}A_{2}(n-x^{+}) & 1.109 & 5.35 & 5.63 & 4.44 & 4.81 & 4.25 & 4.49 & 4.9 & 4.31 & 4.31 & 4.44 \\ 2^{1}A_{2}(n-x^{+}) & 1.109 & 5.35 & 5.63 & 5.44 & 4.85 & 4.77 & 5.22 & 5.25 & 5.18 & 5.18 & 5.20 \\ 2^{1}B_{2}(n-x^{+}) & 1.100 & 0.70 & 6.46 & 6.37 & 6.25 & 6.18 & 6.41 & 6.51 & 6.52 \\ 1^{1}B_{2}(n^{+}-x^{+}) & 1.063 & 7.09 & 6.75 & 6.68 & 6.62 & 6.55 & 6.39 & 6.63 \\ 1^{1}B_{2}(n^{+}-x^{+}) & 1.098 & 0.00 & 7.79 & 7.48 & 7.42 & 7.34 & 7.28 & 7.55 & 7.61 & 7.29 \\ 2^{1}B_{2}(n^{+}-x^{+}) & 1.099 & 4.72 & 4.46 & 4.54 & 4.49 & 4.78 & 4.85 & 4.00 & 4.00 & 4.70 \\ 1^{1}A_{2}^{0}(n^{+}-x^{+}) & 1.094 & 4.99 & 4.72 & 4.64 & 4.55 & 4.49 & 4.78 & 4.85 & 4.00 & 4.00 & 4.70 \\ 1^{1}A_{2}^{0}(n^{+}-x^{+}) & 1.094 & 4.99 & 4.72 & 4.64 & 4.55 & 4.49 & 4.78 & 4.81 & 4.89 & 4.00 & 4.70 & 4.75 \\ 1^{1}A_{2}^{0}(n^{+}-x^{+}) & 1.094 & 4.99 & 4.72 & 4.64 & 4.55 & 4.49 & 4.78 & 4.81 & 4.89 & 4.00 & 4.70 & 4.75 \\ 1^{1}A_{2}^{0}(n^{+}-x^{+}) & 1.094 & 5.02 & 4.79 & 4.71 & 4.59 & 4.54 & 4.81 & 4.89 & 4.70 & 4.75 \\ 1^{1}A_{2}^{0}(n^{+}-x^{+}) & 1.097 & 7.51 & 7.19 & 7.13 & 7.07 & 7.00 & 7.41 & 7.44 & 7.25 \\ 1^{1}A_{2}^{0}(n^{+}-x^{+}) & 1.098 & 8.25 & 7.98 & 7.91 & 7.82 & 7.76 & 8.04 & 8.13 & 7.05 & 7.71 \\ 1^{1}A_{2}^{0}(n^{+}-x^{+}) & 1.088 & 8.28 & 7.99 & 7.91 & 7.82 & 7.76 & 8.04 & 8.13 & 7.05 \\ 1^{1}A_{2}^{0}(n^{+}-x^{+}) & 1.084 & 8.28 & 7.99 & 9.91 & 9.09 & 9.32 \\ 1^{1}A_{2}^{0}(n^{+}-x^{+}) & 1.081 & 9.02 & 9.09 & 9.13 & 9.07 \\ 1^{1}A_{2}^{0}(n^{+}-x^{+}) & 1.118 & 1.004 & 9.73 & 9.59 & 9.42 & 9.31 \\ 1^{1}A_{2}^{0}(n^{+}-x^{+}) & 1.118 & 1.004 & 9.73 & 9.59 & 9.42 & 9.31 \\ 1^{1}A_{2}^{0}(n^{+}-x^{+}) & 1.118 & 1.004 & 9.73 & 9.59 & 9.42 & 9.31 \\ 1^{1}B_{2}^{0}(n^{+}-x^{+}) & 1.118 & 1.004 & 9.73 & 9.59 & 9.42 & 9.31 \\ 1^{1}B_{2}^{0}(n^{+}-x^{+}) & 1.109 & 0.33 & 5.01 & 4.92 & 4.81 & 4.73 & 4.97 & 5.11 & 4.73 & 4.79$			1.078		7.96	7.90	7.81	7.75	8.01	8.08	7.64	8.01^{n}	
$\begin{array}{c} 1 & 1_{A_{2}}(n-\pi^{+}) & 1,100 & 4,76 & 4,12 & 4,44 & 4,31 & 4,25 & 4,49 & 4,59 & 4,31 & 4,31 & 4,44 \\ & 2 & 1_{A_{3}}(n-\pi^{+}) & 1,098 & 6,00 & 5,73 & 5,55 & 5,54 & 5,48 & 5,74 & 5,82 & 5,77 & 5,77 & 5,66 \\ & 2 & 1_{B_{3}}(n-\pi^{+}) & 1,008 & 6,00 & 5,73 & 5,55 & 5,54 & 5,48 & 5,74 & 5,82 & 5,18 & 5,20 \\ & 1 & 1_{B_{2}}(\pi^{-}\pi^{+}) & 1,003 & 7,09 & 6,46 & 6,37 & 6,25 & 6,18 & 6,41 & 6,51 & 6,51 & 6,52 \\ & 2 & 1_{B_{3}}(\pi^{-}\pi^{+}) & 1,07 & 7,79 & 7,48 & 7,42 & 7,34 & 7,28 & 7,55 & 7,61 & 7,22 \\ & 3 & 1_{A_{1}}(\pi^{-}\pi^{+}) & 1,079 & 7,79 & 7,48 & 7,42 & 7,34 & 7,28 & 7,55 & 7,61 & 7,22 \\ & 2 & 1_{B_{3}}(\pi^{-}\pi^{+}) & 1,095 & 4,96 & 4,78 & 4,88 & 4,54 & 4,49 & 4,76 & 4,84 & 4,66 & 4,66 & 4,60 & 4,70 \\ & 1 & 1_{A_{3}}(\pi^{-}\pi^{+}) & 1,094 & 4,99 & 4,72 & 4,64 & 4,55 & 4,49 & 4,76 & 4,84 & 4,66 & 4,66 & 4,66 & 4,71 \\ & 1 & 1_{A_{3}}(\pi^{-}\pi^{+}) & 1,094 & 5,92 & 4,79 & 4,70 & 4,59 & 4,54 & 4,81 & 4,89 & 4,70 & 4,70 & 4,75 \\ & 2 & 1_{A_{3}}(\pi^{-}\pi^{+}) & 1,108 & 5,84 & 5,53 & 5,43 & 5,34 & 5,54 & 5,54 & 5,74 & 5,79 & 5,71 \\ & 2 & 1_{A_{3}}(\pi^{-}\pi^{+}) & 1,108 & 5,84 & 5,53 & 5,43 & 5,34 & 5,54 & 5,54 & 5,74 & 5,79 & 5,71 \\ & 1 & 1_{B_{3}}(\pi^{-}\pi^{+}) & 1,108 & 8,28 & 7,98 & 7,91 & 7,82 & 7,76 & 8,04 & 8,13 & 7,50 \\ & 1 & 1_{B_{3}}(\pi^{-}\pi^{+}) & 1,108 & 8,28 & 7,98 & 7,91 & 7,82 & 7,76 & 8,04 & 8,13 & 7,50 \\ & 1 & 1_{B_{3}}(\pi^{-}\pi^{+}) & 1,108 & 1,002 & 9,88 & 9,96 & 9,03 \\ & 1 & 1_{B_{3}}(\pi^{-}\pi^{+}) & 1,108 & 1,002 & 9,88 & 9,96 & 9,03 \\ & 1 & 1_{B_{3}}(\pi^{-}\pi^{+}) & 1,108 & 1,002 & 9,88 & 9,97 & 9,49 & 9,35 & 9,44 & 9,64 & 8,99 \\ & 2 & 1_{B_{3}}(\pi^{-}\pi^{+}) & 1,108 & 1,002 & 9,88 & 9,96 & 9,32 \\ & 2 & 1_{B_{3}}(\pi^{-}\pi^{+}) & 1,108 & 1,002 & 9,88 & 9,96 & 9,32 \\ & 2 & 1_{B_{3}}(\pi^{-}\pi^{+}) & 1,108 & 1,002 & 9,88 & 9,96 & 9,32 \\ & 2 & 1_{B_{3}}(\pi^{-}\pi^{+}) & 1,108 & 1,002 & 9,88 & 9,96 & 9,32 \\ & 2 & 1_{B_{3}}(\pi^{-}\pi^{+}) & 1,108 & 2,72 & 4,40 & 4,79 & 4,48 & 4,43 & 4,46 & 4,48 \\ & 1 & 1_{B_{3}}(\pi^{-}\pi^{+}) & 1,108 & 1,002 & 9,88 & 9,96 & 9,32 \\ & 2 & 1_{B_{3}}(\pi^{-}\pi^{+}) & 1,108 & 3,70 & 3,88 & 3,71 & 3,88 & $												7.65^{n}	
$\begin{array}{c} 1 & 1_{A_{2}}(n-\pi^{+}) & 1,100 & 4,76 & 4,12 & 4,44 & 4,31 & 4,25 & 4,49 & 4,59 & 4,31 & 4,31 & 4,44 \\ & 2 & 1_{A_{3}}(n-\pi^{+}) & 1,098 & 6,00 & 5,73 & 5,55 & 5,54 & 5,48 & 5,74 & 5,82 & 5,77 & 5,77 & 5,66 \\ & 2 & 1_{B_{3}}(n-\pi^{+}) & 1,008 & 6,00 & 5,73 & 5,55 & 5,54 & 5,48 & 5,74 & 5,82 & 5,18 & 5,20 \\ & 1 & 1_{B_{2}}(\pi^{-}\pi^{+}) & 1,003 & 7,09 & 6,46 & 6,37 & 6,25 & 6,18 & 6,41 & 6,51 & 6,51 & 6,52 \\ & 2 & 1_{B_{3}}(\pi^{-}\pi^{+}) & 1,07 & 7,79 & 7,48 & 7,42 & 7,34 & 7,28 & 7,55 & 7,61 & 7,22 \\ & 3 & 1_{A_{1}}(\pi^{-}\pi^{+}) & 1,079 & 7,79 & 7,48 & 7,42 & 7,34 & 7,28 & 7,55 & 7,61 & 7,22 \\ & 2 & 1_{B_{3}}(\pi^{-}\pi^{+}) & 1,095 & 4,96 & 4,78 & 4,88 & 4,54 & 4,49 & 4,76 & 4,84 & 4,66 & 4,66 & 4,60 & 4,70 \\ & 1 & 1_{A_{3}}(\pi^{-}\pi^{+}) & 1,094 & 4,99 & 4,72 & 4,64 & 4,55 & 4,49 & 4,76 & 4,84 & 4,66 & 4,66 & 4,66 & 4,71 \\ & 1 & 1_{A_{3}}(\pi^{-}\pi^{+}) & 1,094 & 5,92 & 4,79 & 4,70 & 4,59 & 4,54 & 4,81 & 4,89 & 4,70 & 4,70 & 4,75 \\ & 2 & 1_{A_{3}}(\pi^{-}\pi^{+}) & 1,108 & 5,84 & 5,53 & 5,43 & 5,34 & 5,54 & 5,54 & 5,74 & 5,79 & 5,71 \\ & 2 & 1_{A_{3}}(\pi^{-}\pi^{+}) & 1,108 & 5,84 & 5,53 & 5,43 & 5,34 & 5,54 & 5,54 & 5,74 & 5,79 & 5,71 \\ & 1 & 1_{B_{3}}(\pi^{-}\pi^{+}) & 1,108 & 8,28 & 7,98 & 7,91 & 7,82 & 7,76 & 8,04 & 8,13 & 7,50 \\ & 1 & 1_{B_{3}}(\pi^{-}\pi^{+}) & 1,108 & 8,28 & 7,98 & 7,91 & 7,82 & 7,76 & 8,04 & 8,13 & 7,50 \\ & 1 & 1_{B_{3}}(\pi^{-}\pi^{+}) & 1,108 & 1,002 & 9,88 & 9,96 & 9,03 \\ & 1 & 1_{B_{3}}(\pi^{-}\pi^{+}) & 1,108 & 1,002 & 9,88 & 9,96 & 9,03 \\ & 1 & 1_{B_{3}}(\pi^{-}\pi^{+}) & 1,108 & 1,002 & 9,88 & 9,97 & 9,49 & 9,35 & 9,44 & 9,64 & 8,99 \\ & 2 & 1_{B_{3}}(\pi^{-}\pi^{+}) & 1,108 & 1,002 & 9,88 & 9,96 & 9,32 \\ & 2 & 1_{B_{3}}(\pi^{-}\pi^{+}) & 1,108 & 1,002 & 9,88 & 9,96 & 9,32 \\ & 2 & 1_{B_{3}}(\pi^{-}\pi^{+}) & 1,108 & 1,002 & 9,88 & 9,96 & 9,32 \\ & 2 & 1_{B_{3}}(\pi^{-}\pi^{+}) & 1,108 & 1,002 & 9,88 & 9,96 & 9,32 \\ & 2 & 1_{B_{3}}(\pi^{-}\pi^{+}) & 1,108 & 2,72 & 4,40 & 4,79 & 4,48 & 4,43 & 4,46 & 4,48 \\ & 1 & 1_{B_{3}}(\pi^{-}\pi^{+}) & 1,108 & 1,002 & 9,88 & 9,96 & 9,32 \\ & 2 & 1_{B_{3}}(\pi^{-}\pi^{+}) & 1,108 & 3,70 & 3,88 & 3,71 & 3,88 & $	Pyridazine	$1 \stackrel{1}{R_1} (n \rightarrow \pi^*)$	1.087	4 19	3.85	3.78	3.68	3 63	3 92	4.00	3.78	3.78	3.85
$\begin{array}{c c c c c c c c c c c c c c c c c c c $	1 yrraazine												
$\begin{array}{c} 2 \ ^{1}A_{2}(n-\pi^{+}) & 1.09 & 6.00 \\ 2 \ ^{1}B_{1}(n-\pi^{+}) & 1.00 & 6.70 & 6.46 & 6.37 & 6.25 \\ 1 \ ^{1}B_{2}(n-\pi^{+}) & 1.00 & 7.09 & 6.75 & 6.68 & 6.62 & 6.18 & 6.41 & 6.51 & 6.52 \\ 2 \ ^{1}B_{2}(n-\pi^{+}) & 1.09 & 7.99 & 6.75 & 6.68 & 6.62 & 6.55 & 6.38 & 6.90 & 6.31 \\ 3 \ ^{1}A_{1}(n-\pi^{+}) & 1.09 & 1.09 & 1.079 & 7.79 & 7.48 & 7.42 & 7.34 & 7.28 & 7.55 & 7.61 & 7.29 \\ 3 \ ^{1}A_{1}(n-\pi^{+}) & 1.09 & 1.09 & 1.079 & 7.79 & 7.48 & 7.42 & 7.34 & 7.28 & 7.55 & 7.61 & 7.29 \\ 3 \ ^{1}A_{1}(n-\pi^{+}) & 1.095 & 1.99 & 4.72 & 4.64 & 4.55 & 4.49 & 4.78 & 4.85 & 4.60 & 4.60 & 4.71 \\ 1 \ ^{1}A_{2}(n-\pi^{+}) & 1.094 & 1.09 & 4.72 & 4.64 & 4.55 & 4.9 & 4.76 & 4.84 & 4.66 & 4.66 & 4.71 \\ 1 \ ^{1}A_{2}(n-\pi^{+}) & 1.095 & 4.99 & 4.72 & 4.64 & 4.55 & 4.9 & 4.76 & 4.84 & 4.66 & 4.66 & 4.71 \\ 1 \ ^{1}A_{2}(n-\pi^{+}) & 1.095 & 4.99 & 4.72 & 4.70 & 4.59 & 4.54 & 4.81 & 4.89 & 4.70 & 4.70 & 4.75 \\ 2 \ ^{1}A_{1}(n-\pi^{+}) & 1.095 & 4.84 & 5.53 & 5.43 & 5.34 & 5.26 & 5.71 & 5.74 & 5.79 & 5.79 & 5.71 \\ 2 \ ^{1}A_{2}(n-\pi^{+}) & 1.010 & 5.81 & 7.19 & 7.13 & 7.07 & 7.00 & 7.41 & 7.44 & 7.25 \\ 2 \ ^{1}A_{2}(n-\pi^{+}) & 1.010 & 5.75 & 2.99 & 9.19 & 9.07 & 8.99 & 7.95 & 7.71 \\ 1 \ ^{1}B_{2}(n-\pi^{+}) & 1.095 & 1.95 & 9.57 & 9.29 & 9.19 & 9.07 & 8.99 & 9.12 \\ 1 \ ^{1}B_{2}(n-\pi^{+}) & 1.081 & 5.22 & 2.26 & 9.20 & 9.13 & 9.07 \\ 1 \ ^{1}B_{2}(n-\pi^{+}) & 1.018 & 1.004 & 9.73 & 9.59 & 9.42 & 9.31 & 9.07 \\ 1 \ ^{1}B_{2}(n-\pi^{+}) & 1.105 & 10.28 & 9.85 & 9.67 & 9.49 & 9.35 & 9.44 & 9.64 & 8.99 & 9.22 & 9.22 & 2.22 & 2.22 & 2.25 $													
$ \begin{array}{c c c c c c c c c c c c c c c c c c c $													
$ \begin{array}{c} 1 \cdot B_{p}(r \rightarrow \pi^{+}) & 1.063 & 7.09 & 6.75 & 6.68 & 6.62 & 6.55 & 6.33 & 6.93 & 6.94 \\ -1 \cdot B_{p}(r \rightarrow \pi^{+}) & 1.079 & 1.79 & 7.48 & 7.42 & 7.34 & 7.28 & 7.55 & 7.61 & 7.29 \\ -1 \cdot A_{1}(r \rightarrow \pi^{+}) & 1.080 & 8.11 & 7.77 & 7.71 & 7.64 & 7.56 & 7.82 & 7.91 & 7.62 \\ -1 \cdot A_{1}(r \rightarrow \pi^{+}) & 1.080 & 8.11 & 7.77 & 7.71 & 7.64 & 7.56 & 7.82 & 7.91 & 7.62 \\ -1 \cdot A_{1}(r \rightarrow \pi^{+}) & 1.095 & 4.96 & 4.78 & 4.68 & 4.54 & 4.49 & 4.78 & 4.85 & 4.60 & 4.70 \\ -1 \cdot A_{1}(r \rightarrow \pi^{+}) & 1.094 & 5.02 & 4.79 & 4.70 & 4.59 & 4.51 & 4.81 & 4.89 & 4.70 & 4.70 \\ -1 \cdot A_{2}(r \rightarrow \pi^{+}) & 1.094 & 5.02 & 4.79 & 4.70 & 4.59 & 4.51 & 4.81 & 4.89 & 4.70 & 4.70 \\ -1 \cdot A_{2}(r \rightarrow \pi^{+}) & 1.070 & 7.51 & 7.19 & 7.13 & 7.07 & 7.00 & 7.41 & 7.44 & 7.25 \\ -2 \cdot B_{2}(r \rightarrow \pi^{+}) & 1.070 & 7.51 & 7.19 & 7.13 & 7.07 & 7.00 & 7.41 & 7.44 & 7.25 \\ -2 \cdot B_{2}(r \rightarrow \pi^{+}) & 1.084 & 8.28 & 7.98 & 7.94 & 7.86 & 7.74 & 7.67 & 7.80 & 7.95 & 7.71 \\ -1 \cdot B_{2}(r \rightarrow \pi^{+})^{2} & 1.087 & 9.33 & 9.24 & 9.18 & 9.06 & 9.03 \\ -1 \cdot B_{2}(r \rightarrow \pi^{+})^{2} & 1.087 & 9.33 & 9.24 & 9.18 & 9.06 & 9.03 \\ -1 \cdot A_{2}^{*}(r \rightarrow \pi^{+})^{*} & 1.181 & 10.04 & 9.73 & 9.59 & 9.42 & 9.31 \\ -2 \cdot B_{2}^{*}(r \rightarrow \pi^{+})^{*} & 1.118 & 10.04 & 9.73 & 9.59 & 9.42 & 9.31 \\ -2 \cdot B_{2}^{*}(r \rightarrow \pi^{+})^{*} & 1.108 & 10.02 & 9.68 & 9.59 & 9.50 & 9.42 \\ -2 \cdot B_{2}^{*}(r \rightarrow \pi^{+})^{*} & 1.081 & 10.02 & 9.68 & 9.59 & 9.50 & 9.42 \\ -2 \cdot B_{2}^{*}(r \rightarrow \pi^{+})^{*} & 1.081 & 10.02 & 9.68 & 9.59 & 9.50 & 9.42 \\ -2 \cdot B_{2}^{*}(r \rightarrow \pi^{+})^{*} & 1.081 & 10.02 & 9.68 & 9.59 & 9.50 & 9.42 \\ -2 \cdot B_{2}^{*}(r \rightarrow \pi^{+})^{*} & 1.081 & 10.02 & 9.68 & 9.59 & 9.50 & 9.42 \\ -2 \cdot B_{2}^{*}(r \rightarrow \pi^{+})^{*} & 1.081 & 10.02 & 9.68 & 9.59 & 9.50 & 9.42 \\ -2 \cdot B_{2}^{*}(r \rightarrow \pi^{+})^{*} & 1.091 & 1.07 & 6.89 & 5.76 & 6.34 & 5.04 & 5.12 & 5.16 & 4.33 & 4.93 & 5.08 \\ -1 \cdot B_{2}^{*}(r \rightarrow \pi^{+})^{*} & 1.091 & 5.71 & 5.37 & 5.27 & 5.16 & 5.07 & 5.34 & 5.44 & 5.50 & 5.20 & 5.28 \\ -2 \cdot A_{2}^{*}(r \rightarrow \pi^{+})^{*} & 1.091 & 5.71 & 5.37 & 5.27 & 5.16 & 5.07 & 5.34 & 5.44 & 5.50 & 5.20 & 5.28 \\ -2 \cdot B_{2}^{*}(r \rightarrow \pi^{+})^{*} & 1.101 & 5.71 & 5.37$												0.11	5.00
$ \begin{array}{c} 2 \mid D_3 \left(n \rightarrow \pi^* \right) \\ 3 \mid A_1 \left(n \rightarrow \pi^* \right) \\ 1 \mid 0.079 7.799 7.48 7.42 7.34 7.28 7.58 7.61 7.29 \\ 3 \mid A_1 \left(n \rightarrow \pi^* \right) \\ 1 \mid 0.079 7.799 7.48 4.68 4.54 4.49 4.76 4.88 4.85 4.60 4.60 4.70 \\ 1 \mid A_1 \left(n \rightarrow \pi^* \right) 1.095 4.96 4.78 4.68 4.55 4.49 4.76 4.84 4.49 4.76 4.84 4.49 4.76 4.84 4.40 4.70 4.70 4.70 \\ 1 \mid A_2 \left(n \rightarrow \pi^* \right) 1.094 4.99 4.72 4.70 4.70 4.59 4.54 4.49 4.76 4.84 4.89 4.70 4.70 4.76 4.70 $													
$s. Triazine \\ s. Triazine \\ Triazine \\ s. Triazine \\ Triazine \\ s. Triazine \\ Triazine$													
$\begin{array}{c ccccccccccccccccccccccccccccccccccc$		$3 {}^{1}A_{1}(\pi \rightarrow \pi^{*})$											
$\begin{array}{c ccccccccccccccccccccccccccccccccccc$	m· ·	1 1 4/// *>	1.005	4.00	4.50	4.00		4.40	4.50	4.05	1.00	4.00	4.70
$\begin{array}{c ccccccccccccccccccccccccccccccccccc$	s-Triazine												
$\begin{array}{c c c c c c c c c c c c c c c c c c c $													
$\begin{array}{c ccccccccccccccccccccccccccccccccccc$													
$\begin{array}{c ccccccccccccccccccccccccccccccccccc$												5.79	5.71
$\begin{array}{c c c c c c c c c c c c c c c c c c c $		$2 {}^{1}A'_{1}(\pi \to \pi^{*})$											
$ \begin{array}{c c c c c c c c c c c c c c c c c c c $													
$\begin{array}{c ccccccccccccccccccccccccccccccccccc$		$1 {}^{1}E'(\pi \rightarrow \pi^{*})$							8.04	8.13	7.50		
$\begin{array}{c ccccccccccccccccccccccccccccccccccc$				9.57		9.19		8.99					
$ \begin{array}{c ccccccccccccccccccccccccccccccccccc$			1.087	9.33	9.24	9.18	9.06	9.03					
$\begin{array}{c ccccccccccccccccccccccccccccccccccc$		${}^{1}A_{2}^{\prime\prime}(n \rightarrow \sigma^{*})^{k}$	1.081	9.52	9.26	9.20	9.13	9.07					
$ \begin{array}{c} {}^{1}A_{1}''(n\rightarrow\pi^{*})^{k} \\ {}^{8} \text{ I.103} & 10.02 \\ {}^{9} \text{ 68} \\ {}^{8} \text{ 9.59} \\ {}^{9} \text{ 50} \\ {}^{9} \text{ 50} \\ {}^{9} \text{ 42} \\ {}^{1} \\ {}^{1}A_{u}(\pi\rightarrow\pi^{*}) \\ {}^{1} \\ {}^{1}A_{u}(\pi\rightarrow\pi^{*}) \\ {}^{1} \\ {}^{1} \\ {}^{1}A_{u}(\pi\rightarrow\pi^{*}) \\ {}^{1} \\ {}^{$			1.118	10.04	9.73	9.59	9.42	9.31					
Fetrazine 1 \$^1B_{3u}(n \rightarrow \pi^*)\$ 1.086 \$2.72\$ 2.40 \$2.32 \$2.22\$ 2.15 \$2.53\$ 2.60 \$2.29\$ 2.29 \$2.46 \$1^2A_u(\pi \rightarrow \pi^*)\$ 1.099 4.08 3.80 3.71 3.58 3.51 3.79 3.90 3.51 3.51 3.78 \$1^1B_{10}(n \rightarrow \pi^*)\$ 1.100 5.33 5.01 4.92 4.81 4.73 4.97 5.11 4.73 4.73 4.73 4.87 \$1^1B_{2u}(\pi \rightarrow \pi^*)\$ 1.105 5.27 4.90 4.79 4.68 4.58 5.12 5.16 4.93 4.93 5.08 \$2^2A_u(n^2 \rightarrow \pi^*)^2\$ 1.954 11.47 6.89 5.76 6.34 5.04 \$		$2 {}^{1}E'(\pi \to \pi^{*})$	1.155	10.28	9.85	9.67	9.49	9.35	9.44	9.64	8.99		
$\begin{array}{c ccccccccccccccccccccccccccccccccccc$		${}^1A_1''(n\to\pi^*)^k$	1.103	10.02	9.68	9.59	9.50	9.42					
$\begin{array}{c ccccccccccccccccccccccccccccccccccc$	s-Tetrazine	$1 {}^{1}B_{3u}(n \to \pi^{*})$	1.086	2.72	2.40	2.32	2.22	2.15	2.53	2.60	2.29	2.29	2.46
$\begin{array}{c ccccccccccccccccccccccccccccccccccc$			1.099	4.08	3.80	3.71	3.58	3.51	3.79	3.90	3.51	3.51	3.78
$\begin{array}{c ccccccccccccccccccccccccccccccccccc$				5.33	5.01				4.97	5.11	4.73	4.73	
$\begin{array}{c ccccccccccccccccccccccccccccccccccc$		$1 {}^{1}B_{2u}(\pi \to \pi^{*})$	1.110	5.27		4.79	4.68	4.58	5.12	5.16	4.93	4.93	
$\begin{array}{c ccccccccccccccccccccccccccccccccccc$		$2 {}^{1}A_{a}(n^{2} \rightarrow \pi^{*2})^{k}$											
$\begin{array}{c ccccccccccccccccccccccccccccccccccc$									5.34	5.44		5.20	5.28
$\begin{array}{c ccccccccccccccccccccccccccccccccccc$		$2 {}^{1}A_{n}(n \rightarrow \pi^{*})$											
$\begin{array}{c ccccccccccccccccccccccccccccccccccc$		$1 {}^{1}B_{2a}(n^{2} \rightarrow \pi^{*2})^{o}$											
$\begin{array}{c ccccccccccccccccccccccccccccccccccc$		$2 {}^{1}B_{2}(n \rightarrow \pi^{*})$							6.23	6.43		0.10	0.10
$\begin{array}{c ccccccccccccccccccccccccccccccccccc$		$2 \stackrel{1}{B_{1}} (n \rightarrow \pi^*)$											
$\begin{array}{c ccccccccccccccccccccccccccccccccccc$		$2 B_{1g}(n \rightarrow n)$ $3 1_{B_{4}}(n \rightarrow \pi^{*})$											
$\begin{array}{c ccccccccccccccccccccccccccccccccccc$													
$\begin{array}{c ccccccccccccccccccccccccccccccccccc$													
$\begin{array}{c ccccccccccccccccccccccccccccccccccc$		$1 D_{1u}(\pi \rightarrow \pi)$ $1 D_{1u}(\pi \rightarrow \pi)$							7.40	1.49	0.94		
$\begin{array}{c ccccccccccccccccccccccccccccccccccc$		$D_{3g}(n^- \rightarrow \pi^{})^{\cdots}$							7 70	7.07	7.40		
$\begin{array}{c ccccccccccccccccccccccccccccccccccc$		$2^{-1}D_{1u}(\pi \rightarrow \pi^+)$ $1^{-1}D_{1u}(\pi \rightarrow \pi^+)$							1.19	1.81	1.42		
$\begin{array}{cccccccccccccccccccccccccccccccccccc$													
$\begin{array}{c ccccccccccccccccccccccccccccccccccc$									0 = -	0.00	0.11		
$ 2 ^1\overline{B}_{3g}(\pi \to \pi^*) \qquad 1.169 9.43 \qquad 8.90 \qquad 8.69 \qquad 8.49 \qquad 8.32 \qquad 8.47 \qquad 8.72 \qquad 8.34 $ Formaldehyde $ 1 ^1A_2(n \to \pi^*) \qquad 1.074 3.97 \qquad 3.86 \qquad 3.79 \qquad 3.77 \qquad 3.74 \qquad 3.95 3.96 \qquad 3.99 \qquad 3.88 \qquad 3.88 $ $ ^1B_2(n \to \sigma^*)^k \qquad 1.078 8.27 \qquad 8.37 \qquad 8.29 \qquad 8.12 \qquad 8.08 $ $ 1 ^1B_1(\sigma \to \pi^*) \qquad 1.074 9.26 \qquad 9.11 \qquad 9.03 \qquad 9.00 \qquad 8.96 \qquad 9.18 9.20 \qquad 9.14 \qquad 9.1 \qquad 9.04 $ $ 2 ^1A_1(\pi \to \pi^*)^p \qquad 1.086 9.77 \qquad 9.57 \qquad 9.50 \qquad 9.44 \qquad 9.37 \qquad 9.29^q \qquad 9.32 \qquad 9.3 \qquad 9.29 $ $ ^1B_2(n \to \sigma^*)^k \qquad 1.067 9.52 \qquad 9.60 \qquad 9.53 \qquad 9.42 \qquad 9.40 $ $ ^1A_2(\pi \to \pi^*)^k \qquad 1.109 10.52 \qquad 10.23 \qquad 10.14 \qquad 10.15 \qquad 10.06 $		$2 {}^{1}B_{2u}(\pi \to \pi^{*})$							8.51		8.14		
Formaldehyde $1 \ ^{1}A_{2}(n \to \pi^{*})$ $1.074 \ ^{3.97}$ $3.86 \ ^{3.79}$ $3.77 \ ^{3.74}$ $3.95 \ ^{3.96}$ $3.99 \ ^{3.88}$ $3.88 \ ^{1}B_{2}(n \to \sigma^{*})^{k}$ $1.078 \ ^{8.27}$ $8.37 \ ^{8.29}$ $8.12 \ ^{8.08}$ $1 \ ^{1}B_{1}(\sigma \to \pi^{*})$ $1.074 \ ^{9.26}$ $9.11 \ ^{9.03}$ $9.00 \ ^{8.96}$ $9.18 \ ^{9.20}$ $9.14 \ ^{9.1}$ $9.04 \ ^{2}A_{1}(\pi \to \pi^{*})^{p}$ $1.086 \ ^{9.77}$ $9.57 \ ^{9.50}$ $9.44 \ ^{9.37}$ 9.29^{q} $9.32 \ ^{9.32}$ $9.3 \ ^{9.29}$ $1 \ ^{1}B_{2}(n \to \sigma^{*})^{k}$ $1.067 \ ^{9.52}$ $9.60 \ ^{9.53}$ $9.42 \ ^{9.40}$ $1 \ ^{1}A_{2}(\pi \to \pi^{*})^{k}$ $1.109 \ ^{10.52}$ $10.23 \ ^{10.14}$ $10.15 \ ^{10.06}$		$^{1}B_{3g}(n \rightarrow \pi^{*})$							o :-		0.21		
$\begin{array}{cccccccccccccccccccccccccccccccccccc$		$2 {}^{*}B_{3g}(\pi \to \pi^*)$	1.169	9.43	8.90	8.69	8.49	8.32	8.47	8.72	8.34		
$\begin{array}{cccccccccccccccccccccccccccccccccccc$	Formaldehyde								3.95	3.96	3.99	3.88	3.88
$\begin{array}{cccccccccccccccccccccccccccccccccccc$													
$^{1}B_{2}(n \to \sigma^{*})^{k}$ 1.067 9.52 9.60 9.53 9.42 9.40 $^{1}A_{2}(\pi \to \pi^{*})^{k}$ 1.109 10.52 10.23 10.14 10.15 10.06			1.074	9.26	9.11	9.03	9.00	8.96		9.20	9.14	9.1	9.04
$^{1}A_{2}(\pi \to \pi^{*})^{k}$ 1.109 10.52 10.23 10.14 10.15 10.06		$2 {}^{1}A_{1}(\pi \rightarrow \pi^{*})^{p}$	1.086	9.77	9.57	9.50		9.37	9.29^{q}		9.32	9.3	9.29
$^{1}A_{2}(\pi \to \pi^{*})^{k}$ 1.109 10.52 10.23 10.14 10.15 10.06			1.067	9.52	9.60	9.53	9.42	9.40					
$^{1}A_{1}(n \to \pi^{*})^{p}$ 1.077 10.54 10.59 10.52 10.36 10.32 10.45 10.49			1.109	10.52	10.23	10.14	10.15	10.06					
		${}^{1}A_{1}(n \to \pi^{*})^{p}$	1.077	10.54	10.59	10.52	10.36	10.32	10.45	10.49			

Table 3.3 (cont'd).

Molecule	State	REL^c	SD^d	δ -CR(T),IA e	δ -CR(T),ID ^e	δ -CR(2,3),A ^f	δ -CR(2,3),D ^f	$CC3^g$	$SDT-3^h$	$CASPT2^{i}$	TBE-1 i	TBE- 2^i
Acetone	$1 {}^{1}A_{2}(n \rightarrow \pi^{*})$	1.076	4.44	4.29	4.24	4.18	4.15	4.40	4.41	4.44	4.40	4.38
	${}^{1}B_{2}(n \rightarrow \sigma^{*})^{k}$	1.088	7.54	7.54	7.46	7.30	7.25					
	${}^{1}A_{1}(\pi \to \pi^{*}/n \to \sigma^{*})^{k}$	1.091	9.14	8.99	8.93	8.82	8.77	0.15	0.10	0.05	0.1	0.04
	$1 {}^{1}B_{1}(\sigma \rightarrow \pi^{*})$	1.073	9.26	9.08	9.02	8.97	8.93	9.17	9.19	9.27	9.1	9.04
	${}^{1}A_{2}(\sigma \to \pi^{*})^{k}$ ${}^{1}B_{2}(n \to \sigma^{*})^{k}$	1.083	9.54	9.27	9.21	9.17	9.11					
	$^{1}A_{2}(n \rightarrow \sigma^{*})^{n}$ $^{1}A_{2}(n \rightarrow \pi^{*})^{k}$	1.085 1.092	9.59 9.69	9.57 9.66	9.51 9.57	9.34 9.41	9.29 9.35					
	$A_2(n \rightarrow \pi)$ $2 {}^1A_1(\pi \rightarrow \pi^*)$	1.092	9.88	9.76	9.70	9.41	9.53	9.65	9.73	9.31	9.4	8.90^{r}
	± \											
p-Benzoquinone		1.100	3.19	2.94	2.88	2.71	2.65	2.85	2.95	2.77	2.77	2.86
	$^{1}{}^{1}B_{1g}(n \to \pi^{*})$ $^{1}{}^{1}B_{3g}(\pi \to \pi^{*})$	1.097 1.093	$\frac{3.07}{4.93}$	2.81 4.49	2.75 4.42	2.59 4.30	2.54 4.21	2.75 4.59	2.85 4.68	2.76 4.26	2.76 4.26	2.74 4.44
	$1 \stackrel{\text{B}_{3g}(\pi \to \pi)}{1} \stackrel{\text{B}_{1u}(\pi \to \pi^*)}$	1.093	5.90	5.52	5.45	5.30	5.23	5.62	5.69	5.28	5.28	5.47
	$1 \stackrel{\text{B}_{1u}}{\text{B}_{3u}} (n \to \pi^*)$	1.120	6.55	6.34	6.25	5.96	5.88	5.82	6.05	5.64	5.64	5.55
	$\frac{1}{2} {}^{1}\mathrm{B}_{2q}(n \to \pi^{*})^{k}$	1.128	6.78	6.58	6.48	6.13	6.03	0.02	0.00	5.66	0.01	0.00
	${}^{1}\mathrm{B}_{3u}(n,\pi\to\pi^{*2})^{k}$	1.932	12.36	8.30	7.47	7.64	6.70					
	${}^{1}\mathrm{B}_{2a}(n, \pi \to \pi^{*2})^{k}$	1.873	12.17	8.49	7.75	7.79	6.92					
	$2^{1}B_{2a}(n \rightarrow \pi^*)^k$	1.100	7.56	7.25	7.18	6.99	6.93			6.60		
	$2 {}^{1}B_{3a}(\pi \rightarrow \pi^{*})$	1.111	7.63	7.32	7.25	7.08	7.01	7.27	7.37	6.96	6.96	7.16
	$\underline{1}$ $^{1}B_{2u}(\pi \rightarrow \pi^{*})^{k}$	1.155	8.59	8.10	8.02	7.85	7.75			7.32		
	$2 {}^{1}\mathrm{B}_{1u}(\pi \to \pi^{*})$	1.103	8.47	8.08	8.02	7.88	7.80	7.82	7.98	7.92		
Formamide	$1 {}^{1}A''(n \to \pi^*)$	1.074	5.66	5.55	5.48	5.43	5.40	5.65	5.66	5.63	5.63	5.55
	$2 {}^{1}A'(\pi \to \pi^{*})^{s}$	1.096	7.52	7.31	7.23	7.16	7.09	7.24^{t}		7.39	7.39	7.35
	$^{1}A'(\pi \rightarrow \pi^{*})^{s'}$	1.092	8.50	8.45	8.36	8.21	8.16	8.27	8.35			
	$3 {}^{1}A'(\pi \to \pi^*)$	1.100	11.40	11.07	10.99	10.96	10.89	10.93	11.09	10.54		
Acetamide	$1 {}^{1}A''(n \to \pi^*)$	1.075	5.72	5.59	5.54	5.46	5.43	5.69	5.71	5.69	5.69	5.62
ricciamine	${}^{1}A''(\pi \to \sigma^*)^{k}$	1.072	7.32	7.18	7.14	7.10	7.06	0.00	0.11	0.00	0.00	0.02
	${}^{1}A'(\pi \to \pi^*/n \to \sigma^*)^{k}$	1.098	7.48	7.35	7.28	7.12	7.07					
	$2^{1}A'(\pi \to \pi^*/n \to \sigma^*)$	1.090	7.88	7.75	7.68	7.57	7.52	7.67	7.76	7.27	7.27	7.14
	${}^{1}A''(\pi \rightarrow \sigma^{*})^{k}$	1.069	8.74	8.60	8.57	8.52	8.49					
	${}^{1}A'(n \rightarrow \sigma^{*})^{k}$	1.097	9.07	9.01	8.95	8.76	8.71					
	${}^{1}A'(n \rightarrow \sigma^{*})^{k}$	1.099	9.49	9.42	9.35	9.15	9.10					
	${}^{1}A^{\prime\prime}(\pi \rightarrow \sigma^{*})^{k}$	1.083	9.44	9.31	9.26	9.19	9.15					
	${}^{1}A'(n \rightarrow \sigma^{*})^{k}$	1.085	10.20	10.18	10.12	9.95	9.91					
	${}^{1}A^{\prime\prime}(n \rightarrow \pi^{*})^{k}$	1.073	10.32	10.15	10.09	10.02	9.98					
	${}^{1}A^{\prime\prime}(n \to \pi^{*})^{k}$	1.092	10.50	10.45	10.37	10.20	10.16					
	$3 {}^{1}A'(\pi \to \pi^*)$	1.088	10.78	10.58	10.52	10.43	10.38	10.50	10.60	10.09		
Propanamide	$1 {}^{1}A''(n \to \pi^*)$	1.075	5.74	5.62	5.58	5.48	5.45	5.72	5.73	5.72	5.72	5.65
	$^{1}A''(\pi \rightarrow \sigma^{*})^{k}$	1.072	7.32	7.19	7.16	7.10	7.06					
	$2 {}^{1}A'(\pi \to \pi^{*})$	1.090	7.87	7.76	7.71	7.56	7.51	7.62	7.74	7.20	7.20	7.09
	${}^{1}A^{\prime\prime}(\pi\to\sigma^{*})^{\acute{k}}$	1.070	8.70	8.57	8.54	8.48	8.44					
	${}^{1}A^{\prime\prime}(\pi\to\sigma^*)^{k}$	1.083	9.14	9.01	8.97	8.89	8.84					
	${}^1A^{\prime\prime}(n \to \pi^*)^k$	1.080	10.01	9.90	9.85	9.72	9.68					
	$3 {}^{1}A'(\pi \to \pi^*)$	1.089	10.35	10.18	10.12	10.01	9.96	10.06	10.15	9.94		
Cytosine	$2 {}^{1}A'(\pi \to \pi^{*})$	1.101	4.98	4.69	4.63	4.47	4.41	4.72		4.67	4.66	4.66
	$1 {}^{1}A''(n \to \pi^{*})$	1.095	5.45	5.22	5.17	5.00	4.95	5.16		5.12	4.87	4.87
	$2 {}^{1}A''(n \to \pi^{*})$	1.092	6.00	5.81	5.75	5.58	5.53	5.52		5.53	5.26	5.26
	$3 {}^{1}A'(\pi \rightarrow \pi^*)$	1.110	5.95	5.66	5.60	5.44	5.38	5.61		5.53	5.62	5.62
	$4 {}^{1}A'(\pi \rightarrow \pi^*)$	1.094	6.81	6.55	6.49	6.37	6.32	6.61		6.40		
	$5 {}^{1}A'(\pi \rightarrow \pi^*)$	1.104	7.24	6.92	6.85	6.70	6.63			6.97		
	$6 {}^{1}A'(\pi \to \pi^*)$	1.107	8.67	8.45	8.40	8.18	8.12			8.23		
Thymine	$1 {}^{1}A''(n \to \pi^*)$	1.090	5.14	4.97	4.93	4.75	4.71	4.94		4.95	4.82	4.82
	$2 {}^{1}A'(\pi \to \pi^{*})$	1.087	5.60	5.30	5.25	5.11	5.05	5.34		5.06	5.20	5.20
	$3 {}^{1}A'(\pi \rightarrow \pi^*)$	1.113	6.78	6.47	6.41	6.21	6.13	6.34		6.15	6.27	6.27
	$2 {}^{1}A''(n \to \pi^*)$	1.081	6.58	6.44	6.40	6.24	6.21	6.59		6.38	6.16	6.16
	$4 {}^{1}A'(\pi \to \pi^*)$	1.099	7.05	6.71	6.65	6.49	6.42	6.71		6.53	6.53	6.53
	$3 {}^{1}A''(n \to \pi^{*})$ $4 {}^{1}A''(n \to \pi^{*})$	1.118	7.68	7.36	7.27	6.92	6.83			6.85		
	$4 {}^{1}A''(n \to \pi^{*})$ $5 {}^{1}A'(\pi \to \pi^{*})$	1.114 1.101	7.87 7.90	7.62 7.65	7.53 7.59	7.21 7.41	7.13 7.36			7.43 7.43		
	· ´											
Uracil	$1 {}^{1}A''(n \to \pi^{*})$ $2 {}^{1}A'(\pi \to \pi^{*})$	1.092 1.091	5.12 5.70	4.94 5.39	4.89 5.34	4.72 5.22	4.68 5.16	4.90 5.44		4.91 5.23	4.80 5.35	5.00 5.25
	$3 {}^{1}A'(\pi \to \pi^*)$	1.118	6.76	6.43	6.36	6.16	6.08	6.29		6.15	6.26	6.26
	$2 {}^{1}A''(n \rightarrow \pi^{*})$	1.082	6.50^{q}	6.37	6.31	6.16	6.12	6.32		6.28	6.10	6.10
	$3 {}^{1}A''(n \rightarrow \pi^*)$	1.118	7.69^{q}	7.40	7.29	6.97	6.87	6.87		6.98	6.56	6.56
	$4 {}^{1}A'(\pi \rightarrow \pi^*)$	1.100	7.20	6.84	6.77	6.64	6.56	6.84		6.74	6.70	6.70
		1.114	7.74	7.48	7.38	7.07	6.99	7.12		7.28		
	$4 {}^{1}A''(n \to \pi^{*})$ $5 {}^{1}A'(\pi \to \pi^{*})$	1.114	1.17	1.10	1.00	1.01		1.12		1.20		

Table 3.3 (cont'd).

Molecule	State	REL^c	SD^d	δ -CR(T),IA e	δ -CR(T),ID ^e	δ -CR(2,3),A ^f	δ -CR(2,3),D ^f	$CC3^g$	$SDT-3^h$	$\mathrm{CASPT2}^i$	TBE-1 i	TBE- 2^i
Adenine	$2 {}^{1}A'(\pi \to \pi^{*})$	1.101	5.37	5.06	5.00	4.84	4.78	5.18		5.20	5.25	5.25
	$3 {}^{1}A'(\pi \to \pi^*)$	1.089	5.61	5.29	5.24	5.09	5.03	5.39		5.29	5.25	5.25
	$1 {}^{1}A''(n \to \pi^{*})$	1.094	5.58	5.35	5.29	5.11	5.07	5.34		5.19	5.12	5.12
	$2 {}^{1}A''(n \rightarrow \pi^{*})$	1.091	6.19	5.95	5.89	5.72	5.68	5.96		5.96	5.75	5.75
	$4 {}^{1}A'(\pi \to \pi^{*})$	1.096	6.84	6.52	6.47	6.31	6.25	6.53		6.34		
	${}^{1}A'(\pi \rightarrow \pi^{*})^{k}$	1.105	7.07	6.69	6.63	6.45	6.38					
	$5 {}^{1}A'(\pi \to \pi^{*})$	1.100	7.17	6.87	6.81	6.63	6.57			6.64		
	$6 {}^{1}A'(\pi \to \pi^*)$	1.102	7.72	7.38	7.33	7.16	7.10			6.87		
	${}^{1}A'(\pi \rightarrow \pi^{*})^{k}$	1.106	8.10	7.78	7.72	7.51	7.44					
	$7 \stackrel{1}{A'}(\pi \to \pi^*)$	1.117	8.48	8.09	8.02	7.79	7.71			7.56		

^a MP2/6-31G* equilibrium geometries were taken from Ref. [17].

b All excitation energies were computed in this work, unless stated otherwise.

^c Reduced excitation level diagnostic; for one-electron transitions REL ≈ 1 and for two-electron transitions REL ≈ 2 .

^d EOMCCSD results (recalculated for the previously reported 149 singlet states, new for the additional 54 singlet states found in this work).

^e δ -CR-EOMCCSD(T),X (X = IA, ID) results.

f δ -CR-EOMCC(2.3),X (X = A, D) results.

⁹ CC3 results taken from Ref. [17], except for those for the nucleobases which were reported in Ref. [25].

h EOMCCSDT-3 values taken from Ref. [24].

ⁱ CASPT2 and TBE-1 excitation energies taken from Ref. [17], with updates from Ref. [21], and TBE-2 values taken from Ref. [21].

 $[^]j$ In Ref. [17] these states were reported as having doubly excited character. However, as determined in the present study, they are predominantly one-electron transitions (REL for 2 $^1A_1(\pi \to \pi^*)$ is 1.153 and REL for 3 $^1A_1(\pi \to \pi^*)$ is 1.055) and, thus, double excitations have a small effect on these states.

^k Additional excited states not included among the 149 singlet excitations listed in Table I of Ref. [17]. States in this category that have been characterized in the Supporting Information to Ref. [17] are designated as \underline{n} ¹X, where X is the irreducible representation and \underline{n} indicates the state number within symmetry X (n is underlined to distinguish from the 149 states included in Table I of Ref. [17], which are labeled as n ¹X). States that have not been found in Ref. [17] and other prior benchmark work [18–25] are designated as ¹X, i.e., without the state number in front of the term symbol. In ordering these additional states, we use the δ-CR-EOMCC(2,3),D values.

l This state is dominated by comparable single excitations from HOMO to LUMO+1 and from HOMO to LUMO+5. The authors of Ref. [17] stated that it is dominated by a HOMO \rightarrow LUMO single excitation, which is not what our EOMCCSD calculations imply.

 $[^]m$ This state is largely dominated by a single excitation from HOMO to LUMO+1, with two other significant, though slightly smaller, contributions from one-electron HOMO-1 \rightarrow LUMO+1 and HOMO \rightarrow LUMO+5 transitions. According to Ref. [17], this state is dominated by the HOMO-1 \rightarrow LUMO and HOMO \rightarrow LUMO+1 transitions, but our EOMCC calculations do not confirm this.

ⁿ These two TBE-1 values had to be taken from Ref. [195], since Ref. [17] provided no information what the best estimates for them might be.

Table 3.3 (cont'd).

^O This state is the only almost purely doubly excited state among the 149 singlet excited states included in Table I of Ref. [17]. Because of the absence of the CC3 and EOMCCSDT-3 reference data and the uncertainty about the quality of the CASPT2 and TBE values for this state, we have excluded it from the statistical error analyses discussed in Section 3.5. For example, the NEVPT2 results for this state are 6.30–6.35 eV [23], in excellent agreement with our best δ-CR-EOMCC(2,3),D value of 6.59 eV.

 p The authors of Ref. [17] confused the 2 $^1A_1(\pi \to \pi^*)$ and $^1A_1(n \to \pi^*)$ states for formaldehyde shown in the table. They assigned the 2 $^1A_1(\pi \to \pi^*)$ state to the EOMCCSD and CC3 roots at 10.54 and 10.45 eV, respectively, producing large discrepancies, of more than 1 eV, with the CASPT2 and TBE-1 values reported in Ref. [17], of 9.31 and 9.3 eV, and the CC3/aug-cc-pVQZ value of 9.29 eV obtained in Ref. [21]. We have found another EOMCCSD root of the 1A_1 symmetry at 9.77 eV, which results in δ-CR-EOMCC values in the 9.37–9.57 eV range, in very good agreement with the above CASPT2, TBE-1, and CC3/aug-cc-pVQZ data. Thus, the new EOMCC root that we have found must be the 2 $^1A_1(\pi \to \pi^*)$ state, whereas the 1A_1 state interpreted in Ref. [17] as the 2 $^1A_1(\pi \to \pi^*)$ state is the next state of the 1A_1 symmetry, designated in our table as $^1A_1(n \to \pi^*)$.

 q CC3/aug-cc-pVQZ results taken from Ref. [21].

^r The CC3/aug-cc-pVTZ result reported in Ref. [21]. Our δ-CR-EOMCC excitation energies for the 2 $^1A_1(\pi \to \pi^*)$ state of acetone and the corresponding CC3/TZVP, EOMCCSDT-3/TZVP, and TBE values reported in Refs. [17, 22, 24] suggest that the CC3/aug-cc-pVTZ root at 8.90 eV found in Ref. [21] does not represent the 2 $^1A_1(\pi \to \pi^*)$ excitation. Based on our δ-CR-EOMCC analysis, the CC3/aug-cc-pVTZ root at 8.90 eV corresponds, most likely, to the $^1A_1(\pi \to \pi^*/n \to \sigma^*)$ state that has not been considered in the previous benchmark studies [17–25]. For this reason, in comparisons of our δ-CR-EOMCC and EOMCCSD data for the 2 $^1A_1(\pi \to \pi^*)$ state of acetone with a TBE-2 result we use the TBE-1 value taken from Ref. [17] instead.

⁸ The authors of Ref. [17] missed the EOMCCSD root of the $^1A'$ symmetry at 7.52 eV, which corresponds to the CC3 root at 7.24 eV found in Ref. [25] and which matches the TBE values reported in Refs. [17, 21] of about 7.4 eV. As a result, they incorrectly interpreted the higher-energy EOMCCSD and CC3 roots at 8.52 (in our calculations, 8.50) and 8.27 eV, respectively, as the $^1A'(\pi \to \pi^*)$ state. To avoid relabeling of all $^1A'(\pi \to \pi^*)$ states, we designate the state at 8.50 (EOMCCSD) and 8.27 (CC3) eV as the $^1A'(\pi \to \pi^*)$ excitation and assign the 2 $^1A'(\pi \to \pi^*)$ state to the EOMCCSD root at 7.52 eV and CC3 root found in Ref. [25] at 7.24 eV, in perfect agreement with the δ-CR-EOMCC values that range from 7.09 to 7.31 eV when the MP2/6-31G* geometry is employed.

^t Taken from Ref. [25].

^u The EOMCCSD excitation energies for the 2 $^1A''(n \to \pi^*)$ and 3 $^1A''(n \to \pi^*)$ states of uracil are 6.50 and 7.69 eV, respectively, not the other way around, as reported in Ref. [17].

Table 3.4: Vertical excitation energies (in eV) for singlet states of all molecules in the test set using, in the case of the EOMCCSD and δ -CR-EOMCC results, the geometries optimized at the CR-CC(2,3),D/TZVP level.^a

at the CR- Molecule	State	REL^b	SD^c	δ -CR(T),IA ^d	δ -CR(T),ID ^d	δ -CR(2,3),A ^e	δ -CR(2,3),D ^e	$CC3^f$	$SDT-3^g$	$CASPT2^h$	TBE-1 ^h	TBE- 2^h
Ethene	$1 {}^{1}B_{1u}(\pi \to \pi^{*})$	1.034	8.50	8.25	8.21	8.24	8.17	8.37	8.40	8.54	7.80	7.80
T.D II	. ln (*)	4.050		0.40	0.40	0.00	0.00	0.50	0.04	0.45	0.40	0.40
E-Butadiene	$1 {}^{1}B_{u}(\pi \to \pi^{*})$ $2 {}^{1}A_{q}(\pi \to \pi^{*})$	1.056 1.218	6.74 7.42	6.46 6.93	6.40 6.79	6.39 6.75	6.32 6.62	6.58 6.77	6.61 6.89	6.47 6.62	6.18 6.55	6.18 6.55
	2 Fig(n -> n)	1.210	1.42	0.93	0.13	0.75	0.02	0.11	0.03	0.02	0.55	0.55
all-E-Hexatriene	$1 ^1B_u(\pi \to \pi^*)$	1.064	5.76	5.47	5.42	5.35	5.30	5.58	5.61	5.31	5.10	5.10
	$2 {}^{1}A_{g}(\pi \to \pi^{*})$	1.222	6.65	6.08	5.97	5.84	5.72	5.72	5.88	5.42	5.09	5.09
all-E-Octatetraene	$2 {}^{1}A_{q}(\pi \rightarrow \pi^{*})$	1.207	6.07	5.50	5.42	5.21	5.11	4.97	5.17	4.64	4.47	4.47
an 2 octaveració	$1 {}^{1}B_{u}(\pi \rightarrow \pi^{*})$	1.069	5.14	4.85	4.81	4.69	4.65	4.94	4.97	4.70	4.66	4.66
	1= (
Cyclopropene	$1 {}^{1}B_{1}(\sigma \to \pi^{*})$ $1 {}^{1}B_{2}(\pi \to \pi^{*})$	1.066 1.048	6.49	6.73	6.68	6.69	6.64	6.90	6.92	6.76	6.76	6.67
	$1 D_2(\pi \to \pi)$	1.046	7.30	7.06	7.01	7.02	6.95	7.10	7.14	7.06	7.06	6.68
Cyclopentadiene	$1 {}^{1}B_{2}(\pi \to \pi^{*})$	1.055	5.91	5.62	5.57	5.54	5.48	5.73	5.75	5.51	5.55	5.55
	$2 {}^{1}A_{1}(\pi \to \pi^{*})^{i}$	1.153	7.09	6.74	6.63	6.56	6.46	6.61	6.71	6.31	6.31	6.28
	$3 {}^{1}A_{1}(\pi \to \pi^{*})^{i}$ ${}^{1}B_{2}(\pi \to \pi^{*})^{j}$	1.054 1.073	8.98 8.99	8.68 8.77	8.64 8.73	8.62 8.69	8.55 8.64	8.69	8.76	8.52		
	D2(n / n)	1.010	0.55	0.11	0.10	0.03	0.04					
Norbornadiene	$1 {}^{1}A_{2}(\pi \to \pi^{*})$	1.064	5.87	5.60	5.55	5.48	5.42	5.64	5.68	5.34	5.34	5.37
	$1 {}^{1}B_{2}(\pi \to \pi^{*})$ $2 {}^{1}B_{2}(\pi \to \pi^{*})$	1.076	6.72	6.46	6.41	6.32	6.27	6.49	6.55	6.11	6.11	6.21
	$2 \stackrel{\cdot}{}_{B_2}(\pi \rightarrow \pi^*)$ $2 \stackrel{1}{}_{A_2}(\pi \rightarrow \pi^*)$	1.061 1.067	7.87 7.85	7.61 7.62	7.57 7.57	7.50 7.50	7.44 7.46	7.64 7.71	7.68 7.74	7.32 7.45		
	${}^{1}B_{1}(\pi \to \pi^{*})^{j}$	1.079	7.98	7.77	7.73	7.65	7.61			1.10		
	$\underline{2}^{1}A_{1}(\pi \to \sigma^{*}/\pi \to \pi^{*})^{j}$	1.062	8.02	7.85	7.82	7.76	7.73			7.97		
Benzene	$1 {}^{1}B_{2u}(\pi \to \pi^{*})$	1.104	5.18	4.90	4.82	4.75	4.68	5.07	5.10	5.04	5.08	5.08
Denzene	$1 B_{2u}(\pi \rightarrow \pi)$ $1 B_{1u}(\pi \rightarrow \pi^*)$	1.053	6.74	6.47	6.42	6.38	6.32	6.68	6.69	6.42	6.54	6.54
	$1 {}^{1}E_{1u}(\pi \to \pi^{*})$	1.069	7.65	7.37	7.32	7.27	7.21	7.45	7.52	7.13	7.13	7.13
	$2 {}^{1}E_{2g}(\pi \to \pi^{*})$	1.166	9.20	8.79	8.62	8.46	8.33	8.43	8.60	8.18	8.41	8.15
Naphthalene	$1 {}^{1}B_{3u}(\pi \to \pi^{*})$	1.109	4.45	4.14	4.09	3.94	3.89	4.27	4.30	4.24	4.24	4.25
raphenaiche	$1 {}^{1}B_{2u}(\pi \to \pi^{*})$	1.075	5.28	4.97	4.92	4.77	4.72	5.03	5.09	4.77	4.77	4.82
	$2 {}^{1}A_{g}(\pi \rightarrow \pi^{*})$	1.117	6.20	5.91	5.85	5.69	5.64	5.98	6.05	5.87	5.87	5.90
	$1 {}^{1}B_{1g}(\pi \to \pi^{*})$	1.107	6.56	6.22	6.15	5.97	5.90	6.07	6.22	5.99	5.99	5.75
	$2 {}^{1}B_{3u}(\pi \to \pi^{*})$ $2 {}^{1}B_{1g}(\pi \to \pi^{*})$	1.079 1.078	6.57 6.99	6.27 6.69	6.23 6.65	6.09 6.52	6.04 6.46	6.33 6.79	6.41 6.84	6.06 6.47	6.06 6.47	6.11 6.46
	$2 {}^{1}B_{2u}(\pi \to \pi^*)$	1.080	6.77	6.48	6.44	6.30	6.25	6.57	6.64	6.33	6.33	6.36
	$3 {}^{1}A_{q}(\pi \rightarrow \pi^{*})$	1.150	7.80	7.39	7.29	7.03	6.94	6.90	7.14	6.67	6.67	6.49
	$3 {}^{1}B_{2u}(\pi \to \pi^{*})$	1.084	8.74	8.47	8.42	8.28	8.23	8.44	8.56	8.17		
	$3 {}^{1}B_{3u}(\pi \to \pi^{*})$	1.176	9.04	8.62	8.52	8.24	8.14	8.12	8.33	7.74		
Furan	$1 {}^{1}B_{2}(\pi \to \pi^{*})$	1.061	6.87	6.50	6.45	6.44	6.36	6.60	6.64	6.39	6.32	6.32
	$2 {}^{1}A_{1}(\pi \to \pi^{*})$	1.119	6.93	6.61	6.52	6.44	6.37	6.62	6.69	6.50	6.57	6.57
	$3 {}^{1}A_{1}(\pi \to \pi^{*})$	1.077	8.87	8.54	8.49	8.46	8.38	8.53	8.61	8.17	8.13	8.13
Pyrrole	$^{1}A_{2}(\pi \rightarrow \sigma^{*})^{j}$	1.075	6.34	6.09	6.05	6.02	5.97					
v	$2 {}^{1}A_{1}(\pi \rightarrow \pi^{*})$	1.108	6.61	6.32	6.23	6.17	6.10	6.40	6.46	6.31	6.37	6.37
	$1 {}^{1}B_{2}(\pi \rightarrow \pi^{*})$	1.067	6.91	6.59	6.54	6.52	6.45	6.71	6.75	6.33	6.57	6.57
	${}^{1}B_{1}(\pi \rightarrow \sigma^{*})^{j}$ ${}^{1}A_{2}(\pi \rightarrow \sigma^{*})^{j}$	1.077 1.070	6.97 7.69	6.79 7.47	6.74 7.43	6.71 7.40	6.67 7.36					
	${}^{1}B_{1}(\pi \rightarrow \sigma^{*})^{j}$	1.066	7.84	7.62	7.59	7.56	7.52					
	$3 {}^{1}A_{1}(n \to \pi^{*})$	1.084	8.46	8.14	8.09	8.06	7.99	8.17	8.24	8.17	7.91	7.91
	${}^{1}A_{2}(\pi \rightarrow \sigma^{*})^{j}$	1.072	8.33	8.11	8.07	8.04	8.00					
	$^{1}B_{1}(\pi \to \sigma^{*})^{j}$	1.065	8.34	8.14	8.11	8.08	8.04					
Imidazole	$1 {}^{1}A''(\pi \to \pi^*)$	1.090	7.04	6.82	6.75	6.66	6.60	6.82	6.89	6.81	6.81	6.65
	$2 {}^{1}A'(\pi \to \pi^{*})^{k}$	1.096	6.85	6.53	6.45	6.39	6.32	6.58	6.64	6.19	6.19	6.25
	$3 {}^{1}A'(\pi \rightarrow \pi^{*})^{l}$	1.081	7.31	7.00	6.94	6.90	6.84	7.10	7.14	6.93	6.93	6.73
	$2 {}^{1}A''(\pi \to \pi^{*})$ $4 {}^{1}A'(\pi \to \pi^{*})$	1.085 1.091	8.18 8.69	7.95 8.41	7.88 8.35	7.81 8.30	7.75 8.23	7.93 8.45	8.01 8.51	7.90 8.16		
	1 11 (" , ")	1.001	0.00	0.11	0.00	0.00	0.20	0.10	0.01	0.10		
Pyridine	$1 {}^{1}B_{2}(\pi \to \pi^{*})$	1.104		4.97	4.89	4.81	4.74	5.15	5.18	5.02	4.85	4.85
	$1 {}^{1}B_{1}(n \to \pi^{*})$	1.090	5.28	5.03	4.96	4.88	4.83	5.05	5.12	5.17	4.59	4.59
	$2 {}^{1}A_{2}(n \to \pi^{*})$ $2 {}^{1}A_{1}(\pi \to \pi^{*})$	1.096 1.057	5.75 6.94	5.55 6.65	5.47 6.59	5.34 6.55	5.28 6.48	5.50 6.85	5.59 6.87	5.51 6.39	5.11 6.26	5.11 6.26
	$3 {}^{1}A_{1}(\pi \to \pi^{*})$	1.073	7.94	7.64	7.59	7.52	7.46	7.70	7.78	7.46	7.18	7.18
	$2 {}^{1}B_{2}(\pi \rightarrow \pi^{*})$	1.079	7.81	7.52	7.46	7.39	7.33	7.59	7.66	7.27	7.27	7.27
	${}^{1}A_{2}(\pi \rightarrow \sigma^{*})^{j}$ ${}^{1}A_{2}(n \rightarrow \pi^{*})^{j}$	1.068	8.21	8.00	7.96	7.90	7.86					
	${}^{1}A_{2}(n \rightarrow \pi^{*})^{j}$ ${}^{1}B_{1}(n \rightarrow \pi^{*}/\pi \rightarrow \sigma^{*})^{j}$	1.079 1.069	8.50 8.76	8.24 8.55	8.18 8.52	8.10 8.46	8.05 8.42					
	$^{1}B_{1}(n \rightarrow \pi^{*}/\pi \rightarrow \sigma^{*})^{j}$	1.084	8.86	8.62	8.55	8.49	8.44					
	$4 {}^{1}A_{1}(\pi \to \pi^{*})$	1.144	9.46	9.11	8.97	8.81	8.70	8.68	8.86	8.69		
	${}^{1}B_{1}(n \to \pi^{*}/\pi \to \sigma^{*})^{j}$ ${}^{1}B_{2}(\pi \to \pi^{*})$	1.074	9.07	8.85	8.81	8.75	8.71	0 77	9.07	8.60		
	$\sigma = D_2(\pi \to \pi^+)$	1.172	9.63	9.20	9.01	8.83	8.68	8.77	8.97	0.00		

Table 3.4 (cont'd).

Molecule	State	REL^b	SD^c	δ -CR(T),IA ^d	δ -CR(T),ID ^d	δ -CR(2,3),A ^e	δ -CR(2,3),D ^e	$CC3^f$	$SDT-3^g$	$CASPT2^h$	TBE-1 h	TBE- 2^h
Pyrazine	$1 {}^{1}B_{3u}(n \to \pi^{*})$	1.082	4.44	4.16	4.09	4.02	3.96	4.24	4.30	4.12	3.95	4.13
	$1 ^1A_u(n \rightarrow \pi^*)$	1.094	5.29	5.06	4.97	4.86	4.80	5.05	5.13	4.70	4.81	4.98
	$1 ^{1}B_{2u}(\pi \to \pi^{*})$	1.102	5.14	4.82	4.74	4.66	4.58	5.02	5.05	4.85	4.64	4.97
	$1 ^{1}B_{2g}(n \rightarrow \pi^{*})$	1.096	6.09	5.81	5.73	5.65	5.58	5.74	5.83	5.68	5.56	5.65
	$1 ^{1}B_{1g}(n \rightarrow \pi^{*})$	1.115	7.18	6.96	6.85	6.69	6.60	6.75	6.89	6.41	6.60	6.69
	$1 ^{1}B_{1u}(\pi \to \pi^{*})$	1.054	7.18	6.86	6.81	6.77	6.70	7.07	7.09	6.89	6.58	6.83
	$2 ^{1}B_{1u}(\pi \to \pi^{*})$	1.075	8.38	8.03	7.97	7.89	7.82	8.06	8.15	7.79	7.72	7.86
	$2 {}^{1}B_{2u}(\pi \to \pi^{*})$	1.082	8.32	8.02	7.95	7.87	7.79	8.05	8.12	7.66	7.60	7.81
	$1 {}^{1}B_{3g}(\pi \to \pi^{*})$	1.181	9.75	9.27	9.06	8.88	8.72	8.77	9.00	8.47		
	$2 {}^{1}A_{g}(\pi \rightarrow \pi^{*})$	1.160	9.58	9.13	8.96	8.78	8.64	8.69	8.90	8.61		
Pyrimidine	$1 {}^{1}B_{1}(n \to \pi^{*})$	1.092	4.74	4.49	4.42	4.32	4.26	4.50	4.57	4.44	4.55	4.43
	$1 {}^{1}A_{2}(n \to \pi^{*})$	1.093	5.15	4.95	4.86	4.74	4.69	4.93	5.00	4.80	4.91	4.85
	$1 {}^{1}B_{2}(\pi \to \pi^{*})$	1.105	5.50	5.20	5.11	5.02	4.95	5.36	5.39	5.24	5.44	5.34
	$2 {}^{1}A_{1}(\pi \to \pi^{*})$	1.062	7.17	6.86	6.81	6.76	6.69	7.06	7.09	6.63	6.95	6.82
	$2 {}^{1}B_{2}(\pi \rightarrow \pi^{*})$	1.078	8.25	7.97	7.91	7.83	7.76	8.01	8.08	7.64	8.01^{m}	
	$3 {}^{1}A_{1}(\pi \to \pi^{*})$	1.086	7.99	7.68	7.61	7.53	7.47	7.74	7.81	7.21	7.65^{m}	
Pyridazine	$1 {}^{1}B_{1}(n \to \pi^{*})$	1.088	4.14	3.87	3.80	3.71	3.65	3.92	4.00	3.78	3.78	3.85
	$1 {}^{1}A_{2}(n \to \pi^{*})$	1.099	4.75	4.51	4.42	4.30	4.24	4.49	4.59	4.31	4.31	4.44
	$2 {}^{1}A_{1}(\pi \to \pi^{*})$	1.109	5.39	5.07	4.98	4.89	4.81	5.22	5.25	5.18	5.18	5.20
	$2 {}^{1}A_{2}(n \rightarrow \pi^{*})$	1.098	6.03	5.76	5.68	5.57	5.51	5.74	5.82	5.77	5.77	5.66
	$2 {}^{1}B_{1}(n \to \pi^{*})$	1.099	6.69	6.46	6.37	6.24	6.18	6.41	6.51	6.52		
	$1 {}^{1}B_{2}(\pi \to \pi^{*})$	1.063	7.11	6.77	6.71	6.65	6.58	6.93	6.96	6.31		
	$2 {}^{1}B_{2}(\pi \to \pi^{*})$	1.080	7.81	7.52	7.45	7.37	7.31	7.55	7.61	7.29		
	$3 {}^{1}A_{1}(\pi \to \pi^{*})$	1.080	8.13	7.79	7.73	7.66	7.58	7.82	7.91	7.62		
s-Triazine	$1 {}^{1}A_{1}''(n \to \pi^{*})$	1.095	4.99	4.80	4.71	4.57	4.52	4.78	4.85	4.60	4.60	4.70
	$1 {}^{1}A_{2}^{"}(n \to \pi^{*})$	1.094	5.02	4.74	4.67	4.58	4.52	4.76	4.84	4.66	4.66	4.71
	$1 {}^{1}E''(n \to \pi^{*})$	1.094	5.05	4.82	4.73	4.62	4.56	4.81	4.89	4.70	4.70	4.75
	$1 {}^{1}A'_{2}(\pi \to \pi^{*})$	1.108	5.86	5.55	5.45	5.36	5.28	5.71	5.74	5.79	5.79	5.71
	$2 {}^{1}A'_{1}(\pi \to \pi^{*})$	1.070	7.53	7.20	7.14	7.09	7.02	7.41	7.44	7.25	0.10	0.11
	$2 {}^{1}E''(n \rightarrow \pi^*)$	1.110	8.23	7.98	7.88	7.76	7.69	7.80	7.95	7.71		
	$1 {}^{1}E'(\pi \rightarrow \pi^*)$	1.084	8.30	8.00	7.93	7.84	7.78	8.04	8.13	7.50		
	${}^{1}E''(n \rightarrow \pi^{*})^{j}$	1.094	9.59	9.31	9.21	9.10	9.02	0.01	0.10	1.00		
	${}^{1}E'(n \rightarrow \sigma^{*})^{j}$	1.087	9.35	9.27	9.21	9.09	9.06					
	${}^{1}A_{2}^{\prime\prime}(n \to \sigma^{*})^{j}$	1.080	9.52	9.26	9.20	9.13	9.07					
	${}^{1}E''(n \rightarrow \pi^{*})^{j}$	1.119	10.06	9.74	9.61	9.43	9.32					
	$2 {}^{1}E'(\pi \to \pi^*)$	1.154	10.31	9.88	9.70	9.53	9.39	9.44	9.64	8.99		
	${}^1A_1''(n \to \pi^*)^j$	1.102	10.02	9.68	9.58	9.50	9.42	0.11	5.01	0.00		
s-Tetrazine	$1 {}^{1}B_{3u}(n \to \pi^*)$	1.005	2.72	2.40	0.20	2.22	2.16	2.53	2.60	2.29	2.29	2.46
s- retrazine	$1 B_{3u}(n \to \pi)$ $1 A_{u}(\pi \to \pi^{*})$	1.085 1.098	$\frac{2.72}{4.01}$	2.40 3.74	2.32 3.65	3.53	2.16 3.46	3.79	3.90	3.51	3.51	2.46 3.78
	$1 \stackrel{A_u(n \to n)}{\longrightarrow} 1 \stackrel{1}{B_{1g}}(n \to \pi^*)$	1.099	5.34	5.03	4.93	4.83	4.75	4.97	5.11	4.73	4.73	4.87
	$1 \stackrel{B_{1g}(n \to \pi)}{1} 1 \stackrel{B_{2u}(\pi \to \pi^*)}{1}$	1.1099	5.33	4.96	4.86	4.75	4.65	5.12	5.16	4.73	4.73	5.08
	$\frac{1}{2} \stackrel{D2u(n \to n)}{}{}^{1}A_g(n^2 \to \pi^{*2})^j$	1.957	11.47	6.87	5.73	6.36	5.07	0.12	0.10	4.55	4.50	5.00
	$\frac{2}{1} {}^{1}B_{2g}(n \rightarrow \pi^{*})$	1.110	5.82	5.48	5.38	5.27	5.20	5.34	5.44	5.20	5.20	5.28
	$2 {}^{1}A_{u}(n \rightarrow \pi^{*})$	1.093	5.78	5.46	5.38	5.27	5.20	5.46	5.54	5.50	5.50	5.39
	$1 {}^{1}B_{3g}(n^2 \to \pi^{*2})^n$	1.974	13.18	8.44	7.20	7.94	6.55	5.40	0.04	5.86	5.79	5.76
	$2 ^{1}B_{-} (n (\pi^{*}))$	1.122	6.72	6.44	6.31	6.15	6.05	6.23	6.43	6.06	0.13	5.10
	$2 {}^{1}B_{2g}(n \to \pi^{*})$ $2 {}^{1}B_{1g}(n \to \pi^{*})$	1.110	7.30	7.04	6.93	6.79	6.71	6.87	7.00	6.45		
		1.156	8.38	7.92	7.70	7.44	7.26	7.08	7.43	6.73		
	$3 {}^{1}B_{1g}(n \to \pi^{*})$	1.100			6.64			6.67	6.79	6.77		
	$2 {}^{1}B_{3u}(n \to \pi^{*})$		7.02	6.74		6.52	6.45					
	${}^{1}B_{1u}(\pi \to \pi^*) \atop {}^{1}B_{3g}(n^2 \to \pi^{*2})^j$	1.059	7.70	7.31	7.23	7.18	7.09	7.45	7.49	6.94		
	$2 {}^{1}B_{1u}(\pi \to \pi^{*2})^{j}$ $2 {}^{1}B_{1u}(\pi \to \pi^{*})$	1.986	15.13	9.72	8.21	9.12	7.39 7.50	7 70	707	7.40		
	$\stackrel{\angle}{1}_{D} \stackrel{D_{1u}(\pi \to \pi^+)}{}_{U}$	1.082	8.15	7.76	7.68	7.59	7.50	7.79	7.87	7.42		
	${}^{1}B_{1g}(n^{2} \rightarrow \pi^{*2})^{j}$	1.937	14.35	9.88	8.74	9.32	8.01					
	${}^{1}B_{1u}(n^{2} \to \pi^{*2})^{j}$	1.995	15.09	10.14	8.78	9.63	8.10		0.40			
	${}^{1}B_{3g}(n \rightarrow \pi^{*})^{j}$	1.089	8.64	8.46	8.40	8.30	8.26	0 = 1	8.43	0.14		
	$2 {}^{1}B_{2u}(\pi \to \pi^{*})$ $2 {}^{1}B_{3g}(\pi \to \pi^{*})$	1.083 1.164	8.94 9.56	8.55 9.06	8.47 8.86	8.38 8.66	8.28 8.50	8.51 8.47	8.62 8.72	8.14 8.34		
Formaldehyde	$1 {}^{1}A_{2}(n \rightarrow \pi^{*})$ ${}^{1}B_{2}(n \rightarrow \sigma^{*})^{j}$	1.072 1.077	4.03 8.27	3.92 8.36	3.85 8.28	3.83 8.12	3.80 8.08	3.95	3.96	3.99	3.88	3.88
	$1 {}^{1}B_{1}(\sigma \rightarrow \pi^{*})$	1.074	9.36	9.21	9.14	9.11	9.06	9.18	9.20	9.14	9.1	9.04
	$\begin{array}{c} 1 B_1(o \to \pi) \\ 2 A_1(\pi \to \pi^*)^o \end{array}$	1.074	9.86	9.70	9.14	9.11	9.48	9.18 9.29^p	3.20	9.14	9.1	9.04
	${}^{1}B_{2}(n \rightarrow \sigma^{*})^{j}$	1.065	9.80	9.70	9.81	9.54	9.48	3.43°		5.32	<i>3.</i> 3	<i>9.</i> ∠9
	$^{1}A_{2}(\pi \rightarrow \sigma)^{j}$	1.109	10.63	10.34	10.25	10.26	10.18					
	$^{1}A_{1}(n \rightarrow \pi^{*})^{o}$	1.075	10.58	10.60	10.23	10.20	10.15	10.45	10.49			
	211(10 / 11)	1.010	10.00	10.00	10.00	10.03	10.00	10.40	10.43			

Table 3.4 (cont'd).

Molecule	State	REL^b	SD^c	δ -CR(T),IA ^d	δ -CR(T),ID ^d	δ -CR(2,3),A e	δ -CR(2,3),D ^e	$CC3^f$	$SDT-3^g$	$CASPT2^h$	TBE-1 h	TBE- 2^h
Acetone	$1 {}^{1}A_{2}(n \rightarrow \pi^{*})$	1.074	4.50	4.36	4.30	4.25	4.22	4.40	4.41	4.44	4.40	4.38
	$^{1}B_{2}(n \rightarrow \sigma^{*})^{j}$	1.087	7.54	7.53	7.47	7.30	7.25					
	${}^{1}A_{1}(\pi \to \pi^{*}/n \to \sigma^{*})^{j}$	1.090	9.21	9.07	9.02	8.90	8.85	0.45	0.10	0.05	0.1	0.04
	$1 {}^{1}B_{1}(\sigma \rightarrow \pi^{*})$	1.072	9.38	9.20	9.14	9.09	9.05	9.17	9.19	9.27	9.1	9.04
	${}^{1}A_{2}(\sigma \rightarrow \pi^{*})^{j}$	1.087	9.61	9.48	9.41	9.30	9.24					
	$^{1}B_{2}(n \rightarrow \sigma^{*})^{j}$ $^{1}A_{2}(n \rightarrow \pi^{*})^{j}$	1.085	9.58	9.56	9.49	9.33	9.28					
	$A_2(n \to \pi^*)^3$ $2 {}^1A_1(\pi \to \pi^*)$	1.086 1.087	9.70 9.94	9.52 9.80	9.44 9.74	9.36 9.63	9.30 9.58	9.65	9.73	9.31	9.4	8.90^{q}
	2 11(" / ")	1.001	0.01	3.00	0.14	5.00	5.50	5.00	3.10	5.01	5.1	0.50
p-Benzoquinone		1.098	3.32	3.07	3.01	2.84	2.79	2.85	2.95	2.77	2.77	2.86
	$1 {}^{1}B_{1g}(n \to \pi^{*})$	1.095	3.15	2.89	2.83	2.68	2.63	2.75	2.85	2.76	2.76	2.74
	$1 {}^{1}B_{3g}(\pi \to \pi^{*})$	1.091	5.04	4.61	4.54	4.42	4.34	4.59	4.68	4.26	4.26	4.44
	$1 {}^{1}B_{1u}(\pi \to \pi^{*})$	1.093	6.01	5.63	5.57	5.42	5.35	5.62	5.69	5.28	5.28	5.47
	$1 {}^{1}B_{3u}(n \to \pi^{*})$ $1 {}^{1}B_{2g}(n \to \pi^{*})^{j}$	1.117 1.127	6.54	6.33 6.64	6.24 6.54	5.97	5.90	5.82	6.05	5.64 5.66	5.64	5.55
	${}^{1}_{1}B_{3u}(n, \pi \rightarrow \pi^{*2})$	1.930	6.84 12.54	8.52	7.70	6.20 7.86	6.11 6.93			5.00		
	$\frac{2}{2} {}^{1}\mathrm{B}_{2g}(n \to \pi^{*})^{j}$	1.097	7.74	7.44	7.70	7.30	7.13			6.60		
	$\frac{2}{2} {}^{1}B_{3q}(\pi \to \pi^{*})$	1.108	7.75	7.44	7.37	7.13	7.14	7.27	7.37	6.96	6.96	7.16
	${}^{1}B_{2g}(n,\pi \to \pi^{*2})^{j}$	1.861	12.30	8.71	7.99	8.01	7.16	1.21	1.01	0.50	0.50	1.10
	$\frac{1}{2} {}^{1}\mathrm{B}_{2u}(\pi \to \pi^{*})^{i}$	1.147	8.67	8.21	8.12	7.97	7.86			7.32		
	$2 {}^{1}B_{1u}(\pi \to \pi^{*})$	1.086	8.55	8.19	8.13	8.02	7.94	7.82	7.98	7.92		
	- 1 - 11/ *>											
Formamide	$1 {}^{1}A''(n \to \pi^{*})$	1.073	5.73	5.62	5.55	5.50	5.47	5.65	5.66	5.63	5.63	5.55
	$2 {}^{1}A'(\pi \to \pi^*)^{r}$ ${}^{1}A'(\pi \to \pi^*)^{r}$	1.095	7.58	7.38	7.30	7.22	7.16	7.24 ^s	0.95	7.39	7.39	7.35
	$3 {}^{1}A'(\pi \to \pi^{*})'$	1.090 1.100	8.54 11.49	8.49 11.17	8.41 11.09	8.26 11.06	8.22 10.99	8.27 10.93	8.35 11.09	10.54		
	$3 A (\pi \rightarrow \pi)$	1.100	11.49	11.17	11.09	11.00	10.99	10.95	11.09	10.54		
Acetamide	$1 {}^{1}A''(n \to \pi^*)$	1.074	5.79	5.66	5.61	5.54	5.51	5.69	5.71	5.69	5.69	5.62
	${}^{1}A^{\prime\prime}(\pi \rightarrow \sigma^{*})^{j}$	1.071	7.34	7.21	7.17	7.13	7.09					
	${}^{1}A'(\pi \to \pi^*/n \to \sigma^*)^{j}$	1.098	7.52	7.40	7.33	7.17	7.12					
	$2 {}^{1}A'(\pi \to \pi^*/n \to \sigma^*)$	1.089	7.93	7.78	7.72	7.62	7.57	7.67	7.76	7.27	7.27	7.14
	${}^{1}A^{\prime\prime}(\pi\to\sigma^{*})^{j}$	1.068	8.76	8.63	8.59	8.55	8.51					
	${}^{1}A'(n \to \sigma^{*})^{j}$	1.096	9.10	9.04	8.98	8.79	8.75					
	${}^{1}A'(n \to \sigma^{*})^{j}$	1.098	9.52	9.45	9.38	9.18	9.13					
	${}^{1}A''(\pi \to \sigma^*)^{j}$	1.083	9.50	9.37	9.32	9.26	9.21					
	${}^{1}A'(n \to \sigma^{*})^{j}$	1.084	10.22	10.19	10.13	9.97	9.93					
	${}^1A''(n \to \pi^*)^j$	1.074	10.40	10.25	10.19	10.11	10.07					
	${}^{1}A''(n \to \pi^*)^{j}$ $3 {}^{1}A'(\pi \to \pi^*)$	1.090 1.088	10.51 10.87	10.45 10.65	10.37 10.59	10.22 10.51	10.17 10.47	10.50	10.60	10.09		
	, ,	1.000	10.01	10.00	10.00	10.01	10.11	10.00	10.00	10.00		
Propanamide	$1 \stackrel{1}{A}''(n \to \pi^*)$	1.075	5.81	5.69	5.65	5.56	5.53	5.72	5.73	5.72	5.72	5.65
	${}^{1}A''(\pi \to \sigma^*)^{j}$	1.071	7.35	7.23	7.20	7.14	7.11	= 00		= 00	= 00	= 00
	$2 {}^{1}A'(\pi \rightarrow \pi^*)$	1.090	7.91	7.79	7.74	7.60	7.56	7.62	7.74	7.20	7.20	7.09
	${}^{1}A''(\pi \to \sigma^{*})^{j}$ ${}^{1}A''(\pi \to \sigma^{*})^{j}$	1.069	8.73	8.60	8.57	8.51	8.48					
	${}^{1}A''(n \to \sigma^{*})^{j}$ ${}^{1}A''(n \to \pi^{*})^{j}$	1.083	9.22	9.08	9.04	8.96	8.91					
	$A (n \rightarrow \pi)^{3}$ $3 {}^{1}A'(\pi \rightarrow \pi^{*})$	1.085 1.089	10.04 10.44	9.96 10.24	9.90 10.19	9.75 10.10	9.71 10.05	10.06	10.15	9.94		
	, ,	1.000	10.11	10.21	10.10	10.10	10.00	10.00	10.10	0.01		
Cytosine	$2 {}^{1}A'(\pi \to \pi^{*})$	1.100	5.04	4.75	4.68	4.53	4.47	4.72		4.67	4.66	4.66
	$1 {}^{1}A''(n \to \pi^*)$	1.094	5.49	5.26	5.21	5.05	5.00	5.16		5.12	4.87	4.87
	$2 {}^{1}A''(n \rightarrow \pi^*)$	1.091	6.05	5.87	5.81	5.64	5.60	5.52		5.53	5.26	5.26
	$3 {}^1A'(\pi \to \pi^*)$	1.109	6.01	5.72	5.65	5.50	5.44	5.61		5.53	5.62	5.62
	$4 \stackrel{1}{A} A'(\pi \rightarrow \pi^*)$	1.093	6.85	6.59	6.53	6.41	6.36	6.61		6.40		
	$5 {}^{1}A'(\pi \rightarrow \pi^*)$	1.104	7.27	6.96	6.89	6.74	6.67			6.97		
	$6 {}^{1}A'(\pi \to \pi^{*})$	1.106	8.73	8.53	8.48	8.26	8.20			8.23		
Thymine	$1 {}^{1}A''(n \to \pi^*)$	1.089	5.23	5.06	5.02	4.84	4.80	4.94		4.95	4.82	4.82
	$2 {}^{1}A'(\pi \rightarrow \pi^{*})$	1.086	5.68	5.38	5.33	5.19	5.13	5.34		5.06	5.20	5.20
	$3 {}^{1}A'(\pi \to \pi^*)$	1.112	6.86	6.56	6.50	6.30	6.23	6.34		6.15	6.27	6.27
	$2 {}^{1}A''(n \rightarrow \pi^{*})$	1.081	6.65	6.52	6.48	6.32	6.29	6.59		6.38	6.16	6.16
	$4 {}^{1}A'(\pi \to \pi^{*})$	1.099	7.14	6.80	6.74	6.58	6.51	6.71		6.53	6.53	6.53
	$3 {}^{1}A''(n \rightarrow \pi^*)$	1.118	7.76	7.44	7.35	7.01	6.92			6.85		
	$4 {}^1A''(n \to \pi^*)$	1.112	7.95	7.70	7.61	7.31	7.23			7.43		
	$5^{1}A'(\pi \to \pi^*)$	1.100	7.99	7.73	7.67	7.50	7.48			7.43		
Uracil	$1 {}^{1}A''(n \to \pi^*)$	1.091	5.20	5.03	4.98	4.81	4.77	4.90		4.91	4.80	5.00
	$2 {}^{1}A'(\pi \rightarrow \pi^{*})$	1.090	5.76	5.45	5.40	5.28	5.22	5.44		5.23	5.35	5.25
	$3 {}^{1}A'(\pi \rightarrow \pi^*)$	1.116	6.84	6.52	6.44	6.25	6.17	6.29		6.15	6.26	6.26
	$2 {}^{1}A''(n \rightarrow \pi^{*})$	1.082	6.58	6.44	6.39	6.24	6.20	6.32		6.28	6.10	6.10
	$3 {}^{1}A''(n \rightarrow \pi^*)$	1.117	7.76	7.47	7.36	7.06	6.96	6.87		6.98	6.56	6.56
	$4 {}^{1}A'(\pi \rightarrow \pi^*)$	1.099	7.27	6.91	6.84	6.71	6.64	6.84		6.74	6.70	6.70
	$4 {}^{1}A''(n \to \pi^{*}) 5 {}^{1}A'(\pi \to \pi^{*})$	1.113	7.82	7.56	7.46	7.17	7.08	7.12		7.28		

Table 3.4 (cont'd).

Molecule	State	REL^b	SD^c	δ -CR(T),IA ^d	δ -CR(T),ID ^d	δ -CR(2,3),A ^e	δ -CR(2,3),D ^e	$CC3^f$	$SDT-3^g$	$CASPT2^h$	TBE-1 h	TBE- 2^h
Adenine	$2 {}^{1}A'(\pi \to \pi^{*})$	1.101	5.39	5.08	5.03	4.87	4.81	5.18		5.20	5.25	5.25
	$3 {}^{1}A'(\pi \to \pi^*)$	1.089	5.67	5.35	5.31	5.15	5.10	5.39		5.29	5.25	5.25
	$1 {}^{1}A''(n \to \pi^*)$	1.093	5.62	5.39	5.34	5.16	5.11	5.34		5.19	5.12	5.12
	$2 {}^{1}A''(n \to \pi^{*})$	1.091	6.21	5.97	5.91	5.74	5.70	5.96		5.96	5.75	5.75
	$4 {}^{1}A'(\pi \to \pi^{*})$	1.097	6.85	6.54	6.48	6.32	6.26	6.53		6.34		
	$^{1}A'(\pi \rightarrow \pi^{*})^{j}$	1.101	7.13	6.80	6.74	6.56	6.50					
	$5 {}^{1}A'(\pi \to \pi^{*})$	1.100	7.20	6.87	6.81	6.63	6.57			6.64		
	$6 {}^{1}A'(\pi \to \pi^{*})$	1.102	7.72	7.39	7.33	7.16	7.10			6.87		
	$^{1}A'(\pi \rightarrow \pi^{*})^{j}$	1.106	8.14	7.81	7.74	7.54	7.47					
	$7 {}^{1}A'(\pi \to \pi^*)$	1.116	8.49	8.11	8.04	7.82	7.73			7.56		

^a All excitation energies were computed in this work, unless stated otherwise. The δ-CR-EOMCC vertical excitation energies were computed using the CR-CC(2,3),D/TZVP optimized geometries, while the CC3, EOMCCSDT-3, and CASPT2 results were obtained using the MP2/6-31G* geometries from Ref. [17].

^b Reduced excitation level diagnostic; for one-electron transitions REL ≈ 1 and for two-electron transitions REL ≈ 2 .

^c EOMCCSD results.

 $^{^{}d}$ δ-CR-EOMCCSD(T),X (X = IA, ID) results.

^e δ -CR-EOMCC(2,3),X (X = A, D) results.

f CC3 results taken from Ref. [17], except for those for the nucleobases which were reported in Ref. [25].

g EOMCCSDT-3 values taken from Ref. [24].

^h CASPT2 and TBE-1 excitation energies taken from Ref. [17], with updates from Ref. [21], and TBE-2 values taken from Ref. [21].

ⁱ In Ref. [17] these states were reported as having doubly excited character. However, as determined in this work, they are predominantly one-electron transitions (REL for 2 $^1A_1(\pi \to \pi^*)$ is 1.153 and REL for 3 $^1A_1(\pi \to \pi^*)$ is 1.054) and, thus, double excitations have a small effect on these states.

J Additional excited states not included among the 149 singlet excitations listed in Table I of Ref. [17]. States in this category that have been characterized in the Supporting Information to Ref. [17] are designated as \underline{n} 1X , where X is the irreducible representation and \underline{n} indicates the state number within symmetry X (n is underlined to distinguish from the 149 states included in Table I of Ref. [17], which are labeled as n 1X). States that have not been found in Ref. [17] and other prior benchmark work [18–25] are designated as 1X , i.e., without the state number in front of the term symbol. In ordering these additional states, we use the δ-CR-EOMCC(2,3),D values.

 $[^]k$ This state is dominated by comparable single excitations from HOMO to LUMO+1 and from HOMO to LUMO+5. The authors of Ref. [17] stated that it is dominated by a HOMO \rightarrow LUMO single excitation, which is not what our EOMCC calculations imply.

^l This state is largely dominated by a single excitation from HOMO to LUMO+1, with two other significant, though slightly smaller, contributions from one-electron HOMO-1 \rightarrow LUMO+1 and HOMO \rightarrow LUMO+5 transitions. According to Ref. [17], the state is dominated by the HOMO-1 \rightarrow LUMO and HOMO \rightarrow LUMO+1 transitions, but our EOMCC calculations do not confirm this.

LUMO+1 transitions, but our EOMCC calculations do not confirm this.

These two TBE-1 values had to be taken from Ref. [195], since Ref. [17] provided no information what the best estimates for them might be.

ⁿ This state is the only almost purely doubly excited state among the 149 singlet excited states included in Table I of Ref. [17]. The large discrepancies between our δ-CR-EOMCC results, including the most accurate δ-CR-EOMCC(2,3),D value of 6.55 eV, and the previously reported [17, 21] CASPT2 and TBE data do not necessarily imply that CASPT2 and TBE results are more accurate. Although we do not know what the CC3 and EOMCCSDT-3 results for this state might be, our best δ-CR-EOMCC(2,3),D value of 6.55 eV is in excellent agreement with the NEVPT2 results reported in Ref. [23], which range from 6.30 to 6.35 eV.

Table 3.4 (cont'd).

- ⁰ As explained in footnote p to Table 3.3, the authors of Ref. [17] confused the 2 $^1A_1(\pi \to \pi^*)$ state of formaldehyde with the higher-energy $^1A_1(n \to \pi^*)$ solution. See footnote p to Table 3.3 for further information.
- p CC3/aug-cc-pVQZ results taken from Ref. [21].
- The CC3/aug-cc-pVTZ result reported in Ref. [21]. Our δ-CR-EOMCC excitation energies for the 2 $^1A_1(\pi \to \pi^*)$ state of acetone and the corresponding CC3/TZVP, EOMCCSDT-3/TZVP, and TBE values reported in Refs. [17, 22, 24] suggest that the CC3/aug-cc-pVTZ root at 8.90 eV found in Ref. [21] does not represent the 2 $^1A_1(\pi \to \pi^*)$ excitation. Based on our δ-CR-EOMCC analysis, the CC3/aug-cc-pVTZ root at 8.90 eV corresponds, most likely, to the $^1A_1(\pi \to \pi^*/n \to \sigma^*)$ state that has not been considered in the previous benchmark studies [17–25]. For this reason, in comparisons of our δ-CR-EOMCC and EOMCCSD data for the 2 $^1A_1(\pi \to \pi^*)$ state of acetone with a TBE-2 result we use the TBE-1 value taken from Ref. [17] instead.
- As explained in footnote s to Table 3.3, the previous assignment of the 2 $^1A'(\pi \to \pi^*)$ state to the higher-energy CC3 solution at 8.27 eV (or the corresponding EOMCCSD root at \sim 8.5 eV), presented in Ref. [17], is incorrect. See footnote s to Table 3.3 for further information.
- S Taken from Ref. [25].

3.4.2 Remarks on the Calculated Vertical Excitation Spectra for Molecules in the Database of Ref. [17]

As already mentioned, the 203 singlet excitation energies of the 28 molecules constituting the benchmark set of Ref. [17] determined in this dissertation are collected in Tables 3.3 and 3.4. We compare the EOMCCSD, δ -CR-EOMCCSD(T),IA, δ -CR-EOMCCSD(T),ID, δ -CR-EOMCC(2,3),A, and δ -CR-EOMCC(2,3),D results, obtained in this work using the MP2/6-31G* (Table 3.3) and CR-CC(2,3),D/TZVP (Table 3.4) geometries, with the previously reported CASPT2 [17, 21], CC3 [17, 19, 21, 25], EOMCCSDT-3 [22, 24], and theoretical best estimate, TBE-1 [17] and TBE-2 [21], values. In addition to dominant orbital excitations, the nature of each computed excited state (singly, doubly, or somewhere in-between) is characterized using the reduced excitation level (REL) diagnostic [66] resulting from the EOMCCSD calculations (REL ≈ 1 implies a one-electron transition, whereas REL close to 2 indicates a doubly excited state). The main part of the original benchmark set of Ref. [17], presented in Table I of this reference, contains 149 $\pi \to \pi^*$, $n \to \pi^*$, and $\sigma \to \pi^*$ vertical singlet excitations, the majority of which have REL values close to 1, with only relatively few (45 or $\sim 30\%$) states having non-negligible, though still small, doubles contributions (1.1 < REL < 1.2). Even fewer (4 or $\sim 3\%$) states have a more substantial two-electron transition character (REL ≥ 1.2). Only one state among the 149 singlet excited states included in Table I of Ref. [17], i.e., the 1 $^1B_{3g}(n^2 \to \pi^{*2})$ state of s-tetrazine, is a truly multi-reference-type two-electron transition with REL ≈ 2 . Thus, the majority of the singlet excitations found in Ref. [17] consists of states that have a predominantly one-electron excitation nature. The doubly excited 1 $^1B_{3g}(n^2 \to \pi^{*2})$ state of s-tetrazine will be excluded from our statistical error evaluations discussed in Section 3.5, since we have no access to the corresponding CC3 and EOMCCSDT-3 reference data, while the existing CASPT2 and TBE values are, in our view, unreliable (see footnote o to Table 3.3 and the discussion below). In other words, in our overall statistical error analyses discussed in Section 3.5, we start with the 148 singlet excited states, taken from Table I of Ref. [17], as described above, and then, in each comparison of our δ -CR-EOMCC data with another method, we use as many states from this set as computed with this other method.

In addition to the 149 excited states listed in Table I of Ref. [17], we have found 54 states which lie below the threshold set for each molecule as the highest of the CC3, EOMCCSDT-3, and CASPT2 excitation energy values obtained in the previously reported calculations [17, 21, 22, 24, 25]. Among these 54 additional states, there are five excitations that can be found in the Supporting Information to Ref. [17], which include the 2 ${}^{1}A_{1}(\pi \to \pi^{*}/\pi \to \sigma^{*})$ state of norbornadiene, 2 $^1A_g(n^2 \rightarrow \pi^{*2})$ state of s-tetrazine, and 1 $^1B_{2g}(n \rightarrow \pi^*)$, 2 $^{1}B_{2g}(n \to \pi^{*})$, and 1 $^{1}B_{2u}(\pi \to \pi^{*})$ states of p-benzoquinone and which are designated in Tables 3.3 and 3.4 in this dissertation as $\underline{2}$ $^{1}A_{1}(\pi \to \pi^{*}/\pi \to \sigma^{*})$, $\underline{2}$ $^{1}A_{g}(n^{2} \to \pi^{*2})$, and $\underline{1}\ ^1B_{2g}(n\to\pi^*)$, $\underline{2}\ ^1B_{2g}(n\to\pi^*)$, and $\underline{1}\ ^1B_{2u}(\pi\to\pi^*)$, respectively (underlining the state numbers to distinguish them from the main set of 149 states listed in Table I of Ref. [17], where the state numbers are not underlined). The remaining 49 excitations found in the present study and not considered in the earlier work [17–25], which are designated in our tables using multiplicity and spatial symmetry without the state number (i.e., as ${}^{1}X$ rather than $n^{-1}X$, where X is the relevant irreducible representation), consist of six $\pi \to \pi^*$, ten $n \to \pi^*$, one $\sigma \to \pi^*$, two $\pi \to \pi^*/n \to \sigma^*$, three $n \to \pi^*/\pi \to \sigma^*$, thirteen $\pi \to \sigma^*$, nine $n \to \sigma^*$, three $n^2 \to \pi^{*2}$, and two $n, \pi \to \pi^{*2}$ states. While all of these additional 54 states are made up of mostly one-electron transitions, six of them (four $n^2 \to \pi^{*2}$ and two $n, \pi \to \pi^{*2}$) have REL values close to 2. Although we do not include any of these additional

54 states in the overall statistical error analyses discussed in this work, since the previous studies containing the reference CC3, EOMCCSDT-3, and TBE data [17, 21, 22, 24, 25] have not found them, the information about these states, including our new δ -CR-EOMCC data, may help future work on assessing quantum chemistry methods for excited electronic states.

Before examining the overall performance of the δ -CR-EOMCCSD(T),IA, δ -CR-EOMCCSD(T),ID, δ -CR-EOMCC(2,3),A, and δ -CR-EOMCC(2,3),D approaches through appropriate statistical error analyses involving the 148 singlet excitations from Table I of Ref. [17] excluding the aforementioned 1 $^1B_{3g}(n^2 \to \pi^{*2})$ doubly excited state of s-tetrazine, in the next few paragraphs we highlight some of the key findings of our δ -CR-EOMCC calculations for the various molecules in the database of Ref. [17] organized in the following seven subgroups: linear polyenes, unsaturated cyclic hydrocarbons, aromatic hydrocarbons, heterocycles, aldehydes and ketones, amides, and nucleobases. In order to make our comparisons with the original [17] and subsequent [18–25] benchmark studies straightforward and clear, we keep the original state labeling and ordering used in Ref. [17], with updates provided in Ref. [21], as much as possible. All of the additional states found in the present study, beyond the 149 states from Table I of Ref. [17], are ordered according to the δ -CR-EOMCC(2,3),D energies, which we regard as generally most accurate among all δ -CR-EOMCC approaches. In comparing our δ -CR-EOMCC excitation energies with the previously published data [17– 25], we focus on the CC3 [17, 25], EOMCCSDT-3 [22, 24], CASPT2 [17, 21], and TBE-2 [21] values. We do not discuss comparisons with TBE-1 data, which are the TBE values included in Ref. [17], since the updated TBE-2 excitation energies from Ref. [21] are generally more reliable.

3.4.2.1 Linear Polyenes: Ethene, E-butadiene, all-E-hexatriene, and all-E-octatetraene

Comparing the δ -CR-EOMCC vertical excitation energies of the seven states of ethene, Ebutadiene, all-E-hexatriene, and all-E-octatetraene, shown in Table 3.3, with their CASPT2 and TBE-2 counterparts from Refs. [17] and [21], the corresponding MUE values are relatively small, with the δ -CR-EOMCC(2,3) methods yielding smaller deviations from the CASPT2 and TBE-2 data (0.19–0.20 and 0.28–0.34 eV, respectively) than the δ -CR-EOMCCSD(T) approaches (0.26–0.31 and 0.41–0.49 eV, respectively). Compared to the iterative triples EOMCCSDT-3 approximation [22, 24], the non-iterative δ -CR-EOMCCSD(T),IX and δ -CR-EOMCC(2,3), X (X = A, D) schemes have MUEs in the 0.16-0.27 eV range. Compared to CC3 [17], the δ -CR-EOMCC methods show similar MUE characteristics ($\sim 0.2 \text{ eV}$). The MaxE values characterizing the δ -CR-EOMCC results vs the CC3 and EOMCCSDT-3 reference data for the seven states of linear polyenes discussed here, which range from 0.23 to 0.44 eV, are on the same order. Thus, for the linear polyene molecules in the database of Ref. [17], all four δ -CR-EOMCC approaches accurately reproduce the results of the considerably more expensive CC3 and EOMCCSDT-3 calculations. This includes the 2 $^1A_g(\pi \to \pi^*)$ states of E-butadiene, all-E-hexatriene, and all-E-octatetraene, which have a partially doubly excited character (REL ≈ 1.2). The differences between the δ -CR-EOMCCSD(T),IA and δ -CR-EOMCCSD(T),ID excitation energies of the 2 $^1A_g(\pi \to \pi^*)$ states of all-E-hexatriene and all-E-octatetraene and the corresponding CASPT2 and TBE-2 data, of 0.61–0.77 and 0.94 eV, respectively, in the δ -CR-EOMCCSD(T),IA case and 0.49–0.68 and 0.82–0.85 eV, respectively, in the δ -CR-EOMCCSD(T),ID case, are larger, but the δ -CR-EOMCC(2,3),A and δ -CR-EOMCC(2,3),D approaches reduce them to 0.37–0.47 and 0.64–0.70 eV in the δ - CR-EOMCC(2,3),A case and 0.25–0.37 and 0.54–0.58 eV in the δ -CR-EOMCC(2,3),D case. Thus, we can conclude that the δ -CR-EOMCC(2,3) methods produce excitation energies which are consistent with both the high-level single-reference CC data of the CC3 and EOMCCSDT-3 type and with the results of the multi-reference CASPT2 calculations, while improving the δ -CR-EOMCCSD(T) excitation energies and being reasonably close to the TBE-2 reference values, which carry their own uncertainties.

The authors of Ref. [17] state that the 2 $^1A_g(\pi \to \pi^*)$ states of E-butadiene, all-E-hexatriene, and all-E-octatetraene have large contributions from two-electron transitions. As a result, they and other authors [17, 19, 20, 23–25] remove these states from some of their statistical error evaluations, particularly when CC vs CASPT2 comparisons are made, but we will not do this in the present work. The REL values of ~ 1.2 characterizing the 2 $^1A_g(\pi \to \pi^*)$ states of E-butadiene, all-E-hexatriene, and all-E-octatetraene indicate that these three states are predominantly one-electron transitions, with relatively small contributions from double excitations, which higher and more robust EOMCC levels, such as our δ -CR-EOMCC(2,3) approaches, should be able to handle quite well.

3.4.2.2 Unsaturated Cyclic Hydrocarbons: Cyclopropene, Cyclopentadiene, and Norbornadiene

For this group of molecules, the results of our δ -CR-EOMCC calculations for the nine states included in Table I of Ref. [17] are of a similar quality as the CASPT2 and TBE-2 data [17, 21], with MaxE and MUE values ranging from 0.16 to 0.42 eV and 0.08 to 0.21 eV, respectively. Compared to the CC3 [17] and EOMCCSDT-3 [22, 24] calculations, the δ -CR-EOMCC results for the nine states of unsaturated cyclic hydrocarbons included in Table I of Ref. [17] are characterized by MaxE values in the 0.16–0.32 eV range and MUEs ranging

from 0.09 to 0.28 eV.

Among the various excited electronic states in this group of molecules, the $1\,^{1}B_{2}(\pi \to \pi^{*})$ state of cyclopentadiene is of particular note, as it has been the focus of several theoretical studies where the location of this state has been disputed by various high-level single- and multi-reference quantum chemistry approaches (see Refs. [196, 197] and references therein). Our δ -CR-EOMCC vertical excitation energies for this state agree very well with the CASPT2 and TBE-1 or TBE-2 (both equal to EOMCCSDT in this case [17, 197]) values of 5.51 and 5.55 eV, respectively, with the δ -CR-EOMCC(2,3),D approach yielding the experimental band maximum, which is, after correcting for vibronic interactions, 5.43 eV [197]. Both the CC3 and EOMCCSDT-3 results place this state ~ 0.2 –0.3 eV higher in energy compared to our δ -CR-EOMCC values, suggesting that the δ -CR-EOMCC excitation energies, which almost perfectly match the TBE/EOMCCSDT and experimental data for this state, may be more accurate.

The authors of Ref. [17] mention that the valence excited states of cyclopentadiene, 2 $^1A_1(\pi \to \pi^*)$ and 3 $^1A_1(\pi \to \pi^*)$, contain significant contributions from double excitations. Their argument is based on the \sim 0.3–0.4 eV lowering when going from EOMCCSD to CC3. However, as can be seen in our tables and as shown in several previous studies [69, 135–137], it is not unusual to observe errors of this magnitude in EOMCCSD calculations for singly excited states. Indeed, the REL values characterizing the 2 $^1A_1(\pi \to \pi^*)$ and 3 $^1A_1(\pi \to \pi^*)$ states of cyclopentadiene, of about 1.153 and 1.055, respectively, when the MP2/6-31G* geometry is employed, show that these states are predominantly one-electron transitions and that double excitations do not significantly contribute to their electronic wave functions. Thus, in analogy to the 2 $^1A_g(\pi \to \pi^*)$ excitations in linear polyenes, there is no reason to exclude them from the statistical error analyses of various methods, as has

been done in some of the earlier benchmark studies [17, 19, 20, 23–25]. The 2 $^1A_1(\pi \to \pi^*)$ and 3 $^1A_1(\pi \to \pi^*)$ states of cyclopentadiene are included in our statistical error analyses discussed in Section 3.5.

In addition to the nine excited states of unsaturated cyclic hydrocarbons included in Table I of Ref. [17], we found three extra states for cyclopentadiene and norbornadiene within the prescribed energy range. Two of these states, namely, the ${}^{1}B_{2}(\pi \to \pi^{*})$ state of cyclopentadiene and the ${}^{1}B_{1}(\pi \to \pi^{*})$ state of norbornadiene, have not been considered in the prior benchmark studies [17–25]. The $\underline{2}$ ${}^{1}A_{1}(\pi \to \pi^{*}/\pi \to \sigma^{*})$ state of norbornadiene has been considered in the Supporting Information of Ref. [17]. All of these additional states are dominated by one-electron $\pi \to \pi^{*}$ transitions, with the $\underline{2}$ ${}^{1}A_{1}(\pi \to \pi^{*}/\pi \to \sigma^{*})$ state of norbornadiene being different from the other two excitations in that it has comparable contributions from $\pi \to \pi^{*}$ and $\pi \to \sigma^{*}$ one-electron transitions. The authors of Ref. [17] characterize it as having only $\pi \to \pi^{*}$ character, but our wave function analysis indicates a mixed $\pi \to \pi^{*}/\pi \to \sigma^{*}$ nature.

3.4.2.3 Aromatic Hydrocarbons: Benzene and Naphthalene

In analogy to the unsaturated cyclic hydrocarbons, the δ -CR-EOMCC results for the four excited states of benzene and ten excited states of naphthalene included in Table I of Ref. [17] are in generally good agreement with the CASPT2 and TBE-2 results of Refs. [17, 21]. This is particularly true for the δ -CR-EOMCC(2,3),D calculations, which are characterized by the MUE and MaxE values of 0.17 and 0.39 eV, respectively, when compared to CASPT2, and 0.20 and 0.40 eV, respectively, when compared to TBE-2. The remaining three δ -CR-EOMCC approaches have very similar MUE values relative to the CASPT2 and TBE-2 data, of 0.17–0.29 and 0.20–0.27 eV, respectively, but the corresponding MaxE values are somewhat

higher, especially in the δ -CR-EOMCCSD(T),IA case, where MaxE relative to CASPT2 is 0.87 eV and relative to TBE-2 0.86 eV. Comparing to the iterative triples CC3 and EOMCCSDT-3 approaches exploited in Refs. [17, 22, 24, 25], we see that the non-iterative δ -CR-EOMCCSD(T) corrections produce MUEs of 0.18 and 0.16–0.18 eV, respectively. The δ -CR-EOMCC(2,3) approaches give similar deviations from CC3 and EOMCCSDT-3 (all in the \sim 0.2–0.3 eV range).

The fourteen excited states of benzene and naphthalene considered in this work are predominantly one-electron transitions. In particular, the four states of naphthalene, namely, $2^{-1}A_g(\pi \to \pi^*)$, $1^{-1}B_{1g}(\pi \to \pi^*)$, $3^{-1}A_g(\pi \to \pi^*)$, and $3^{-1}B_{3u}(\pi \to \pi^*)$, in contrast to their characterization in Ref. [17] as having strong contributions from doubly excited configurations, are shown to be predominantly one-electron transitions, with REL values ranging from 1.109 to 1.177. Therefore, unlike in the earlier *ab initio* benchmark studies [17, 19, 20, 23–25], we do not exclude them from the statistical error analyses in Section 3.5, as there are no reasons to do so.

3.4.2.4 Heterocycles: Furan, Pyrrole, Imidazole, Pyridine, Pyrazine, Pyrimidine, Pyridazine, s-Triazine, and s-Tetrazine

This group of molecules is the largest subgroup among the 28 molecules in the database of Ref. [17]. As shown in Tables 3.3 and 3.4, our δ -CR-EOMCC calculations have identified a total of 87 excited states for the molecules in this group. Among them are 66 states listed in Table I of Ref. [17], the $2^{-1}A_g(n^2 \to \pi^{*2})$ state of s-tetrazine that can be found in the Supporting Information to Ref. [17], and 20 other additional states found in this work, but not considered in the prior benchmark studies [17–25]. As already alluded to above and as further elaborated on below, one of the states of s-tetrazine, namely, $1^{-1}B_{3g}(n^2 \to \pi^{*2})$,

included in Table I of Ref. [17], is an almost pure two-electron transition, which is excluded from our statistical analyses due to the absence of sufficiently many reliable data for it. If we compare the results of our δ -CR-EOMCC calculations for the remaining 65 states of the heterocycles considered here and listed in Table I of Ref. [17], for which the CASPT2, CC3, and EOMCCSDT-3 reference data are available [17, 22, 24, 25] and which are of predominantly single excitation nature, we can see a great deal of consistency among the various theoretical values. Indeed, the MUEs characterizing the δ -CR-EOMCC calculations for these states relative to the corresponding CASPT2, CC3, and EOMCCSDT-3 excitation energies are 0.17–0.24, 0.14–0.27, and 0.15–0.36 eV, respectively. Not surprising, the corresponding MaxE values are larger, particularly when one compares the δ -CR-EOMCCSD(T),IA and CASPT2 results, where MaxE is 1.16 eV, but the δ -CR-EOMCC(2,3) approaches, especially variant D, are very effective in reducing them to an acceptable level. The largest deviation between the δ -CR-EOMCC(2,3),D and CASPT2/CC3/EOMCCSDT-3 excitation energies of the 65 states of heterocycles included in Table I of Ref. [17], other than the 1 $^1B_{3g}(n^2 \to \pi^{*2})$ doubly excited state excluded from our statistics, is 0.58 eV. Similar remarks apply to a comparison of our δ -CR-EOMCC excitation energies with the TBE-2 data reported in Ref. [21]. The MUE and MaxE values characterizing the differences between the δ -CR-EOMCC and TBE-2 excitation energies of the 65 states of heterocycles included in Table I of Ref. [17], other than the two-electron 1 $^1B_{3g}(n^2 \to \pi^{*2})$ transition in s-tetrazine, are 0.13–0.20 and 0.40–0.50 eV, respectively. In other words, if we limit ourselves to excited states of heterocycles dominated by one-electron transitions, the δ -CR-EOMCC approaches, especially the triples corrections defining the δ -CR-EOMCC(2,3) approximations, are capable of providing CC3/EOMCCSDT-3-quality data, while matching the results of the multi-reference CASPT2 calculations and TBE-2 values. An interesting question arises if the above observations apply to the aforementioned doubly excited 1 $^1B_{3g}(n^2 \to \pi^{*2})$ state of s-tetrazine excluded from the above error analysis and disregarded in all of the previously published CC/EOMCC work [17, 19–25].

According to Refs. [17, 21], the CASPT2/TZVP calculation places the 1 $^1B_{3g}(n^2 \to \pi^{*2})$ state of s-tetrazine at 5.79 or 5.86 eV. The TBE value for this state reported in Table I of Ref. [17] (TBE-1 data in Ref. [21]) is 5.79 eV. The TBE-2 result recommended by the authors of Ref. [21], which utilizes the CASPT2/aug-cc-pVTZ data, is 5.76 eV. None of these results agree too well with our EOMCC computations. In the case of EOMCCSD, the excitation energy of the 1 $^1B_{3g}(n^2 \to \pi^{*2})$ state of s-tetrazine is placed at 13.19 eV, which is not surprising, since EOMCCSD fails when strongly multi-reference doubly excited states are considered. However, the discrepancy between the δ -CR-EOMCC and CASPT2/TBE results needs additional comments, since the δ -CR-EOMCC triples corrections, especially δ -CR-EOMCCSD(T), ID and δ -CR-EOMCC(2,3), D, have a successful track record in accurately describing excited states dominated by two-electron transitions (cf. Refs. [63–68, 74, 111, 149, 152, 155, 162, 179, 182 for examples). According to Table 3.3, the triples corrections of the δ -CR-EOMCCSD(T),IA, δ -CR-EOMCCSD(T),ID, δ -CR-EOMCC(2,3),A, and δ -CR-EOMCC(2,3),D approaches lower the EOMCCSD excitation energy of the 1 $^1B_{3g}(n^2 \rightarrow$ π^{*2}) state, of 13.19 eV, to 8.46, 7.23, 7.97, and 6.59 eV, respectively. The fact that the δ -CR-EOMCCSD(T),IA and δ -CR-EOMCC(2,3),A values are too high compared to the CASPT2 and TBE data is not surprising, since by relying on the Møller–Plesset rather than Epstein–Nesbet denominators in defining the corresponding triples corrections, as in Eq. (3.10), these methods tend to overestimate excitation energies for doubly excited states [63, 68]. A question arises though why there is a relatively large, $\sim 0.7-0.8$ eV, discrepancy between the CASPT2/TBE and δ -CR-EOMCC(2,3),D data, given the excellent performance

of the δ -CR-EOMCC(2,3),D approach, which uses the more robust Epstein-Nesbet-type denominator, Eq. (3.9), in past applications involving doubly excited states [67, 68, 74, 179, 182. We believe that our δ -CR-EOMCC(2,3),D result for the vertical excitation energy of the 1 $^1B_{3g}(n^2 \to \pi^{*2})$ state, of 6.59 eV, when the MP2/6-31G* geometry of s-tetrazine is employed, or 6.55 eV, when the CR-CC(2,3),D/TZVP geometry is adopted, is more reliable than the previously reported CASPT2 and TBE values that range between 5.76 and 5.86 eV [17, 21]. Indeed, as pointed out in footnote o to Table 3.3 (cf., also, footnote n to Table 3.4), our δ -CR-EOMCC(2,3),D excitation energies, of 6.55 eV or 6.59 eV, agree very well with the more recent second-order multi-reference perturbation theory calculations of the NEVPT2 type, which give 6.30–6.35 eV [23]. It is also well known that CASPT2 often underestimates the excitation energies and the $\sim 0.5-1$ eV underestimation is not unheard of. For all these reasons, we do not include the 1 $^1B_{3g}(n^2 \to \pi^{*2})$ state in our statistical error analyses, since we do not have access to the high-level EOMCC results with an accurate treatment of triple excitations other than our own δ -CR-EOMCC(2,3),D values and we cannot rely on the CASPT2 or TBE excitation energies reported in Refs. [17, 21], which seem to be inaccurate. It would be desirable to perform full EOMCCSDT or active-space EOMCCSDt calculations for the 1 $^1B_{3g}(n^2 \to \pi^{*2})$ state of s-tetrazine, along with the corresponding CC3, EOMCCSDT-3, and multi-reference CI computations, to determine the accuracy of our δ -CR-EOMCC(2,3),D results.

Among the 21 additional states of the heterocycles considered in this work, six $\pi \to \sigma^*$ excitations in pyrrole, five states of pyridine representing $n \to \pi^*$, $\pi \to \sigma^*$, and $n \to \pi^*/\pi \to \sigma^*$ excitations, five states of s-triazine of the $n \to \sigma^*$ and $n \to \pi^*$ types, and one $n \to \pi^*$ excitation in s-tetrazine are predominantly one-electron transitions, as demonstrated by their REL values being close to 1. As a result, all triples corrections to EOMCCSD are

quite small ($\sim 0.1-0.4 \text{ eV}$) and all δ -CR-EOMCC approaches provide similar values. This is especially true when we compare the δ -CR-EOMCC(2,3),A and δ -CR-EOMCC(2,3),D data, which agree to within 0.1 eV. Based on our experience, such an agreement typically implies that the δ -CR-EOMCC(2,3) excitation energies are reasonably well converged. Thus, in the absence of other high-level CC/EOMCC data for the 21 additional states of the heterocycles considered in the present work, we can treat our δ -CR-EOMCC(2,3) values for the 17 singly excited states among them as reference data for future benchmark studies. Among all the heterocycles listed in Tables 3.3 and 3.4, s-tetrazine is the only molecule that has doubly excited states in the prescribed energy range, which are characterized by REL close to 2. One of them is the 1 ${}^{1}B_{3g}(n^2 \to \pi^{*2})$ excitation, which we have already discussed above. The remaining doubly excited states of s-tetrazine, which we have found, are the $2^{-1}A_g(n^2 \to \pi^{*2})$ state, which was also found by the authors of Ref. [17] (cf. the Supporting Information to Ref. [17]), and the $n^2 \to \pi^{*2}$ excitations of the $^1B_{3g}$, $^1B_{1g}$, and ${}^{1}B_{1u}$ symmetries that have not been considered before. As in the previously discussed $1^{-1}B_{3g}(n^2 \to \pi^{*2})$ state, the excitation energies for all of these doubly excited states lie quite high in the EOMCCSD spectrum. However, when triples are properly accounted for, using, for example, our δ -CR-EOMCC(2,3),D approach, we see a significant lowering of the EOMCCSD excitation energies. For example, for the $2^{-1}A_g(n^2 \to \pi^{*2})$ state found by the authors of Ref. [17], the more robust triples correction of the δ -CR-EOMCC(2,3),D type lowers the EOMCCSD energy of 11.47 eV to 5.04 eV. This result is in reasonable agreement with the CASPT2 excitation energy of 4.55 eV reported in the Supporting Information to Ref. [17], to which our aforementioned comments on the underestimation of excitation energies by CASPT2 still apply. For the ${}^1B_{3g}(n^2 \to \pi^{*2})$ two-electron transition that has not been considered before, the EOMCCSD excitation energy of 15.10 eV is lowered by almost 8 eV when the δ -CR-EOMCC(2,3),D method is employed, resulting in 7.31 eV, and for the remaining two doubly excited states of s-tetrazine, namely, ${}^{1}B_{1g}(n^{2} \to \pi^{*2})$ and ${}^{1}B_{1u}(n^{2} \to \pi^{*2})$, the δ -CR-EOMCC(2,3),D corrections to the EOMCCSD values of 14.31 and 15.04 eV, respectively, result in the final excitation energies of 7.96 and 8.07 eV, respectively. As discussed above, the δ -CR-EOMCC(2,3),D method has been demonstrated to provide an accurate description of the challenging electronically excited states dominated by two-electron transitions. Thus, we expect our δ -CR-EOMCC(2,3),D estimates for all five doubly excited states of s-tetrazine considered in this work to be reasonable, possibly serving as reference data in future benchmark studies.

3.4.2.5 Aldehydes and Ketones: Formaldehyde, Acetone, and p-Benzoquinone

While this subgroup is much smaller than the previous one, with only three molecules and thirteen one-electron excitations reported in Table I of Ref. [17], it is of interest, as we have found several additional excited states for it in the prescribed energy range, including three states of p-benzoquinone characterized in the Supporting Information to Ref. [17] (the $1^{-1}B_{2g}(n \to \pi^*)$, $2^{-1}B_{2g}(n \to \pi^*)$, and $1^{-1}B_{2u}(\pi \to \pi^*)$ states) and eleven other states that have not been considered before. Among the other states, two are dominated by $n, \pi \to \pi^{*2}$ two-electron transitions, which we elaborate on below. Comparing to the high-level iterative CC3 and EOMCCSDT-3 methods, we can see that the results of our δ -CR-EOMCC calculations for this group of molecules are in good agreement with the available CC3 [17] and EOMCCSDT-3 [22, 24] data. The MUE values characterizing the deviations of the δ -CR-EOMCC excitation energies from the CC3 and EOMCCSDT-3 results are in the 0.11 to 0.29 eV range. The corresponding MaxE values range from 0.32 to 0.52 eV, when the

 δ -CR-EOMCC energies are compared to CC3, and from 0.26 to 0.47 eV, when we replace CC3 by EOMCCSDT-3. Similar remarks apply to comparisons of the δ -CR-EOMCC excitation energies characterizing the thirteen states of formaldehyde, acetone, and p-benzoquinone listed in Table I of Ref. [17] with their CASPT2 and TBE-2 counterparts reported in Refs. [17, 21]. In this case, the MUE values characterizing the differences between the δ -CR-EOMCC and CASPT2 data are 0.16–0.24 eV. For the differences between the δ -CR-EOMCC and TBE-2 excitation energies, we obtain 0.14–0.18 eV. Once again, the corresponding MaxE values are somewhat higher, but the δ -CR-EOMCC(2,3),D approach reduces them to an acceptable level, especially when compared with CASPT2, where we obtain 0.34 eV. In comparing the δ -CR-EOMCC and TBE-2 excitation energies for formaldehyde, acetone, and p-benzoquinone, we treat one of the twelve states for which such comparison can be made, namely, the 2 ${}^1A_1(\pi \to \pi^*)$ state of acetone, differently than the remaining states. As explained in footnote r to Table 3.3 (cf., also, footnote q to Table 3.4), the TBE-2 value for the 2 $^1A_1(\pi \to \pi^*)$ state of acetone reported in Ref. [21] is a result of an incorrect assignment of the CC3/aug-cc-pVTZ root at 8.90 eV. Based on our δ -CR-EOMCC results for acetone, we think that the CC3/aug-cc-pVTZ root at 8.90 eV found in Ref. [21] corresponds to the ${}^{1}A_{1}(\pi \to \pi^{*}/n \to \sigma^{*})$ state of acetone, which has not been considered in the previous benchmark studies [17–25], not to the 2 ${}^{1}A_{1}(\pi \to \pi^{*})$ excitation. Indeed, we observe a virtually perfect agreement between our δ -CR-EOMCC excitation energies for the ${}^{1}A_{1}(\pi \rightarrow \pi)$ $\pi^*/n \to \sigma^*$) state of acetone, which range from 8.77 to 8.99 eV when the MP2/6-31G* geometry is employed, and the CC3/aug-cc-pVTZ value of 8.90 eV reported in Ref. [21].

We now move to the fourteen additional states of formaldehyde, acetone, and p-benzoquinone, which are not included in Table I of Ref. [17] and which we have found in our calculations. As already alluded to above, three of these additional states are the

 $1^{-1}B_{2g}(n \to \pi^*)$, $2^{-1}B_{2g}(n \to \pi^*)$, and $1^{-1}B_{2u}(\pi \to \pi^*)$ excitations in p-benzoquinone described in the Supporting Information to Ref. [17], where the authors characterized them using the CASPT2 approach. As shown in Table I, our best δ -CR-EOMCC(2,3),D results for these three predominantly singly excited states agree with the corresponding CASPT2 data reported in the Supporting Information to Ref. [17] to within ~ 0.3 –0.4 eV. We can view this as a good agreement given the fact that CASPT2 tends to underestimate excitation energies.

For the remaining eleven states that have not been considered before, we have to make the following two comments. The first one deals with the confusion regarding the 2 $^1A_1(\pi \to \pi^*)$ and ${}^{1}A_{1}(n \to \pi^{*})$ states of formaldehyde (see footnotes p and q in Table 3.3). The authors of Ref. [17] have interpreted the EOMCCSD and CC3 roots at 10.54 and 10.45 eV, respectively, as the 2 $^1A_1(\pi \to \pi^*)$ state, producing large discrepancies, of more than 1 eV, with the CASPT2 and TBE values reported in Ref. [17], of 9.31 and 9.3 eV, respectively, and the CC3/aug-cc-pVQZ value of 9.29 eV obtained in Ref. [21]. It is hard to understand such a discrepancy given the fact that all excited states of formaldehyde considered in Ref. [17] are almost pure single excitations. After thorough examination of the problem, we have found another EOMCCSD root of the ${}^{1}A_{1}$ symmetry at 9.77 eV, which results in the δ -CR-EOMCC values that range from 9.37 in the δ -CR-EOMCC(2,3),D case to 9.57 eV when the δ -CR-EOMCCSD(T),IA approach is employed, in very good agreement with the above CASPT2, TBE, and CC3 values, particularly when our best δ -CR-EOMCC(2,3),D result of 9.37 eV is considered. Thus, the new EOMCC root that we have found in this work must be the 2 $^1A_1(\pi \to \pi^*)$ state, whereas the 1A_1 state at 10.54 eV in the EOMCCSD calculations and at 10.45 eV in the CC3 calculations, interpreted in Ref. [17] as the 2 $^1A_1(\pi \to \pi^*)$ excitation, is the next state of the ${}^{1}A_{1}$ symmetry, designated in our Tables 3.3 and 3.4 as

$$^{1}A_{1}(n \rightarrow \pi^{*}).$$

Our second comment regarding the additional states of aldehydes and ketones found in this work deals with the ${}^{1}B_{3u}(n,\pi\to\pi^{*2})$ and ${}^{1}B_{2g}(n,\pi\to\pi^{*2})$ doubly excited states of p-benzoquinone. In analogy to the previously discussed two-electron transitions in stetrazine, these two challenging multi-reference states cannot be properly characterized by EOMCCSD. When our best δ -CR-EOMCC(2,3),D approach is used, we see the excitation energies of the ${}^{1}B_{3u}(n,\pi\to\pi^{*2})$ and ${}^{1}B_{2g}(n,\pi\to\pi^{*2})$ states of p-benzoquinone lower by about 5 eV compared to EOMCCSD, giving 6.70 and 6.92 eV, respectively. The energy lowering provided by the remaining three δ -CR-EOMCC approaches, particularly in the δ -CR-EOMCCSD(T),IA case, is not as large, but this is consistent with our earlier experiences with the δ -CR-EOMCC methods. It would be desirable to perform the full EOMCCSDT or active space EOMCCSDt calculations for p-benzoquinone to verify if our best δ -CR-EOMCC(2,3),D estimates of the vertical excitation energies of the ${}^{1}B_{3u}(n,\pi\to\pi^{*2})$ and ${}^{1}B_{2g}(n,\pi\to\pi^{*2})$ doubly excited states of p-benzoquinone are accurate.

3.4.2.6 Amides: Formamide, Acetamide, and Propanamide

Unlike in the previous group of aldehydes and ketones, all of the excited states of the three amides considered in this work, including nine states listed in Table I of Ref. [17] and four-teen additional states found in our calculations, but not considered in the prior benchmark studies [17–25], are dominated by one-electron transitions. As a result, there is a very good agreement between our δ -CR-EOMCC excitation energies and the previously published [17, 21, 22, 24] CASPT2, CC3, EOMCCSDT-3, and TBE-2 values for the subsets of nine (CASPT2, CC3), eight (EOMCCSDT-3), and six (TBE-2) states of formamide, acetamide, and propanamide, for which the latter data are available. Indeed, the MUE values

characterizing the deviations of the δ -CR-EOMCC excitation energies for the nine states of the three amides included in Table I of Ref. [17] from the corresponding CASPT2 data, reported in Ref. [17] as well, range from 0.25 to 0.30 eV, with the largest deviation (MaxE) of 0.56 eV observed when the δ -CR-EOMCCSD(T),IA and CASPT2 results are compared with each other. As in the case of the other molecular groups examined in this work, the δ -CR-EOMCC(2,3),D approach improves the agreement with CASPT2, reducing the above MaxE value of 0.56 eV to 0.35 eV. Similar remarks apply to a comparison of the δ -CR-EOMCC results with the available TBE-2 values [21]. In this case, the MUE values characterizing the differences between the δ -CR-EOMCC and TBE-2 data are 0.23–0.27 eV and, once again, the δ -CR-EOMCC(2,3),D approach produces the smallest MaxE value of 0.42 eV. The agreement between our δ -CR-EOMCC excitation energies for formamide, acetamide, and propanamide and the previously published reference values improves even further when the results of the δ -CR-EOMCC calculations are compared with the CC3 and EOMCCSDT-3 data reported in Refs. [17, 22, 24]. The MUE and MaxE values characterizing the differences between our δ -CR-EOMCC results and their CC3 counterparts reported in Ref. [17] are 0.08–0.16 and 0.14–0.27 eV, respectively. They are 0.05–0.24 and 0.12–0.28 eV, respectively, when the excitation energies obtained in the δ -CR-EOMCC and EOMCCSDT-3 calculations are compared with each other.

As has been the case with the other subgroups of molecules examined in this work, we have found several additional excited states of formamide, acetamide, and propanamide that have not been considered in the previous benchmark studies [17–25], with acetamide having the richest variation of the excitation types. Of the fourteen additional excited states we have found in the prescribed energy range, there are one $\pi \to \pi^*$ excitation in formamide (which we will further comment on below), two $n \to \pi^*$, three $n \to \sigma^*$, three $\pi \to \sigma^*$,

and one $\pi \to \pi^*/n \to \sigma^*$ excitations in acetamide, and one $n \to \pi^*$ and three $\pi \to \sigma^*$ excitations in propanamide. As already mentioned, all of these additional excited states are predominantly one-electron transitions. Thus, as in the case of the previously discussed nine states of formamide, acetamide, and propanamide considered in the prior benchmark studies [17–25], the triples corrections to the EOMCCSD excitation energies resulting from our δ -CR-EOMCC calculations for the fourteen additional states of the three amides found in this work are rather small (~ 0.1 –0.3 eV). Our best δ -CR-EOMCC(2,3),A and δ -CR-EOMCC(2,3),D values, in analogy to the aldehydes and ketones, agree almost perfectly, differing by ~ 0.05 eV. Thus, in the absence of other high-level CC/EOMCC results for the fourteen additional excited states of formamide, acetamide, and propanamide found in the present work, our δ -CR-EOMCC(2,3) excitation energies can be used as accurate reference data in future benchmark calculations or applications involving these three molecules.

The 2 $^1A'(\pi \to \pi^*)$ state of formamide considered in the previous benchmark work [17–23, 25] and the extra $^1A'(\pi \to \pi^*)$ state of the same molecule found in the present study require an additional comment. As explained in footnote s to Table 3.3, the authors of Ref. [17] have incorrectly assigned the EOMCCSD and CC3 roots at 8.52 (8.50 in our calculations) and 8.27 eV, respectively, to the $2\,^1A'(\pi \to \pi^*)$ transition, where the corresponding CASPT2, TBE-1, and TBE-2 values are 7.39, 7.39, and 7.35 eV, respectively. The $2\,^1A'(\pi \to \pi^*)$ state of formamide is an almost pure one-electron transition (REL = 1.096 when the MP2/6-31G* geometry is employed) and so differences between the CASPT2 and CC3 results on the order of 1 eV are unlikely. Our EOMCCSD calculations show that there is another root of the $^1A'$ symmetry and dominated by $\pi \to \pi^*$ excitations, designated in Tables 3.3 and 3.4 as $^1A'(\pi \to \pi^*)$ and located at 7.52 eV, which has the δ -CR-EOMCC excitation energies ranging from 7.09 to 7.31 eV, in excellent agreement with the above CASPT2 and TBE

values. We have, thus, reassigned the previously reported [17] EOMCCSD and CC3 roots at 8.52 (in our calculations, 8.50) and 8.27 eV, respectively, to the higher energy ${}^{1}A'(\pi \to \pi^{*})$ state, while interpreting the EOMCCSD root at 7.52 eV as the 2 ${}^{1}A'(\pi \to \pi^{*})$ state. The authors of Ref. [25] have found a CC3 root of formamide of ${}^{1}A'$ symmetry and $\pi \to \pi^{*}$ character at 7.24 eV, lending support to the above state reassignment.

3.4.2.7 Nucleobases: Cytosine, Uracil, Thymine, and Adenine

For this final group of molecules included in the database of Ref. [17], there are a total of 31 excited states listed in Table I of Ref. [17]. Our δ -CR-EOMCC calculations have also found two additional states in the prescribed energy range that have not been considered before (two $\pi \to \pi^*$ excitations in adenine). As shown in Tables 3.3 and 3.4, all of these states are dominated by one-electron transitions. The 31 states included in Table I of Ref. [17] have been characterized by CASPT2 and nineteen of them have been assigned the TBE values of the corresponding excitation energies [17, 21]. Due to prohibitive computational costs of the high-level iterative triples CC3 and EOMCCSDT-3 calculations, none of the initial benchmark studies [17–24] using the database of Ref. [17] have provided the CC3 and EOMCCSDT-3 data for nucleobases. The CC3 reference data for 22 of the 31 excitations of nucleobases listed in Table I of Ref. [17] have finally become available in Ref. [25]. All of this means that in assessing the performance of the δ -CR-EOMCC approaches in calculations for nucleobases, we are somewhat limited, although comparisons with the available CASPT2 [17], CC3 [25], and TBE [17, 21] data allow us to make some useful observations. Compared with the CASPT2 excitation energies for all 31 states included in Table I of Ref. [17], our δ -CR-EOMCC results are characterized by MUE values of 0.12–0.19 eV. As one might expect, the corresponding MaxE values are somewhat larger, but our best δ -CR-EOMCC(2,3) calculations bring them down to a ~ 0.4 eV level. Similar remarks apply to comparisons of δ -CR-EOMCC excitation energies with the available TBE-2 values, where the corresponding MUEs range from 0.14 to 0.22 eV and MaxEs from about 0.4 eV in the case of the δ -CR-EOMCC(2,3) calculations to ~ 0.7 –0.8 eV in the case of the δ -CR-EOMCCSD(T) data. For the 22 excitation energies of nucleobases computed at the CC3 level of theory [25], the MUE and MaxE values characterizing the differences between the δ -CR-EOMCC and CC3 data are 0.10–0.24 and 0.35–0.53 eV, respectively, with the smallest MaxE values provided by δ -CR-EOMCC(2,3) calculations. As in the case of the remaining 24 molecules included in the benchmark set of Ref. [17], it is encouraging to observe the very good agreement between our best δ -CR-EOMCC(2,3) calculations and the considerably more demanding CC3 computations.

3.5 Statistical Error Analysis for the Entire Benchmark Set

We now turn to the examination of the overall quality of the δ -CR-EOMCCSD(T),IA, δ -CR-EOMCCSD(T),ID, δ -CR-EOMCC(2,3),A, and δ -CR-EOMCC(2,3),D excitation energies obtained in this work, as compared to the previously published CASPT2 [17, 21], TBE-2 [21], CC3 [17, 25], and EOMCCSDT-3 [22, 24] data and the underlying EOMCCSD results, using a larger set of 148 singlet excited states of 28 molecules considered in this work, taken from Table I of Ref. [17], as a starting point for the corresponding statistical error evaluations. As explained in the beginning of Section 3.4.2, the list of 148 singlet excited states used to initiate the statistical error analyses discussed in this section has been obtained by excluding the doubly excited 1 ${}^{1}B_{3g}(n^{2} \to \pi^{*2})$ state of s-tetrazine, for which the CC3 and

EOMCCSDT-3 reference data are unavailable and the existing CASPT2 and TBE excitation energies reported in Refs. [17, 21] unreliable, from the 149 singlet excitations collected in Table I of Ref. [17]. As a result, the vast majority of states entering the statistical error analysis presented in this section are dominated by one-electron transitions, with only 45 out of the above 148 states having 1.1 < REL < 1.2, three states having $REL \ge 1.2$, and no state having REL greater than 1.225. As pointed out in Section 3.4.2, we have identified several additional states with significant contributions from double excitations, including, in addition to the above 1 $^1B_{3g}(n^2 \to \pi^{*2})$ state of s-tetrazine, six other states with REL close to 2 that can be found among the 54 extra roots outside the set of 149 states listed in Table I of Ref. [17] obtained in our EOMCC calculations, but none of these additional states can be considered in the overall error evaluation, since we do not have access to the appropriate high-level reference data which would allow us to assess performance of the δ -CR-EOMCC approaches in this case. On the basis of our past experiences with the δ -CR-EOMCC calculations [63–68, 74, 111, 149, 179, 182] and the previously discussed comparison of the δ -CR-EOMCC(2,3),D and NEVPT2 [23] results for the doubly excited 1 $^{1}B_{3g}(n^{2} \rightarrow \pi^{*2})$ state of s-tetrazine (cf. footnotes o and n to Tables 3.3 and 3.4, respectively), we may expect the results of our overall best δ -CR-EOMCC(2,3),D calculations for the excited states with REL close to 2 identified in this work to be accurate to within $\sim 0.2-0.3$ eV, but we would need to perform additional high-level EOMCCSDT/EOMCCSDt or multireference CI calculations, which are beyond the scope of the present study, to verify such a statement.

The results of our statistical error analyses involving various *ab initio* methods considered in this work and the 148 singlet excited states of 28 molecules taken from Table I of Ref. [17], as described above, or their appropriate subsets for which the relevant data are available,

as further elaborated on below, are summarized in Tables 3.5–3.8. Table 3.5 compares the MUE, MSE, and MaxE values characterizing the differences between the excitation energies obtained in our EOMCCSD and δ -CR-EOMCC calculations, the CC3 calculations reported in Refs. [17, 25], and the EOMCCSDT-3 calculations reported in Refs. [22, 24] from the corresponding CASPT2 data given in Ref. [17], with updates provided in Ref. [21]. Table 3.6 does the same for comparisons of the EOMCCSD, δ -CR-EOMCC, CC3, and EOMCCSDT-3 data with their TBE-2 counterparts taken from Ref. [21]. Tables 3.7 and 3.8 compare the MUE, MSE, and MaxE values characterizing the differences between the excitation energies resulting from our EOMCCSD and δ -CR-EOMCC calculations with the CC3 (Table 3.7) and EOMCCSDT-3 (Table 3.8) data reported in Refs. [17, 22, 24, 25]. To make sure that our statistical analyses of errors are as systematic and as fair as possible, we focus on the δ -CR-EOMCCSD(T),IA, δ -CR-EOMCCSD(T),ID, δ -CR-EOMCC(2,3),A, and δ -CR-EOMCC(2,3), D excitation energies, and their EOMCCSD counterparts summarized in Table 3.3, i.e., those obtained using the TZVP basis set and the MP2/6-31G* geometries, since the reference CASPT2, CC3, and EOMCCSDT-3 results reported in Refs. [17, 21, 24, 25] and collected in Table 3.3 as well have been obtained using the TZVP basis and the geometries resulting from the MP2/6-31G* optimizations.

Table 3.5: Statistical error analyses of the various CC/EOMCC data, including EOM-CCSD, δ -CR-EOMCCSD(T),IA (δ -CR(T),IA), δ -CR-EOMCCSD(T),ID (δ -CR(T),ID), δ -CR-EOMCC(2,3),A (δ -CR(2,3),A), δ -CR-EOMCC(2,3),D (δ -CR(2,3),D), CC3, and EOMCCSDT-3, from their CASPT2 counterparts.

	SD	δ -CR(T),IA	δ -CR(T),ID	δ -CR(2,3),A	δ -CR(2,3),D	CC3	SDT-3
-Count ^a	148	148	148	148	148	139	115
MSE^b	0.49	0.20	0.12	0.00	-0.06	0.18	0.28
MUE^b	0.50	0.24	0.21	0.17	0.18	0.20	0.29
$MaxE^b$	1.63	1.16	0.95	0.68	0.53	0.62	0.70

^a Total number of states considered.

Table 3.6: Statistical error analyses of the various CC/EOMCC data, including EOM-CCSD, δ -CR-EOMCCSD(T),IA (δ -CR(T),IA), δ -CR-EOMCCSD(T),ID (δ -CR(T),ID), δ -CR-EOMCC(2,3),A (δ -CR(2,3),A), δ -CR-EOMCC(2,3),D (δ -CR(2,3),D), CC3, and EOMCCSDT-3, from their TBE-2 counterparts.

	SD	δ -CR(T),IA	δ -CR(T),ID	δ -CR(2,3),A	δ -CR(2,3),D	CC3	SDT-3
Count^a	102	102	102	102	102	102	82
MSE^b	0.45	0.18	0.11	0.00	-0.07	0.19	0.27
MUE^b	0.45	0.22	0.19	0.19	0.19	0.20	0.27
$MaxE^b$	1.52	0.94	0.85	0.70	0.58	0.63	0.79

^a Total number of states considered.

^b Mean signed error (MSE), mean unsigned error (MUE), and maximum energy difference (MaxE) with respect to CASPT2 (in eV).

^b Mean signed error (MSE), mean unsigned error (MUE), and maximum energy difference (MaxE) with respect to TBE-2 (in eV).

Table 3.7: Statistical error analyses of the EOMCCSD, δ -CR-EOMCCSD(T),IA (δ -CR(T),IA), δ -CR-EOMCCSD(T),ID (δ -CR(T),ID), δ -CR-EOMCC(2,3),A (δ -CR(2,3),A), and δ -CR-EOMCC(2,3),D (δ -CR(2,3),D) data from their CC3 counterparts.

	SD	δ -CR(T),IA	δ -CR(T),ID	δ -CR(2,3),A	δ -CR(2,3),D
-Count ^a	139	139	139	139	139
MSE^b	0.30	0.01	-0.06	-0.17	-0.24
MUE^b	0.30	0.13	0.15	0.19	0.25
MaxE^b	1.28	0.81	0.60	0.44	0.54

^a Total number of states considered.

Table 3.8: Statistical error analyses of the EOMCCSD, δ-CR-EOMCCSD(T),IA (δ-CR(T),IA), δ-CR-EOMCCSD(T),ID (δ-CR(T),ID), δ-CR-EOMCC(2,3),A (δ-CR(2,3),A), and δ-CR-EOMCC(2,3),D (δ-CR(2,3),D) data from their EOMCCSDT-3 counterparts.

	SD	δ -CR(T),IA	δ -CR(T),ID	δ -CR(2,3),A	δ -CR(2,3),D
-Count ^a	115	115	115	115	115
MSE^b	0.22	-0.08	-0.15	-0.26	-0.33
MUE^b	0.22	0.14	0.18	0.26	0.33
$MaxE^b$	0.93	0.46	0.37	0.48	0.58

^a Total number of states considered.

^b Mean signed error (MSE), mean unsigned error (MUE), and maximum energy difference (MaxE) with respect to CC3 (in eV).

 $[^]b$ Mean signed error (MSE), mean unsigned error (MUE), and maximum energy difference (MaxE) with respect to EOMCCSDT-3 (in eV).

Clearly, our δ -CR-EOMCC excitation energies would change somewhat if we used basis sets larger than TZVP, but comparing the results obtained with various methods where different calculations use different basis sets would make our comparisons less systematic. The same applies to comparisons of vertical excitation energies using different ground-state geometries in different excited-state calculations, although comparing vertical excitation spectra at the ground-state geometries obtained with the same method as used in excited-state calculations for each of the ab initio approaches analyzed in this study would be interesting. As explained in Section 3.4.1 and as implied by Fig. 3.2 (or by a comparison of the results shown in Tables 3.3 and 3.4), the effect of ground-state geometries on the vertical excitation spectra resulting from the δ -CR-EOMCC calculations is generally very small and unlikely to have an effect on our main conclusions regarding performance of the δ -CR-EOMCC methods relative to other approaches, but the topic of nuclear geometries used in the various computations for the 28 molecules comprising the benchmark set of Ref. [17] is worth further exploration. The effect of the basis set on the δ -CR-EOMCC calculations summarized in Tables 3.3 and 3.4 is interesting too and we plan to examine it in the future work. We should also point out that while in the original benchmark set presented in Table I of Ref. [17] there are a total of 149 excited states, including the aforementioned 148 excitations that provide the basis for the statistical error analyses discussed in this section, we do not have access to all 148 vertical excitation energies for every approach providing the reference data for judging the δ -CR-EOMCC methods. Thus, in making comparisons of the δ -CR-EOMCC and CC3 results, we have to limit ourselves to the subset of 139 excited states, for which the CC3 results are available [17, 25]. When comparing the δ -CR-EOMCC and EOMCCSDT-3 excitation energies, we have to limit ourselves to the subset of 115 states, for which the EOMCCSDT-3 results are available [22, 24]. Comparisons of our δ -CR-EOMCC excitation energies with the corresponding TBE-2 values are limited to the subset of 102 states, for which the latter values are available [21]. The only comparison that can utilize all 148 excited states, obtained by excluding the 1 ${}^{1}B_{3g}(n^{2} \to \pi^{*2})$ state of s-tetrazine from the 149 states listed in Table I of Ref. [17], in determining the corresponding MUE, MSE, and MaxE values is that involving the δ -CR-EOMCC and CASPT2 approaches, where the relevant CASPT2 data can be found in Ref. [17], with updates provided in Ref. [21]. Information about the numbers of excited states included in the statistical error analyses involving various methods considered in this work can be found in Tables 3.5–3.8.

In addition to tables that summarize the overall MUE, MSE, and MaxE values characterizing the differences between the results of the various calculations, we present comparisons of the EOMCCSD and δ -CR-EOMCC excitation energies with their CASPT2, TBE-2, CC3, and EOMCCSDT-3 counterparts in the form of the correlation and error distribution plots shown in Figs. 3.3–3.26. The correlation plots shown in Figs. 3.3–3.7 compare the vertical excitation energies of the 148 singlet excited states of 28 molecules listed in Table I of Ref. [17], i.e., all excitations listed in Table I of Ref. [17] other than the doubly excited 1 $^1B_{3g}(n^2 \to \pi^{*2})$ state of s-tetrazine, which had to be excluded from our statistical error analyses, obtained in the EOMCCSD, δ -CR-EOMCCSD(T),IA, δ -CR-EOMCCSD(T),ID, δ -CR-EOMCC(2,3),A, and δ -CR-EOMCC(2,3),D calculations using the TZVP basis set and MP2/6-31G* geometries with the corresponding CASPT2 values taken from Ref. [17], with updates provided in Ref. [21]. The analogous plots presented in Figs. 3.8–3.12 compare the EOMCCSD/TZVP and δ -CR-EOMCC/TZVP excitation energies calculated at MP2/6-31G* geometries with the TBE-2 data for the subset of 102 states reported in Ref. [21]. Figures 3.13–3.17 compare the EOMCCSD/TZVP//MP2/6-31G* and δ -CR- $\rm EOMCC/TZVP//MP2/6-31G^*$ excitation energies with the corresponding $\rm CC3/TZVP//$

MP2/6-31G* results for the subset of 139 states that can be found in Refs. [17, 25]. The correlation plots shown in Figs. 3.18–3.22 compare the EOMCCSD and δ -CR-EOMCC excitation energies with the results of the EOMCCSDT-3 calculations, all using the TZVP basis set and MP2/6-31G* geometries, for the subset of 115 states reported in Refs. [22, 24]. In addition to the excitation energies and their scatter along the diagonal representing perfect agreement, each of the correlation plots shown in Figs. 3.3–3.22 provides information about the MUE, MSE, and MaxE values characterizing the pair of methods under consideration, the corresponding R^2 correlation coefficient, and the list of outlier states for which the absolute values of the differences between the excitation energies obtained in the two calculations compared in the plot exceed a particular threshold value. For the comparisons of the EOMCCSD and δ -CR-EOMCC excitation energies with their CASPT2 and TBE-2 counterparts, shown in Figs. 3.3–3.12, we have chosen a cutoff threshold of 0.75 eV to show the corresponding outlier states. When comparing the EOMCCSD and δ -CR-EOMCC excitation energies with the results of the CC3 and EOMCCSDT-3 calculations in Figs. 3.13–3.22, we have chosen a somewhat smaller cutoff threshold of 0.50 eV to display the outliers. The remaining Figs. 3.23–3.26 present the error distribution curves characterizing the deviations of the δ -CR-EOMCCSD(T),IA (Fig. 3.23), δ -CR-EOMCCSD(T),ID (Fig. 3.24), δ -CR-EOMCC(2,3), A (Fig. 3.25), and δ -CR-EOMCC(2,3), D (Fig. 3.26) excitation energies, calculated using the TZVP basis set and MP2/6-31G* geometries, from the available CASPT2/TZVP, CC3/TZVP, EOMCCSDT-3/TZVP, and TBE-2 data reported in Refs. [17, 21, 22, 24, 25].

Examining the error values in Tables 3.5–3.8 and the correlation plots shown in Figs. 3.3–3.22, we can immediately see that all four δ -CR-EOMCC approaches considered in this work provide significant improvements in the EOMCCSD excitation energies relative to the

CASPT2, TBE-2, CC3, and EOMCCSDT-3 data. In the case of comparisons with CASPT2 and TBE-2 (Tables 3.5 and 3.6 and Figs. 3.3–3.12), we see steady error decreases when going from EOMCCSD, through δ -CR-EOMCCSD(T),IA, δ -CR-EOMCCSD(T),ID, and δ -CR-EOMCC(2,3),A, to δ -CR-EOMCC(2,3),D, with the δ -CR-EOMCC(2,3),D approach providing the most accurate description which seems better than that provided by CC3 and EOMCCSDT-3, whereas comparisons with CC3 and EOMCCSDT-3 (Tables 3.7 and 3.8 and Figs. 3.13–3.22) indicate a more uniform performance of all four δ -CR-EOMCC methods, although, as further elaborated on below, one may also argue that the overall agreement with the CC3 and EOMCCSDT-3 data continues to be best in the case of the δ -CR-EOMCC(2,3) triples corrections. Let us discuss these observations some more, starting with comparisons of the various CC/EOMCC approaches with the CASPT2 and TBE-2 data.

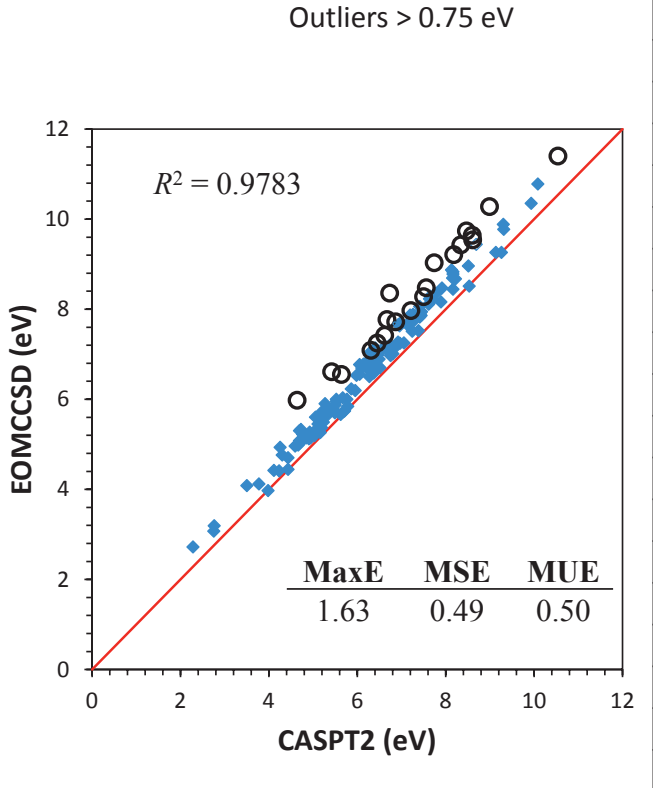
As shown in Table 3.5, the MUE, MSE, and MaxE values relative to CASPT2 decrease from 0.50, 0.49, and 1.63 eV, respectively, when the EOMCCSD results are considered, to 0.18, -0.06, and 0.53 eV, when the EOMCCSD excitation energies are corrected for triples using the δ -CR-EOMCC(2,3),D approach. Variant A of the δ -CR-EOMCC(2,3) method, which is characterized by the MUE, MSE, and MaxE values relative to CASPT2 of 0.17, 0.00, and 0.68 eV, respectively, is essentially equally accurate from the point of view of these three error measures, but the triples corrections of δ -CR-EOMCCSD(T),IA and δ -CR-EOMCCSD(T),ID, although offering significant improvements in the EOMCCSD results, are not as effective as their biorthogonal δ -CR-EOMCC(2,3) counterparts. This becomes particularly evident when the MSE and MaxE values relative to CASPT2 characterizing the various δ -CR-EOMCC approaches in Table 3.5 are examined. Similar improvements in the accuracy of the calculated excitation energies relative to CASPT2, when going from EOMCCSD, through δ -CR-EOMCCSD(T),IA, δ -CR-EOMCCSD(T),ID, and δ -CR-EOMCC(2,3),A, to

 δ -CR-EOMCC(2,3),D, can be seen when analyzing the correlation plots in Figs. 3.3–3.7. Indeed, we observe a systematic decrease in the number of the outlier states whose energies differ from the CASPT2 data by more than 0.75 eV, from 21 in the EOMCCSD case, to 5 and 2 in the case of the δ -CR-EOMCCSD(T),IA and δ -CR-EOMCCSD(T),ID calculations, respectively, and to the absence of such outlier states when the δ -CR-EOMCC(2,3), A and δ -CR-EOMCC(2,3),D approaches are considered. At the same time, one can see a steady increase in the R^2 correlation factor when going from EOMCCSD, through δ -CR-EOMCCSD(T),IA, δ -CR-EOMCCSD(T),ID, and δ -CR-EOMCC(2,3),A, to δ -CR-EOMCC(2,3),D, from 0.9783 when the EOMCCSD and CASPT2 excitation energies are compared to 0.9869 when we compare the δ -CR-EOMCC(2,3),D and CASPT2 data. The improvements in the EOMCCSD results offered by the non-iterative triples δ -CR-EOMCC(2,3),D correction are so substantial that one can regard them as competitive with the considerably more expensive iterative CC3 and EOMCCSDT-3 calculations. Indeed, as shown in Table 3.5, the MUE, MSE, and MaxE values relative to CASPT2 characterizing the δ -CR-EOMCC(2,3),D excitation energies are smaller than those characterizing the CC3 and EOMCCSDT-3 computations. This is especially true in the latter case, suggesting that the linear-response CC3 approach is somewhat more accurate than its EOMCC-based EOMCCSDT-3 analog, when both are compared to CASPT2, and that our δ -CR-EOMCC(2,3),D calculations are even more accurate. We would not be surprised by such a statement if our statistical error evaluation involved doubly excited states, since the MMCC-based CR-EOMCC approaches are generally more robust than the perturbative CC3 and EOMCCSDT-3 approximations in applications involving quasidegenerate excited states (cf., e.g., Refs. [63–67, 122]), but it is interesting to see that similar might be true when the excited states of interest are of a predominantly single excitation character.

One might, of course, argue that the CASPT2 approach itself is not accurate enough to make definitive claims regarding the relative accuracy of the CC3 and EOMCCSDT-3 vs δ -CR-EOMCC(2,3),D calculations. We can, however, compare the CC3, EOMCCSDT-3, and δ -CR-EOMCC(2,3),D results, and their EOMCCSD, δ -CR-EOMCCSD(T),IA, δ -CR-EOMCCSD(T), ID, and δ -CR-EOMCC(2,3), A counterparts with other sources of information about the electronic spectra of the 28 molecules constituting the database of Ref. [17], such as the TBE-2 data reported in Ref. [21]. As shown in Table 3.6, the MUE, MSE, and MaxE values relative to TBE-2 characterizing the δ -CR-EOMCC(2,3),D excitation energies, of 0.19, -0.07, and 0.58 eV, respectively, are once again smaller than those characterizing the CC3 and EOMCCSDT-3 calculations, especially in the latter case. At the same time, the MUE, MSE, and MaxE values relative to TBE-2 characterizing the δ -CR-EOMCC(2,3),D results are similar to those obtained with the δ -CR-EOMCC(2,3), A approach and smaller than their δ -CR-EOMCCSD(T),IA and δ -CR-EOMCCSD(T),ID counterparts, although all four δ -CR-EOMCC methods considered in this work offer significant improvements in the EOMCCSD results when compared to the TBE-2 data. Once again, similar improvements in the accuracy of the calculated excitation energies relative to their TBE-2 values reported in Ref. [21], when going from EOMCCSD, through δ -CR-EOMCCSD(T),IA, δ -CR-EOMCCSD(T),ID, and δ -CR-EOMCC(2,3),A, to δ -CR-EOMCC(2,3),D, are observed when Figs. 3.8–3.12 are examined. In analogy to Figs. 3.3–3.7, the number of the outlier states whose energies differ from the TBE-2 data by more than 0.75 eV reduces from 11 in the EOMCCSD case to 5 and 3, respectively, in the case of the δ -CR-EOMCCSD(T),IA and δ -CR-EOMCCSD(T),ID calculations, and to none when the δ -CR-EOMCC(2,3),A and δ -CR-EOMCC(2,3),D methods are considered. We also observe a systematic increase in the R^2 correlation factor when going from EOMCCSD, through δ -CR-EOMCCSD(T),IA, δ -CR-EOMCCSD(T),ID, and δ -CR-EOMCC(2,3),A, to δ -CR-EOMCC(2,3),D, from 0.9721 when one compares the EOMCCSD and TBE-2 excitation energies to 0.9797 when the δ -CR-EOMCC(2,3),D and TBE-2 data are compared.

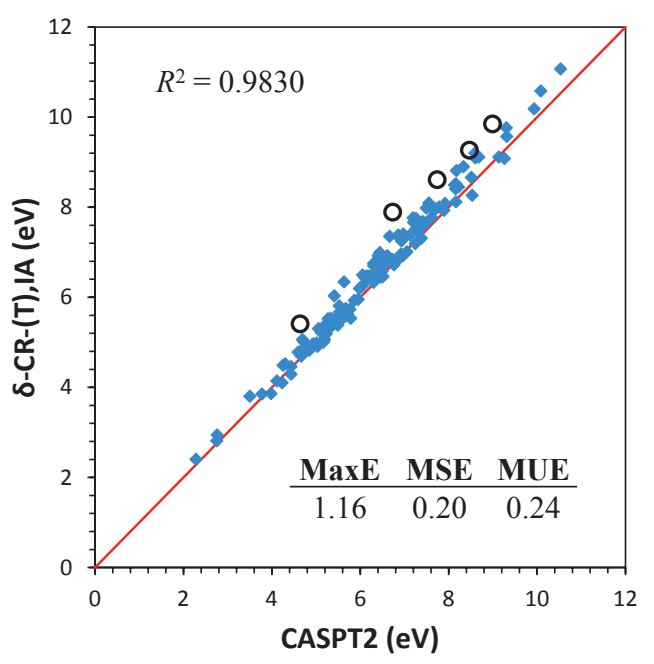
It is encouraging to observe the improvements in the overall accuracy of the EOMCCSD, CC3, and EOMCCSDT-3 calculations offered by the δ -CR-EOMCC(2,3),D approach, when compared to the CASPT2 and TBE-2 excitation energies, and the improvements in the accuracy of the EOMCCSD results by all four δ -CR-EOMCC methods examined in this dissertation, but one would also like to know how accurate the various non-iterative triples δ -CR-EOMCC corrections are when compared with their iterative CC3 and EOMCCSDT-3 counterparts. This is examined in Tables 3.7 and 3.8 and Figs. 3.13–3.26. The MUE and MSE values shown in Table 3.7 and the MUE, MSE, and MaxE values shown in Tables 3.8 may create an impression that the δ -CR-EOMCCSD(T),IA and δ -CR-EOMCCSD(T),ID approaches are somewhat more accurate, when compared to the CC3 and EOMCCSDT-3 results, than their biorthogonal δ -CR-EOMCC(2,3),A and δ -CR-EOMCC(2,3),D counterparts, but given the fact that the MUE and MSE values characterizing the average differences between the δ-CR-EOMCC and CC3/EOMCCSDT-3 excitation energies are all very small this might be a somewhat misleading conclusion. Indeed, when we look at the correlation plots in Figs. 3.13–3.17 we can see a fairly systematic decrease in the number of the outlier states whose energies differ from the CC3 data by more than 0.50 eV when going from EOMCCSD, through the δ -CR-EOMCCSD(T) approximations, to the δ -CR-EOMCC(2,3) approaches, from 18 in the EOMCCSD case, to 3 and 1 in the case of the δ -CR-EOMCCSD(T),IA and δ -CR-EOMCCSD(T),ID calculations, to none and 1 when the δ -CR-EOMCC(2,3),A and δ -CR-EOMCC(2,3), D excitation energies are considered. From the point of view of the outlier states, or, as shown in Table 3.7, the MaxE values obtained in the various δ -CR-EOMCC calculations, the δ -CR-EOMCC(2,3),A approach seems to reproduce the CC3 data most effectively, with variants ID and D of δ -CR-EOMCCSD(T) and δ -CR-EOMCC(2,3), respectively, falling slightly behind, but this is not necessarily the case when the R^2 correlation factors in Figs. 3.13–3.17 and the error distribution curves shown in Figs. 3.23–3.26 are inspected. Indeed, we observe a steady increase in the R^2 correlation factor when going from EOMCCSD, through δ -CR-EOMCCSD(T),IA, δ -CR-EOMCCSD(T),ID, and δ -CR-EOMCC(2,3),A, to δ -CR-EOMCC(2,3),D, from 0.9835 when the EOMCCSD and CC3 excitation energies are compared to 0.9866, 0.9879, 0.9902, and 0.9906 when the CC3 data are compared with their δ -CR-EOMCCSD(T),IA, δ -CR-EOMCCSD(T),ID, δ -CR-EOMCC(2,3),A, and δ -CR-EOMCC(2,3),D counterparts, respectively.

We can see the same systematic pattern when examining the error distribution curves shown in Figs. 3.23–3.26; the error distribution relative to the CC3 data becomes increasingly narrower as we go from EOMCCSD, through δ -CR-EOMCCSD(T),IA, δ -CR-EOMCCSD(T),ID, and δ -CR-EOMCC(2,3),A, to δ -CR-EOMCC(2,3),D. One might always argue that MUE and MSE values characterizing the overall deviations of the δ -CR-EOMCCSD(T),IA, δ -CR-EOMCCSD(T),ID, and δ -CR-EOMCC(2,3),A excitation energies from their CC3 counterparts, particularly those obtained in the δ -CR-EOMCCSD(T),IA and δ -CR-EOMCCSD(T),ID calculations, are smaller than the MUE and MSE values characterizing the δ -CR-EOMCC(2,3),D approach, but knowing that the error distribution relative to the CC3 data is narrowest in the δ -CR-EOMCC(2,3),D case and keeping in mind that the CC3 approach is not necessarily more accurate than the δ -CR-EOMCC(2,3),D method, especially when the excited states in question have some contributions from double excitations, makes us believe that the overall best approach among the four types of triples corrections to EOMCCSD excitation energies considered in this study is δ -CR-EOMCC(2,3),D, with



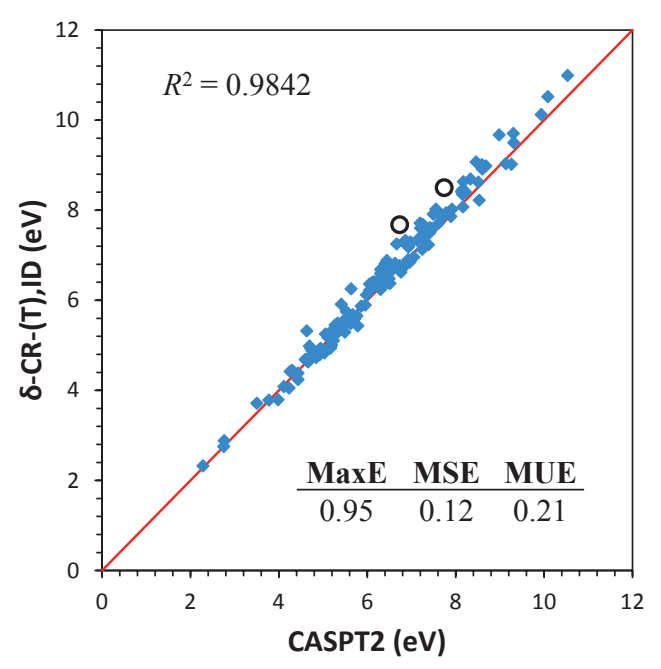
St	tate	CASPT2	EOMCCSD	REL
Butadiene	$2~^1A_g(\pi{\longrightarrow}~\pi^*)$	6.62	7.42	1.22
Hexatriene	$2^{-1}A_g(\pi \rightarrow \pi^*)$	5.42	6.61	1.23
Octatetraene	$2~^1A_g(\pi{\longrightarrow}~\pi^*)$	4.64	5.98	1.21
Benzene	$2 {}^{1}E_{2g}(\pi \rightarrow \pi^{*})$	8.18	9.21	1.17
Naphthalene	$3 {}^{1}A_{g}(\pi \rightarrow \pi^{*})$	6.67	7.77	1.15
Naphthalene	$3~^{1}\mathrm{B}_{3\mathrm{u}}(\pi{ ightarrow}\pi^{*})$	7.74	9.03	1.18
Pyridine	$3 {}^{1}\text{B}_{2}(\pi \rightarrow \pi^{*})$	8.60	9.64	1.17
Pyrazine	$1~^{1}\mathrm{B}_{3g}(\pi{\longrightarrow}~\pi^{*})$	8.47	9.74	1.18
Pyrazine	$2~^1A_g(\pi{\to}~\pi^*)$	8.61	9.54	1.16
Pyrimidine	$3 {}^{1}A_{1}(\pi \rightarrow \pi^{*})$	7.21	7.97	1.09
Pyridazine	$1 {}^{1}\text{B}_{2}(\pi \rightarrow \pi^{*})$	6.31	7.09	1.06
Triazine	$1 {}^{1}\mathrm{E}'(\pi \rightarrow \pi^*)$	7.50	8.28	1.08
Triazine	$2 {}^{1}\mathrm{E}'(\pi \rightarrow \pi^{*})$	8.99	10.28	1.16
Tetrazine	$2 {}^{1}B_{1g}(n \rightarrow \pi^{*})$	6.45	7.25	1.11
Tetrazine	$3 {}^{1}B_{1g}(n \rightarrow \pi^{*})$	6.73	8.36	1.16
Tetrazine	$2^{1}B_{3g}(\pi \rightarrow \pi^{*})$	8.34	9.43	1.17
Benzoquinone	$1 {}^{1}B_{3u}(n \rightarrow \pi^{*})$	5.64	6.55	1.12
Formamide	$3 {}^{1}\text{A}'(\pi \rightarrow \pi^*)$	10.54	11.40	1.10
Thymine	$3 ^1A''(n \rightarrow \pi^*)$	6.85	7.68	1.12
Adenine	$6^{1} A'(\pi \rightarrow \pi^*)$	6.87	7.72	1.10
Adenine	$7^{1}A'(\pi \rightarrow \pi^*)$	7.56	8.48	1.12

Figure 3.3: Correlation plot for the calculated singlet excited states: EOMCCSD/TZVP vs CASPT2/TZVP vertical excitation energies (in eV) at $MP2/6-31G^*$ geometries. The table on the right hand side shows the list of outliers, marked with open circles in the plot.



State		CASPT2	δ-CR-(T),IA	REL
Octatetraene	$2 {}^{1}A_{g}(\pi \rightarrow \pi^{*})$	4.64	5.41	1.21
Naphthalene	$3 {}^{1}B_{3u}(\pi \rightarrow \pi^{*})$	7.74	8.61	1.18
Pyrazine	$1 {}^{1}B_{3g}(\pi \rightarrow \pi^{*})$	8.47	9.27	1.18
Triazine	$2 ^{1}\text{E}'(\pi \rightarrow \pi^{*})$	8.99	9.85	1.16
Tetrazine	$3 {}^{1}B_{1g}(n \rightarrow \pi^{*})$	6.73	7.89	1.16

Figure 3.4: Correlation plot for the calculated singlet excited states: δ -CR-EOMCCSD(T),IA/TZVP (δ -CR-(T),IA) vs CASPT2/TZVP vertical excitation energies (in eV) at MP2/6-31G* geometries. The table on the right hand side shows the list of outliers, marked with open circles in the plot.



State	CASPT2	δ-CR-(T),ID	REL
Naphthalene $3 {}^{1}B_{3u}(\pi \rightarrow \pi^{*})$	7.74	8.50	1.18
Tetrazine $3 {}^{1}B_{1g}(n \rightarrow \pi^{*})$	6.73	7.68	1.16

Figure 3.5: Correlation plot for the calculated singlet excited states: δ -CR-EOMCCSD(T),ID/TZVP (δ -CR-(T),ID) vs CASPT2/TZVP vertical excitation energies (in eV) at MP2/6-31G* geometries. The table on the right hand side shows the list of outliers, marked with open circles in the plot.

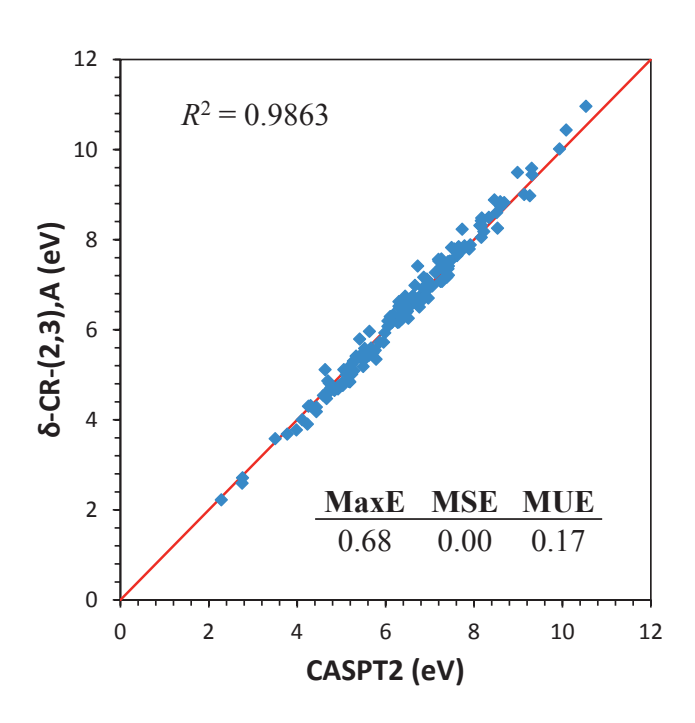


Figure 3.6: Correlation plot for the calculated singlet excited states: δ -CR-EOM CC(2,3),A/TZVP (δ -CR-(2,3),A) vs CASPT2/TZVP vertical excitation energies (in eV) at MP2/6-31G* geometries. The absence of the table on the right hand side indicates that there are no outliers.

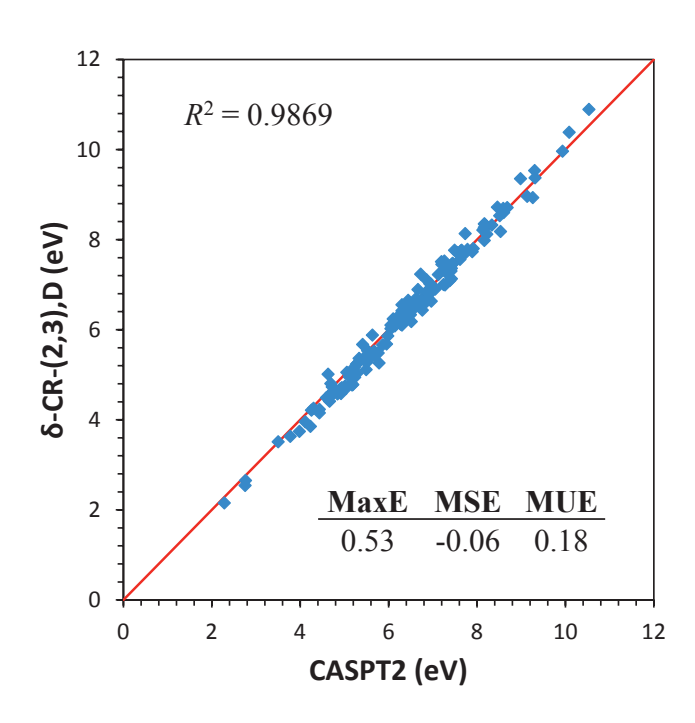
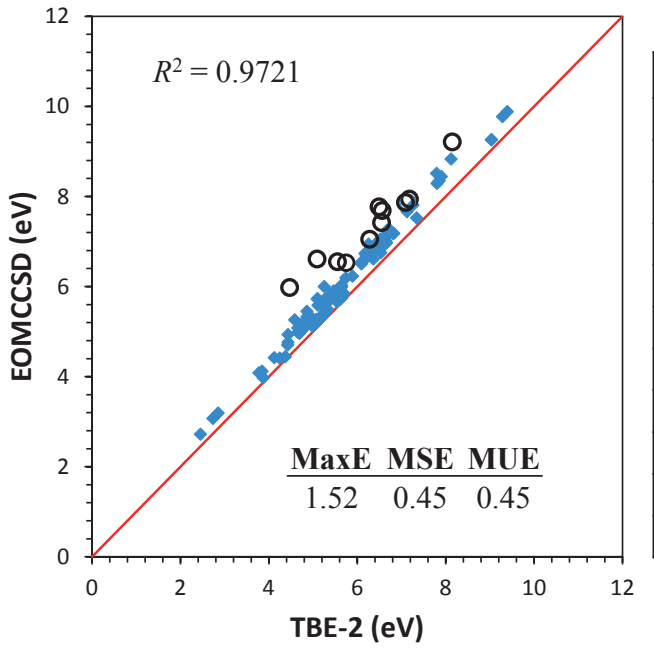
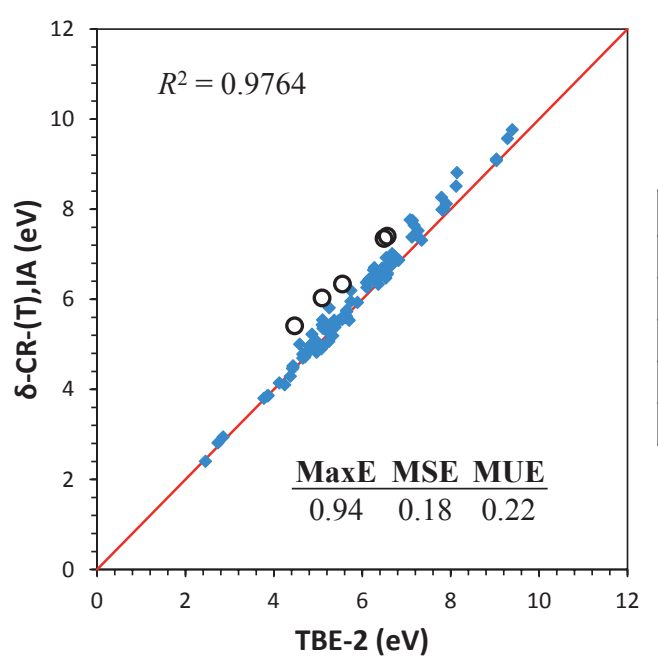


Figure 3.7: Correlation plot for the calculated singlet excited states: δ -CR-EOM CC(2,3),D/TZVP (δ -CR-(2,3),D) vs CASPT2/TZVP vertical excitation energies (in eV) at MP2/6-31G* geometries. The absence of the table on the right hand side indicates that there are no outliers.



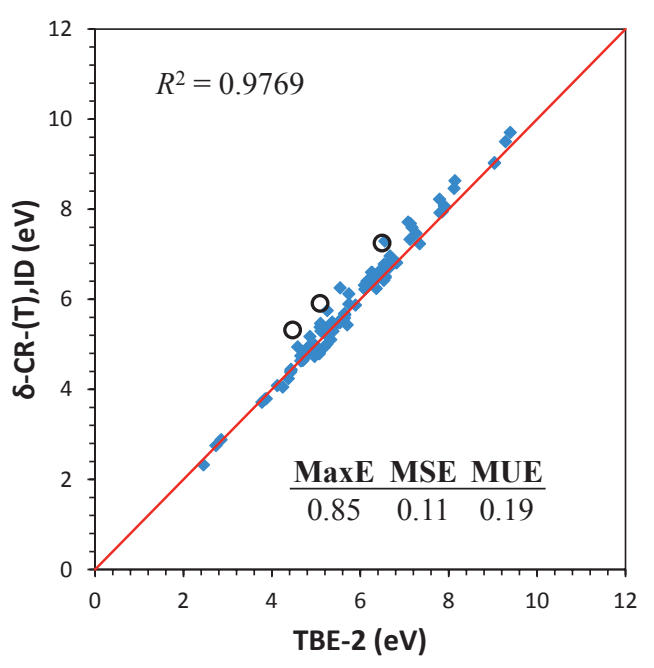
State		TBE-2	EOMCCSD	REL
Butadiene	$2 {}^{1}A_{g}(\pi \rightarrow \pi^{*})$	6.55	7.42	1.22
Hexatriene	$2^{-1}A_g(\pi \rightarrow \pi^*)$	5.09	6.61	1.23
Octatetraene	$2 {}^{1}A_{g}(\pi \rightarrow \pi^{*})$	4.47	5.98	1.21
Cyclopentadien	e 2 ${}^{1}A_{1}(\pi \rightarrow \pi^{*})$	6.28	7.05	1.15
Benzene	$2 {}^{1}E_{2g}(\pi \rightarrow \pi^{*})$	8.15	9.21	1.17
Naphthalene	$1 {}^{1}B_{1g}(\pi \rightarrow \pi^{*})$	5.75	6.53	1.11
Naphthalene	$3 {}^{1}A_{g}(\pi \rightarrow \pi^{*})$	6.49	7.77	1.15
Pyridine	$3 {}^{1}A_{1}(\pi \rightarrow \pi^{*})$	7.18	7.94	1.07
Benzoquinone	$1 {}^{1}B_{3u}(n \rightarrow \pi^{*})$	5.55	6.55	1.12
Propanamide	$2^{1}A'(\pi \rightarrow \pi^*)$	7.09	7.87	1.09
Uracil	$3 {}^{1}A''(n \rightarrow \pi^*)$	6.56	7.69	1.12

Figure 3.8: Correlation plot for the calculated singlet excited states: EOMCCSD/TZVP vertical excitation energies (in eV) at $MP2/6-31G^*$ geometries vs TBE-2 data. The table on the right hand side shows the list of outliers, marked with open circles in the plot.



State		TBE-2	δ-CR-(T),IA	REL
Hexatriene	$2 {}^{1}A_{g}(\pi \rightarrow \pi^{*})$	5.09	6.03	1.23
Octatetraene	$2^{1}A_{g}(\pi \rightarrow \pi^{*})$	4.47	5.41	1.21
Naphthalene	$3 {}^{1}\text{A}_{g}(\pi \rightarrow \pi^{*})$	6.49	7.35	1.15
Benzoquinone	$1 {}^{1}B_{3u}(n \rightarrow \pi^{*})$	5.55	6.34	1.12
Uracil	$3 ^1A''(n \rightarrow \pi^*)$	6.56	7.40	1.12

Figure 3.9: Correlation plot for the calculated singlet excited states: δ -CR-EOM CCSD(T),IA/TZVP vertical excitation energies (in eV) at MP2/6-31G* geometries (δ -CR-(T),IA) vs TBE-2 data. The table on the right hand side shows the list of outliers, marked with open circles in the plot.



S	tate	TBE-2	δ-CR-(T),ID	REL
Hexatriene	$2^{1}A_{g}(\pi \rightarrow \pi^{*})$	5.09	5.91	1.23
Octatetraene	$2 {}^{1}A_{g}(\pi \rightarrow \pi^{*})$	4.47	5.32	1.21
Naphthalene	$3 {}^{1}A_{g}(\pi \rightarrow \pi^{*})$	6.49	7.25	1.15

Figure 3.10: Correlation plot for the calculated singlet excited states: δ -CR-EOM CCSD(T),ID/TZVP vertical excitation energies (in eV) at MP2/6-31G* geometries (δ -CR-(T),ID) vs TBE-2 data. The table on the right hand side shows the list of outliers, marked with open circles in the plot.

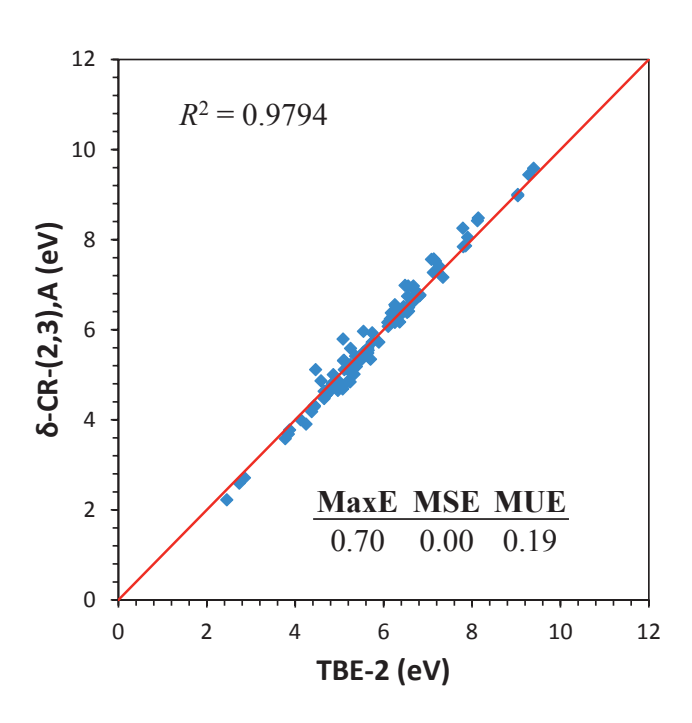


Figure 3.11: Correlation plot for the calculated singlet excited states: δ -CR-EOM CC(2,3),A/TZVP vertical excitation energies (in eV) at MP2/6-31G* geometries (δ -CR-(2,3),A) vs TBE-2 data. The absence of the table on the right hand side indicates that there are no outliers.

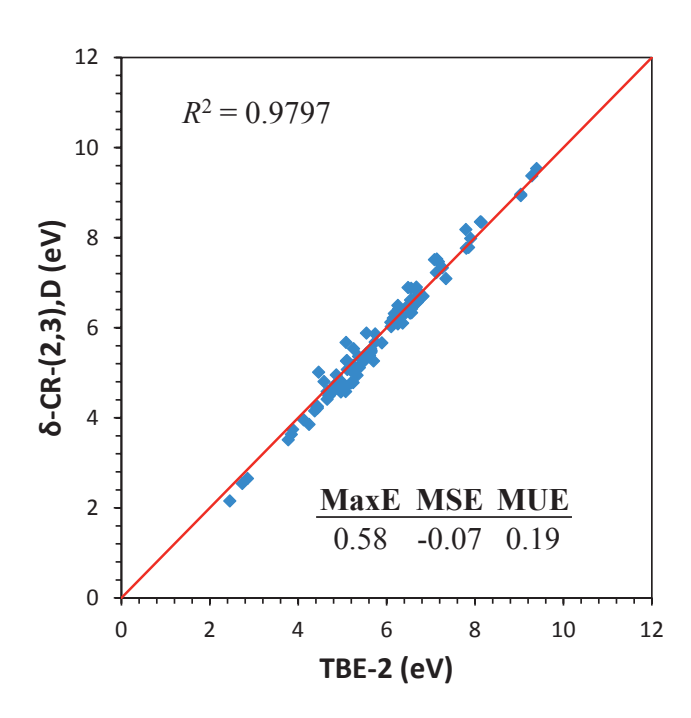
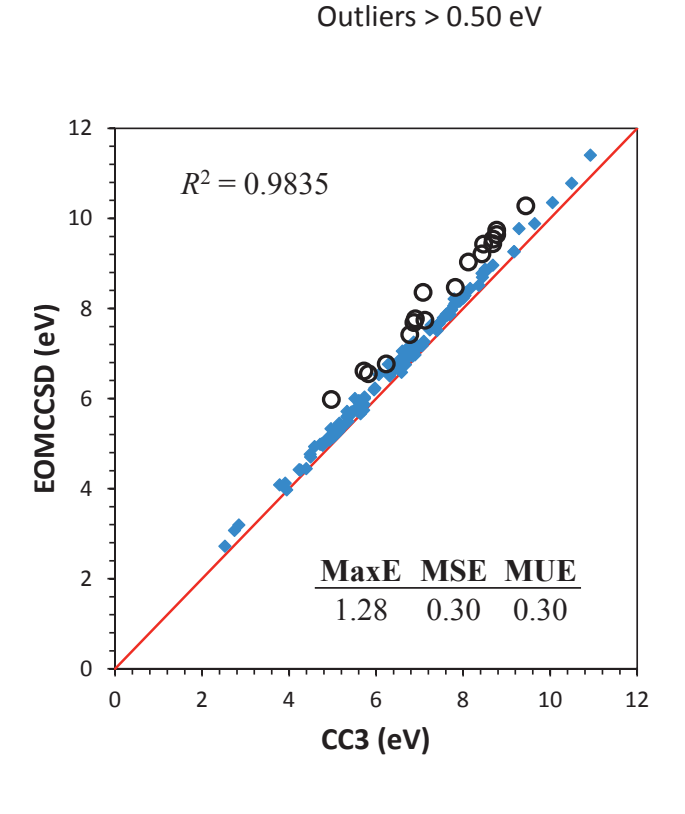
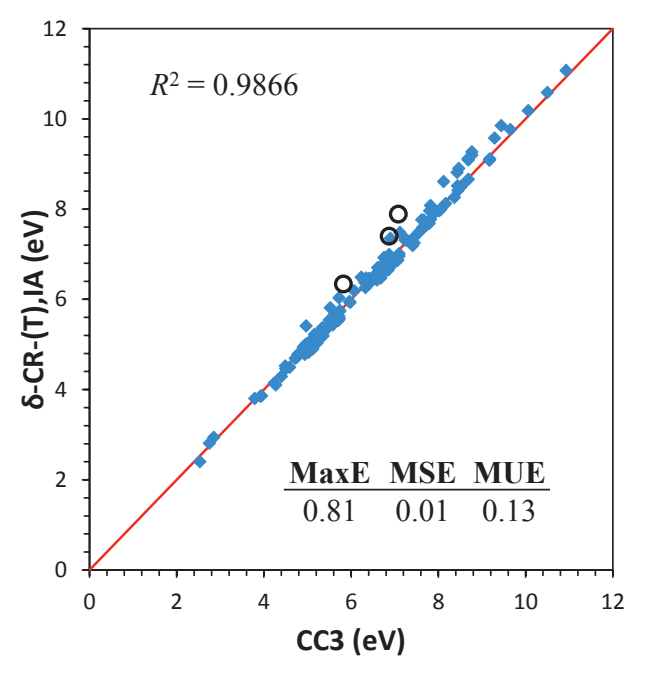


Figure 3.12: Correlation plot for the calculated singlet excited states: δ -CR-EOM CC(2,3),D/TZVP vertical excitation energies (in eV) at MP2/6-31G* geometries (δ -CR-(2,3),D) vs TBE-2 data. The absence of the table on the right hand side indicates that there are no outliers.



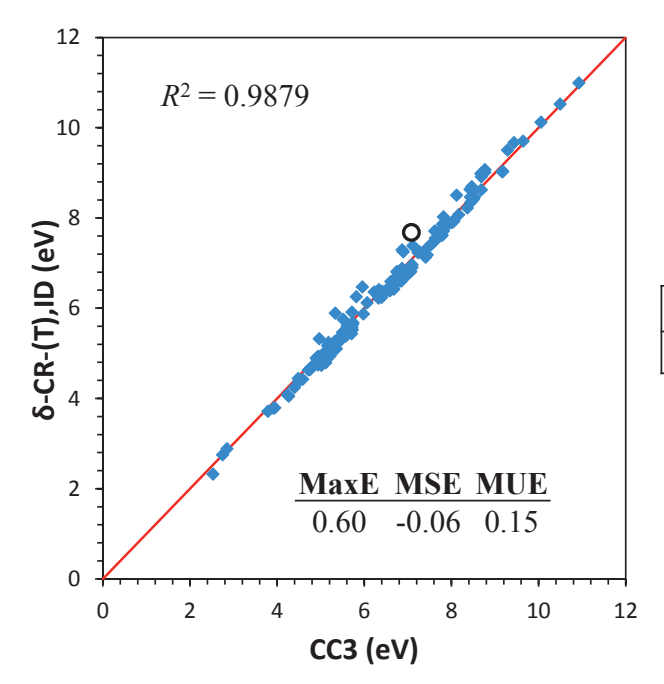
C+	ate	CC3	EOMCCSD	REL
31	ate	CC3	EOMICCSD	KEL
Butadiene	$2 {}^{1}A_{g}(\pi \rightarrow \pi^{*})$	6.77	7.42	1.22
Hexatriene	$2 {}^{1}A_{g}(\pi \rightarrow \pi^{*})$	5.72	6.61	1.23
Octatetraene	$2 {}^{1}A_{g}(\pi \rightarrow \pi^{*})$	4.97	5.98	1.21
Benzene	$2 {}^{1}E_{2g}(\pi \rightarrow \pi^{*})$	8.43	9.21	1.17
Naphthalene	$3 {}^{1}A_{g}(\pi \rightarrow \pi^{*})$	6.90	7.77	1.15
Naphthalene	$3 {}^{1}\mathrm{B}_{3\mathrm{u}}(\pi \rightarrow \pi^{*})$	8.12	9.03	1.18
Pyridine	$4 {}^{1}A_{1}(\pi \rightarrow \pi^{*})$	8.68	9.44	1.14
Pyridine	$3 {}^{1}\text{B}_{2}(\pi \rightarrow \pi^{*})$	8.77	9.64	1.17
Pyrazine	1 ${}^{1}B_{3g}(\pi \rightarrow \pi^{*})$	8.77	9.74	1.18
Pyrazine	$2 {}^{1}A_{g}(\pi \rightarrow \pi^{*})$	8.69	9.54	1.16
Triazine	$2 {}^{1}E'(\pi \rightarrow \pi^{*})$	9.44	10.28	1.16
Tetrazine	$2 {}^{1}B_{2g}(n \rightarrow \pi^{*})$	6.23	6.77	1.12
Tetrazine	$3 {}^{1}B_{1g}(n \rightarrow \pi^{*})$	7.08	8.36	1.16
Tetrazine	$2 {}^{1}B_{3g}(\pi \rightarrow \pi^{*})$	8.47	9.43	1.17
Benzoquinone	$1 {}^{1}B_{3u}(n \rightarrow \pi^{*})$	5.82	6.55	1.12
Benzoquinone	$2 {}^{1}B_{1u}(\pi \rightarrow \pi^{*})$	7.82	8.47	1.10
Uracil	$3 ^1A''(n \rightarrow \pi^*)$	6.87	7.69	1.12
Uracil	$4 {}^{1}A''(n \rightarrow \pi^*)$	7.12	7.74	1.11

Figure 3.13: Correlation plot for the calculated singlet excited states: EOMCCSD/TZVP vs CC3/TZVP vertical excitation energies (in eV) at MP2/6-31G* geometries. The table on the right hand side shows the list of outliers, marked with open circles in the plot.



State	ссз	δ-CR-(T),IA	REL
Tetrazine $3 {}^{1}B_{1g}(n \rightarrow \pi^{*})$	7.08	7.89	1.16
Benzoquinone $1 {}^{1}B_{3u}(n \rightarrow \pi^{*})$	5.82	6.34	1.12
Uracil $3^{-1}A''(n \rightarrow \pi^*)$	6.87	7.40	1.12

Figure 3.14: Correlation plot for the calculated singlet excited states: δ -CR-EOM CCSD(T),IA/TZVP (δ -CR-(T),IA) vs CC3/TZVP vertical excitation energies (in eV) at MP2/6-31G* geometries. The table on the right hand side shows the list of outliers, marked with open circles in the plot.



State		ссз	δ-CR-(T),ID	REL
Tetrazine	$3 {}^{1}\mathrm{B}_{1g}(\mathrm{n} \rightarrow \pi^{*})$	7.08	7.68	1.16

Figure 3.15: Correlation plot for the calculated singlet excited states: δ -CR-EOM CCSD(T),ID/TZVP (δ -CR-(T),ID) vs CC3/TZVP vertical excitation energies (in eV) at MP2/6-31G* geometries. The table on the right hand side shows the list of outliers, marked with open circles in the plot.

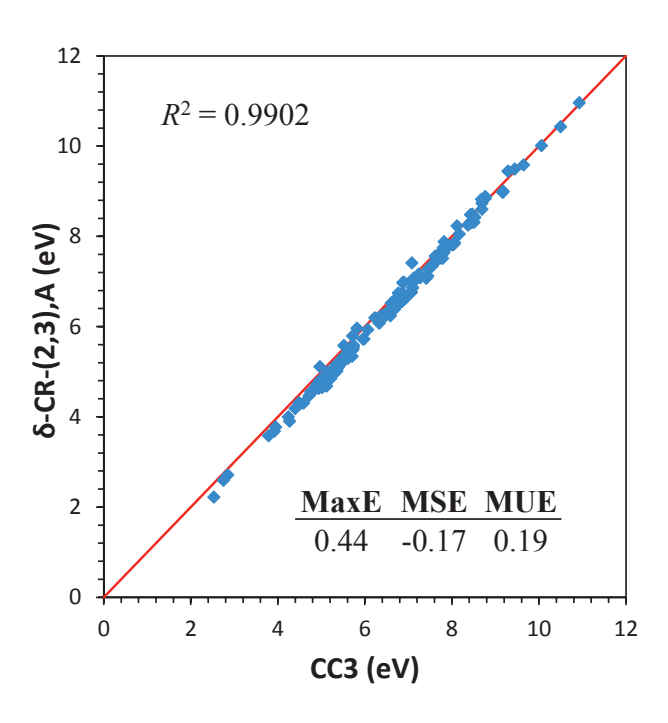
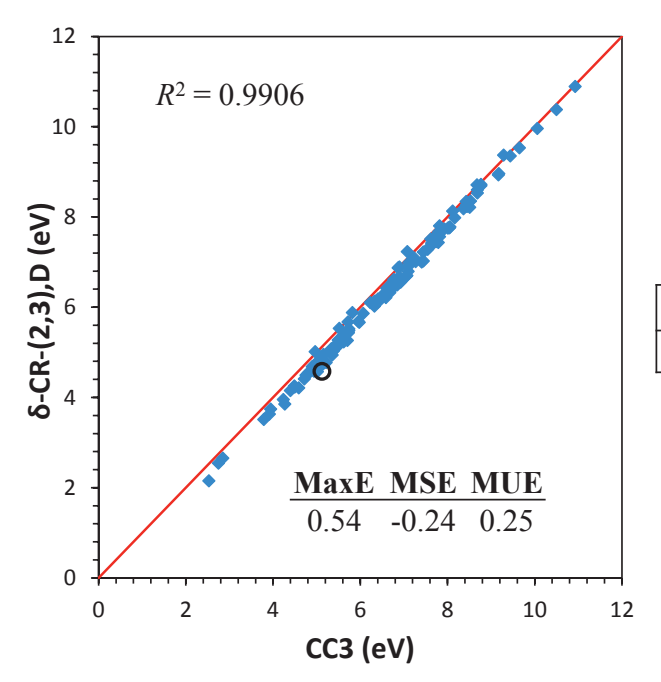
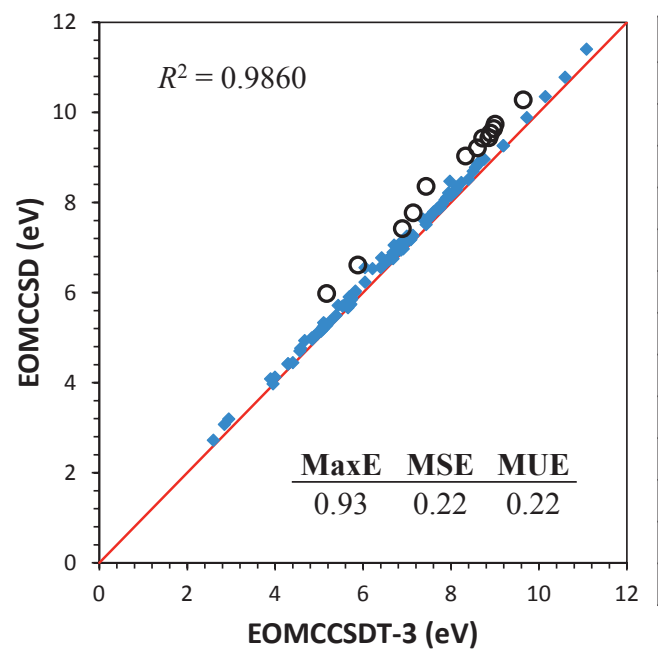


Figure 3.16: Correlation plot for the calculated singlet excited states: δ -CR-EOM CC(2,3),A/TZVP (δ -CR-(2,3),A) vs CC3/TZVP vertical excitation energies (in eV) at MP2/6-31G* geometries. The absence of the table on the right hand side indicates that there are no outliers.



State	ссз	δ-CR-(2,3),D	REL
Tetrazine 1 ${}^{1}B_{2u}(\pi \rightarrow \pi^{*})$	5.12	4.58	1.11

Figure 3.17: Correlation plot for the calculated singlet excited states: δ -CR-EOM CC(2,3),D/TZVP (δ -CR-(2,3),D) vs CC3/TZVP vertical excitation energies (in eV) at MP2/6-31G* geometries. The table on the right hand side shows the list of outliers, marked with open circles in the plot.



State		EOMCCSDT-3	EOMCCSD	REL
Butadiene	$2 {}^{1}A_{g}(\pi \rightarrow \pi^{*})$	6.89	7.42	1.22
Hexatriene	$2 {}^{1}A_{g}(\pi \rightarrow \pi^{*})$	5.88	6.61	1.23
Octatetraene	$2^{1}A_{g}(\pi \rightarrow \pi^{*})$	5.17	5.98	1.21
Benzene	$2 {}^{1}\text{E}_{2g}(\pi \rightarrow \pi^{*})$	8.60	9.21	1.17
Naphthalene	$3 {}^{1}A_{g}(\pi \rightarrow \pi^{*})$	7.14	7.77	1.15
Naphthalene	$3 {}^{1}\mathrm{B}_{3\mathrm{u}}(\pi \rightarrow \pi^{*})$	8.33	9.03	1.18
Pyridine	$4^{1}A_{1}(\pi \rightarrow \pi^{*})$	8.86	9.44	1.14
Pyridine	$3~^{1}\mathrm{B}_{2}(\pi \rightarrow \pi^{*})$	8.97	9.64	1.17
Pyrazine	$1~^{1}\mathrm{B}_{3g}(\pi{\longrightarrow}~\pi^{*})$	9.00	9.74	1.18
Pyrazine	$2 {}^{1}A_{g}(\pi \rightarrow \pi^{*})$	8.90	9.54	1.16
Triazine	$2 ^{1}\text{E}'(\pi \rightarrow \pi^{*})$	9.64	10.28	1.16
Tetrazine	$3 {}^{1}B_{1g}(n \rightarrow \pi^{*})$	7.43	8.36	1.16
Tetrazine	$2 {}^{1}\mathrm{B}_{3g}(\pi \rightarrow \pi^{*})$	8.72	9.43	1.17

Figure 3.18: Correlation plot for the calculated singlet excited states: EOMCCSD/TZVP vs EOMCCSDT-3/TZVP vertical excitation energies (in eV) at MP2/6-31G* geometries. The table on the right hand side shows the list of outliers, marked with open circles in the plot.

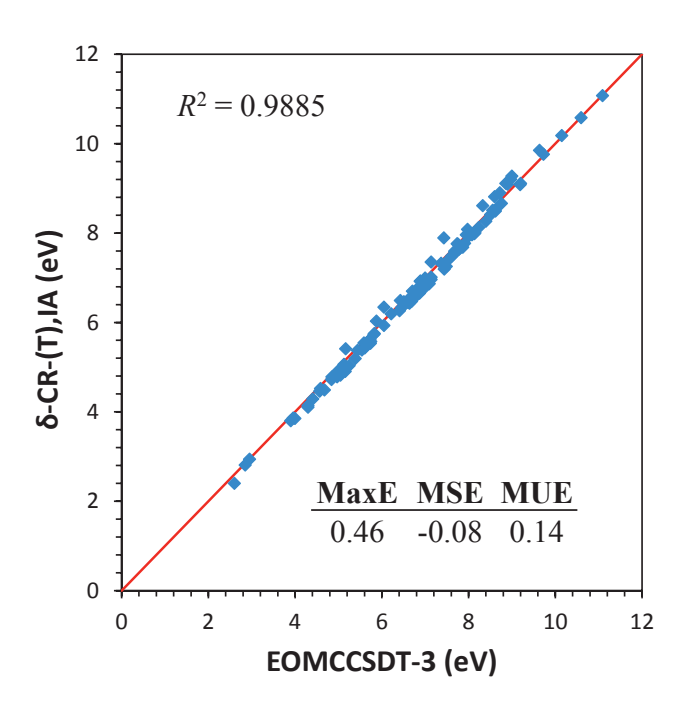


Figure 3.19: Correlation plot for the calculated singlet excited states: δ -CR-EOM CCSD(T),IA/TZVP (δ -CR-(T),IA) vs EOMCCSDT-3/TZVP vertical excitation energies (in eV) at MP2/6-31G* geometries. The absence of the table on the right hand side indicates that there are no outliers.

Outliers > 0.50 eV

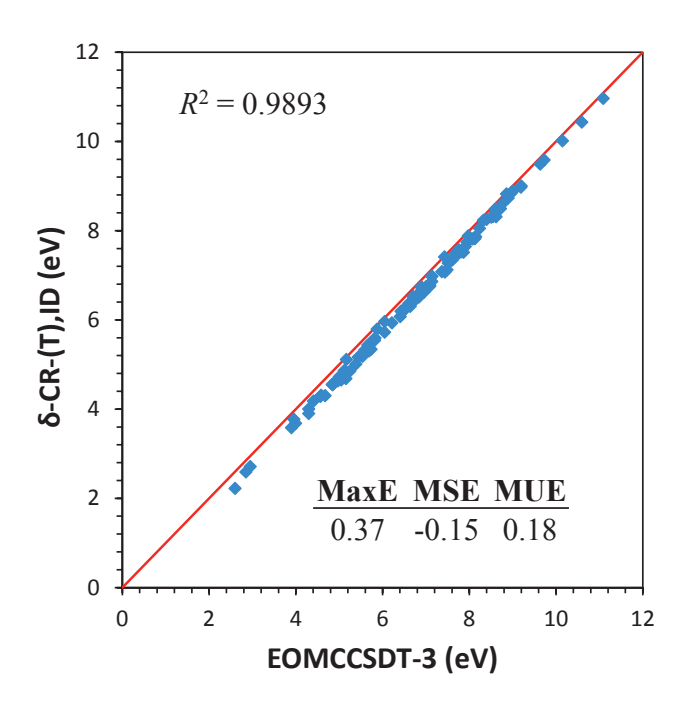


Figure 3.20: Correlation plot for the calculated singlet excited states: δ -CR-EOM CCSD(T),ID/TZVP (δ -CR-(T),ID) vs EOMCCSDT-3/TZVP vertical excitation energies (in eV) at MP2/6-31G* geometries. The absence of the table on the right hand side indicates that there are no outliers.

Outliers > 0.50 eV

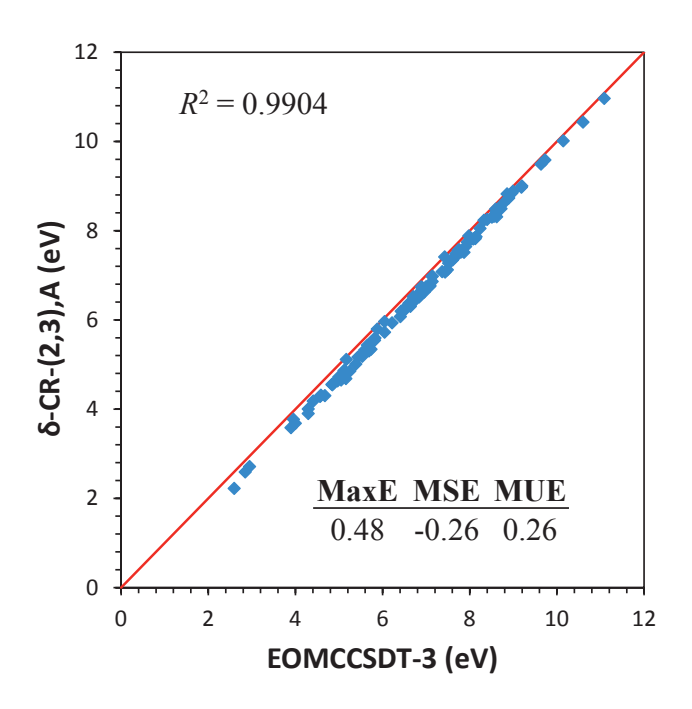
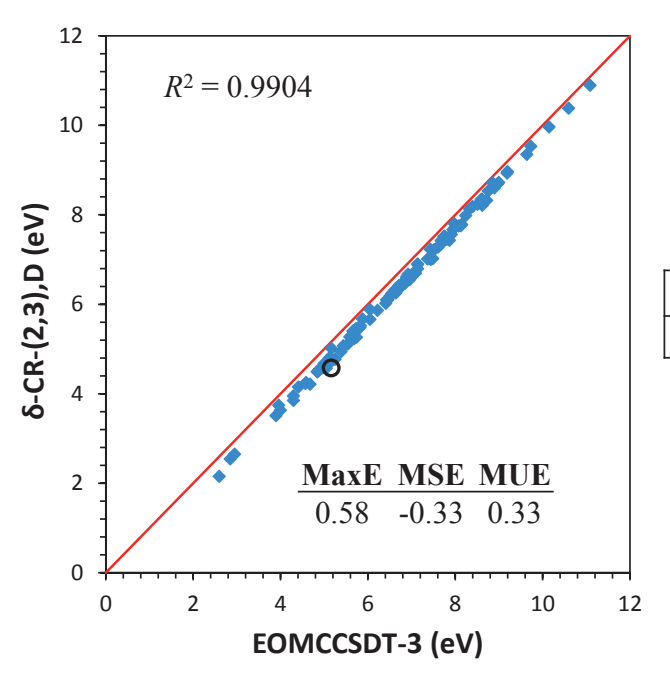


Figure 3.21: Correlation plot for the calculated singlet excited states: δ -CR-EOM CC(2,3),A/TZVP (δ -CR-(2,3),A) vs EOMCCSDT-3/TZVP vertical excitation energies (in eV) at MP2/6-31G* geometries. The absence of the table on the right hand side indicates that there are no outliers.

Outliers > 0.50 eV



	State	EOMCCSDT-3	δ-CR-(2,3),D	REL
Tetrazine	$1~^{1}\mathrm{B}_{2\mathrm{u}}(\pi{\to}\pi^{*})$	5.16	4.58	1.11

Figure 3.22: Correlation plot for the calculated singlet excited states: δ -CR-EOM CC(2,3),D/TZVP (δ -CR-(2,3),D) vs EOMCCSDT-3/TZVP vertical excitation energies (in eV) at MP2/6-31G* geometries. The table on the right hand side shows the list of outliers, marked with open circles in the plot.

variant A of δ -CR-EOMCC(2,3) offering a similar performance as long as the excited states of interest are not dominated by two-electron transitions, which is the case here. As already alluded to above, using the 1 $^{1}B_{3g}(n^{2} \to \pi^{*2})$ state of s-tetrazine as an example, and as shown in our past work [67, 68], variants D of the CR-EOMCC(2,3) and δ -CR-EOMCC(2,3) methodologies are generally more robust than other CR-EOMCC/ δ -CR-EOMCC corrections when the doubly excited states are considered.

Most of the above remarks related to statistical comparisons of the δ -CR-EOMCC and CC3 excitation energies apply to the analogous comparisons of the δ -CR-EOMCC and EOMCCSDT-3 data. With the cutoff threshold of 0.50 eV used in the examination of the EOMCCSD and δ -CR-EOMCC vs CC3 and EOMCCSDT-3 results, we cannot say as much about the relative performance of the various non-iterative triples δ -CR-EOMCC corrections relative to EOMCCSDT-3 as in the case of the analogous comparisons with CC3, since all four corrections work equally well, producing no outliers, but we continue to observe a steady increase in the R^2 correlation factor when going from EOMCCSD, through δ -CR-EOMCCSD(T),IA, δ -CR-EOMCCSD(T),ID, and δ -CR-EOMCC(2,3),A, to δ -CR-EOMCC(2,3),D, from 0.9860 when the EOMCCSD and EOMCCSDT-3 excitation energies are compared to 0.9885, 0.9893, 0.9904, and 0.9904 when we compare the EOMCCSDT-3 data with their δ -CR-EOMCCSD(T),IA, δ -CR-EOMCCSD(T),ID, δ -CR-EOMCC(2,3),A, and δ -CR-EOMCC(2,3),D counterparts, respectively. This is reflected in the error distribution curves shown in Figs. 3.23–3.26, where we can see that the error distribution relative to the EOMCCSDT-3 data becomes increasingly narrower as we go from EOMCCSD, through δ -CR-EOMCCSD(T),IA, δ -CR-EOMCCSD(T),ID, and δ -CR-EOMCC(2,3),A, to δ -CR-EOMCC(2,3),D. Once again, based on the MUE and MSE values collected in Table 3.8, one might argue that δ -CR-EOMCCSD(T),IA and δ -CR-EOMCCSD(T),ID approaches are more effective in reproducing the EOMCCSDT-3 results than their biorthogonal δ -CR-EOMCC(2,3),A and δ -CR-EOMCC(2,3),D counterparts, but knowing that the error distribution relative to the excitation energies obtained in the EOMCCSDT-3 calculations is narrowest in the δ -CR-EOMCC(2,3),D case and keeping in mind that the EOMCCSDT-3 method is not necessarily more accurate than the δ -CR-EOMCC(2,3),D approach, particularly when the excited states in question have some contributions from double excitations, reinforces our belief that the overall best approach among the four types of triples corrections to EOMCCSD excitation energies investigated in this work is δ -CR-EOMCC(2,3),D, with δ -CR-EOMCC(2,3),A offering similar accuracies as long as the excited states of interest are not dominated by two-electron transitions.

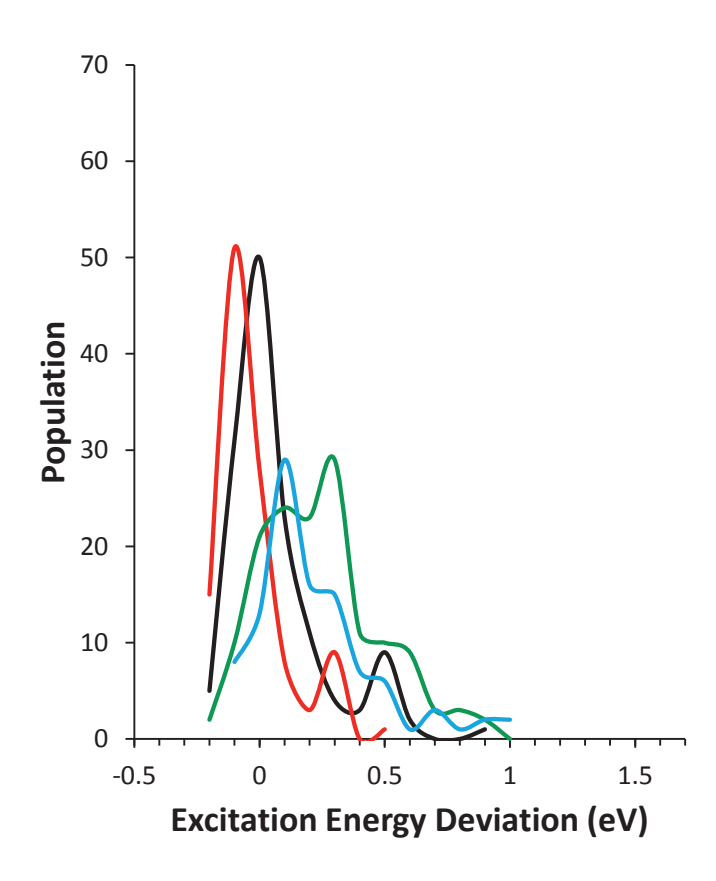


Figure 3.23: Normal distribution curves for the deviation of the δ -CR-EOMCCSD(T),IA excitation energies at MP2/6-31G* geometries from the CASPT2/TZVP (green), CC3/TZVP (black), EOMCCSDT-3/TZVP (red) and TBE-2 (blue) results.

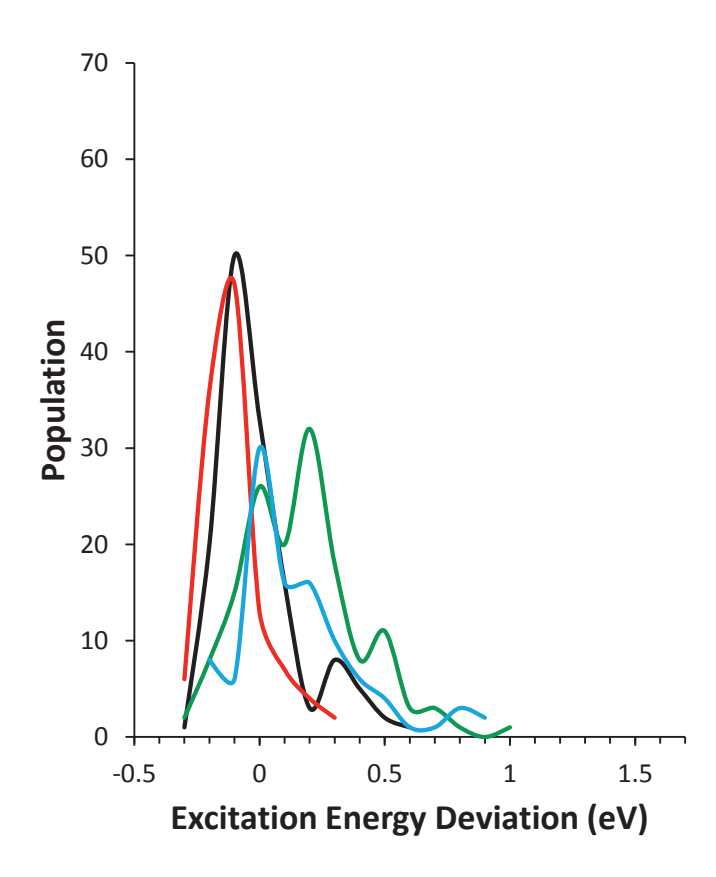


Figure 3.24: Normal distribution curves for the deviation of the δ -CR-EOMCCSD(T),ID excitation energies at MP2/6-31G* geometries from the CASPT2/TZVP (green), CC3/TZVP (black), EOMCCSDT-3/TZVP (red) and TBE-2 (blue) results.

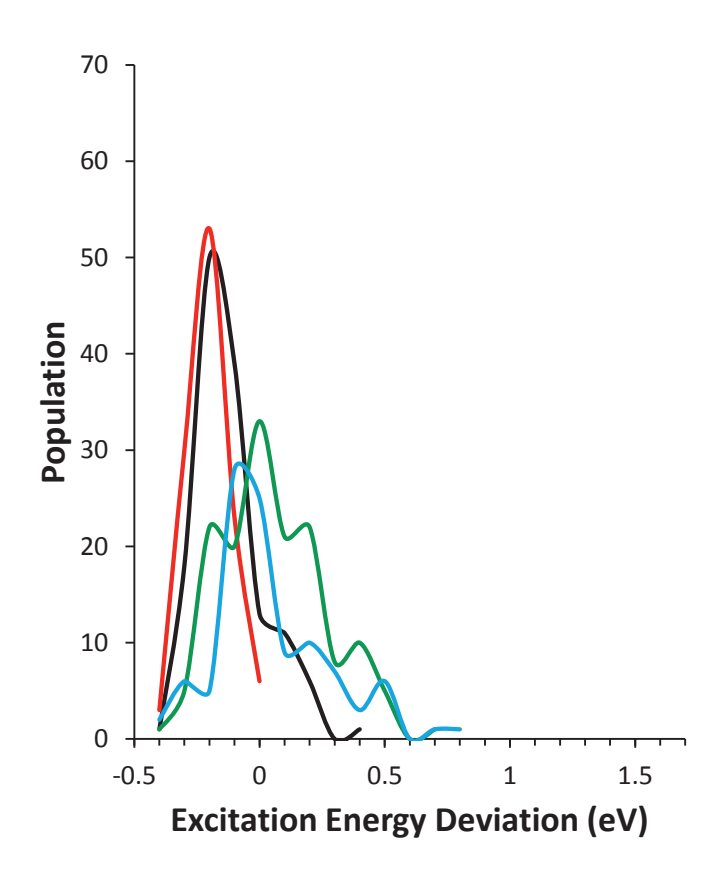


Figure 3.25: Normal distribution curves for the deviation of the δ -CR-EOMCC(2,3),A excitation energies at MP2/6-31G* geometries from the CASPT2/TZVP (green), CC3/TZVP (black), EOMCCSDT-3/TZVP (red) and TBE-2 (blue) results.

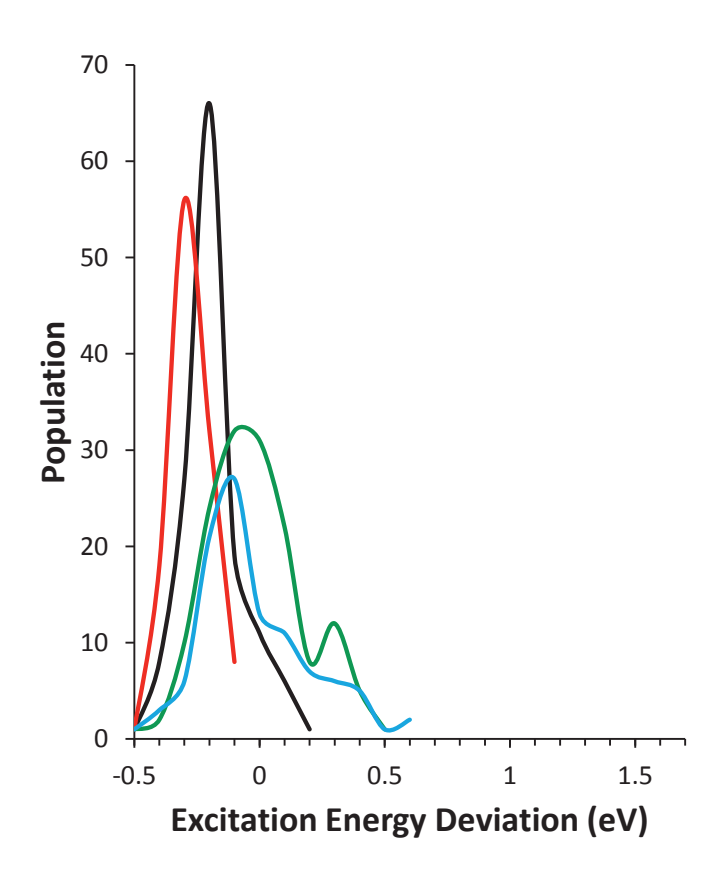


Figure 3.26: Normal distribution curves for the deviation of δ -CR-EOMCC(2,3),D excitation energies at MP2/6-31G* geometries from the CASPT2/TZVP (green), CC3/TZVP (black), EOMCCSDT-3/TZVP (red) and TBE-2 (blue) results.

3.6 Conclusions

We have used a comprehensive test set of 148 singlet excited states of 28 medium-size organic molecules taken from Ref. [17] to benchmark two variants of the approximately size-intensive CR-EOMCC method with singles, doubles, and non-iterative triples, abbreviated as δ -CR-EOMCCSD(T),IA and δ -CR-EOMCCSD(T),ID [63], derived from the MMCC formalism [65, 68, 122, 125–129], and the analogous two variants of the rigorously size-intensive δ -CR-EOMCC(2,3) approach, designated as δ -CR-EOMCC(2,3),A and δ -CR-EOMCC(2,3),D, respectively [69], based on the generalization of the biorthogonal MMCC formalism [127–129] to excited states [67, 122–124], against the previously published CASPT2 [17, 21], TBE [17, 21] (especially, TBE-2 [21]), CC3 [17, 25] and EOMCCSDT-3 [22, 24] results. The list of 148 singlet excited states used to initiate the various statistical error analyses reported in this study has been obtained by excluding the doubly excited 1 $^1B_{3g}(n^2 \to \pi^{*2})$ state of s-tetrazine, for which the CC3 and EOMCCSDT-3 reference data are unavailable and the existing CASPT2 and TBE excitation energies reported in Refs. [17, 21] unreliable, from the 149 singlet excitations collected in Table I of Ref. [17]. We have, however, determined the δ -CR-EOMCCSD(T),IA, δ -CR-EOMCCSD(T),ID, δ -CR-EOMCC(2,3),A, and δ -CR-EOMCC(2,3),D vertical excitation energies, as well as their EOMCCSD counterparts, for all 149 excited states listed in Table I of Ref. [17], along with the 54 additional excitations. All of the δ -CR-EOMCC calculations performed in this work and the underlying EOMCCSD computations were performed using the TZVP basis set used in the previous studies [17– 20, 22–25] and two sets of the ground-state nuclear geometries, including the MP2/6-31G* geometries taken from Ref. [17] and the CR-CC(2,3),D geometries obtained in this work, were used to determine the EOMCCSD, δ -CR-EOMCCSD(T),IA, δ -CR-EOMCCSD(T),ID, δ -CR-EOMCC(2,3),A, and δ -CR-EOMCC(2,3),D vertical excitation spectra.

 δ -CR-EOMCCSD(T),IA, δ -CR-EOMCCSD(T),ID. δ -CR-By comparing our EOMCC(2,3),A, and δ -CR-EOMCC(2,3),D excitation energies for the 148 excited states of 28 molecules taken from Table I of Ref. [17], as described above, or their appropriate subsets for which the relevant reference CASPT2, TBE-2, CC3, and EOMCCSDT-3 data are available, we have shown that the non-iterative triples corrections to the EOMCCSD excitation energies defining the relatively inexpensive, single-reference, black-box δ -CR-EOMCC approaches provide significant improvements in the EOMCCSD data, while closely matching the results of the iterative and considerably more expensive CC3 and EOMCCSDT-3 calculations and their CASPT2 and TBE counterparts, typically to within $\sim 0.1-0.2$ eV, i.e., to within intrinsic errors of the CC3, EOMCCSDT-3, CASPT2, and TBE estimates. We have also demonstrated that the δ -CR-EOMCC methods, especially the most robust δ -CR-EOMCC(2,3),D approach that works well for singly as well as doubly excited states, are capable of bringing the results of the CC3 and EOMCCSDT-3 calculations to a closer agreement with the CASPT2 and TBE data, demonstrating the utility of the cost effective δ -CR-EOMCC methods in applications involving molecular electronic spectra. This has allowed us to conclude that the overall best balanced approach among the four types of triples corrections to EOMCCSD excitation energies investigated in this work is δ -CR-EOMCC(2,3),D, with δ -CR-EOMCC(2,3),A offering similar accuracies as long as the excited states of interest are not dominated by two-electron transitions. We have reached these conclusions by performing a variety of full and partial statistical error analyses and examining the suitably designed correlation and error distribution plots.

We have also used the four δ -CR-EOMCC approaches considered in this study to identify and accurately characterize 54 additional singlet excited states in the energy range covered by

Table I of Ref. [17], including five states that can be found in the Supporting Information to Ref. [17] and 49 states that have not been considered in the earlier benchmark work [17–25], which can be used in future benchmark studies. The aforementioned 1 $^1B_{3g}(n^2 \to \pi^{*2})$ state of s-tetrazine, listed in Table I of Ref. [17], which could not be used in our overall statistical error analyses due to the absence of the reliable benchmark data to judge our δ -CR-EOMCC results, and six other states among the 54 states outside the set of 149 states listed in Table I of Ref. [17] are almost pure two-electron transitions, which many quantum chemistry methods have problems with, but we have provided arguments, based on the successful track record involving various CR-EOMCC or δ -CR-EOMCC calculations, including quasi-degenerate excited states dominated by double excitations [63–68, 74, 111, 149, 152, 155, 162, 179, 182] and the comparison of our best δ -CR-EOMCC(2,3),D excitation energies for the 1 $^1B_{3g}(n^2 \rightarrow$ π^{*2}) state of s-tetrazine with the recently published NEVPT2 data [23], that our δ -CR-EOMCC calculations for the doubly excited states found in this work and other additional states that have not been considered in the prior work [17–25] are accurate to within \sim 0.2-0.3 eV. We have suggested full EOMCCSDT, active-space EOMCCSDt, or accurate multi-reference CI calculations for all of the additional excited states found in our calculations to verify if our assessment of the accuracy of the δ -CR-EOMCC calculations for these extra states is correct.

In summary, we have identified the δ -CR-EOMCC(2,3) methodology, especially its δ -CR-EOMCC(2,3),D variant, as a useful and, at the same time, rigorously size-intensive approach for the routine and highly accurate calculations of molecular electronic spectra, even when the excited states of interest have more substantial two-electron contributions, with the δ -CR-EOMCC(2,3),A approximation offering an equally good description as long as the excited states of interest are dominated by one-electron transitions.

Chapter 4

Economical Doubly Electron-Attached

Equation-of-Motion

Coupled-Cluster Methods with an

Active-Space Treatment of

3-particle—1-hole and 4-particle—2-hole

Excitations

The second part of this dissertation is concerned with the development and application of economical DEA-EOMCC approximations that have emerged following our group's initial implementation of the full DEA-EOMCC(3p-1h) and DEA-EOMCC(4p-2h) methods and the active-space DEA-EOMCC(4p-2h) approach, in which 4p-2h terms are treated using active orbitals [92, 93]. We begin by reviewing fundamental elements of the DEA-EOMCC theory defining the existing full DEA-EOMCC(3p-1h) and full and active-space DEA-EOMCC(4p-2h) approaches introduced prior to my method development work [92, 93]. Then, we discuss the new generation of DEA-EOMCC approaches truncated at either 4p-2h

or 3p-1h excitations, where both 3p-1h and 4p-2h terms are treated using active orbitals, resulting in major savings in the computational effort compared to their all-orbital counterparts. In addition to the discussion of the key equations, details of computer codes, and examples of CPU timings, we present the results of the various DEA-EOMCC calculations, including methods developed in this thesis project, focusing on the determination of electronic spectra of diradicals, especially their singlet-triplet gaps, and one example of single bond breaking where the DEA-EOMCC approaches can be useful too. Much of our discussion is tied up to our original work published in Refs. [94] and [117].

4.1 Background Information and Motivation

Quantum chemistry methods based on the exponential wave function ansatz [198, 199] of single-reference CC theory [34–37, 200, 201] and their extensions to excited states and properties other than energy exploiting the EOM [48–50, 118, 119] and linear response [38–42, 120, 121, 202] frameworks have witnessed considerable success in a wide range of molecular applications (cf., e.g., Refs. [203] and [204] for selected reviews). As pointed out in the Introduction, this includes extensions of the EOMCC formalism to open-shell systems obtained by adding electron(s) to or removing electron(s) from the corresponding closed-shell cores via the EA [75–81] or IP [59–62, 77, 79–85] methodologies, their linear response [205] and SAC-CI [96, 206–208] counterparts, and their multiply attached/ionized generalizations, such as the DEA- and DIP-EOMCC schemes [53, 86–94] or the EOMCC approach to triple electron attachment [209]. There is growing interest in the EA/IP-EOMCC, DEA/DIP-EOMCC, and similar approaches, as a way to handle ground and excited states of open-shell species around closed shells, such as radicals and diradicals, since they offer

several advantages over the conventional particle-conserving CC/EOMCC treatments that rely on the spin-integrated, but not spin-adapted, spin-orbital formulation employing the unrestricted or restricted open-shell references. The EA- and IP-EOMCC methods and their multiply electron-attached and multiply ionized extensions, in which one diagonalizes the similarity-transformed Hamiltonian of the CC theory obtained in the calculations for the reference closed-shell system in the appropriate sector of the Fock space corresponding to the open-shell species of interest, provide a rigorously spin-adapted description, while offering a potential of being very accurate when suitable approximations, including those developed in this work are applied.

Recently, our group has developed high-level variants of the DEA- and DIP-EOMCC approaches with up to 4p-2h and 4h-2p excitations, abbreviated as DEA-EOMCC(4p-2h) and DIP-EOMCC(4h-2p), respectively, and their less expensive active-space counterparts, designated as DEA-EOMCC(4p-2h) $\{N_u\}$ and DIP-EOMCC(4h-2p) $\{N_o\}$, where N_u and N_o indicate the numbers of active unoccupied and active occupied orbitals used to select the corresponding 4p-2h and 4h-2p contributions, as promising new ways to describe multireference systems having two electrons outside the corresponding closed-shell cores [92, 93]. The active-space DEA-EOMCC(4p-2h) $\{N_u\}$ and DIP-EOMCC(4h-2p) $\{N_o\}$ approaches of Refs. [92] and [93] have been shown to be highly successful in challenging test cases involving single bond breaking in closed-shell molecules leading to doublet dissociation fragments and electronic spectra of diradicals, producing excellent results when compared to full CI or experiment, independent of the type of molecular orbitals (MOs) employed in the calculations, and almost perfectly reproducing the parent full DEA-EOMCC(4p-2h) and DIP-EOMCC(4h-2p) data at the fraction of the computer cost. Unfortunately, even with the help of active orbitals to select the dominant 4p-2h excitations, calculations at the DEA-EOMCC(4p-2h) level remain quite expensive, especially when larger basis sets have to be employed. This has prompted our interest in investigating new types of approximations to the existing active-space DEA-EOMCC(4p-2h) $\{N_u\}$ and full DEA-EOMCC(4p-2h) methods [92, 93], with the goal of developing more economical and cost-effective approaches [94] that can reduce the computer effort further without sacrificing high accuracy the DEA-EOMCC(4p-2h)-level theories offer. This work reports my contributions to this area.

To appreciate the new DEA-EOMCC methods proposed and tested in this work, and the advantages they offer compared to the existing schemes in this category, we first examine the computer costs of the high-level DEA-EOMCC(4p-2h) calculations. The most expensive CPU steps of the DEA-EOMCC(4p-2h) computations with a full treatment of 3p-1h and 4p-2h contributions scale as $n_o^2 n_u^6$ or \mathcal{N}^8 (see Refs. [92] and [93]). As a result, the DEA-EOMCC(4p-2h) approach, although highly accurate in applications involving single bond breaking in closed-shell molecules and diradical electronic spectra [92, 93], is usually prohibitively expensive (for the examples of timings, see Section II.B of Ref. [92]). The active-space analog of the DEA-EOMCC(4p-2h) method, designated as DEA- $\mathrm{EOMCC}(4p\text{-}2h)\{N_u\}$, which uses a subset of N_u unoccupied orbitals to select the dominant 4p-2h excitations, developed in Refs. [92] and [93] reduces the most expensive $n_o^2 n_u^6$ steps of the full DEA-EOMCC(4p-2h) approach to a considerably more manageable $N_u^2 n_o^2 n_u^4$ or $\sim \mathcal{N}^6$ level, which is equivalent to costs of the standard EOMCCSD calculations or costs of the ground-state CCSD computations times a relatively small prefactor if $N_u \ll n_u$, but does not solve the problem in its entirety. Indeed, although the resulting activespace DEA-EOMCC(4p-2h) $\{N_u\}$ approach offers substantial savings in the computer effort compared to its full DEA-EOMCC(4p-2h) parent without loss of accuracy [92, 93], the DEA-EOMCC(4p-2h) $\{N_u\}$ calculations remain expensive when larger basis sets are employed. This is due to the fact that in the existing implementation of the active-space DEA-EOMCC(4p-2h){ N_u } method described in Refs. [92] and [93] the lower-rank 3p-1h components are still treated fully using all orbitals in the basis set, and this becomes a serious problem in applications using larger bases, since computer costs associated with 3p-1h contributions can be high too. Indeed, the full treatment of 3p-1h excitations within the DEA-EOMCC framework requires CPU steps that scale as $n_o n_u^5$, which can be as demanding as or, in some cases, more time consuming than the $N_u^2 n_o^2 n_u^4$ steps of the DEA-EOMCC(4p-2h){ N_u } method associated with 4p-2h terms, especially when n_u becomes larger, since typical values of N_u and n_o are much smaller than n_u . Clearly, the same analysis applies to the lower-level DEA-EOMCC(3p-1h) approach [53, 86, 88, 89, 92, 93], in which the electron-attaching operator of the DEA-EOMCC formalism is truncated at 3p-1h component. The DEA-EOMCC(3p-1h) calculations, in which 4p-2h contributions are neglected, can be quite expensive too due to the $n_o n_u^5$ steps resulting from a full treatment of 3p-1h excitations.

There clearly is a need to address the above concerns if we want the DEA-EOMCC methodology, especially its presently highest DEA-EOMCC(4p-2h) level, to be more widely exploited in molecular applications. It is, therefore, essential that the expensive CPU steps of the $n_o n_u^5$ and $n_o^2 n_u^6$ types, which originate from the presence of 3p-1h and 4p-2h components in the DEA-EOMCC wave function expansions, are replaced by steps that are considerably more manageable. The previous DEA-EOMCC(4p-2h) $\{N_u\}$ method described in Refs. [92] and [93] addresses this issue, but only partly, since it focuses on 4p-2h excitations without doing anything about their 3p-1h counterparts, which lead to high costs too if treated fully.

abbreviated as DEA-EOMCC(3p-1h) $\{N_u\}$ and DEA-EOMCC(3p-1h,4p-2h) $\{N_u\}$. In analogy to the DEA-EOMCC(4p-2h){ N_u } and DIP-EOMCC(4h-2p){ N_o } methods of Refs. [92] and [93] and their active-space CC [98–109], EOMCC [71, 72, 110–112, 114], and EA/IP-EOMCC [79–81, 96] predecessors (see Ref. [115] for a review), the DEA-EOMCC(3p-1h){ N_u } and DEA-EOMCC(3p-1h,4p-2h) $\{N_u\}$ schemes developed in this work are based on the idea of employing active orbitals to capture dominant excitation (in this case, electron attaching) amplitudes. Thus, the DEA-EOMCC(3p-1h) $\{N_u\}$ approach uses N_u active unoccupied orbitals to select a small subset of the dominant 3p-1h amplitudes within the standard DEA-EOMCC(3p-1h) framework, in which the operator attaching two electrons to the corresponding closed-shell core is truncated at 3p-1h component. Similarly, the DEA-EOMCC(3p-1h,4p-2h) $\{N_u\}$ method uses N_u active unoccupied orbitals to select the dominant 3p-1h and 4p-2h amplitudes within the higher-level DEA-EOMCC(4p-2h) scheme. In other words, the DEA-EOMCC(3p-1h) $\{N_u\}$ approach is a natural approximation to its DEA-EOMCC(3p-1h) parent, which becomes full DEA-EOMCC(3p-1h) when all unoccupied orbitals in the basis set are active (i.e., $N_u = n_u$). Similarly, the DEA-EOMCC $(3p-1h,4p-2h)\{N_u\}$ approach is a natural approximation to its DEA-EOMCC(4p-2h) parent or to the previously developed DEA-EOMCC(4p-2h) $\{N_u\}$ method of Refs. [92] and [93], becoming full DEA-EOMCC(4p-2h) when $N_u = n_u$. The DEA-EOMCC(3p-1h) $\{N_u\}$ and DEA-EOMCC(3p-1h,4p-2h) $\{N_u\}$ approaches proposed in this work offer significant savings in the computer effort compared to their full DEA-EOMCC(3p-1h) and DEA-EOMCC(4p-2h) counterparts by reducing the expensive \mathcal{N}^6 -like $n_o n_u^5$ steps associated with 3p-1h excitations to a \mathcal{N}^5 -like $N_u n_o n_u^4$ level, which for larger systems is less expensive than costs of the underlying CCSD calculations. As in the case of the previously proposed DEA- ${\rm EOMCC}(4p\text{-}2h)\{N_u\} \text{ approximation [92, 93], the DEA-EOMCC}(3p\text{-}1h, 4p\text{-}2h)\{N_u\} \text{ method } \{N_u\} \text{ approximation [92, 93], the DEA-EOMCC}(3p\text{-}1h, 4p\text{-}2h)\{N_u\} \text{ method } \{N_u\} \text{ approximation [92, 93], the DEA-EOMCC}(3p\text{-}1h, 4p\text{-}2h)\{N_u\} \text{ method } \{N_u\} \text{ approximation [92, 93], the DEA-EOMCC}(3p\text{-}1h, 4p\text{-}2h)\{N_u\} \text{ method } \{N_u\} \text{ approximation } \{N_u\} \text{ method } \{N_u\} \text{ approximation } \{N_u\} \text{ approximation } \{N_u\} \text{ approximation } \{N_u\} \text{ method } \{N_u\} \text{ approximation }$ replaces the \mathcal{N}^8 -like $n_o^2 n_u^6$ steps associated with 4p-2h contributions by the much more affordable, CCSD-type, $N_u^2 n_o^2 n_u^4$ steps, in addition to using the relatively inexpensive, \mathcal{N}^5 -like, $N_u n_o n_u^4$ steps in handling the lower-order 3p-1h terms.

In order to test the performance of the DEA-EOMCC(3p-1h) $\{N_u\}$ and DEA-EOMCC $(3p-1h,4p-2h)\{N_u\}$ approaches developed in this work, especially when compared to the previously examined [92, 93] DEA-EOMCC(3p-1h), DEA-EOMCC(4p-2h) $\{N_u\}$, and full DEA-EOMCC(4p-2h) methods, we investigate adiabatic excitation energies characterizing low-lying states of methylene, singlet-triplet gaps in trimethylenemethane (TMM), a series of cyclobutadiene and its derivatives and cyclopentadienyl cation, and bond breaking in the F₂ molecule. We show that the new DEA-EOMCC(3p-1h,4p-2h) $\{N_u\}$ approach with the activespace treatment of 3p-1h and 4p-2h excitations and its lower-level DEA-EOMCC(3p-1h) $\{N_u\}$ counterpart ignoring 4p-2h contributions, while using active orbitals to select the dominant 3p-1h components, accurately reproduce the results obtained with the considerably more expensive parent DEA-EOMCC methods with a full treatment of 3p-1h and full or activespace treatment of 4p-2h excitations at the small fraction of the computer effort. This is particularly valuable when the higher-level DEA-EOMCC(3p-1h,4p-2h){ N_u } approach is employed, since the explicit inclusion of 4p-2h excitations in the DEA-EOMCC wave function expansions leads to a robust and highly accurate description of the electronic structure and spectra of diradicals and single bond breaking in closed shells leading to doublet dissociation fragments, independent of the MO basis exploited in such calculations [92–94].

4.2 Theory and Algorithmic Details

4.2.1 Basic Elements of the DEA-EOMCC Formalism and the Previously Developed DEA-EOMCC(3p-1h), DEA-EOMCC(4p-2h), and DEA-EOMCC(4p-2h) $\{N_u\}$ Approximations

In the DEA-EOMCC formalism exploited in this work, one represents the ground ($\mu = 0$) and excited ($\mu > 0$) states $|\Psi_{\mu}^{(N)}\rangle$ of the N-electron system obtained by adding two electrons to the closed-shell core using the following wave function ansatz [53, 86, 88, 89, 92–94]:

$$|\Psi_{\mu}^{(N)}\rangle = R_{\mu}^{(+2)}|\Psi_{0}^{(N-2)}\rangle,$$
 (4.1)

where

$$|\Psi_0^{(N-2)}\rangle = e^T |\Phi^{(N-2)}\rangle \tag{4.2}$$

is the CC ground state of the (N-2)-electron closed-shell species, with $|\Phi^{(N-2)}\rangle$ designating the corresponding reference determinant that serves as the Fermi vacuum. The operator T entering Eq. (4.2) is the usual particle-conserving cluster operator, obtained in the ground-state CC calculations for the (N-2)-electron reference system, and

$$R_{\mu}^{(+2)} = \sum_{n=2}^{M_R} R_{\mu,np-(n-2)h},$$
(4.3)

where $M_R = N$ in the exact case and $M_R < N$ in approximate schemes, is the EOM operator attaching two electrons to the corresponding (N-2)-electron closed-shell core,

while allowing excitations of the remaining electrons via the $R_{\mu,np-(n-2)h}$ components with n > 2. Once we decide on specific truncations in the many-body expansions representing the T and $R_{\mu}^{(+2)}$ operators (assuming that the highest many-body rank in T (abbreviated as M_T) is, as explained in Refs. [92] and [93], at least $(M_R - 2)$) and once the relevant components of T are determined by solving the ground-state CC equations for the (N-2)-electron reference system, we obtain the $R_{\mu,np-(n-2)h}$ components of the $R_{\mu}^{(+2)}$ operator and the corresponding vertical electron-attachment energies

$$\omega_{\mu}^{(N)} = E_{\mu}^{(N)} - E_{0}^{(N-2)}, \tag{4.4}$$

where $E_{\mu}^{(N)}$ is the energy of the N-electron state $|\Psi_{\mu}^{(N)}\rangle$ and $E_{0}^{(N-2)}$ is the ground-state CC energy of the (N-2)-electron reference system, by solving the following non-Hermitian eigenvalue problem [92–94]:

$$(\bar{H}_{N,\text{open}} R_{\mu}^{(+2)})_C |\Phi^{(N-2)}\rangle = \omega_{\mu}^{(N)} R_{\mu}^{(+2)} |\Phi^{(N-2)}\rangle$$
 (4.5)

in the space of N-electron determinants corresponding to the $R_{\mu,np-(n-2)h}$ components included in $R_{\mu}^{(+2)}$. Here, $\bar{H}_{N,\text{open}}$ is the open part of the similarity-transformed form of the Hamiltonian H, written in the normal-ordered representation $H_N = H - \langle \Phi^{(N-2)} | H | \Phi^{(N-2)} \rangle$, i.e., the open part of the

$$\bar{H}_N = e^{-T} H_N e^T = (H_N e^T)_C$$
 (4.6)

operator obtained in the underlying CC calculations for the (N-2)-electron reference system, and subscript C designates the connected operator product. Thus, $\bar{H}_{N,\text{open}}$ is this part of \bar{H}_N , Eq. (4.6), which corresponds to diagrams of $(H_N e^T)_C$ that have external fermion lines. It is easy to show that $\bar{H}_{N,\text{open}}$ is equivalent to $\bar{H} - E_0^{(N-2)} \mathbf{1}$, where $\bar{H} = e^{-T} H e^T$ is the similarity-transformed form of H and $\mathbf{1}$ is the unit operator. the aforementioned condition $M_R - 2 \leq M_T$ has to be satisfied to obtain the connected form of the eigenvalue problem represented by Eq. (4.5), which is, in turn, key to retaining the desired property of size intensivity of the resulting electron-attachment energies $\omega_{\mu}^{(N)}$.

Different truncations in the cluster and electron attaching operators, T and $R_{\mu}^{(+2)}$, respectively, which enter the above equations and which satisfy the condition $M_R - 2 \leq M_T$, lead to various DEA-EOMCC schemes. In particular, in the full DEA-EOMCC(4p-2h) method developed in Refs. [92] and [93], which presently is the highest implemented level of the DEA-EOMCC theory, we truncate the cluster operator T at double excitations, i.e., we use the standard CCSD approach to determine the (N-2)-electron reference ground state $|\Psi_0^{(N-2)}\rangle$, and set M_R in Eq. (4.3) at 4, obtaining

$$R_{\mu}^{(+2)} = R_{\mu,2p} + R_{\mu,3p-1h} + R_{\mu,4p-2h}, \tag{4.7}$$

where

$$R_{\mu,2p} = \sum_{a < b} r_{ab}(\mu) \ a^a a^b, \tag{4.8}$$

$$R_{\mu,3p-1h} = \sum_{k,a < b < c} r_{abc}^{\ k}(\mu) a^a a^b a^c a_k, \tag{4.9}$$

and

$$R_{\mu,4p-2h} = \sum_{k>l,a < b < c < d} r_{abcd}^{\ kl}(\mu) \ a^a a^b a^c a^d a_l a_k \tag{4.10}$$

are the relevant 2p, 3p-1h, and 4p-2h components of the electron-attaching operator $R_{\mu}^{(+2)}$. We determine these components of $R_{\mu}^{(+2)}$, or the amplitudes $r_{ab}(\mu)$, $r_{abc}^{\ \ k}(\mu)$, and $r_{abcd}^{\ \ kl}(\mu)$ that represent them, along with the corresponding vertical electron-attachment energies $\omega_{\mu}^{(N)}$, Eq. (4.4), by diagonalizing the similarity-transformed Hamiltonian of CCSD obtained in the calculations for the (N-2)-electron reference system, given by Eq. (4.6) in which T is truncated at two-body clusters, in the space spanned by the N-electron $|\Phi^{ab}\rangle = a^a a^b |\Phi^{(N-2)}\rangle$, $|\Phi^{abc}\rangle = a^a a^b a^c a_k |\Phi^{(N-2)}\rangle$, and $|\Phi^{abcd}\rangle = a^a a^b a^c a^d a_l a_k |\Phi^{(N-2)}\rangle$ determinants. The older and simpler DEA-EOMCC(3p-1h) approximation [53, 86, 88, 89], which we implemented in Refs. [92] and [93] as well, is obtained by neglecting the 4p-2h component of $R_{\mu}^{(+2)}$, $R_{\mu,4p-2h}$, in Eq. (4.7), i.e., by setting M_R in Eq. (4.3) at 3. In this case, we diagonalize the similarity-transformed Hamiltonian of CCSD in the space spanned by the $|\Phi^{abc}\rangle$ and $|\Phi^{abc}\rangle$ determinants. We use the conventional notation in which i, j, k, l, \ldots (a, b, c, d, \ldots) indices are the spin-orbitals occupied (unoccupied) in the reference determinant $|\Phi^{(N-2)}\rangle$ and and a^p (a_p) are the creation (annihilation) operators associated with the spin-orbital basis $\{|p\rangle\}$.

 $R_{\mu}^{\left(+2\right)}$, Eq. (4.7), by its active-space counterpart $r_{\mu,4p\text{-}2h}$ given by

$$r_{\mu,4p-2h} = \sum_{k>l,\mathbf{A}<\mathbf{B}< c< d} r_{\mathbf{A}\mathbf{B}cd}^{\quad kl}(\mu) a^{\mathbf{A}} a^{\mathbf{B}} a^c a^d a_l a_k, \tag{4.11}$$

where the capital-case bold symbols **A** and **B** in Eq. (4.11) designate the active spin-orbitals unoccupied in the (N-2)-electron reference determinant $|\Phi^{(N-2)}\rangle$ (formally, any subset of unoccupied spin-orbitals, which we hope to be small in practical DEA-EOMCC(4p-2h) $\{N_u\}$ calculations). The resulting $R_{\mu}^{(+2)}\{N_u\}$ operator defining the DEA-EOMCC(4p-2h) $\{N_u\}$ method is given by

$$R_{\mu}^{(+2)}\{N_u\} = R_{\mu,2p} + R_{\mu,3p-1h} + r_{\mu,4p-2h},\tag{4.12}$$

where $R_{\mu,2p}$, $R_{\mu,3p-1h}$, and $r_{\mu,4p-2h}$ are defined by Eqs. (4.8, 4.9, and 4.11), respectively. We obtain the relevant $r_{ab}(\mu)$, $r_{abc}^{\ \ k}(\mu)$, and $r_{\mathbf{AB}cd}^{\ \ kl}(\mu)$ amplitudes entering Eq. (4.12) by diagonalizing the similarity-transformed Hamiltonian $\bar{H}_{N,\mathrm{open}}$ obtained in the CCSD calculations for the (N-2)-electron reference system in the subspace of the N-electron Hilbert space spanned by the $|\Phi^{ab}\rangle$, $|\Phi^{abc}_{\ \ k}\rangle$, and $|\Phi^{\mathbf{AB}cd}_{\ \ kl}\rangle$ determinants. If the number of active unoccupied spin-orbitals, N_u , is small compared to the number of all unoccupied spin-orbitals (n_u) , the number of 4p-2h amplitudes to be determined in DEA-EOMCC(4p-2h) $\{N_u\}$ calculations, which equals the number of double excitations times a prefactor on the order of N_u^2 , is much smaller than the number of all $r_{abcd}^{\ \ kl}(\mu)$ amplitudes, which scales as $n_o^2 n_u^4$. This is precisely the source of savings in the computer effort offered by the active-space DEA-EOMCC(4p-2h) $\{N_u\}$ approach, when compared to full DEA-EOMCC(4p-2h), which we have elaborated on earlier.

4.2.2 The Active-Space DEA-EOMCC(3p-1h){ N_u } and DEA-EOMCC(3p-1h,4p-2h){ N_u } Approaches Developed in this Thesis Project

The active-space DEA-EOMCC(4p-2h) $\{N_u\}$ method described in Section 4.2.1 offers major savings in the computer effort compared to its full DEA-EOMCC(4p-2h) parent, replacing the prohibitively expensive $n_o^2 n_u^6$ steps of the latter approach by steps that scale as $N_u^2 n_o^2 n_u^4$, but, as explained earlier, the CPU time associated with 3p-1h component $R_{\mu,3p-1h}$, which scales as $n_o n_u^5$, can be significant too, especially when larger basis sets are employed. In order to respond to this problem, in this work we develop and test a new, more economical variant of the active-space DEA-EOMCC(4p-2h) approach, designated DEA-EOMCC(3p-1h,4p-2h) $\{N_u\}$, in which both 3p-1h and 4p-2h components of the electron attaching operator $R_{\mu}^{(+2)}$, Eq. (4.7), are treated using active orbitals. This is done by replacing the $R_{\mu,3p-1h}$ and $R_{\mu,4p-2h}$ components of $R_{\mu}^{(+2)}$ by their active-space counterparts, $r_{\mu,3p-1h}$ and $r_{\mu,4p-2h}$, respectively, to obtain a new form of the $R_{\mu}^{(+2)}$ operator, designated $\tilde{R}_{\mu}^{(+2)}$ $\{N_u\}$, which is defined as

$$\tilde{R}_{\mu}^{(+2)}\{N_u\} = R_{\mu,2p} + r_{\mu,3p-1h} + r_{\mu,4p-2h},\tag{4.13}$$

where $r_{\mu,4p\text{-}2h}$ is given by Eq. (4.11) and

$$r_{\mu,3p-1h} = \sum_{k,\mathbf{A} < b < c} r_{\mathbf{A}bc}^{\ k}(\mu) a^{\mathbf{A}} a^b a^c a_k.$$
 (4.14)

In analogy to Eq. (4.11), the capital-case bold index **A** in Eq. (4.14) runs over active spin-orbitals unoccupied in $|\Phi^{(N-2)}\rangle$. If we want to limit ourselves to the simpler DEA-

EOMCC(3p-1h) level and reduce costs of the DEA-EOMCC(3p-1h) calculations further as well, we can consider the active-space variant of the DEA-EOMCC(3p-1h) approach, designated in this work as DEA-EOMCC(3p-1h){ N_u }, which is obtained by neglecting $r_{\mu,4p-2h}$ in Eq. (4.13).

In defining the above $r_{\mu,3p-1h}$ component, we adopt the general philosophy of all activespace CC and EOMCC theories [71, 72, 79–81, 92, 93, 96, 98–112, 114, 115], especially the previously formulated [92, 93] DEA-EOMCC(4p-2h) $\{N_u\}$ method. Indeed, let us recall that the definition of the higher-rank $r_{\mu,4p\text{-}2h}$ component, Eq. (4.11), entering the DEA- $\mathrm{EOMCC}(4p\text{-}2h)\{N_u\}$ and $\mathrm{DEA\text{-}EOMCC}(3p\text{-}1h,4p\text{-}2h)\{N_u\}$ expressions, reflects on the intuitive picture of the formation of the N-electron diradical system from the related (N-2)electron closed-shell species, which is certainly valid when the low-lying electronic states of the diradical are considered. In this picture, the N-electron diradical is viewed as a system obtained, at least in the zeroth-order description, by attaching two electrons to the lowest-energy unoccupied orbitals of the related closed-shell species, followed by the relaxation of the remaining electrons [92]. Assuming that the relaxation of the (N-2) electrons in the closed-shell core is characterized by substantial 2p-2h correlations (i.e., doubles) and assuming that the lowest-energy unoccupied orbitals are the most important orbitals for the electron attachment process of interest, we can replace the full form of 4p-2h component of $R_{\mu}^{(+2)}$, Eq. (4.10), by its active-space $r_{\mu,4p-2h}$ analog defined by Eq. (4.11). Following a similar reasoning, if the relaxation of the (N-2) electrons in the closed-shell core is characterized by larger 1p-1h correlations (i.e., singles) and assuming, once again, the dominant role of the lowest-energy unoccupied orbitals in the electron attachment process of interest that leads to the formation of the N-electron diradical species, we can replace the full form of 3p-1h component of $R_{\mu}^{(+2)}$, Eq. (4.9), by its active-space $r_{\mu,3p$ -1h counterparts defined by Eq. (4.14).

In analogy to the previously discussed full and active-space DEA-EOMCC(4p-2h) approaches [92, 93], in the DEA-EOMCC(3p-1h,4p-2h) $\{N_u\}$ calculations we determine the $R_{\mu,2p}$, $r_{\mu,3p-1h}$, and $r_{\mu,4p-2h}$ components of the electron attaching operator $\tilde{R}_{\mu}^{(+2)}\{N_u\}$, Eq. (4.13), by diagonalizing the similarity-transformed Hamiltonian $\bar{H}_{N,\text{open}}$ obtained in the CCSD calculations for the (N-2)-electron reference system, but now the diagonalization subspace is much smaller if $N_u \ll n_u$. Indeed, in the DEA-EOMCC(3*p*-1*h*,4*p*-2*h*){ N_u } method, we diagonalize $\bar{H}_{N,\text{open}}$ in the subspace spanned by the $|\Phi^{ab}\rangle$, $|\Phi^{\mathbf{A}bc}_{k}\rangle$, and $|\Phi^{\mathbf{AB}cd}_{kl}\rangle$ determinants that correspond to the definition of $\tilde{R}_{\mu}^{(+2)}\{N_u\}$, Eq. (4.13). Thus, instead of having to deal with $\sim n_o n_u^3$ 3p-1h and $\sim n_o^2 n_u^4$ 4p-2h amplitudes and determinants defining the eigenvalue problem of DEA-EOMCC(4p-2h), we consider $\sim N_u n_o n_u^2$ amplitudes and determinants of the 3p-1h type and $\sim N_u^2 n_o^2 n_u^2$ amplitudes and determinants of the 4p-2h type, which reflect on the content of $\tilde{R}_{\mu}^{(+2)}\{N_u\}$. This results in enormous savings in the computer effort compared to full DEA-EOMCC(4p-2h) calculations by reducing the expensive $n_o n_u^5$ steps associated with 3p-1h excitations and even more expensive $n_o^2 n_u^6$ steps associated with 4p-2h contributions to the much more affordable $N_u n_o n_u^4$ and $N_u^2 n_o^2 n_u^4$ levels. As shown in Section 4.2.4, the active-space DEA-EOMCC(3p-1h,4p-2h) $\{N_u\}$ approach proposed in this work is also substantially less expensive than its previously proposed [92, 93] DEA-EOMCC(4p-2h) $\{N_u\}$ counterpart, which reduces the $n_o^2 n_u^6$ steps associated with 4p-2h excitations to the $N_u^2 n_o^2 n_u^4$ level, but treats 3p-1h contributions fully using expensive CPU steps that scale as $n_o n_u^5$. Similar remarks apply to the active-space DEA-EOMCC(3p-1h) $\{N_u\}$ method, where we diagonalize $\bar{H}_{N,\text{open}}$ in the small subspace spanned by $|\Phi^{ab}\rangle$ and $|\Phi^{\mathbf{A}bc}\rangle$ determinants, so that instead of having to deal with $\sim n_o n_u^3$ 3p-1h amplitudes and determinants nants defining the full DEA-EOMCC(3p-1h) eigenvalue problem, we consider a much smaller number of such amplitudes and determinants that scales as $\sim N_u n_o n_u^2$. As illustrated in Section 4.2.4, this leads to significant reductions in the CPU time needed to perform the DEA-EOMCC(3p-1h)-level calculations, since the CPU steps of DEA-EOMCC(3p-1h) that normally scale as $n_o n_u^5$ are reduced to a relatively inexpensive $N_u n_o n_u^4$ level.

4.2.3 Key Details of the Efficient Computer Implementation of the Active-Space DEA-EOMCC(3p-1h) $\{N_u\}$ and DEA-EOMCC (3p-1h,4p-2h) $\{N_u\}$ Methods

In this section we discuss our efficient implementations of the active-space DEA-EOMCC $(3p-1h)\{N_u\}$ and DEA-EOMCC $(3p-1h,4p-2h)\{N_u\}$ schemes discussed in Section 4.2.2. In analogy to the previously developed DEA-EOMCC(3p-1h), DEA-EOMCC(4p-2h), and DEA- $EOMCC(4p-2h)\{N_u\}$ codes and their DIP counterparts described and tested in Refs. [92] and [93],present computer implementation of the active-space DEA-EOMCC $(3p-1h)\{N_u\}$ and DEA-EOMCC $(3p-1h,4p-2h)\{N_u\}$ approaches proposed in this work has been interfaced with the atomic integral, RHF as well as restricted open-shell Hartree–Fock (ROHF), and integral transformation routines available in the GAMESS software package [192, 193]. We have benefited from the previously developed spin-free CCSD GAMESS routines [194], to obtain the singly and doubly excited cluster amplitudes, t_a^i and t_{ab}^{ij} , respectively. The (N-2)-electron CCSD calculations prior to the DEA-EOMCC diagonalization steps can be run using any set of orbitals, as long as the underlying reference determinant $|\Phi^{(N-2)}\rangle$ is of the closed-shell type. In this work, we have taken advantage of the algebraic expressions and routines that were used in some of our earlier EOMCC studies [63, 66, 68], where we utilize converged t_a^i and t_{ab}^{ij} amplitudes and one- and two-electron integrals, f_p^q , $f_p^q = \langle p|f|q \rangle$ (f is the Fock operator) and $v_{pq}^{rs} = \langle pq|v|rs \rangle - \langle pq|v|sr \rangle$ (v is the electron-electron interaction), respectively, defining the normal-ordered Hamiltonian to construct the one- and two-body matrix elements of the similarity-transformed Hamiltonian of CCSD $\bar{H}_{N,\text{open}}^{(\text{CCSD})}$, \bar{h}_p^q and \bar{h}_{pq}^{rs} , respectively, defining the one- and two-body components of $\bar{H}_{N,\text{open}}^{(\text{CCSD})}$ within the second quantized formalism,

$$\bar{H}_1^{(CCSD)} = \bar{h}_p^q a^p a_q, \tag{4.15}$$

and

$$\bar{H}_{2}^{(CCSD)} = \frac{1}{4} \bar{h}_{pq}^{rs} N[a^{p} a^{q} a_{s} a_{r}],$$
 (4.16)

respectively, where N[...] is the normal product of the operators between the brackets (we use Einstein's summation convention over repeated upper and lower indices). The compact DEA-EOMCC(3p-1h){ N_u } and DEA-EOMCC(3p-1h,4p-2h){ N_u } equations shown below are expressed in terms of \bar{h}_p^q and \bar{h}_{pq}^{rs} matrix elements, which have been derived in Refs. [50, 66, 68, 119, 210] and can also be found in Table 4.1.

In programming the active-space DEA-EOMCC(3p-1h) $\{N_u\}$ and DEA-EOMCC (3p-1h,4p-2h) $\{N_u\}$ approaches developed in this work, we have taken advantage of the explicit, computationally efficient, equations defining the DEA-EOMCC(3p-1h) and DEA-EOMCC(4p-2h) eigenvalue problems in terms of one- and two-body matrix elements of the similarity-transformed Hamiltonian of CCSD and other recursively generated intermediates, reported in the appendix of Ref. [92], imposing suitable active-space logic on these equations with the help of our home-grown automated derivation and implementation software, which was previously exploited in coding the DEA-EOMCC(4p-2h) $\{N_u\}$ approach and its DIP counterpart [92] and a number of other CC/EOMCC methods that rely on similar logic,

Table 4.1: Explicit algebraic expressions for the one- and two-body matrix elements of $\bar{H}_{N,\text{open}}^{(\text{CCSD})}$ (\bar{h}_p^q and \bar{h}_{pq}^{rs} , respectively) taken from [66, 68].

Intermediate	Expression a
$ar{h}_i^a$	$f_i^a + v_{im}^{ae} t_e^m$
$ar{h}_i^j$	$f_{i}^{j}+v_{im}^{je}t_{e}^{m}+rac{1}{2}v_{mi}^{ef}t_{ef}^{mj}+ar{h}_{i}^{e}t_{e}^{j}$
$ar{h}_a^b$	$I_a^b - ar{h}_m^b t_a^m$
$ar{h}_{ai}^{bc}$	$v_{ai}^{bc} - v_{mi}^{bc} t_a^m$
$ar{h}_{ij}^{ka}$	$v_{ij}^{ka}+v_{ij}^{ea}t_{e}^{k}$
$ar{h}_{ab}^{cd}$	$v_{ab}^{cd} + \frac{1}{2}v_{mn}^{cd}t_{ab}^{mn} - \bar{h}_{am}^{cd}t_{b}^{m} + v_{bm}^{cd}t_{a}^{m}$
$ar{h}_{ij}^{kl}$	$v^{kl}_{ij} + rac{1}{2} v^{ef}_{ij} t^{kl}_{ef} - ar{h}^{le}_{ij} t^{k}_{e} + v^{ke}_{ij} t^{l}_{e}$
$ar{h}_{ia}^{jb}$	$I_{ia}^{\prime jb}-v_{im}^{eb}t_{ea}^{jm}-ar{h}_{im}^{jb}t_{a}^{m}$
$ar{h}^{ic}_{ab}$	$v_{ab}^{ic} + v_{ab}^{ec} t_e^i - \bar{h}_{mb}^{ic} t_a^m + I_{ma}^{'ic} t_b^m - \bar{h}_m^c t_{ab}^{im} + \bar{h}_{bm}^{ce} t_{ae}^{im} - v_{am}^{ce} t_{be}^{im} + \frac{1}{2} \bar{h}_{nm}^{ic} t_{ab}^{nm}$
$ar{h}_{ia}^{jk}$	$v_{ia}^{jk}+ar{h}_{mi}^{jk}t_a^m-v_{ia}^{ke}t_e^j+\mathscr{A}^{jk}ar{h}_{im}^{je}t_{ae}^{km}$
	$+\bar{h}_{i}^{e}t_{ea}^{jk}+I_{ia}^{'je}t_{e}^{k}-\frac{1}{2}v_{ai}^{ef}t_{ef}^{jk}$
$I_a^{'b}$	$f_a^b + v_{am}^{be} t_e^m$
I_a^b	$I_a^{'b}-rac{1}{2}v_{mn}^{eb}t_{ea}^{mn}$
$I_{ia}^{\prime jb}$	$v_{ia}^{jb} + v_{ia}^{eb} t_e^j$

^a Summation over repeated upper and lower indices is assumed. $f_p^q = \langle p|f|q \rangle$ and $v_{pq}^{rs} = \langle pq|v|rs \rangle - \langle pq|v|sr \rangle$ are the one- and two-body matrix elements of the Hamiltonian in the normal-ordered form (one- and two-electron integrals), and the t_a^i and t_{ab}^{ij} are the singly and doubly excited cluster amplitudes defining the ground-state CCSD wave function of the (N-2)-electron reference system. The antisymmetrizer is defined by $\mathscr{A}^{jk} = 1 - (jk)$, where (jk) is the transposition of indices j and k.

including those developed in Refs. [129, 211, 212].

Following our earlier EOMCC programming work [63, 66–68, 71, 72, 79, 81, 92, 110– 112, 123, 124, 182], including the DEA-EOMCC(3p-1h), DEA-EOMCC(4p-2h), and DEA-EOMCC(4p-2h) $\{N_u\}$ codes and their DIP counterparts described and tested in Refs. [92] and [93], in solving the DEA-EOMCC(3p-1h){ N_u } and DEA-EOMCC(3p-1h,4p-2h){ N_u } equations for the amplitudes defining the corresponding $R_{\mu}^{(+2)}$ operators we have adopted the Hirao-Nakatsuji generalization [213] of the Davidson diagonalization algorithm [214] to non-Hermitian eigenvalue problems. Since we are interested in capturing challenging electronic states of diradicals that may have a substantial multi-reference character, which manifests itself via the presence of larger 3p-1h components, in addition to the simplest 2pinitial guesses for the $R_{\mu}^{(+2)}$ vectors, in which one diagonalizes the Hamiltonian in the small subspace spanned by 2p determinants only, we have also implemented the more sophisticated ones, where one performs simplified DEA-EOMCC(3p-1h) calculations in which the threebody matrix elements of the similarity-transformed Hamiltonian of CCSD are ignored and the 3p-1h amplitudes are limited to the purely active excitations of the $r_{\mathbf{ABC}}^{\mathbf{K}}(\mu)$ type. Such simplified DEA-EOMCC(3p-1h) calculations rely only on one- and two-body matrix elements of $\bar{H}_{N,\mathrm{open}}$, which one can easily determine after the CCSD equations are converged, and are characterized by the relatively small dimensions of the resulting eigenvalue problems that make them trivially solvable with the standard library diagonalization routines exploited in the initial guess work. We used this strategy in our earlier DEA-EOMCC work [92, 93], finding it quite helpful in situations where 3p-1h amplitudes are larger, so we use it here as well.

In order to derive the DEA-EOMCC(3p-1h,4p-2h){ N_u } equations, we begin with the working equations defining the parent DEA-EOMCC(4p-2h) approximations, which are pre-

sented in Appendix B. Generally, the DEA-EOMCC(3p-1h,4p-2h){ N_u } equations are obtained by imposing the active-space constraint on the spin-orbital indices defining the $|\Phi^{abc}_{k}\rangle$ and $|\Phi^{abcd}_{k}\rangle$ determinants and on the indices defining the corresponding $r_{abc}^{\ k} \equiv r_{abc}^{\ k}(\mu)$ and $r_{abcd}^{\ kl} \equiv r_{abcd}^{\ kl}(\mu)$ amplitudes to each term in DEA-EOMCC(3p-1h,4p-2h){ N_u } equations (to make our expressions more compact, we will drop the state index μ from the EOM r amplitudes). In order to appreciate the inner workings of this procedure, we will demonstrate the underlying logic by deriving few terms which enter these set of equations based on the appendix in Ref. [92]. We begin by analyzing the following contribution to Eq. (B.2) in Appendix B, corresponding to the projection on $|\Phi^{abc}_{k}\rangle$, which we label as $D^{abc}_{k}(1)$:

$$D^{abc}_{k}(1) = -\frac{1}{3}\bar{h}_{m}^{k}r_{abc}^{m} + \frac{1}{3}\bar{h}_{m}^{e}r_{abce}^{km}, \tag{4.17}$$

where in analogy to all other expressions shown in this section and Appendix B, we use Einstein's summation convention over repeated upper and lower indices. In the DEA-EOMCC(3p-1h){ N_u } approach, we only consider 3p-1h projections of the type $|\Phi^{\mathbf{A}bc}\rangle$, and so we must restrict the indices in Eq. (4.17) as follows:

$$D^{\mathbf{A}bc}_{k}(1) = -\frac{1}{3}\bar{h}_{m}^{k}r_{\mathbf{A}bc}^{m} + \frac{1}{3}\bar{h}_{m}^{e}r_{\mathbf{A}bce}^{km}.$$
 (4.18)

As we can see, we have replaced the generic unoccupied label a in Eq. (4.17) that corresponds to the projection on $|\Phi^{abc}_{k}\rangle$ by the active index **A**. Since the $r_{\mathbf{A}bc}^{k}$ and $r_{\mathbf{A}bce}^{km}$ amplitudes which enter Eq. (4.18) contain an active unoccupied index, conforming to the proper form dictated by Eq. (4.14), we do not require further restrictions to the indices defining the $D^{abc}_{k}(1)$, thus, completing the derivation of the final formula for this particular contribution to the

DEA-EOMCC(3p-1h) $\{N_u\}$ equations. However, most of the terms which enter the activespace DEA-EOMCC equations are not so easily obtained, and so it is useful to examine more difficult cases. For example, let us consider the following contribution to Eq. (B.2) in Appendix B, which we label as $D^{abc}_{k}(2)$:

$$D^{abc}_{\ k}(2) = -\frac{1}{2}\bar{h}^{ef}_{ab}r^{\ k}_{cef}. \tag{4.19}$$

If we employ the same approach as used in the previous case, we obtain the following expression:

$$D^{\mathbf{A}bc}_{k}(2) = -\frac{1}{2}\bar{h}^{ef}_{\mathbf{A}b}r_{cef}^{k}.$$

$$(4.20)$$

Again, we have replaced the generic unoccupied label a in Eq. (4.19) by the active index \mathbf{A} defining the $|\Phi^{\mathbf{A}bc}_{k}\rangle$ determinant. However, unlike in the previous example, the r_{cef}^{k} amplitudes that enter the above equation do not have at least one active unoccupied index, and so it is not automatically of the form required by Eq. (4.14). Furthermore, whether or not these amplitudes satisfy the active-space restrictions depends on whether the unoccupied indices b and c belong to active or inactive virtual spin-orbitals. Hence, instead of the generic projection $|\Phi^{\mathbf{A}bc}_{k}\rangle$, that converts Eq. (4.19) into Eq. (4.20), we must consider four more distinct types of the restricted 3p-1h projections that belong to the general $|\Phi^{\mathbf{A}bc}_{k}\rangle$ class, given in Table 4.2 below.

Applying the 3p-1h projection of type 1 in Table 4.2 to the term given in Eq. (4.19), that is, the projection on the $|\Phi^{\mathbf{ABC}}_{k}\rangle$ determinant, one obtains

$$D^{\mathbf{ABC}}_{k}(2) = -\frac{1}{2}\bar{h}^{ef}_{\mathbf{AB}}r_{\mathbf{C}ef}^{k}.$$
(4.21)

Table 4.2: The various classes of restricted projections that must be considered when generating the computationally efficient form of the equations defining the DEA-EOMCC(3p-1h, 4p-2h){ N_u } eigenvalue problem.

	DEA-E	DEA-EOMCC $(3p-1h, 4p-2h)\{N_u\}$		
Projection Type	2p	3p- $1h$	4p- $2h$	
1	$ \Phi^{\mathbf{A}\mathbf{B}} angle$	$ \Phi^{\mathbf{A}\mathbf{B}\mathbf{C}}_{}k} angle$	$ \Phi^{\mathbf{ABCD}}_{}}}}}$	
2	$ \Phi^{\mathbf{A}\mathbf{b}} angle$	$ \Phi^{\mathbf{A}\mathbf{B}\mathbf{c}}_{}k} angle$	$ \Phi^{\mathbf{A}\mathbf{B}\mathbf{C}\mathbf{d}}_{\mathbf{d}}} angle$	
3	$ \Phi^{{f a}{f B}} angle$	$ \Phi_{k}^{\mathbf{AbC}} angle$	$ \Phi^{\mathbf{ABcD}}_{}kl}\rangle$	
4	$ \Phi^{{f a}{f b}} angle$	$ \Phi_{k}^{\mathbf{Abc}} angle$	$ \Phi^{\mathbf{A}\mathbf{B}\mathbf{c}\mathbf{d}}_{kl}} angle$	

Since the 3p-1h amplitude $r_{\mathbf{C}ef}^{k}$ has at least one active unoccupied index, it satisfies the active-space demands of Eq. (4.14), and so requires no additional restrictions on the spin-orbital indices. Continuing on the same logic, if we consider the projection on $|\Phi^{\mathbf{AbC}}\rangle$ (type 3 projection in Table 4.2, with lower-case index representing inactive virtual orbitals), one obtains

$$D^{\mathbf{AbC}}_{k}(2) = -\frac{1}{2}\bar{h}^{ef}_{\mathbf{Ab}}r_{\mathbf{C}ef}^{k}, \tag{4.22}$$

which also requires no further constraints on the spin-orbital indices, since 3p-1h amplitude $r_{\mathbf{C}ef}^{\ k}$ has at least one active unoccupied indices. The main difference between Eqs. (4.21) and (4.22) is in the restriction on the label b, which is restricted to active unoccupied spin-orbital set in Eq. (4.21) and to inactive virtual spin-orbitals in Eq. (4.22). This barefaced relationship between Eqs. (4.21) and (4.22) allows us to recombine these two contributions into one, somewhat more general expression of the form

$$D^{\mathbf{A}b\mathbf{C}}_{k}(2) = -\frac{1}{2}\bar{h}^{ef}_{\mathbf{A}b}r_{\mathbf{C}ef}^{k}.$$
(4.23)

where the unoccupied index b can be active or inactive. We now consider the projection on

 $|\Phi^{\mathbf{Abc}}_{k}\rangle$ (projection type 2 in Table 4.2). The resulting expression for this contribution is

$$D^{\mathbf{ABc}}_{k}(2) = -\frac{1}{2}\bar{h}^{ef}_{\mathbf{AB}}r_{\mathbf{c}ef}^{k}, \tag{4.24}$$

where, unlike in the previous cases the $r_{\mathbf{c}ef}^{\ k}$ amplitude which enters this equation does not automatically have at least one unoccupied index constrained to active unoccupied spin-orbitals. In order to necessarily impose such a condition, we must restrict the summation over all particle spin-orbitals e in Eq. (4.24) to active spin-orbital labels only since \mathbf{c} is an inactive index. The resulting expression is given by

$$\tilde{D}^{\mathbf{ABc}}_{k}(2) = -\frac{1}{2}\bar{h}^{\mathbf{E}f}_{\mathbf{AB}}r_{\mathbf{cE}f}^{k}, \tag{4.25}$$

where the overtilde denotes the fact that we applied restrictions on the summations appearing in $D^{\mathbf{ABc}}_{k}(2)$. Finally, we consider the projection on $|\Phi^{\mathbf{Abc}}_{k}\rangle$ (projection type 4 in Table 4.2). The resulting expression for this contribution is

$$D^{\mathbf{Abc}}_{k}(2) = -\frac{1}{2}\bar{h}^{ef}_{\mathbf{Ab}}r_{\mathbf{c}ef}^{k}.$$
(4.26)

Again, the $r_{\mathbf{c}ef}^{\ k}$ amplitude which enters this term does not automatically have at least one unoccupied index constrained to active unoccupied spin-orbitals. As a result, we restrict the summation over all particle spin-orbitals e in Eq. (4.26) to active spin-orbital labels only since \mathbf{b} and \mathbf{c} are virtual (i.e., inactive) indices. The resulting expression is given by

$$\tilde{D}_{k}^{\mathbf{Abc}}(2) = -\frac{1}{2}\bar{h}_{\mathbf{Ab}}^{\mathbf{E}f}r_{\mathbf{c}\mathbf{E}f}^{k}.$$
(4.27)

Furthermore, comparing Eqs. (4.25) and (4.27) reveals that the only difference between these two terms is in the restriction on the index b, which in Eq. (4.25) is restricted to active unoccupied spin-orbitals and in Eq. (4.27) to inactive virtual spin-orbitals. Like in the previous examples of projection types considered earlier, we combine these two contributions into one general term of the following form:

$$\tilde{D}^{\mathbf{A}b\mathbf{c}}_{k}(2) = -\frac{1}{2}\bar{h}^{\mathbf{E}f}_{\mathbf{A}b}r_{\mathbf{c}\mathbf{E}f}^{k}.$$
(4.28)

where the unoccupied index b can be active or inactive. Equations (4.23) and (4.28) represent all contributions to the active-space DEA-EOMCC working equations stemming from one of the terms in the DEA-EOMCC(3p-1h){ N_u } equations projected on 3p-1h excited determinants given by Eq. (4.19). With this kind of analysis in view, we are now at a pole position to apply the above procedure to each term that enters the explicit form of the equations defining the DEA-EOMCC(3p-1h, 4p-2h){ N_u } approximation (Eqs. (B.1), (B.2), and (B.3) in appendix B), with the help of the projection types in Table 4.2. After collecting all of these contributions together, one obtains the final form of the fully factorized, computationally efficient DEA-EOMCC(3p-1h, 4p-2h){ N_u } equations, which are systematically presented below. The factorized equations defining the projections of the DEA-EOMCC(3p-1h, 4p-2h){ N_u } eigenvalue problem on the 2p determinants | Φ^{ab} ⟩ are

$$\langle \Phi^{ab} | (\bar{H}_{N,\text{open}}^{(\text{CCSD})} R_{\mu}^{(+2)})_C | \Phi \rangle = \mathscr{A}_{ab} \mathscr{T}_{ab} = \omega_{\mu}^{(N)} r_{ab}, \tag{4.29}$$

where

$$\mathscr{T}_{\mathbf{A}b} = \chi_{\mathbf{A}b} + \alpha_{\mathbf{A}b} - \sum_{\mathbf{E} < f} (\bar{h}_{\mathbf{A}m}^{\mathbf{E}f} r_{\mathbf{E}fb}^{\ m} - \frac{1}{4} v_{mn}^{\mathbf{E}f} r_{\mathbf{A}b\mathbf{E}f}^{\ mn}), \tag{4.30}$$

$$\mathscr{T}_{\mathbf{a}\mathbf{B}} = \Delta_{\mathbf{a}\mathbf{B}} - \alpha_{\mathbf{B}\mathbf{a}},\tag{4.31}$$

and

$$\mathscr{T}_{ab} = \Delta_{ab}, \tag{4.32}$$

with

$$\chi_{ab} = -\bar{h}_a^e r_{be} + \frac{1}{4} \bar{h}_{ab}^{ef} r_{ef}, \tag{4.33}$$

$$\alpha_{\mathbf{A}b} = \frac{1}{2}\bar{h}_{m}^{e}r_{\mathbf{A}be}^{m},\tag{4.34}$$

$$\Delta_{\mathbf{aB}} = \chi_{\mathbf{aB}} - \frac{1}{2} \bar{h}_{\mathbf{a}m}^{ef} r_{\mathbf{B}ef}^{m} + \frac{1}{4} \sum_{\mathbf{E} < f} v_{mn}^{\mathbf{E}f} r_{\mathbf{aBE}f}^{mn}, \tag{4.35}$$

and

$$\Delta_{\mathbf{ab}} = \chi_{\mathbf{ab}} + \frac{1}{2} \bar{h}_{m}^{\mathbf{E}} r_{\mathbf{Eab}}^{m} - \sum_{\mathbf{E} < f} \bar{h}_{\mathbf{am}}^{\mathbf{E}f} r_{\mathbf{bE}f}^{m} + \frac{1}{8} v_{mn}^{\mathbf{EF}} r_{\mathbf{ab}\mathbf{EF}}^{mn}. \tag{4.36}$$

The DEA-EOMCC(3p-1h, 4p-2h) $\{N_u\}$ equations on the selected 3p-1h determinants $|\Phi^{\mathbf{A}bc}_{k}\rangle$ have the following computationally efficient form:

$$\langle \Phi_{k}^{\mathbf{A}bc} | (\bar{H}_{N,\text{open}}^{(\text{CCSD})} R_{\mu}^{(+2)})_{C} | \Phi \rangle = \mathscr{A}_{bc} \mathscr{T}_{\mathbf{A}bc}^{k} = \omega_{\mu}^{(N)} r_{\mathbf{A}bc}^{k}, \tag{4.37}$$

where

$$\mathscr{T}_{\mathbf{AB}c}^{c} = \chi_{\mathbf{AB}c}^{c} + \Delta_{\mathbf{AB}c}^{c}, \tag{4.38}$$

$$\mathscr{T}_{\mathbf{AbC}}^{\quad k} = \Delta_{\mathbf{AbC}}^{\quad k}, \tag{4.39}$$

and

$$\mathscr{T}_{\mathbf{Abc}}^{\quad k} = \Delta_{\mathbf{Abc}}^{\quad k}, \tag{4.40}$$

with

$$\chi_{\mathbf{A}bc}^{k} = -\bar{h}_{\mathbf{A}b}^{e} r_{ce} - \frac{1}{3} \bar{h}_{m}^{k} r_{\mathbf{A}bc}^{m} + \frac{1}{2} I_{\mathbf{A}m} t_{bc}^{km} + \frac{1}{3} \bar{h}_{m}^{\mathbf{E}} r_{\mathbf{A}bc}^{km} - \frac{1}{3} \bar{h}_{m}^{\mathbf{E}} r_{\mathbf{A}bc}^{km},$$

$$(4.41)$$

$$\Delta_{\mathbf{A}bc}^{bc} = \bar{h}_{\mathbf{A}}^{\mathbf{E}} r_{bc}^{\mathbf{E}}^{\mathbf{E}} + \bar{h}_{\mathbf{A}m}^{\mathbf{k}\mathbf{E}} r_{bc}^{\mathbf{E}}^{m} + \sum_{\mathbf{E} < f} \bar{h}_{\mathbf{A}b}^{\mathbf{E}f} r_{\mathbf{E}fc}^{k} + \frac{1}{2} \bar{h}_{\mathbf{A}m}^{\mathbf{E}\mathbf{F}} r_{bc}^{\mathbf{E}\mathbf{F}}, \tag{4.42}$$

$$\Delta_{\mathbf{AbC}}^{k} = \chi_{\mathbf{AbC}}^{k} + \frac{1}{2}\bar{h}_{\mathbf{Ab}}^{ef}r_{\mathbf{C}ef}^{k} + \sum_{\mathbf{E} < f} \bar{h}_{\mathbf{A}m}^{\mathbf{E}f}r_{\mathbf{b}\mathbf{C}\mathbf{E}f}^{km}, \tag{4.43}$$

and

$$\Delta_{\mathbf{Abc}}^{k} = \chi_{\mathbf{Abc}}^{k} + \bar{h}_{\mathbf{A}}^{\mathbf{E}} r_{\mathbf{Ebc}}^{k} + \bar{h}_{\mathbf{A}m}^{k\mathbf{E}} r_{\mathbf{Ebc}}^{m} + \sum_{\mathbf{E} < f} \bar{h}_{\mathbf{Ab}}^{\mathbf{E}f} r_{\mathbf{E}fc}^{k} + \frac{1}{2} \bar{h}_{\mathbf{A}m}^{\mathbf{EF}} r_{\mathbf{bc}\mathbf{EF}}^{km}.$$

$$(4.44)$$

Finally, the DEA-EOMCC(3p-1h, 4p-2h) $\{N_u\}$ equations defining the projections on the selected 4p-2h determinants $|\Phi^{\mathbf{AB}cd}\rangle$ have the following form:

$$\langle \Phi^{\mathbf{AB}cd}_{kl} | (\bar{H}_{N.\text{open}}^{(\text{CCSD})} R_{\mu}^{(+2)})_C | \Phi \rangle = \mathscr{A}_{\mathbf{AB}} \mathscr{A}_{cd} \mathscr{A}^{kl} \mathscr{T}_{\mathbf{AB}cd}^{cd} = \omega_{\mu}^{(N)} r_{\mathbf{AB}cd}^{cd}, \tag{4.45}$$

where

$$\mathscr{T}_{\mathbf{ABC}d}^{\quad kl} = \chi_{\mathbf{ABC}d}^{\quad kl} + \Delta_{\mathbf{ABC}d}^{\quad kl}, \tag{4.46}$$

$$\mathscr{T}_{\mathbf{ABcD}}^{kl} = -\beta_{\mathbf{DBcA}}^{kl} - \Delta_{\mathbf{ADcB}}^{kl}, \tag{4.47}$$

and

$$\mathscr{T}_{\mathbf{ABcd}}^{\quad kl} = \Delta_{\mathbf{ABcd}}^{\quad kl},\tag{4.48}$$

with

$$\chi_{\mathbf{A}\mathbf{B}cd}^{kl} = -\frac{1}{6}\bar{h}_{\mathbf{A}m}^{kl}r_{\mathbf{B}cd}^{m} + I_{\mathbf{A}\mathbf{B}m}^{k}t_{cd}^{lm} + \frac{1}{2}I_{\mathbf{A}\mathbf{B}c}^{e}t_{de}^{kl} + \frac{1}{12}\bar{h}_{m}^{k}r_{\mathbf{A}\mathbf{B}cd}^{lm} + \frac{1}{48}\bar{h}_{mn}^{kl}r_{\mathbf{A}\mathbf{B}cd}^{mn},$$
(4.49)

$$\beta_{\mathbf{ABcD}}^{kl} = \frac{1}{2} \bar{h}_{\mathbf{DB}}^{ke} r_{\mathbf{cA}}^{l}_{e}, \tag{4.50}$$

$$\Delta_{\mathbf{ABC}d}^{kl} = \frac{1}{2} \bar{h}_{\mathbf{AB}}^{ke} r_{\mathbf{C}de}^{l} - \frac{1}{6} \bar{h}_{\mathbf{A}}^{e} r_{\mathbf{BC}de}^{kl} + \frac{1}{3} \bar{h}_{\mathbf{A}m}^{ke} r_{\mathbf{BC}de}^{lm} + \frac{1}{4} \sum_{\mathbf{E} < f} \bar{h}_{\mathbf{AB}}^{\mathbf{E}f} r_{\mathbf{C}d\mathbf{E}f}^{kl},$$

$$(4.51)$$

$$\Delta_{\mathbf{DBcA}}^{kl} = \chi_{\mathbf{DBcA}}^{kl} - \frac{1}{6} \bar{h}_{\mathbf{A}}^{e} r_{\mathbf{BcDe}}^{kl} + \frac{1}{3} \bar{h}_{\mathbf{A}m}^{ke} r_{\mathbf{BcDe}}^{lm} + \frac{1}{4} \sum_{\mathbf{E} < f} h_{\mathbf{AB}}^{\mathbf{E}f} r_{\mathbf{cDE}f}^{kl}$$

$$(4.52)$$

and

$$\Delta_{\mathbf{ABcd}}^{kl} = \chi_{\mathbf{ABcd}}^{kl} + \frac{1}{2} \bar{h}_{\mathbf{AB}}^{k\mathbf{E}} r_{\mathbf{cdE}}^{l} - \frac{1}{6} \bar{h}_{\mathbf{A}}^{\mathbf{E}} r_{\mathbf{BcdE}}^{kl} + \frac{1}{3} \bar{h}_{\mathbf{Am}}^{k\mathbf{E}} r_{\mathbf{BcdE}}^{lm} + \frac{1}{8} h_{\mathbf{AB}}^{\mathbf{EF}} r_{\mathbf{cdEF}}^{kl}$$

$$(4.53)$$

In addition, the above equations for DEA-EOMCC(3p-1h){ N_u } approximation make use several recursively generated intermediates which are as follows:

$$I_{\mathbf{A}m} = \tilde{I}_{\mathbf{A}m} + v_{mn}^{ef} r_{\mathbf{A}ef}^{n} \tag{4.54}$$

and

$$I_{\mathbf{a}m} = \tilde{I}_{\mathbf{a}m} + 2\sum_{\mathbf{E} < f} v_{mn}^{\mathbf{E}f} r_{\mathbf{a}\mathbf{E}f}^{n}, \tag{4.55}$$

where

$$\tilde{I}_{am} = \bar{h}_{am}^{ef} r_{ef}, \tag{4.56}$$

and

$$I_{\mathbf{A}bm}^{k} = \tilde{I}_{\mathbf{A}bm}^{k} + \frac{1}{2}\bar{h}_{mn}^{ke}r_{\mathbf{A}be}^{n} - \sum_{\mathbf{E} < f}\bar{h}_{\mathbf{A}m}^{\mathbf{E}f}r_{b\mathbf{E}f}^{k}$$
$$+ \frac{1}{2}\sum_{\mathbf{E} < f}v_{mn}^{\mathbf{E}f}r_{\mathbf{A}b\mathbf{E}f}^{kn}, \tag{4.57}$$

$$I_{\mathbf{a}\mathbf{B}m}^{k} = \tilde{I}_{\mathbf{a}\mathbf{B}m}^{k} + \frac{1}{2}\bar{h}_{mn}^{ke}r_{\mathbf{a}\mathbf{B}e}^{n} - \frac{1}{2}\bar{h}_{\mathbf{a}m}^{ef}r_{\mathbf{B}ef}^{k} + \frac{1}{2}\sum_{\mathbf{E}< f}v_{mn}^{\mathbf{E}f}r_{\mathbf{a}\mathbf{B}\mathbf{E}f}^{kn},$$

$$(4.58)$$

and

$$I_{\mathbf{ab}m}^{k} = \tilde{I}_{\mathbf{ab}m}^{k} + \frac{1}{2}\bar{h}_{mn}^{k}r_{\mathbf{ab}E}^{n} - \frac{1}{2}\sum_{\mathbf{E}< f}\bar{h}_{\mathbf{am}}^{\mathbf{E}f}r_{\mathbf{bE}f}^{k} + \frac{1}{4}v_{mn}^{\mathbf{E}F}r_{\mathbf{ab}EF}^{kn}, \tag{4.59}$$

where

$$I_{abm}^{\ k} = \bar{h}_{am}^{ke} r_{be} + \frac{1}{8} I_{mn} t_{ab}^{kn}, \tag{4.60}$$

and

$$I_{\mathbf{A}bc}^{\ e} = \bar{h}_{\mathbf{A}b}^{ef} r_{cf} - \bar{h}_{\mathbf{A}m}^{e\mathbf{F}} r_{bc\mathbf{F}}^{\ m} + \frac{1}{3} \sum_{e>\mathbf{F}} v_{mn}^{e\mathbf{F}} r_{\mathbf{A}bc\mathbf{F}}^{\ mn}, \tag{4.61}$$

$$I_{\mathbf{aBc}}^{e} = \bar{h}_{\mathbf{aB}}^{ef} r_{\mathbf{c}f} - \bar{h}_{\mathbf{a}m}^{ef} r_{\mathbf{Bc}f}^{m} + \frac{1}{3} \sum_{e>\mathbf{F}} v_{mn}^{e\mathbf{F}} r_{\mathbf{aBc}F}^{mn}, \tag{4.62}$$

$$I_{\mathbf{abC}}^{e} = \bar{h}_{\mathbf{ab}}^{ef} r_{\mathbf{C}f} - \bar{h}_{\mathbf{am}}^{ef} r_{\mathbf{bC}f}^{m} + \frac{1}{3} \sum_{e>\mathbf{F}} v_{mn}^{e\mathbf{F}} r_{\mathbf{abCF}}^{mn}, \tag{4.63}$$

and

$$I_{\mathbf{abc}}^{\ e} = \bar{h}_{\mathbf{ab}}^{ef} r_{\mathbf{c}f}. \tag{4.64}$$

The antisymmetrizer $\mathscr{A}_{pq} = \mathscr{A}^{pq}$, which enters the above equations is defined as

$$\mathscr{A}_{pq} \equiv \mathscr{A}^{pq} = 1 - (pq), \tag{4.65}$$

with (pq) representing the transposition of indices p and q.

Next, we consider some key components of the efficient computer implementation of the DEA-EOMCC(3p-1h,4p-2h){ N_u } eigenvalue equations, namely, Eqs. (4.29) - (4.64). Figure (4.1) gives the important details of the algorithm that is used to compute the projection of the DEA-EOMCC eigenvalue problem on the selected 3p-1h determinants. The algorithm for calculating the remaining 2p and 4p-2h projections is similar but we do not discuss it in this dissertation.

One important element of our algorithm is that the explicit loops that are used to construct the DEA-EOMCC(3p-1h,4p-2h){ N_u } equations projected on $|\Phi^{\mathbf{A}bc}_{k}\rangle$, Eq. 4.37, range over active indices represented by the use of bold, uppercase letters for variables in the loop. Within these loops, we have utilized a high degree of vectorization while exploiting efficient matrix multiplication routines from the BLAS library to perform essential computations. In doing so, we have maintained the Einstein summation convention throughout and also imposed the traditional summation symbol Σ in instances where at least one unoccupied free index belongs to the active set of orbitals.

```
Calculate \tilde{I}_{am} for all values of e,f Eq. (4.56)
Set I_{am} = I_{am} for all values of a, m
LOOP OVER D
   Calculate I_{\mathbf{D}m} = I_{\mathbf{D}m} + v_{mn}^{ef} r_{\mathbf{D}ef}^{\ n} for all values of m, Eq. (4.54)
   Calculate I_{\mathbf{a}m}=I_{\mathbf{a}m}+2\sum_{n}\sum_{f(>\mathbf{D})}v_{mn}^{\mathbf{D}f}r_{\mathbf{a}\mathbf{D}f}^{n} for all values of \mathbf{a},m, Eq. (4.55)
END OF LOOP OVER {f D}
LOOP OVER A
   Calculate \chi_{{f A}bc}^{\quad k} and \Delta_{{f A}bc}^{\quad k} for all values b,c,k, Eqs. (4.41) and (4.42)
   Set \Delta_{\mathbf{A}\mathbf{b}c}^{\quad k} = \chi_{\mathbf{A}\mathbf{b}c}^{\quad k} for all values of \mathbf{b}, c, k
   LOOP OVER E
       Calculate \Delta_{\mathbf{Abc}}^{\phantom{\mathbf{bc}}k} = \Delta_{\mathbf{Abc}}^{\phantom{\mathbf{bc}}k} + \bar{h}_{\mathbf{A}}^{\mathbf{E}} r_{\mathbf{Ebc}}^{\phantom{\mathbf{bc}}k} + \bar{h}_{\mathbf{A}m}^{\mathbf{EE}} r_{\mathbf{Ebc}}^{\phantom{\mathbf{Ebc}}m} + \sum_{\mathbf{E} < f} \bar{h}_{\mathbf{Ab}}^{\mathbf{Ef}} r_{\mathbf{Efc}}^{\phantom{\mathbf{Efc}}k} + \frac{1}{2} \bar{h}_{\mathbf{A}m}^{\mathbf{EF}} r_{\mathbf{bc}\mathbf{EF}}^{\phantom{\mathbf{EFc}}k} for
       all values of \mathbf{b}, \mathbf{c}, k, Eq. (4.44)
       Calculate \Delta_{\mathbf{A}\mathbf{b}\mathbf{C}}^{\ k} = \Delta_{\mathbf{A}\mathbf{b}\mathbf{C}}^{\ k} + \frac{1}{2}\bar{h}_{\mathbf{A}\mathbf{b}}^{ef}r_{\mathbf{C}ef}^{\ k} + \sum_{\mathbf{E}< f}\bar{h}_{\mathbf{A}m}^{\mathbf{E}f}r_{\mathbf{b}\mathbf{C}\mathbf{E}f}^{\ km} for all values of \mathbf{b},\mathbf{C},k,
       Eq. (4.43)
   END OF LOOP OVER {f E}
   Set \mathscr{T}_{\mathbf{Abc}}^{\quad k} = \Delta_{\mathbf{Abc}}^{\quad k}, Eq. (4.40)
END OF LOOP OVER A
LOOP OVER A
   LOOP OVER D
       Calculate \mathscr{T}_{\mathbf{AD}_c}^{\ \ k} for all values of c,k, Eq. (4.38)
       Calculate \mathscr{T}_{\mathbf{AbD}}^{k} for all values of \mathbf{b}, k, Eq. (4.39)
   END OF LOOP OVER {f D} Calculate \langle \Phi^{{f A}bc}_{\ k}|(\bar{H}_{N,{
m open}}^{({
m CCSD})}R_{\mu}^{(+2)})_C|\Phi 
angle by antisymmetrizing
\mathscr{T}_{\mathbf{A}bc}^{\phantom{A}k}, Eq. (4.37)
END OF LOOP OVER \mathbf{A}
```

Figure 4.1: The key elements of the algorithm used to compute $\langle \Phi^{\mathbf{A}bc}_{k} | (\bar{H}_{N,\text{open}}^{(\text{CCSD})} R_{\mu}^{(+2)})_{C} | \Phi \rangle$, Eq. (4.37), in the efficient implementation of the DEA-EOMCC(3*p*-1*h*,4*p*-2*h*){*N_u*} method.

4.2.4 The Remaining Algorithmic Details and Illustrative Timings of DEA-EOMCC(3p-1h) $\{N_u\}$ and DEA-EOMCC

 $(3p-1h, 4p-2h)\{N_u\}$ Calculations

As already alluded to above and as illustrated through examples of timings in Ref. [92], the active-space DEA-EOMCC(4p-2h) $\{N_u\}$ method offers a massive reduction in computer effort compared to its DEA-EOMCC(4p-2h) parent with virtually no loss of accuracy. Indeed, as demonstrated in Ref. [92], it is not unusual for the CPU timings of DEA-EOMCC(4p-2h) $\{N_u\}$ calculations to be hundreds of times smaller than the timings of the corresponding full DEA-EOMCC(4p-2h) computations. This is a consequence of the fact that it is sufficient to use small numbers of active unoccupied orbitals in the DEA-EOMCC(4p-2h) $\{N_u\}$ calculations, which represent a tiny fraction of the total number of unoccupied orbitals in the MO basis, to obtain reasonably converged results. The DEA-EOMCC(3p-1h,4p-2h) $\{N_u\}$ approach developed in this study, which treats both 3p-1h and 4p-2h components of the $R_{\mu}^{(+2)}$ operator, not just the 4p-2h components, using active orbitals is even more economical. This is illustrated in Table 4.3, where we compare the CPU times per iteration characterizing the DEA-EOMCC diagonalization steps required by the full and active-space DEA-EOMCC(3p-1h) and activespace DEA-EOMCC(3p-1h,4p-2h) $\{N_u\}$ and DEA-EOMCC(4p-2h) $\{N_u\}$ calculations for the X 3A_2 state of the TMM molecule, as described by the cc-pVDZ and cc-pVTZ basis sets [215].

We recall that our group used the various DEA- and DIP-EOMCC methods to study the TMM system in Refs. [92] and [93]. As explained in Refs. [92] and [93], the TMM molecule is large enough to make the full DEA-EOMCC(4p-2h) calculations using the cc-pVDZ and cc-pVTZ basis sets prohibitively expensive, so the highest DEA-EOMCC level included in

Table 4.3: A comparison of CPU times required by the various DEA-EOMCC calculations characterizing the X 3A_2 state of TMM, as described by the cc-pVDZ and, in parentheses, cc-pVTZ basis sets, along with the formal scalings of the most expensive steps in the diagonalization of $\bar{H}_{N,\text{open}}$ with n_o , n_u , and N_u .

Method	CPU Time Scaling	CPU Time/Iteration $(\min)^b$
DEA-EOMCC(3 p -1 h){ N_u }	$N_u n_o n_u^4$	0.05 (1.5)
DEA-EOMCC $(3p-1h)$	$n_o n_u^5$	0.43 (43.5)
DEA-EOMCC $(3p-1h,4p-2h)\{N_u\}$	$N_u^2 n_o^2 n_u^4 + N_u n_o n_u^4$	2.75(65.0)
DEA-EOMCC $(4p-2h)\{N_u\}$	$N_u^2 n_o^2 n_u^4 + n_o n_u^5$	4.43 (136.0)

 $[^]a$ The TMM²⁺ reference system used in the DEA-EOMCC calculations was obtained by vacating the doubly degenerate valence 1e'' orbitals of the TMM's π system (using the D_{3h} symmetry of the X $^3A'_2$ state). The lowest-energy core orbitals correlating with the 1s shells of the carbon atoms were frozen in the post-SCF calculations and the spherical components of the d and f orbitals were employed throughout. The active space used to select 3p-1h and 4p-2h components consisted of the doubly degenerate 1e'' and non-degenerate $2a''_2$ orbitals, which are the three lowest-energy unoccupied MOs in the TMM²⁺ reference system, so N_u was set at 3.

Table 4.3 is DEA-EOMCC(4p-2h){ N_u }. This is sufficient for the analysis presented here, since the CPU time savings offered by the active-space DEA-EOMCC(4p-2h){ N_u } approach vs. its full DEA-EOMCC(4p-2h) counterpart have already been discussed in Refs. [92] and [93], whereas the main objective of this dissertation is to show additional savings in the computer effort offered by the DEA-EOMCC(3p-1h,4p-2h){ N_u } and DEA-EOMCC(3p-1h){ N_u } approximations developed in the present work. As one can see in Table 4.3, the DEA-EOMCC(3p-1h,4p-2h){ N_u } calculations for the X 3A_2 state of TMM, which use three active orbitals to select the dominant 3p-1h and 4p-2h amplitudes, are about twice as fast as the corresponding DEA-EOMCC(4p-2h){ N_u } computations, in which 3p-1h contributions are treated fully. At the same time, as shown in Section 4.3.3, there is virtually no loss of accuracy when the singlet-triplet gaps in TMM resulting from the DEA-EOMCC(3p-1h,4p-2h){3} and DEA-EOMCC(3p-1h,4p-2h){3} calculations are compared with each other and with experiment.

Interestingly, as shown in Table 4.3 as well, the CPU timings of the higher-level DEA-

^b The CPU time per iteration characterizing the DEA-EOMCC diagonalization step obtained on a single core of the PowerEdge R910 system from Dell using 8-core Intel Xeon X7560 2.26GHz processor boards.

EOMCC $(3p-1h,4p-2h)\{3\}$ calculations for the system, which include 3p-1h and 4p-2h contributions, are on the same order as the timings characterizing the corresponding lowerlevel DEA-EOMCC(3p-1h) computations, which neglect 4p-2h effects altogether. This is especially true when the larger cc-pVTZ basis set is employed. We observe the same when other molecular systems are examined. Thus, with the development of the DEA-EOMCC(3p-1h,4p-2h) $\{N_u\}$ method in this work, we have gained the ability to perform routine electronic structure calculations at the very high DEA-EOMCC(4p-2h) level, at least for medium-sized molecular systems, which, as shown in the next section and our earlier work [92, 93], provide chemical ($\sim 1 \text{ kcal/mol}$) or better accuracy in describing low-lying states of diradicals and single bond breaking in closed-shell species, improving the results of the corresponding DEA-EOMCC(3p-1h) calculations. At the same time, through the development of the active-space DEA-EOMCC(3p-1h) $\{N_u\}$ approach in this work, we have made the DEA-EOMCC(3p-1h) calculations a lot more practical. For example, as shown in Table 4.3, the DEA-EOMCC(3p-1h){3} calculations for TMM are about 30 times faster than the corresponding full DEA-EOMCC(3p-1h) computations, when the cc-pVTZ basis set is employed, and, as demonstrated in Section 4.3.3, there is virtually no loss of accuracy in the description of the singlet-triplet gap in TMM when full DEA-EOMCC(3p-1h) is replaced by its active-space DEA-EOMCC(3p-1h) $\{N_u\}$ counterpart. Similar observations apply to other molecular systems. A few representative examples comparing the accuracy of the full DEA-EOMCC(3p-1h) and active-space DEA-EOMCC(3p-1h) $\{N_u\}$, active-space DEA- $EOMCC(3p-1h,4p-2h)\{N_u\}$ and $DEA-EOMCC(4p-2h)\{N_u\}$, and full $DEA-EOMCC(4p-2h)\{N_u\}$ approaches are discussed next.

4.3 Numerical Examples

In order to assess the performance of the active-space DEA-EOMCC(3p-1h) $\{N_u\}$ and DEA-EOMCC(3p-1h,4p-2h) $\{N_u\}$ methods developed in this work, we have carried out several benchmark calculations that are representative of the types of problems such methods may be useful for, which are low-lying singlet and triplet states of diradical species and single bond breaking in closed-shell molecules leading to doublet radical fragments. Because of the methodological nature of this work, where our main goal is to compare the results obtained in the relatively inexpensive DEA-EOMCC(3p-1h){ N_u } and DEA-EOMCC(3p-1h,4p-2h){ N_u } calculations, in which 3p-1h or 3p-1h and 4p-2h components of the respective $R_{\mu}^{(+2)}$ operators are treated using active orbitals, with the parent full DEA-EOMCC(3p-1h) and DEA-EOMCC(4p-2h) data and the results of the DEA-EOMCC(4p-2h) $\{N_u\}$ computations, in which 4p-2h amplitudes are selected using active orbitals, but 3p-1h contributions are treated fully, in the analysis presented in this dissertation we focus on smaller and medium size molecular systems with up six non-hydrogen (second row) atoms. Some of the benchmark systems discussed are small enough to allow for the exact, full CI, and nearly exact, full DEA-EOMCC(4p-2h) calculations, and all of them can be treated with the DEA-EOMCC(3p-1h)and DEA-EOMCC(4p-2h) $\{N_u\}$ approaches that provide important reference data for their less expensive DEA-EOMCC(3p-1h) $\{N_u\}$ and DEA-EOMCC(3p-1h,4p-2h) $\{N_u\}$ counterparts developed in this work. Most of the test cases considered here have been included in our recent DEA-EOMCC studies [92–94, 117] and some are new in this context.

In the discussion below, we examine the following molecular problems: (i) the adiabatic energy gaps between the triplet ground state $(X \, ^3B_1)$ and the three low-lying singlet excited states $(A \, ^1A_1, \, B \, ^1B_1, \, \text{and} \, C \, ^1A_1)$ of methylene, as described by the [5s3p/3s] triple zeta

basis set of Dunning [216] augmented with two sets of polarization functions, abbreviated as TZ2P, for which the exact, full CI, results have been reported in Ref. [217] (see Table 4.4), (ii) the singlet-triplet gaps of methylene obtained by the DEA-EOMCC approaches with larger, up to quintuple, zeta basis sets, extrapolated to the complete basis set (CBS) limit (see Table 4.5), (iii) the adiabatic separation between the D_{3h} -symmetric X $^3A'_2$ ground state, which has a largely single-reference nature, and the C_{2v} -symmetric $B^{-1}A_1$ excited state, which has a multi-reference, diradical, character, in TMM, as described by the cc-pVDZ and cc-pVTZ basis sets, which has accurately been determined in Ref. [147] by subtracting the theoretical zero-point vibrational energy corrections ($\Delta ZPVE$) resulting from spin-flip density-functional-theory (SF-DFT/6-31G(d)) calculations [147] from the experimental values of the $B^{-1}A_1 - X^{-3}A_2'$ gap obtained in photoelectron spectroscopy measurements in Ref. [218] (see Table 4.6; cf. Table 4.3 for the corresponding CPU timings), (iv) the vertical singlet-triplet gaps in the antiaromatic cyclobutadiene and its derivatives and cyclopentadienyl cation diradicals, as described by the cc-pVDZ and maug-cc-pVTZ basis sets, for which geometries of the triplet states have been optimized in Ref. [219] (see Tables 4.7 and 4.8), and (v) the F-F bond dissociation in the F₂ molecule, as described by the double zeta (DZ) basis set [220], for which the exact, full CI, results can be found in Ref. [221] (see Table 4.9).

One of the important aspects of any DEA-EOMCC work is the choice of orbitals used to construct the corresponding wave function expansions. As explained in Refs. [92–94], one typically has a choice between the symmetry-adapted RHF or ROHF orbitals obtained in the calculations for the singlet (RHF) and triplet (ROHF) states of the N-electron target system or the RHF MOs optimized for the corresponding (N-2)-electron closed-shell core. Both strategies are considered in this work. In doing so, one has to be aware of the fact that the singlet RHF orbitals of the target N-electron system may lift orbital degeneracies

when the N-electron species of interest has a non-Abelian symmetry, resulting in undesirable symmetry-broken DEA-EOMCC wave function expansions [92–94]. As explained in Ref. [93] and as further elaborated on below, this would, for example, happen if we tried to exploit the RHF MOs optimized for the B $^{1}A_{1}$ singlet state of TMM in the calculations for the corresponding D_{3h} -symmetric X $^3A_2'$ triplet state. In cases like this, one can either use the high-spin ROHF orbitals of the N-electron target system or the dicationic RHF orbitals corresponding to the (N-2)-electron closed-shell core, which allow us to maintain the relevant spatial symmetries throughout the DEA-EOMCC calculations (adaptation to spin symmetry is automatic as long as restricted orbitals are employed). This is what we do in this work, i.e., all of the DEA-EOMCC calculations discussed in this dissertation provide spin- and symmetry-adapted results. One of the main findings of our group's previous studies, especially those reported in Ref. [93], has been the observation that the results of the DEA-EOMCC computations including 4p-2h contributions are practically insensitive to the choice of the underlying MO basis, whereas their lower-order DEA-EOMCC(3p-1h) counterparts may display a significant dependence on the type of orbitals used in the calculations. A similar behavior is observed in this work, i.e., the results obtained with the active-space DEA-EOMCC(3p-1h,4p-2h) $\{N_u\}$ approach are not only in very good agreement with the corresponding DEA-EOMCC(4p-2h) $\{N_u\}$ and DEA-EOMCC(4p-2h) data, especially if we take into account the relatively low costs of the DEA-EOMCC(3p-1h,4p-2h) $\{N_u\}$ calculations, but they are also less sensitive to the choice of the underlying MO basis than the corresponding DEA-EOMCC(3p-1h) $\{N_u\}$ and DEA-EOMCC(3p-1h) results. At the same time, the results of the active-space DEA-EOMCC(3p-1h) $\{N_u\}$ calculations display a similar type of dependence on the underlying MO basis as their parent full DEA-EOMCC(3p-1h) counterparts. This reemphasizes the point that the active-space treatment of 3p-1h contributions advocated in this study is sufficient to capture the bulk of 3p-1h effects.

4.3.1 Adiabatic Energy Gaps Involving Low-Lying Singlet and Triplet States of Methylene

We begin our discussion with the various DEA-EOMCC results for the X 3B_1 , A 1A_1 , B 1B_1 , and C 1A_1 electronic states of methylene, as described by the TZ2P basis set used in Ref. [217], where the authors performed the corresponding full CI calculations, optimizing the geometry of each of the four states at the full CI level as well. In performing the DEA-EOMCC calculations with the full and active-space treatments of 3p-1h and 4p-2h excitations, summarized in Table 4.4, we adopted the full CI/TZ2P geometries of the X 3B_1 , A 1A_1 , B 1B_1 , and C 1A_1 states reported in Ref. [217]. In our discussion, we focus on the adiabatic energy gaps between the triplet ground state and the three lowest-energy singlet excited states.

A few decades ago methylene was the subject of serious controversies between theory and experiment concerning the geometry of its triplet ground state and the small energy gap between the X 3B_1 and A 1A_1 states, where theory turned out to be crucial for providing correct answers (cf. Refs. [222–227] for selected historical accounts). Because of its small size, which allows for all kinds of electronic structure calculations, including the aforementioned full CI/TZ2P study [217] and the previously published DEA-EOMCC(3p-1h), DEA-EOMCC(4p-2h), and DEA-EOMCC(4p-2h) $\{N_u\}$ data obtained with the TZ2P basis set as well, which are used in this work to test the DEA-EOMCC(3p-1h) $\{N_u\}$ and DEA-EOMCC(3p-1h,4p-2h) $\{N_u\}$ approaches, and because of its complicated electronic spectrum, which consists of excited states that are difficult to describe in an accurate and balanced

manner, methylene has become an important benchmark system for testing quantum chemistry methods (cf. Refs. [92] and [93], and the long list of references cited therein for some of the most representative examples of the past ab initio computations for the ground and excited states of CH₂). We also recall that while the ground and second excited states, X $^{3}B_{1}$ and B $^{1}B_{1}$, respectively, can be characterized as having a single-reference characterized ter, which is well represented by the high-spin triplet and open-shell singlet configurations of the $(1a_1)^2(2a_1)^2(1b_2)^2(3a_1)^1(1b_1)^1$ type, the first excited $A^{-1}A_1$ state and the third excited $C^{-1}A_1$ state have a manifestly multi-reference nature that originates from mixing the $(1a_1)^2(2a_1)^2(1b_2)^2(3a_1)^2$ and $(1a_1)^2(2a_1)^2(1b_2)^2(1b_1)^2$ configurations, which is particularly severe in the case of the strongly diradical $C^{-1}A_1$ state. Thus, in order to obtain accurate results for the adiabatic energy gaps between the X 3B_1 ground state and the A 1A_1 , B 1B_1 , and $C^{-1}A_1$ excited states, one has to use methods that can provide a well-balanced treatment of the dynamical and non-dynamical electron correlation effects. This makes methylene a valuable benchmark system for testing the active-space DEA-EOMCC(3p-1h) $\{N_u\}$ and DEA-EOMCC(3p-1h,4p-2h) $\{N_u\}$ methods developed in this work.

In all of the DEA-EOMCC calculations summarized in Table 4.4, the (N-2)-electron CH_2^{2+} reference system was obtained by vacating the highest occupied MO (HOMO), $3a_1$, of CH_2 . In order to examine the dependence of the various DEA-EOMCC results on the type of orbitals that are used to define the corresponding wave function expansions, we used both the ground-state RHF orbitals of the CH_2^{2+} reference dication and the RHF or ROHF MOs optimized for the CH_2 target system. In the latter case, we followed Refs. [92] and [93] and adopted three different strategies. In the first strategy, we constructed the DEA-EOMCC wave function expansions for all the calculated states using the ROHF orbitals obtained for the X 3B_1 state of methylene. In the second strategy,

Table 4.4: A comparison of the full CI and various DEA-EOMCC adiabatic excitation energies, along with the corresponding MaxUE and NPE values relative to full CI, characterizing the low-lying states of methylene, as described by the TZ2P basis set.^a

Orbitals	Method	$A^{1}A_{1} - X^{3}B_{1}$	$B^{1}B_{1} - X^{3}B_{1}$	$C^{1}A_{1} - X^{3}B_{1}$	MaxUE	NPE
(N-2)-electron RHF ^b	DEA-EOMCC $(3p-1h)\{2\}^c$	1.30	-0.82	-1.00	1.30	2.30
	DEA-EOMCC $(3p-1h)$	-0.11	-1.89	-3.64	3.64	3.53
	DEA-EOMCC $(3p-1h,4p-2h)\{2\}^c$	1.67	0.82	2.28	2.28	1.46
	DEA-EOMCC $(4p-2h)\{2\}^c$	0.13	-0.35	-0.54	0.54	0.67
	DEA-EOMCC $(4p-2h)$	0.38	-0.02	0.21	0.38	0.40
N-electron ROHF ^{d}	DEA-EOMCC $(3p-1h)\{2\}^c$	1.47	0.63	1.42	1.47	0.84
	DEA-EOMCC $(3p-1h)$	0.64	0.10	0.45	0.64	0.54
	DEA-EOMCC $(3p-1h,4p-2h)\{2\}^c$	0.63	0.48	0.58	0.63	0.16
	DEA-EOMCC $(4p-2h)\{2\}^c$	-0.22	-0.05	-0.29	0.29	0.24
	DEA-EOMCC $(4p-2h)$	0.19	0.08	0.37	0.37	0.29
N -electron RHF e	DEA-EOMCC $(3p-1h)\{2\}^c$	-0.11	-0.50	0.17	0.50	0.67
	DEA-EOMCC $(3p-1h)$	0.29	-0.15	-0.31	0.31	0.60
	DEA-EOMCC $(3p-1h,4p-2h)\{2\}^c$	0.16	-0.42	-0.01	0.42	0.60
	DEA-EOMCC $(4p-2h)\{2\}^c$	0.66	-0.02	-0.28	0.66	0.94
	DEA-EOMCC $(4p-2h)$	0.14	0.09	0.38	0.38	0.29
N -electron ROHF/RHF f	DEA-EOMCC $(3p-1h)\{2\}^c$	2.19	1.79	2.46	2.46	0.67
	DEA-EOMCC $(3p-1h)$	1.53	1.09	0.93	1.53	0.60
	DEA-EOMCC $(3p-1h,4p-2h)\{2\}^c$	0.76	0.18	0.59	0.76	0.58
	DEA-EOMCC $(4p-2h)\{2\}^c$	0.12	-0.56	-0.82	0.82	0.94
	DEA-EOMCC $(4p-2h)$	0.19	0.14	0.43	0.43	0.29
	Full CI^a	11.14	35.59	61.67		

 $[^]a$ The basis set, geometries, and full CI energies were taken from Ref. [217]. The full CI values are the adiabatic excitation energies, in kcal/mol, whereas the remaining values are errors relative to full CI, also in kcal/mol. The CH_2^{2+} reference system used in the DEA-EOMCC calculations was created by vacating the $3a_1$ HOMO of CH_2 . As in Ref. [217], the lowest occupied orbital and the highest unoccupied orbital were frozen in the post-SCF calculations and the spherical components of the carbon d orbital were employed throughout.

b The RHF orbitals obtained for the singlet ground state of CH_2^{2+} were employed.

The active space consisted of the HOMO and LUMO of CH_2 , $3a_1$ and $1b_1$, respectively, which are unoccupied in the CH₂²⁺ reference system used in the DEA-EOMCC calculations.

d The ROHF orbitals obtained for the X 3B_1 state of CH₂ were employed.

 $[^]e$ The RHF orbitals obtained for the A 1A_1 state of CH₂ were employed. f The ROHF orbitals of CH₂ for the X 3B_1 state and the A 1A_1 RHF orbitals of CH₂ for the remaining three states were employed.

we utilized the RHF orbitals optimized for the $A^{-1}A_1$ state. In the third strategy, we used the X 3B_1 ROHF orbitals in the DEA-EOMCC calculations for the triplet ground state and the A $^{1}A_{1}$ RHF orbitals for the remaining three singlet states. For each choice of the MO basis, the active orbitals employed in the DEA-EOMCC(3p-1h) $\{N_u\}$, DEA- $EOMCC(3p-1h,4p-2h)\{N_u\}$, and $DEA-EOMCC(4p-2h)\{N_u\}$ calculations were the HOMO orbital $3a_1$ and the lowest unoccupied MO (LUMO) $1b_1$ of methylene, which are unoccupied in the CH_2^{2+} dication that serves as a reference system for the DEA-EOMCC considerations. In other words, the number of active unoccupied orbitals, N_u , used to define 3p-1h component in the DEA-EOMCC(3p-1h){N_u} calculations, 3p-1h and 4p-2h component in the DEA-EOMCC(3p-1h) ponents in the DEA-EOMCC(3p-1h,4p-2h){ N_u } computations, and 4p-2h component in the DEA-EOMCC(4p-2h) $\{N_u\}$ calculations was set at 2, making the resulting diagonalizations of the similarity-transformed Hamiltonian only a few times more expensive than the conventional closed-shell CCSD calculations in the DEA-EOMCC(3p-1h,4p-2h) $\{N_u\}$ and DEA-EOMCC(4p-2h) $\{N_u\}$ cases and less expensive than CCSD in the case of DEA-EOMCC(3p-1h){ N_u }. As shown in Ref. [92], the DEA-EOMCC(4p-2h){2} calculations for the TZ2P model of methylene considered here are about 400 times faster than the corresponding full DEA-EOMCC(4p-2h) computations and only 4 times slower than the DEA-EOMCC(3p-1h) calculations. The DEA-EOMCC(3p-1h,4p-2h){2} computations are even faster.

The adiabatic $A^{1}A_{1}-X^{3}B_{1}$, $B^{1}B_{1}-X^{3}B_{1}$, and $C^{1}A_{1}-X^{3}B_{1}$ excitation energies collected in Table 4.4 and the corresponding maximum unsigned error (MaxUE) and NPE values demonstrate that there is a generally good agreement between the results of the inexpensive active-space DEA-EOMCC(3p-1h){2} calculations and their full DEA-EOMCC(3p-1h) counterparts and among the results of the active-space DEA-EOMCC(3p-1h,4p-2h){2} and

DEA-EOMCC(4p-2h){2} and full DEA-EOMCC(4p-2h) computations. As opposed to the DIP-EOMCC approach truncated at 3h-1p excitations, which we examined in our previous studies [92, 93] and which in the case of the TZ2P model of methylene may produce errors as large as 10.94 kcal/mol, none of the DEA-EOMCC methods examined in the present work fails, i.e., the DEA-EOMCC calculations truncated at 3p-1h terms are capable of providing reasonable gap values, especially when one uses MOs optimized for the target CH₂ system. Nevertheless, the inclusion of 4p-2h correlations through the relatively inexpensive DEA-EOMCC(3p-1h,4p-2h){2} calculations, which describe 3p-1h and 4p-2h effects using active orbitals, is helpful and worth analyzing here. As shown in Sections 4.2.1 and 4.2.2, 4p-2h contributions become larger when other diradical systems considered in this study are examined, but we begin our discussion with methylene, since we have access to the largest amount of numerical data in this case.

We first observe that the differences between the DEA-EOMCC(3p-1h){2} and DEA-EOMCC(3p-1h) gap values are almost identical to the analogous differences between the gaps obtained in the DEA-EOMCC(3p-1h,4p-2h){2} and DEA-EOMCC(4p-2h){2} calculations. Indeed, if we, for example, examine the $A^{-1}A_1 - X^{-3}B_1$ energy separations calculated using the RHF MOs of the CH_2^{2+} reference system, the ROHF MOs optimized for the triplet ground state of CH_2 , the RHF MOs optimized for the $A^{-1}A_1$ state of CH_2 , and the ROHF MOs of CH_2 for the $X^{-3}B_1$ state combined with the RHF MOs of CH_2 for the singlet states, the differences between the DEA-EOMCC(3p-1h){2} and DEA-EOMCC(3p-1h) results, of 1.41, 0.83, 0.40, and 0.66 kcal/mol, respectively, are almost identical to the analogous differences between the DEA-EOMCC(3p-1h,4p-2h){2} and DEA-EOMCC(4p-2h){2} data, which are 1.54, 0.85, 0.50, and 0.64 kcal/mol. This is not surprising, since the DEA-EOMCC(3p-1h){2} and DEA-EOMCC(3p-1h) calculations and the

DEA-EOMCC(3p-1h,4p-2h){2} and DEA-EOMCC(4p-2h){2} calculations differ in exactly the same manner, namely, DEA-EOMCC $(3p-1h)\{2\}$ and DEA-EOMCC $(3p-1h,4p-2h)\{2\}$ treat 3p-1h terms using active orbitals, whereas DEA-EOMCC(3p-1h) and DEA-EOMCC $(4p-2h)\{2\}$ treat them fully. Because of the approximate treatment of 3p-1h contributions in the DEA-EOMCC $(3p-1h,4p-2h)\{2\}$ calculations, the agreement between the DEA-EOMCC(3p-1h,4p-2h){2} and full DEA-EOMCC(4p-2h) data is not as good as in the case of DEA-EOMCC(4p-2h){2}, which uses active orbitals to select only the higherrank 4p-2h excitations, while treating 3p-1h contributions fully, but the relatively inexpensive DEA-EOMCC $(3p-1h,4p-2h)\{2\}$ calculations, which capture the dominant 3p-1h and 4p-2h correlations, improve the DEA-EOMCC(3p-1h){2} and DEA-EOMCC(3p-1h) results that neglect 4p-2h physics altogether. For example, if we look at the largest unsigned errors relative to full CI obtained in the calculations of the adiabatic $A^{-1}A_1 - X^{-3}B_1$, $B^{-1}B_1 - X^{-3}B_1$, and $C^{-1}A_1 - X^{-3}B_1$ energy gaps, represented in Table 4.4 by the MaxUE values, and focus on the DEA-EOMCC results obtained using the ROHF MOs of CH_2 for the triplet ground state and the RHF MOs of CH_2 for the remaining three singlet states, we can see significant improvement when going from DEA-EOMCC(3p-1h){2} and DEA-EOMCC(3p-1h), which give MaxUEs of 2.46 and 1.53 kcal/mol, respectively, to DEA-EOMCC $(3p-1h,4p-2h)\{2\}$, which gives MaxUE of 0.76 kcal/mol. In fact, the MaxUE value characterizing the DEA-EOMCC $(3p-1h,4p-2h)\{2\}$ calculations is virtually identical to that obtained with the more expensive DEA-EOMCC $(4p-2h)\{2\}$ approach, which gives 0.82 kcal/mol, and not much worse than the MaxUE of 0.43 kcal/mol characterizing the corresponding full DEA-EOMCC(4p-2h) computations. When the ROHF MOs of CH₂ are used in the calculations for all four states, the largest errors obtained with the active-space DEA- $EOMCC(3p-1h,4p-2h)\{2\}$ and full DEA-EOMCC(3p-1h) approaches are virtually identical, but the NPE characterizing the DEA-EOMCC(3p-1h,4p-2h){2} calculations, of 0.16 kcal/mol, is more than three times smaller than the NPE characterizing the corresponding DEA-EOMCC(3p-1h) data (0.54 kcal/mol). The use of ionic MOs obtained in the RHF calculations for the CH₂²⁺ dication worsens the DEA-EOMCC(3p-1h,4p-2h){2} results somewhat, but they are still better than the results of the corresponding DEA-EOMCC(3p-1h) computations, reducing the MaxUE and NPE values characterizing the adiabatic A $^1A_1 - X$ 3B_1 , B $^1B_1 - X$ 3B_1 , and C $^1A_1 - X$ 3B_1 separations by 1.36 and 2.07 kcal/mol, respectively.

In agreement with Ref. [93], where it was demonstrated that the DEA-EOMCC calculations including 4p-2h contributions are less sensitive to the choice of the underlying MO basis than the DEA-EOMCC computations truncated at 3p-1h excitations, we observe a smaller dependence of the A $^1A_1 - X$ 3B_1 , B $^1B_1 - X$ 3B_1 , and C $^1A_1 - X$ 3B_1 gap values obtained with the DEA-EOMCC(3p-1h,4p-2h){2}, DEA-EOMCC(4p-2h){2}, and DEA-EOMCC(4p-2h){2}, EOMCC(4p-2h) approaches on the orbitals used in the calculations than that observed when the lower-order DEA-EOMCC(3p-1h){2} and DEA-EOMCC(3p-1h) methods are employed. Indeed, if we look at the numerical data listed in Table 4.4, we can see that the ranges of the NPE values characterizing the DEA-EOMCC(3p-1h){2} and DEA-EOMCC(3p-1h) results, when all types of MOs are included in the analysis, are 0.67–2.30 and 0.54–3.53 kcal/mol, respectively. The DEA-EOMCC $(3p-1h,4p-2h)\{2\}$, DEA-EOMCC $(4p-2h)\{2\}$, and DEA-EOMCC(4p-2h) calculations reduce these ranges to 0.16–1.46, 0.24–0.94, and 0.29-0.40 kcal/mol, respectively. Clearly, the DEA-EOMCC $(3p-1h,4p-2h)\{2\}$ calculations, in which both 3p-1h and 4p-2h components are treated approximately using a small number of active MOs, have a larger sensitivity to the underlying MO basis than the DEA-EOMCC $(4p-2h)\{2\}$ and DEA-EOMCC(4p-2h) computations, but the variation in the NPE values characterizing the DEA-EOMCC(3p-1h,4p-2h){2} results, of 0.16–1.46 kcal/mol, is relatively small and acceptable in many applications. In fact, the variation in the NPE values characterizing the DEA-EOMCC(3p-1h,4p-2h){2} calculations becomes even smaller when we exclude the results obtained with the ionic MOs optimized for the CH_2^{2+} dication, i.e., when we only consider the various types of orbitals optimized for CH_2 in our analysis. When we do this, the range of the NPE values characterizing the DEA-EOMCC(3p-1h,4p-2h){2} results reduces to 0.16-0.60 kcal/mol; a similarly small error range, of 0.42-0.76 kcal/mol, is obtained in this case, when we examine the corresponding MaxUE data. When the data obtained with the ionic MOs are ignored, the active-space DEA-EOMCC(3p-1h,4p-2h){2} approach becomes competitive with its more expensive DEA-EOMCC(4p-2h){2} counterpart, which produces the NPE and MaxUE ranges of 0.24-0.94 and 0.29-0.82 kcal/mol, respectively.

The methylene/TZ2P example is certainly instructive, and it is encouraging to observe good performance of the DEA-EOMCC(3p-1h,4p-2h){ N_u } method in this case. It is, therefore, interesting to examine if the DEA-EOMCC(3p-1h,4p-2h){ N_u } approach remains accurate when larger basis sets and the CBS limit are investigated.

4.3.2 The Complete Basis Set Limit Investigation of Singlet and Triplet States of Methylene

In order to further explore methylene, we performed a sequence of all-electron calculations using the aug-cc-pCVxZ (x = T, Q, and 5) basis sets [215, 228, 229], abbreviated as ACxZ, with x representing the cardinal number, and the CBS limit extrapolations [230, 231], similar to what was done in one of the previous studies in our group using the CR-EOMCC methodology [74]. In order to an appropriate assessment of the data produced by a variety of our DEA-EOMCC approaches, we have included the previous Quantum Monte Carlo

(QMC) [232–234] study of the ground and three low-lying excited states of methylene by Zimmerman et al. [235] and the available results from experiment. Experimental data for the $A^{-1}A_1 - X^{-3}B_1$ and $B^{-1}B_1 - X^{-3}B_1$ energy gaps are provided. In the case of the $A^{1}A_{1} - X^{3}B_{1}$ energy separation, the experimental estimate of the non-relativistic, purely electronic, adiabatic excitation energy corresponding to the X $^3B_1 \rightarrow A$ 1A_1 transition, of 0.406 eV, was obtained after subtracting the relativistic and Born-Oppenheimer diagonal corrections from the vibrationless adiabatic excitation energy (see Ref. [74] for further details). In the case of $B^{-1}B_1 - X^{-3}B_1$ energy separation, the experimental value of the purely electronic adiabatic excitation energy corresponding to the X $^3B_1 \rightarrow B$ 1B_1 transition, of 1.415 eV, was obtained using the information about the relevant $B^{-1}B_1 - A^{-1}A_1$ and $B^{\ 1}B_1-X^{\ 3}B_1$ gaps from which the zero-point vibrational energies obtained in the full CI/TZ2P calculations were subtracted (see Ref. [74]). In order to compensate for the missing experimental $C^{-1}A_1 - X^{-3}B_1$ energy gap value and to have a complete evaluation of our DEA-EOMCC results, we have included the QMC calculations performed by Zimmerman et al. [235], particularly two different variants of QMC, namely, variational Monte Carlo (VMC) and diffusion Monte Carlo (DMC), where three different active spaces were used to generate complete active space trial functions for the QMC calculations reported in Ref. [235], namely, the (2,2), (4,4), and (6,6) active spaces, with (n,m) denoting an active space of n electrons and m orbitals. For the purpose of our assessment of DEA-EOMCC results, we adopted the highest-level QMC calculations, namely, DMC(6,6) and VMC(6,6). In both the DEA-EOMCC calculations reported in this dissertation and the QMC calculations of Ref. [235], the geometries for each state were taken from Ref. [217], generated using the full CI calculations with the [5s3p/2s] augmented with TZ2P basis set of Dunning [216].

The strategy is similar to our discussion in Section 4.3.1. It should be noted that be-

cause our DEA-EOMCC codes are interfaced with the GAMESS package, the h-functions of the AC5Z basis set were omitted in our calculations. As already mentioned, all electrons were correlated. The spherical components of the d, f, and g orbitals were employed throughout. In the calculations employing the ACxZ basis sets with x = T and Q, we were able to use all of the DEA-EOMCC methods, including the highest DEA-EOMCC(3p-1h, 4p-2h){ N_u } and DEA-EOMCC(4p-2h){ N_u } levels, in which both 3p-1h and 4p-2h components of $R_{\mu}^{(+2)}$ are taken into account. In the case of the largest AC5Z basis set, we could only afford the DEA-EOMCC(3p-1h){ N_u } calculations, in which 4p-2h terms are neglected. The DEA-EOMCC(3p-1h)/AC5Z, DEA-EOMCC(3p-1h)4p-2h){ N_u }/AC5Z, and DEA-EOMCC(4p-2h){ N_u }/AC5Z calculations using our present codes turned out to be quite expensive, so in order to estimate the DEA-EOMCC(3p-1h)/AC5Z, DEA-EOMCC (3p-1h)4p-2h){ N_u }/AC5Z, and DEA-EOMCC(4p-2h){ N_u }/AC5Z results we adopted a simple extrapolation scheme that accounts for both 3p-1h and 4p-2h correlations, and calculated the final total energies as follows:

$$E(3p-1h)/AC5Z = E(3p-1h)/ACQZ + E(3p-1h)\{2\}/AC5Z - E(3p-1h)\{2\}/ACQZ,$$
 (4.66)

$$E(3p-1h, 4p-2h)\{2\}/AC5Z = E(3p-1h, 4p-2h)\{2\}/ACQZ + E(3p-1h)\{2\}/AC5Z - E(3p-1h)\{2\}/ACQZ,$$

$$(4.67)$$

and

$$E(4p-2h)\{2\}/AC5Z = E(4p-2h)\{2\}/ACQZ + E(3p-1h)\{2\}/AC5Z - E(3p-1h)\{2\}/ACQZ.$$

$$(4.68)$$

The first terms on the right-hand sides of Eqs. (4.66–4.68) are the DEA-EOMCC(3p-1h)/ACQZ, DEA-EOMCC(3p-1h, 4p-2h){ N_u }/ACQZ, and DEA-EOMCC(4p-2h){ N_u }/ACQZ energies.

The effect of going from the ACQZ to the AC5Z basis set is estimated by forming the difference of energies obtained in the less expensive DEA-EOMCC(3p-1h) $\{N_u\}$ /AC5Z and DEA-EOMCC(3p-1h) $\{N_u\}$ /ACQZ calculations. We are confident of these extrapolation formulas since the results of DEA-EOMCC(3p-1h) $\{N_u\}$ calculations using the ACTZ, ACQZ, and AC5Z basis sets, which we could calculate for all states, indicate that the effect of the basis set on the singlet-triplet gaps characterizing the low-lying states of methylene examined in this work is small (see Table 4.5). We also provide CBS limits for the DEA-EOMCC calculations. The CBS total energy of each state of interest is directly extrapolated using the formula [228]

$$E(x) = E_{\infty} + Be^{-(x-1)} + Ce^{-(x-1)^2}.$$
(4.69)

The x-variable number entering Eq. (4.69) represents the cardinal number of the ACxZ basis set (x = 3 for ACTZ, x = 4 for ACQZ, and x = 5 for AC5Z). E(x) is the total DEA-EOMCC energy computed with the ACxZ basis set, and E_{∞} is the desired CBS limit of the total DEA-EOMCC energy for a given electronic state of the (N + 2)-electron species.

The results of our large basis set of methylene calculations are shown in Table 4.5. We focus on only one type of MOs, namely, the (N-2)-electron orbitals obtained in RHF calculations for the CH_2^{2+} reference dication. We begin by analyzing the basis set effects among the DEA-EOMCC computations. We observe that the $A^{-1}A_1 - X^{-3}B_1$, $B^{-1}B_1 - X^{-3}B_1$, and $C^{-1}A_1 - X^{-3}B_1$ gaps do not change much, when one goes from ACTZ to the ACT5Z basis sets. In Table 4.5, we also observe that it is sufficient to use active orbitals to select dominant 3p-1h excitations, since the active-space DEA-EOMCC(3p-1h) data accurately reproduce the results of the expensive Monte Carlo methods to within 1 kcal/mol. Accounting for the effects of 4p-2h correlations through the DEA-EOMCC(3p-1h, 4p-2h){ N_u } approach

or the DEA-EOMCC(4p-2h) $\{N_u\}$ method do not significantly alter the values for these gaps.

Methylene is an interesting case, but, as already pointed out above, the lower-level DEA-EOMCC(3p-1h) calculations and their active-space counterparts are capable of providing reasonable results without the presence of 4p-2h terms. Our next examples demonstrate the utility of the DEA-EOMCC(3p-1h, 4p-2h){ N_u } approach in situations where 4p-2h contributions are significant (sometimes, quite large).

4.3.3 Adiabatic Singlet-Triplet Gap in Trimethylenemethane

We now turn to the TMM molecule, a non-Kekulé hydrocarbon characterized by the delocalization of four π electrons over four closely spaced π -type orbitals (see, e.g., Refs. [147] and [241–243] for the relevant information). The four valence MOs of TMM's π network include the non-degenerate $1a_2''$, the doubly degenerate 1e'', and the non-degenerate $2a_2''$ orbitals, when D_{3h} symmetry of the triplet ground state is used, or the $1b_1$, $1a_2$, $2b_1$, and $3b_1$ orbitals, when C_{2v} symmetry relevant to the low-lying singlet states is adopted. Because of its fascinating and challenging electronic structure, the TMM molecule has attracted a lot of attention over the years among many theoretical and experimental groups (cf. Refs. [92] and [93], and references cited therein for the historical account and further information). In particular, a lot of effort has been devoted to an accurate determination of the relatively small energy gaps between the low-lying singlet and triplet states. As implied by Hund's rule and the EPR data [244], TMM has a D_{3h} -symmetric triplet ground state, X $^3A'_2$, dominated by the $|\{\text{core}\}(1a_2'')^2(1e_1'')^1(1e_2'')^1|$ configuration (which in a C_{2v} description becomes the X 3B_2 state dominated by the $|\{\text{core}\}(1b_1)^2(1a_2)^1(2b_1)^1|$ configuration). The next two states in TMM's electronic spectrum are the nearly degenerate singlets stabilized by the Jahn-Teller distortion that lifts their exact degeneracy in a D_{3h} description, which have a

Table 4.5: Comparison of the adiabatic excitation energies (in eV) for the low-lying states of CH₂, as obtained with various DEA-EOMCC approaches using the ACxZ (x=T, Q, and 5) basis sets and (N-2)-electron RHF orbitals, and extrapolating to the CBS limit, with the corresponding QMC results and experiment.

		Adiabatic Excitation Energy (eV)			
Method	Basis Set	$\overline{A^1A_1 - X^3B_1}$	$B^{1}B_{1} - X^{3}B_{1}$	$C^{1}A_{1} - X^{3}B_{1}$	
$\overline{\text{DEA-EOMCC}(3p-1h)\{2\}^b}$	x=T	0.474	1.463	2.520	
(1)	x = Q	0.469	1.449	2.498	
	x=5	0.470	1.449	2.495	
	CBS	0.471	1.450	2.494	
DEA-EOMCC $(3p-1h)$	x=T	0.408	1.408	2.391	
	x = Q	0.400	1.391	2.365	
	x=5	0.401	1.392	2.362	
	CBS	0.402	1.393	2.361	
DEA-EOMCC $(3p-1h,4p-2h)\{2\}^b$	x=T	0.488	1.512	2.661	
	x = Q	0.482	1.496	2.639	
	x=5	0.483	1.497	2.636	
	CBS	0.483	1.498	2.635	
DEA-EOMCC $(4p-2h)\{2\}^b$	x=T	0.415	1.452	2.523	
	x = Q	0.406	1.434	2.496	
	x=5	0.408	1.435	2.494	
	CBS	0.407	1.436	2.493	
DMC: $CAS(6,6)$		0.406(4)	1.416(4)	2.524(4)	
VMC: $CAS(6,6)$		0.430(8)	1.460(8)	2.550(8)	
Experiment		0.406^{c}	1.415^{d}		

 $[^]a$ The geometries were taken from Ref. [217] and were generated using full CI with the TZ2P basis set. In all DEA-EOMCC calculations, all electrons were correlated and the spherical components of the d, f, and g basis functions were employed throughout. Since the integral routines in CC package used in the underlying (N-2)-electron CCSD calculations are currently restricted to g functions, the h functions of the AC5Z basis set were neglected. The CH $_2^{2+}$ reference system used in the DEA-EOMCC calculations was created by vacating the $3a_1$ HOMO of CH $_2$.

^b The active space consisted of the HOMO and LUMO of CH_2 , $3a_1$ and $1b_1$, respectively, which are unoccupied in the CH_2^{2+} reference system used in the DEA-EOMCC calculations.

 $^{^{}c}$ Obtained by correcting the experimentally derived value of the vibrationless adiabatic A $^{1}A_{1}$ – X $^{3}B_{1}$ energy gap reported in Ref. [236] for the relativistic and non-adiabatic (Born-Oppenheimer diagonal correction) effects calculated in Refs. [237] and [238], respectively (as described in Ref. [239]).

^d Obtained by correcting the adiabatic separation between the v=0 vibronic levels of the B 1B_1 and X 3B_1 states, based on the information about the B $^1B_1 - A$ 1A_1 and A $^1A_1 - X$ 3B_1 gaps provided in Refs. [240] and [236], respectively, for the zero-point vibrational energies obtained in the full CI/TZ2P calculations in Ref. [217] (as described in Ref. [235]).

multi-reference, diradical, character. The lower of the two singlets is an open-shell singlet state characterized by a C_s minimum, which can be approximated by a twisted C_{2v} structure, so this state is usually labeled as the A 1B_1 state. The second singlet, abbreviated B 1A_1 , is a C_{2v} -symmetric state dominated by the closed-shell $|\{\text{core}\}(1b_1)^2(1a_2)^2|$ and $|\{\text{core}\}(1b_1)^2(2b_1)^2|$ determinants (see, e.g., Refs. [147], [241], and [242] for more information).

The highest ab initio levels of electronic structure theory applied to TMM to date reproduce the adiabatic, purely electronic, energy gap between the D_{3h} -symmetric X $^3A'_2$ ground state and the C_{2v} -symmetric B $^{1}A_{1}$ excited state, which is estimated at 18.1 kcal/mol [147], to within 1-6 kcal/mol, i.e., some high-level approaches work well, but some struggle (cf. Table 6 in Ref. [212] for a compilation of representative examples). The most accurate previously published [92, 93] full and active-space DIP-EOMCC calculations truncated at 4h-2p excitations and the corresponding active-space DEA-EOMCC computations truncated at 4p-2h excitations using the cc-pVDZ basis set place the adiabatic B $^1A_1 - X$ $^3A_2'$ gap in TMM within 1 kcal/mol from the recommended value of 18.1 kcal/mol, independent of the type of MOs used to define the corresponding wave function expansions. The DIP-EOMCC method truncated at 3h-1p excitations and its DEA-EOMCC counterpart truncated at 3p-1h terms worsen these results, producing values that are very sensitive to the type of MOs used in the calculations, which can be as good as 18.3 kcal/mol and as bad as 23.9 kcal/mol if 3h-1p and 3p-1h components are treated fully (see Refs. [92] and [93] and Table 4.6). As shown in Table 4.6, the use of the larger cc-pVTZ basis set does not significantly alter these conclusions, i.e., the highest-level affordable DEA-EOMCC/cc-pVTZ calculations with a full treatment of 3p-1h contributions and an active-space treatment of 4p-2h terms (as already mentioned, the corresponding full DEA-EOMCC(4p-2h) calculations are prohibitively expensive for us at this time) produce the adiabatic gaps between the $B\ ^1A_1$ and $X\ ^3A_2'$ states in the narrow 18.4–18.7 kcal/mol range, which is in excellent agreement with the recommended value of 18.1 kcal/mol, whereas the DEA-EOMCC approach truncated at 3p-1h excitations treated fully gives generally less accurate values that vary from 21.1 to 23.5 kcal/mol. Our main objective here is to examine if we can reproduce the high-accuracy results provided by the DEA-EOMCC method with a full treatment of 3p-1h and an active-space treatment of 4p-2h terms, summarized in Table 4.6, with the considerably less expensive DEA-EOMCC(3p-1h,4p-2h) $\{N_u\}$ approach (cf. Table 4.3), which approximates 3p-1h and 4p-2h components using active orbitals. We also want to investigate if it is sufficient to handle 3p-1h excitations within the DEA-EOMCC schemes truncated at 3p-1h or 4p-2hcomponents, which in Refs. [92] and [93] were treated fully, using a small subset of active orbitals. As explained in the beginning of this section, the adiabatic $B^{-1}A_1 - X^{-3}A_2'$ gap value of 18.1 kcal/mol reported in Ref. [147], which serves as a key reference value for our DEA-EOMCC calculations, was determined by subtracting the SF-DFT/6-31G(d) Δ ZPVE corrections from the vibronic separation between the X $^3A'_2$ and B 1A_1 states extracted from the photoelectron spectroscopy measurements discussed in Ref. [218]. The other low-energy singlet state, $A^{-1}B_1$, which we mentioned above and which is nearly degenerate with the $B^{-1}A_1$ state, was not observed in the photoelectron spectrum reported in Ref. [218] due to unfavorable Franck-Condon factors, so we do not discuss it in this dissertation. Following our earlier work [92, 93], in performing the DEA-EOMCC calculations with the full and active-space treatments of 3p-1h excitations and the active-space treatment of 4p-2h contributions, we adopted the geometries of the X $^3A_2'$ and B 1A_1 states of TMM optimized at the SF-DFT/6-31G(d) level in Ref. [147].

In all of the DEA-EOMCC calculations for TMM reported in this study, the (N-2)-

Table 4.6: The selected DEA-EOMCC results for the adiabatic singlet-triplet separation, $\Delta E_{\mathrm{S-T}} = E(B\ ^1A_1) - E(X\ ^3A_2')$, in kcal/mol, in trimethylenemethane (TMM), as described by the cc-pVDZ and, in parentheses, cc-pVTZ basis sets, calculated using the SF-DFT/6-31G(d) geometries.^a

	Orbitals				
Method	(N-2)-electron RHF ^b	N-electron ROHF ^{c}	N -electron ROHF/RHF d		
$\overline{\text{DEA-EOMCC}(3p\text{-}1h)\{3\}^e}$	24.2 (24.0)	19.6 (22.3)	21.5 (22.3)		
DEA-EOMCC $(3p-1h)$	23.9(23.5)	19.4 (21.1)	20.9 (21.1)		
DEA-EOMCC $(3p-1h,4p-2h)\{3\}^e$	$19.3\ (18.9)$	18.7 (19.9)	19.4 (19.9)		
DEA-EOMCC $(4p-2h)\{3\}^e$	19.0 (18.4)	18.6 (18.7)	18.9 (18.7)		
$\mathrm{Expt}.^f$		16.1 ± 0.1			
Expt. $-\Delta ZPVE^g$		18.1			

 $[^]a$ The TMM $^{2+}$ reference system used in the DEA-EOMCC calculations was created by vacating the doubly degenerate valence $1e^{\prime\prime}$ (the D_{3h} -symmetric X $^3A_2^\prime$ state) or non-degenerate $1a_2$ and $2b_1$ (the C_{2v} symmetric B 1A_1 state) orbitals of the TMM's π system. The lowest-energy core orbitals correlating with the 1s shells of the carbon atoms were frozen in the post-SCF calculations and the spherical components of the d and f orbitals were employed throughout.

 $[^]b$ The RHF orbitals of the singlet ground state of TMM²⁺ were employed. The ROHF orbitals obtained for the triplet ground state of TMM were employed.

 $[^]d$ The ROHF orbitals of TMM for the X $^3A_2^{\prime\prime}$ state and the RHF orbitals of TMM for the B 1A_1 state

d The ROHF orbitals of TMM for the X^3A_2' state and the RHF orbitals of TMM for the B^1A_1 state were employed.

The active space consisted of the doubly degenerate 1e'' and non-degenerate $2a_2''$ orbitals (using the D_{3h} symmetry of the X $^3A_2'$ state) or the $1a_2$, $2b_1$, and $3b_1$ orbitals (using the C_{2v} symmetry of the B 1A_1 state), which are the three lowest-energy unoccupied MOs in the TMM²⁺ reference system.

 $[^]f$ Ref. [218]. g The estimate of the purely electronic $\Delta E_{\mathrm{S-T}}$ gap obtained by subtracting the zero-point vibrational energy corrections, Δ ZPVE, resulting from the SF-DFT/6-31G(d) calculations reported in Ref. [147] from the experimental singlet-triplet separation determined in Ref. [218].

electron closed-shell TMM^{2+} reference system was obtained by vacating the doubly degenerate 1e'' shell (the D_{3h} -symmetric X $^3A'_2$ state) or the non-degenerate $1a_2$ and $2b_1$ orbitals (the C_{2v} -symmetric B 1A_1 state) of the TMM's valence π network. In analogy to the previously discussed methylene example and following our earlier study [93], in order to examine the dependence of the various DEA-EOMCC results on the type of MO basis that defines the corresponding wave function expansions, we used both the ground-state RHF orbitals of the TMM²⁺ reference dication and the RHF or ROHF orbitals optimized for the TMM target species. When utilizing the orbitals optimized for TMM, we followed Refs. [92] and [93] and adopted two different strategies. In the first strategy in this category, we relied on only one type of orbitals, namely, the high-spin ROHF MOs optimized for the triplet ground state, which we used to perform the DEA-EOMCC calculations for both electronic states of TMM that are examined here. In the second strategy, we used two different sets of MOs, namely, the ROHF orbitals optimized for the $X^{3}A'_{2}$ state in the DEA-EOMCC calculations for this D_{3h} -symmetric triplet ground state and the RHF orbitals obtained for the $B^{-1}A_1$ state in the DEA-EOMCC calculations for the C_{2v} -symmetric $B^{-1}A_1$ state. In analogy to Ref. [93] and as already alluded to above, the third possibility of exploiting the RHF MOs optimized for the B 1A_1 state in the DEA-EOMCC calculations for both states of TMM that interest us here was not pursued, since such orbitals break the degeneracy of the valence 1e'' shell at the D_{3h} geometry of the triplet ground state, resulting in a symmetry-broken description of the X $^3A_2'$ state. The high-spin ROHF MOs optimized for the X $^3A_2'$ state of TMM and the RHF orbitals optimized for the singlet ground state of TMM²⁺ guarantee a symmetry-adapted description of the triplet ground state of TMM at its optimum D_{3h} geometry, when the DEA-EOMCC calculations are performed. The RHF MOs optimized for the C_{2v} -symmetric $B^{-1}A_1$ state are also acceptable as long as we do not use them to determine the D_{3h} -symmetric $X^{3}A'_{2}$ state, i.e., the strategy combining the use of the ROHF orbitals optimized for the $X^{3}A'_{2}$ state in the DEA-EOMCC calculations for the $X^{3}A'_{2}$ state and the RHF orbitals of the $B^{-1}A_1$ state in the DEA-EOMCC calculations for the $B^{-1}A_1$ state is fine. Consistent with the structure of the valence shells of TMM, for each choice of the MO basis, the active orbitals employed in the DEA-EOMCC(3p-1h){ N_u }, DEA-EOMCC(3p-1h,4p-2h){ N_u }, and DEA-EOMCC(4p-2h) $\{N_u\}$ calculations were the doubly degenerate 1e'' and non-degenerate $2a_2''$ MOs in the case of the D_{3h} -symmetric X $^3A_2'$ state and the $1a_2$, $2b_1$, and $3b_1$ orbitals for the C_{2v} -symmetric B $^{1}A_{1}$ state. In other words, the number of active unoccupied orbitals, N_u , used to define 3p-1h component in the DEA-EOMCC(3p-1h) $\{N_u\}$ calculations, 3p-1h and 4p-2h components in the DEA-EOMCC(3p-1h,4p-2h){ N_u } computations, and 4p-2h component in the DEA-EOMCC(4p-2h) $\{N_u\}$ calculations was set at 3, making all of these calculations affordable, even when the cc-pVTZ basis set is employed. As shown in Table 4.3 and as discussed in Section 4.2.4, this is particularly true in the case of the DEA-EOMCC(3p-1h) $\{N_u\}$ and DEA-EOMCC(3p-1h,4p-2h) $\{N_u\}$ methods, which are substantially less expensive than the corresponding DEA-EOMCC(3p-1h) and DEA- $EOMCC(4p-2h)\{N_u\}$ approaches, not to mention full DEA-EOMCC(4p-2h), which becomes prohibitively expensive when the TMM molecule is examined.

It is apparent from Table 4.6 that the agreement between the adiabatic $B^{1}A_{1} - X^{3}A'_{2}$ gap values obtained in the inexpensive DEA-EOMCC(3p-1h){3} calculations, which use only three active unoccupied orbitals to select the dominant 3p-1h excitations, and their counterparts obtained with the considerably more demanding DEA-EOMCC(3p-1h) approach, where 3p-1h excitations are treated fully, is generally very good. Independent of the basis set and independent of the type of MOs used to construct the corresponding wave function expansions, the differences between the active-space DEA-EOMCC(3p-1h){3} and full

DEA-EOMCC(3p-1h) data do not exceed 1.2 kcal/mol, and they are, in most cases, considerably smaller, on the order of 0.2–0.6 kcal/mol. The same is observed when we compare the higher-level DEA-EOMCC(3p-1h,4p-2h){3} and DEA-EOMCC(4p-2h){3} methods, which use active orbitals to select the dominant 4p-2h contributions, but differ in the treatment of 3p-1h component of the electron attaching operator $R_{\mu}^{(+2)}$. The differences between the $B^{-1}A_1 - X^{-3}A_2'$ gap values obtained in the DEA-EOMCC(4p-2h){3} computations, where the 3p-1h component is treated fully, with their counterparts obtained with the considerably less expensive DEA-EOMCC(3p-1h,4p-2h){3} approach vary between 0.1 and 1.2 kcal/mol, with the majority of these differences falling into the 0.1–0.5 kcal/mol range. As mentioned earlier, on the basis of the comparison of the full DEA-EOMCC(3p-1h), active-space DEA-EOMCC(4p-2h){3}, and experimentally derived data for the adiabatic separation between the X $^3A_2^\prime$ and B 1A_1 states in TMM, 4p-2h effects are important if we are to obtain a fully quantitative description. The DEA-EOMCC(3p-1h,4p-2h){3} calculations reflect on this in a proper manner by improving the results of the DEA-EOMCC(3p-1h){3} and DEA-EOMCC(3p-1h) calculations by about 1-5 kcal/mol, with the largest error reductions observed when the ionic orbitals, obtained in the RHF calculations for the TMM^{2+} reference system, are employed. Indeed, when one uses the RHF MOs optimized for the TMM^{2+} dication, the DEA-EOMCC(3p-1h,4p-2h){3} approach brings the results of the DEA-EOMCC(3p-1h){3} and DEA-EOMCC(3p-1h) calculations, which neglect 4p-2h correlations, closer to the recommended $B^{-1}A_1 - X^{-3}A_2'$ gap value of 18.1 kcal/mol by 4.9 and 4.6 kcal/mol, respectively, when the cc-pVDZ basis set is employed, and 5.1 and 4.6 kcal/mol, when the cc-pVTZ basis set is used. As a result, the adiabatic gaps between the X $^3A_2'$ and B 1A_1 states obtained in the DEA-EOMCC(3p-1h,4p-2h){3} calculations, which range from 18.7 and 19.4 kcal/mol, when the cc-pVDZ basis set is used, and 18.9 and 19.9 kcal/mol, when one uses the cc-pVTZ basis, are in generally very good agreement with the experimentally derived value of 18.1 kcal/mol. They are only slightly worse than the corresponding DEA-EOMCC(4p-2h){3} results, which range from 18.6 and 19.0 kcal/mol in the cc-pVDZ case and 18.4 and 18.7 kcal/mol when the cc-pVTZ basis is employed.

In analogy to the DEA-EOMCC(4p-2h){3} approach, the improvements offered by its less expensive DEA-EOMCC(3p-1h,4p-2h){3} counterpart over the DEA-EOMCC calculations truncated at 3p-1h excitations can also be seen when we compare the sensitivity of the various DEA-EOMCC calculations to the type of orbitals used to construct the corresponding wave function expansions. Indeed, when we probe the (N-2)-electron MOs obtained in the RHF calculations for the TMM^{2+} reference dication and the N-electron ROHF or ROHF and RHF orbitals optimized for the TMM target system, as described above, the variation in the DEA-EOMCC(3p-1h){3} and DEA-EOMCC(3p-1h) results for the adiabatic B $^{1}A_{1}-X$ $^{3}A_{2}'$ gap in TMM is 4.6 and 4.5 kcal/mol, respectively, when the cc-pVDZ basis set is employed, and 1.7 and 2.4 kcal/mol, when one uses cc-pVTZ. The DEA-EOMCC(4p-2h){3} calculations reduce these variations to the impressively small 0.3–0.4 kcal/mol level, but it is encouraging to observe that the considerably less expensive DEA-EOMCC(3p-1h,4p-2h){3} computations, in which the resulting gap values vary by 0.7 kcal/mol in the cc-pVDZ case and 1.0 kcal/mol in the case of cc-pVTZ, remain rather insensitive to the type of MOs used to construct the corresponding wave functions. The above discussion shows that the relatively inexpensive DEA-EOMCC calculations with an active-space treatment of 3p-1h and 4p-2h excitations are not only accurate in describing singlet-triplet gaps in diradical systems, but are also quite robust, enabling one to use different types of orbitals without risking that the results dramatically change, as is often the case when DEA-EOMCC computations truncated at 3p-1h excitations are performed.

4.3.4 Vertical Singlet-Triplet Gaps in Antiaromatic Diradicals

We also applied the DEA-EOMCC(3p-1h) $\{N_u\}$ and DEA-EOMCC(3p-1h,4p-2h) $\{N_u\}$ approaches and their more expensive full DEA-EOMCC(3p-1h) and active-space DEA-EOMCC(4p-2h) $\{N_u\}$ counterparts to the vertical energy gaps between the lowest singlet and triplet states of the following antiaromatic diradical systems: D_{4h} -symmetric form of cyclobutadiene (1), D_{5h} -symmetric cyclopentadienyl cation (2), and five cyclobutadiene derivatives with polar substituents, including aminocyclobutadiene (3), formylcyclobutadiene (4), 1-amino-2-formyl-cyclobutadiene (5), 1,2-bis(methylene)cyclobutadiene (6), and 1,3-bis(methylene)cyclobutadiene (7), all shown in Figure 4.2. In doing so, we followed the computational strategy of Ref. [219]. Thus, we adopted the D_{4h} point group for system 1, the D_{5h} point group for system 2, and the C_1 point group for systems 3–7. In each case, the closed-shell (N-2)-electron reference system used to set up the DEA-EOMCC calculations was obtained by vacating the two valence partly occupied orbitals that define the singlet and triplet states of interest, which are exactly degenerate in systems 1 and 2 and nearly degenerate in systems 3-7. For example, the (N-2)-electron reference dication used in the DEA-EOMCC calculations for system 1 was obtained by vacating the two valence singly occupied MOs of e_g symmetry. For system 2, we vacated the degenerate valence e_1'' shell, etc. Consistent with the structure of the valence π shells in systems 1–7, which consist of one doubly occupied, two partly occupied, and one unoccupied MOs in systems 1, 3, and 4 and one doubly occupied, two partly occupied, and two unoccupied MOs in systems 2 and 5-7, the active spaces needed to perform the DEA-EOMCC(3p-1h) $\{N_u\}$, DEA-EOMCC(3p-1h,4p-2h) $\{N_u\}$, and DEA-EOMCC(4p-2h) $\{N_u\}$ calculations were defined in the following manner. For systems 1, 3, and 4, we used the $N_u = 3$ MOs, which are

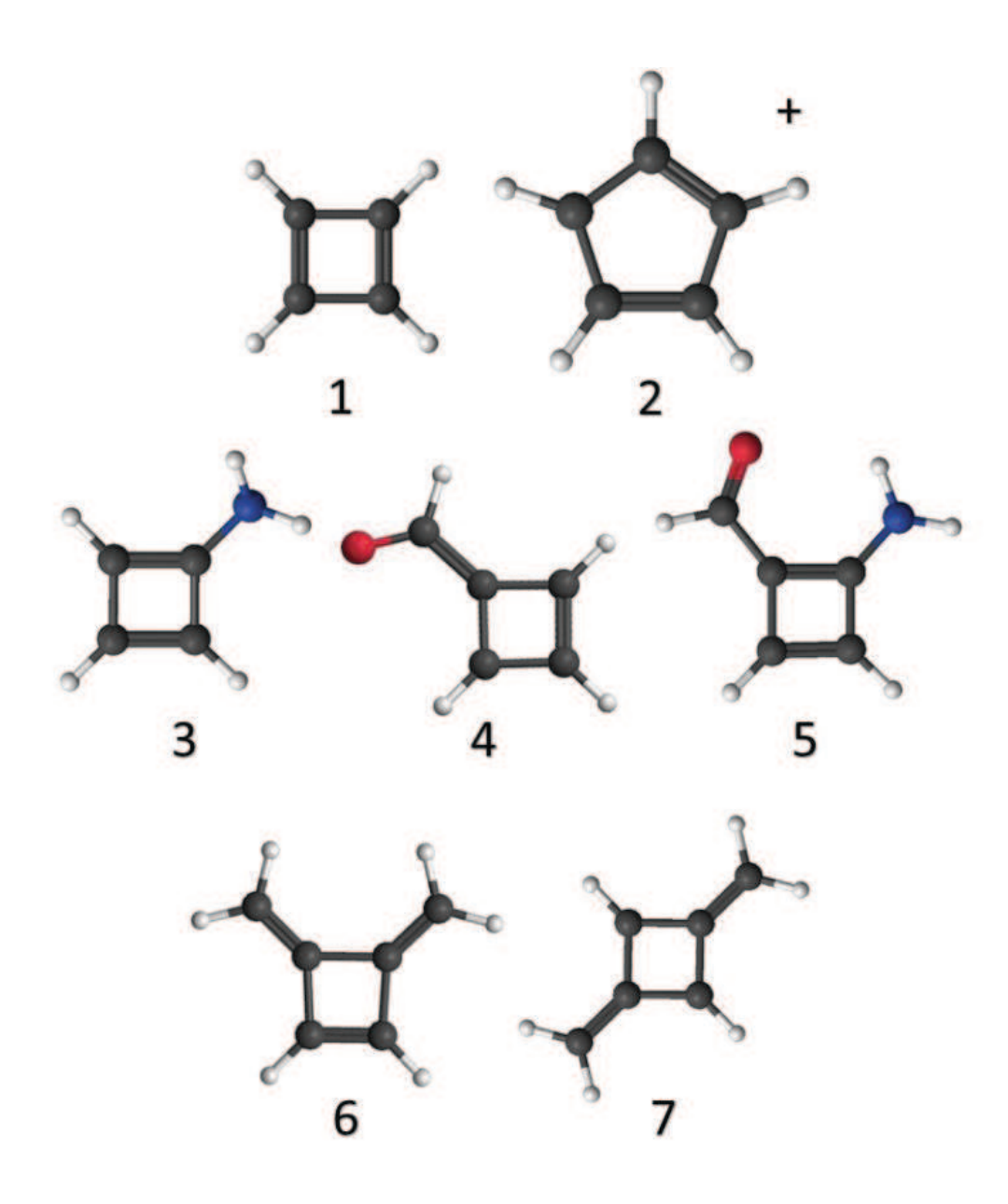


Figure 4.2: Diradical systems considered in this work. **1**: C_4H_4 , **2**: $[C_5H_5]^+$, **3**: $C_4H_3NH_2$, **4**: C_4H_3CHO , **5**: $C_4H_2NH_2CHO$, **6**: C_4H_2-1 , $2-(CH_2)_2$, and **7**: C_4H_2-1 , $3-(CH_2)_2$.

the three lowest-energy unoccupied orbitals in the respective 1^{2+} , 3^{2+} , and 4^{2+} reference dications. For systems 2, 5, 6, and 7, we used the $N_u = 4$ orbitals, which are the four lowest-energy unoccupied MOs in the respective (N-2)-electron 2^{2+} , 5^{2+} , 6^{2+} , and 7^{2+} species. We verified the appropriateness of the above active orbital choices by comparing the full DEA-EOMCC(3p-1h) and active-space DEA-EOMCC(3p-1h){ N_u } data obtained using the cc-pVDZ basis set, abbreviated below as VDZ. In order to examine the dependence of our results on the basis set, we used a larger maug-cc-pVTZ basis [245], abbreviated as mATZ. For some of the systems considered in this work, namely systems 3–7, the DEA-EOMCC(4p-2h){ N_u }/mATZ calculations turned out to be quite expensive, so to estimate the highest level DEA-EOMCC(4p-2h){ N_u }/mATZ-level data, abbreviated as DEA-EOMCC[4p-2h], which we could not obtain in direct calculations, we adopted a simple extrapolation scheme defined as follows:

$$E[4p-2h] = E(4p-2h)\{N_u\}/VDZ + E(3p-1h)\{N_u\}/mATZ - E(3p-1h)\{N_u\}/VDZ.$$
(4.70)

The first term on the right-hand side of Eq. (4.70) is the DEA-EOMCC(4p-2h) $\{N_u\}/\text{VDZ}$ energy. The effect of going from the VDZ basis set to mATZ is estimated by forming the difference of energies obtained in the less expensive DEA-EOMCC(3p-1h) $\{N_u\}/\text{mATZ}$ and DEA-EOMCC(3p-1h) $\{N_u\}/\text{VDZ}$ calculations. In addition to the calculations using the DEA-EOMCC methods entering Eq. (4.70), we performed the full DEA-EOMCC(3p-1h) and active-space DEA-EOMCC(3p-1h,4p-2h) $\{N_u\}$ computations using the VDZ basis set (all seven systems) and the DEA-EOMCC(3p-1h,4p-2h) $\{N_u\}/\text{mATZ}$ calculations for the smallest system 1. We carried out these extra computations to validate the basis set extrapolation scheme based on Eq. (4.70), especially the usefulness of the DEA-EOMCC(3p-1h) $\{N_u\}$ ap-

proach in estimating the effect of going from the VDZ basis set to the mATZ basis. Following Refs. [92–94], in all of the DEA-EOMCC calculations performed in this work, the ground states of the underlying (N-2)-electron closed-shell cores were obtained using CCSD.

Table 4.7: The DEA-EOMCC results for the vertical singlet-triplet gaps, $\Delta E_{S-T} = E(S) - E(T)$, in kcal/mol, in systems 1–7, as described by the VDZ and mATZ basis sets.

	System						
Method	1	2	3	4	5	6	7
				VDZ			
DEA-EOMCC($3p$ - $1h$){ N_u }	-1.37	16.38	0.44	-1.24	-6.90	-81.63	18.26
DEA-EOMCC $(3p-1h)$	-1.42	16.06	0.34	-1.32	-7.46	-81.84	17.95
DEA-EOMCC $(3p-1h,4p-2h)\{N_u\}$	-4.98	14.25	-3.22	-4.32	-4.82	-78.42	20.03
DEA-EOMCC $(4p-2h)\{N_u\}$	-5.04	13.91	-3.30	-4.40	-5.49	-78.75	19.76
	mATZ						
DEA-EOMCC(3 p -1 h){ N_u }	-0.53	16.35	1.09	-0.48	-7.09	-80.56	16.98
DEA-EOMCC $[4p-2h]^a$	-4.20^{b}	13.88	-2.65	-3.65	-5.68	-77.68	18.49
N_u	3	4	3	3	4	4	4

 $[^]a$ Best estimate defined by the extrapolation formula given by Eq. (4.70).

All of the DEA-EOMCC calculations and the underlying CCSD computations were performed using the RHF MOs corresponding to the (N-2)-electron closed-shell cores. In this way, we could maintain all of the relevant symmetries throughout the calculations. We could accomplish the same goal by using other types of orbitals, such as the N-electron ROHF orbitals obtained in the calculations for the triplet states of diradicals examined in this work, but the resulting singlet-triplet gaps turned out to be virtually independent of the type of MOs exploited in the calculations, in agreement with our earlier findings reported in Refs. [92–94]. As in Ref. [219], in all of the post-HF calculations the core orbitals correlating with the 1s shells of the C, N, and O atoms were kept frozen and the spherical components of d and f basis functions were employed throughout.

The results of our various DEA-EOMCC calculations for the singlet-triplet gaps in

 $[^]b$ The DEA-EOMCC(3p-1h,4p-2h){N_u}/mATZ calculation gives -4.08 kcal/mol.

systems 1–7 are summarized in Table 4.7. Our highest-level calculated DEA-EOMCC $(4p-2h)\{N_u\}/\text{VDZ}$ data and their extrapolation to the larger mATZ basis set using Eq. (4.70), abbreviated as DEA-EOMCC[4p-2h], which we treat in this work as best estimates of the ΔE_{S-T} values of interest, indicate that systems 1 and 3–6 have singlet ground states, whereas the ground states of systems 2 and 7 are triplets. As shown in Table 4.8, where we compare our extrapolated DEA-EOMCC[4p-2h] values with the singlet–triplet gaps resulting from the symmetry-broken, UHF-based, calculations using the single-reference CCSD(T) (UCCSD(T)) approach and its Brueckner-orbital UBD(T) analog [246], and the multi-reference MkCCSD computations using the ROHF and CASSCF orbitals, our DEA-EOMCC(4p-2h)-level results agree in this regard with the findings of Saito et al [219].

Before making further comparisons between the results of our DEA-EOMCC calculations and the $\Delta E_{\mathrm{S-T}}$ values reported in Ref. [219], we comment on the extrapolation procedure defined by Eq. (4.70). We begin with the choice of active orbitals used to select the dominant 3p-1h and 4p-2h contributions in the DEA-EOMCC(3p-1h) $\{N_u\}$ and DEA-EOMCC(4p-2h) $\{N_u\}$ computations. A comparison of the results of the full DEA-EOMCC(3p-1h) and active-space DEA-EOMCC(3p-1h) $\{N_u\}$ calculations using the VDZ basis set demonstrates that our choice of active orbitals, which allow us to select the dominant higher-than-2p contributions in the DEA-EOMCC wave function ansatz is appropriate. Indeed, as shown in Table 4.7, the differences between the singlet-triplet gaps resulting from the DEA-EOMCC(3p-1h)/VDZ and DEA-EOMCC(3p-1h) $\{N_u\}$ /VDZ calculations are very small, ranging from 0.05 kcal/mol for system 1 to 0.56 kcal/mol for system 5, where the DEA-EOMCC(3p-1h)/VDZ gap value is -7.46 kcal/mol. In fact, one observes similarly small differences when comparing the results of the higher-level DEA-EOMCC(4p-2h) $\{N_u\}$ /VDZ calculations, in which 4p-2h terms are treated using active orbitals, but 3p-1h terms are

treated fully, with the results obtained with the DEA-EOMCC(3p-1h,4p-2h){ N_u } approach, in which both types of terms are treated using active orbitals. We can certainly conclude that the use of the active-space DEA-EOMCC(3p-1h){ N_u } approach in Eq. (4.70), as a substitute for the considerably more expensive full DEA-EOMCC(3p-1h) parent in estimating the effect of going from the VDZ basis set to the mATZ one, is an appropriate procedure.

Equation (4.70) is also justified by the fact that the effect of going from the smaller VDZ basis to the larger mATZ basis set on the calculated $\Delta E_{\rm S-T}$ values is generally rather small, implying that it is safe to estimate it using the lower-level DEA-EOMCC(3p-1h){ N_u } method, as opposed to the significantly more expensive DEA-EOMCC(4p-2h){ N_u } approach. Indeed, as shown in Table 4.7, the differences between the singlet-triplet gaps resulting from the DEA-EOMCC(3p-1h){ N_u }/VDZ and DEA-EOMCC(3p-1h){ N_u }/mATZ calculations range from 0.03 kcal/mol for system 2 to 1.28 kcal/mol for system 7, where the DEA-EOMCC(3p-1h)/VDZ gap value is 18.26 kcal/mol, for an average of 0.69 kcal/mol. Our extrapolation of the DEA-EOMCC(4p-2h)/mATZ-level result based on Eq. (4.70) gives -4.20 kcal/mol, in virtually perfect agreement with the DEA-EOMCC(3p-1h,4p-2h){3}/mATZ calculation. This means that Eq. (4.70) works well, allowing us to capture the effect of high-order 4p-2h correlations and the effect of going from the VDZ basis set to mATZ in an accurate and computationally manageable manner.

Having established the validity of Eq. (4.70), which, given the above analysis and previous extensive studies of the DEA-EOMCC approaches with up to 4p-2h excitations [92–94], is expected to produce singlet–triplet gap values in systems 1–7 to within 1 kcal/mol or better, we comment on our best DEA-EOMCC[4p-2h] (and the corresponding DEA-EOMCC(4p-2h){ N_u }/VDZ) ΔE_{S-T} values. First, it is important to note that although bulk of the correlation effects is captured at the DEA-EOMCC(3p-1h) level, the high-order 4p-2h

effects can be quite substantial. When we compare the extrapolated DEA-EOMCC|4p-2h|and calculated DEA-EOMCC(3p-1h) $\{N_u\}$ /mATZ gap values, or, equivalently, the DEA- $EOMCC(4p-2h)\{N_u\}/VDZ$ and $DEA-EOMCC(3p-1h)\{N_u\}/VDZ$ data, the 4p-2h effects range, in absolute value, from 1.4 kcal/mol in system 5 to 3.7 kcal/mol in systems 1 and 3. Although they typically reduce the total electronic energies of the individual states, their net effect on the calculated singlet-triplet gaps can go either way. Indeed, we may encounter lowering of the signed ΔE_{S-T} values due to 4p-2h correlations, as in systems 1-4, or we can find cases where the signed singlet-triplet gaps increase, as in systems 5-7. In some cases, the 4p-2h effects can change a tiny singlet-triplet gap near zero to a considerably larger absolute value, as in systems 1 and 4, but there also are situations, such as system 3, where 4p-2h correlations change the state ordering and, thus, the sign of ΔE_{S-T} . It is quite clear from the results shown in Table 4.7 that one has to account for the high-order 4p-2heffects within the DEA-EOMCC framework to obtain reasonably converged values of the singlet-triplet gaps in diradicals. This is consistent with our earlier DEA-EOMCC studies reported in Refs. [92–94].

The high accuracy of our extrapolated DEA-EOMCC[4p-2h] data and the underlying DEA-EOMCC(4p-2h){ N_u }/VDZ calculations, which include sophisticated 4p-2h terms, in addition to their lower-rank 2p and 3p-1h counterparts, on top of CCSD, implies that we should be able to judge other methods. We now comment on the singlet-triplet gaps resulting from the symmetry-broken, UHF-based, computations using the single-reference CCSD(T) (UCCSD(T)) approach and its Brueckner-orbital analog, abbreviated as UBD(T) [246], and the ROHF- and CASSCF-based state-specific multi-reference CCSD approach of Mukherjee (MkCCSD) [247] calculations reported by Saito et al. [219]. We observe that all of these methods agree in predicting the correct state ordering. Unfortunately, as shown in Table 4.8,

they disagree, sometimes rather significantly, in quantitative predictions. In the case of systems 1-4, there is a great deal of consistency among the singlet-triplet gap values provided by UCCSD(T) and UBD(T) and those obtained in our DEA-EOMCC(4p-2h) $\{N_u\}$ /VDZ and DEA-EOMCC[4p-2h] calculations, which agree to within ~ 1 kcal/mol, but one cannot say the same about the MkCCSD data, which seem to be in rather large error, on the order of 3-4 kcal/mol, displaying a significant dependence of the resulting $\Delta E_{\rm S-T}$ values on the type of orbitals used in the calculations in the case of system 2. The poor performance of MkCCSD for system 1 is reinforced by the results of the multi-reference averaged quadratic CC calculations [248], reported in Ref. [219] as well, which give $\Delta E_{\rm S-T}$ of -5.5 kcal/mol, in good agreement with our highest-level DEA-EOMCC[4p-2h] and DEA-EOMCC(4p-2h) $\{N_u\}$ /VDZ calculations and the UCCSD(T) and UBD(T) data, but in sharp disagreement with the ROHF- and CASSCF-based MkCCSD values. Based on the results for systems 1-4 and the MUE values relative to DEA-EOMCC[4p-2h] reported in Table 4.8, one might recommend the use of the symmetry-broken UCCSD(T) and UBD(T) methods in the calculations of singlet-triplet gaps in diradicals, but the results for system 5, where errors relative to DEA-EOMCC(4p-2h) $\{N_u\}$ /VDZ and DEA-EOMCC[4p-2h] in the UCCSD(T) and UBD(T) $\Delta E_{\mathrm{S-T}}$ values are on the order of 5 kcal/mol, show that this would be misleading. The agreement among the UCCSD(T), UBD(T), ROHF-MkCCSD, and CASSCF-MkCCSD $\Delta E_{\mathrm{S-T}}$ values improves when systems 6 and 7 are examined, but one still observes substantial differences among the results obtained with these four methods, on the order of 4-5 kcal/mol. Our extrapolated DEA-EOMCC[4p-2h] data and the underlying DEA-EOMCC(4p-2h) $\{N_u\}$ /VDZ calculations are considerably more reliable in this regard. They do set up a new high-level dataset for benchmarking other methods, such as the CASPT2 and RASPT2 approaches considered in our recent collaboration with the

Table 4.8: A comparison of the $\Delta E_{\rm S-T}$ values (in kcal/mol) characterizing systems 1–7 obtained with the DEA-EOMCC[4p-2h] extrapolation in the DEA-EOMCC(4p-2h){ N_u }/VDZ calculations with the UCCSD(T), UBD(T), ROHF-MkCCSD, and CASSCF-MkCCSD results reported by Saito et al.

Molecule	DEA-EOMCC	Saito et al.								
	$[4p-2h]/(4p-2h)\{N_u\}$	UCCSD(T)	UBD(T)	ROHF-MkCCSD	CASSCF-MkCCSD					
1	-4.2/-5.0	-4.8	-5.1	-8.6	-8.1					
2	13.9/13.9	14.8	14.0	13.5	9.4					
3	-2.7/-3.3	-3.2	-3.6	-6.5	-7.3					
4	-3.6/-4.4	-4.5	-4.5	7.1	-6.9					
5	-5.7/-5.5	-0.6	-0.9	-2.7	-4.5					
6	-77.7/-78.8	-82.7	-79.8	-82.7	-84.2					
7	18.5/19.8	15.0	17.1	20.0	19.5					
MUE^a	0.0/0.7	2.4	1.6	3.1	3.6					

b $\,$ Mean unsigned errors relative to the extrapolated DEA-EOMCC[4p-2h] results.

groups of Professors Laura Gagliardi and Donald Truhlar, which resulted in Ref. [117].

4.3.5 F-F Bond Dissociation in the Fluorine Molecule

Our final example is the potential energy curve of the challenging F_2 molecule, as described by the DZ basis set, for which the results of the exact, full CI calculations were reported in Ref. [221] and which was examined by us earlier, using the full DEA-EOMCC(3p-1h) and DEA-EOMCC(4p-2h) and active-space DEA-EOMCC(4p-2h){ N_u } approaches, and their DIP counterparts, in Ref. [92]. As in the case of other molecular examples discussed in this work, our discussion concentrates on a comparison of the active-space DEA-EOMCC(3p-1h){ N_u } approach with its full DEA-EOMCC(3p-1h) parent and on the ability of the DEA-EOMCC(3p-1h,4p-2h){ N_u } method, in which the dominant 3p-1h and 4p-2h amplitudes are selected with the help of active orbitals, to reproduce the results of the corresponding DEA-EOMCC(4p-2h) and DEA-EOMCC(4p-2h){ N_u } calculations, in which 3p-1h components are treated fully. Following Refs. [92] and [221], all of the DEA-EOMCC calculations for F_2

Table 4.9: A comparison of the full CI and various DEA-EOMCC ground-state energies of F_2 at the equilibrium ($R_e = 2.66816$ bohr) and a few other F-F distances, along with the corresponding MUE and NPE values relative to full CI, obtained with the DZ basis set.^a

Method	R_e	$1.1R_e$	$1.2R_e$	$1.5R_e$	$2R_e$	$3R_e$	$4R_e$	MUE	NPE
DEA-EOMCC $(3p-1h)\{2\}^b$	-3.538	-2.808	-2.210	1.585	1.860	1.360	1.279	3.538	5.398
DEA-EOMCC $(3p-1h)$	-3.947	-3.181	-2.563	1.305	1.485	1.015	0.935	3.947	5.432
DEA-EOMCC $(3p-1h,4p-2h)\{2\}^b$	3.807	3.508	3.193	1.665	1.895	1.656	1.601	3.807	2.206
DEA-EOMCC $(4p-2h)\{2\}^b$	3.437	3.161	2.855	1.371	1.505	1.298	1.244	3.437	2.193
DEA-EOMCC $(4p-2h)$	2.314	2.195	2.061	0.628	0.807	0.762	0.720	2.314	1.686
Full CI^a	0.968128	0.976458	0.972125	0.952558	0.945201	0.944819	0.944831		

The full CI values are total energies, E, taken from Ref. [221], reported as -(E+198) hartree. The remaining energies are errors relative to full CI, in millihartree. The F_2^{2+} reference system used in the DEA-EOMCC calculations was created by vacating the valence σ_g orbital of F_2 . Following Ref. [221], the RHF orbitals of F_2 were employed throughout and the two lowest-energy core orbitals and the corresponding two highest-energy unoccupied orbitals were frozen in the post-SCF calculations.

reported in this work use the RHF orbitals of the target species. The corresponding closed-shell reference F_2^{2+} system, needed to set up the various DEA-EOMCC calculations summarized in Table 4.9, was obtained by vacating the valence σ_g orbital, which is doubly occupied in the RHF determinant for F_2 . The active orbitals used in the DEA-EOMCC(3p-1h){ N_u }, DEA-EOMCC(3p-1h,4p-2h){ N_u }, and DEA-EOMCC(4p-2h){ N_u } computations consisted of the valence σ_g and σ_u MOs involved in the dissociation of the fluorine molecule, which are empty in reference F_2^{2+} system, as defined above. In other words, the value of N_u was set at 2.

As established in the earlier study from our group [92] and as shown in Table 4.9, 4p-2h excitations, treated fully or with active orbitals, play a substantial role in improving the results of the DEA-EOMCC calculations, offering a considerably more accurate description of bond breaking in F_2 than that provided by the DEA-EOMCC(3p-1h) approach. Indeed, the full DEA-EOMCC(4p-2h) and active-space DEA-EOMCC(4p-2h){2} approaches reduce the relatively large NPE value relative to full CI characterizing the DEA-EOMCC(3p-1h) potential energy curve of F_2 , of 5.432 millihartree, to as little as 1.686 and 2.193 millihartree, re-

b The active space consisted of the valence σ_g and σ_u orbitals, which are unoccupied in the F₂²⁺ reference system utilized in the DEA-EOMCC calculations.

spectively. The considerably less expensive DEA-EOMCC $(3p-1h,4p-2h)\{2\}$ calculations are capable of maintaining these high accuracies, providing the NPE of 2.206 millihartree, which is in excellent agreement with the NPEs provided by the parent DEA-EOMCC(4p-2h){2} and DEA-EOMCC(4p-2h) calculations. The largest errors relative to full CI, represented in Table 4.9 by the MUE values, do not change much when going from the DEA-EOMCC(3p-1h) to the DEA-EOMCC $(3p-1h,4p-2h)\{2\}$, DEA-EOMCC $(4p-2h)\{2\}$, and DEA-EOMCC(4p-2h)levels, but the potential energy curves obtained with the latter three approaches are much more parallel to the full CI curve than the curve obtained in the DEA-EOMCC(3p-1h) calculations. As a result, if we define the energy difference $D_e \equiv E(4R_e) - E(R_e)$ as a measure of the dissociation energy characterizing the F_2 molecule, where R_e is the equilibrium geometry, we can see an excellent agreement between the DEA-EOMCC(3p-1h,4p-2h){2}, DEA-EOMCC(4p-2h) $\{2\}$, and DEA-EOMCC(4p-2h) D_e values, which are 13.23, 13.24, and 13.62 kcal/mol, respectively, among themselves and a very good agreement between the active-space DEA-EOMCC $(3p-1h,4p-2h)\{2\}$ and DEA-EOMCC $(4p-2h)\{2\}$ and full DEA-EOMCC(4p-2h) data and the full CI calculations, which give $D_e = 14.62$ kcal/mol. Given its relatively low computer cost compared to the remaining two DEA-EOMCC approaches including 4p-2h excitations considered in this study, the good performance of the DEA-EOMCC(3p-1h,4p-2h){2} method with an active-space treatment of both 3p-1h and 4p-2hcomponents is most encouraging.

The DEA-EOMCC(3p-1h) result for D_e , as defined above, of 17.68 kcal/mol, is substantially worse, largely because of the increase in the corresponding NPE value, from a 2 millihartree level in the DEA-EOMCC(3p-1h,4p-2h){2}, DEA-EOMCC(4p-2h){2}, and DEA-EOMCC(4p-2h) calculations to 5.432 millihartree in the DEA-EOMCC(3p-1h) case, but the good news is that the active-space DEA-EOMCC(3p-1h){2} approach provides the

virtually identical energetics at the small fraction of the cost of the full DEA-EOMCC(3p-1h) computations. Indeed, the DEA-EOMCC(3p-1h){2} values of NPE and D_e , which are 5.398 millihartree and 17.64 kcal/mol, respectively, are in perfect agreement with their full DEA-EOMCC(3p-1h) counterparts. The inexpensive active-space treatment of 3p-1h excitations, which we advocate in this study, is clearly sufficient to capture the relevant 3p-1h correlation effects. Combined with the active-space treatment of 4p-2h contributions, as in the DEA-EOMCC(3p-1h,4p-2h){ N_u } methodology developed in this work, it allows us to study multi-reference situations created by single bond breaking in closed-shell species and diradicals in a formally appealing, spin- and symmetry-adapted manner, while being accurate and computationally efficient at the same time.

4.4 Conclusions

We have demonstrated that the previously developed DEA-EOMCC approaches with full and active-space treatments of 4p-2h excitations, abbreviated as DEA-EOMCC(4p-2h) and DEA-EOMCC(4p-2h){ N_u }, respectively, which represent state-of-the-art methodologies within the DEA-EOMCC framework and which are particularly well-suited to describe electronic structure and spectra of diradical systems and single bond breaking in closed-shell molecules leading to doublet radical fragments, can be made considerably more economical if the corresponding 3p-1h contributions are treated using active orbitals. The resulting DEA-EOMCC(3p-1h,4p-2h){ N_u } approach, developed and implemented in this thesis project, replaces the expensive \mathcal{N}^6 -like $n_o n_u^5$ steps associated with 3p-1h excitations by the much less time consuming \mathcal{N}^5 -like $N_u n_o n_u^4$ operations, where N_u is the number of active unoccupied orbitals in the underlying (N-2)-electron closed-shell core, in addition to downscaling the

prohibitively expensive \mathcal{N}^8 -like $n_o^2 n_u^6$ steps associated with 4p-2h contributions to a manageable \mathcal{N}^6 -like $N_u^2 n_o^2 n_u^4$ level. By examining the low-lying singlet and triplet states of methylene, trimethylenemethane, cyclobutadiene and its derivatives, and cyclopentadienyl cation and bond breaking in F_2 , we have demonstrated that the DEA-EOMCC(3p-1h,4p-2h) $\{N_u\}$ method is practically as accurate as its parent DEA-EOMCC(4p-2h) $\{N_u\}$ and DEA-EOMCC (4p-2h) models at the fraction of the computational cost involved in the DEA-EOMCC (4p-2h) $\{N_u\}$ and DEA-EOMCC(4p-2h) calculations, while preserving all other features of the DEA-EOMCC methodology, such as rigorous spin and symmetry adaptation, which are difficult to achieve within the standard particle-conserving CC/EOMCC framework. We have also demonstrated that the DEA-EOMCC(3p-1h,4p-2h) $\{N_u\}$ scheme is almost as insensitive to the choice of the underlying MO basis used in the calculations as the considerably more expensive DEA-EOMCC(4p-2h) $\{N_u\}$ and DEA-EOMCC(4p-2h) approaches.

The methodological advances reported in this dissertation have also benefited the lower-level DEA-EOMCC approach truncated at 3p-1h excitations, which can be useful in applications involving diradicals too, by replacing the $n_o n_u^5$ steps associated with a full treatment of 3p-1h contributions by the much less demanding $N_u n_o n_u^4$ steps of the active-space DEA-EOMCC(3p-1h) $\{N_u\}$ approach, implemented in this work as well. Just like its DEA-EOMCC(3p-1h) parent, the DEA-EOMCC(3p-1h) $\{N_u\}$ model with an active-space treatment of 3p-1h excitations, which ignores 4p-2h correlation effects, is less accurate than the DEA-EOMCC(3p-1h,4p-2h) $\{N_u\}$, DEA-EOMCC(4p-2h) $\{N_u\}$, and DEA-EOMCC(4p-2h) methods, but it faithfully reproduces the results of DEA-EOMCC(3p-1h) calculations at the small fraction of the computer cost, offering a useful alternative to the DEA-EOMCC(3p-1h) approximation, where 3p-1h terms are treated fully.

Chapter 5

Summary and Future Outlook

In this dissertation, we have employed a comprehensive test set of about 150 singlet excited states of 28 medium-size organic molecules to benchmark two variants of the approximately size-intensive CR-EOMCC method with singles, doubles, and non-iterative triples, abbreviated as δ -CR-EOMCCSD(T),IA and δ -CR-EOMCCSD(T),ID [63], derived from the MMCC formalism [65, 68, 122, 125–129], and the analogous two variants of the rigorously size-intensive δ -CR-EOMCC(2.3) approach, designated as δ -CR-EOMCC(2.3). A and δ -CR-EOMCC(2,3),D, respectively [69], based on the generalization of the biorthogonal MMCC formalism [127-129] to excited states [67, 122-124]. By doing so, we have identified the δ -CR-EOMCC(2,3) methodology, especially its δ -CR-EOMCC(2,3),D variant, as a useful approach for the routine and highly accurate calculations of molecular electronic spectra, with the δ -CR-EOMCC(2,3), A approximation offering a similarly good description. It will be interesting to verify if our conclusions change when basis sets other than TZVP, which was used in this study, are employed and when one examines non-singlet excitations, including, for example, the triplet excited states of the 28 molecules considered in the present work. It will also be interesting to examine if our conclusions change if our δ -CR-EOMCC calculations are compared to the results of EOMCC calculations with a full or active-space treatment of triple excitations, as substitutes for the CC3, EOMCCSDT-3, and TBE values employed in this dissertation to benchmark the δ -CR-EOMCC approaches.

In the second part of this dissertation, we have demonstrated that the previously developed DEA-EOMCC approaches with full and active-space treatments of 4p-2h excitations, abbreviated as DEA-EOMCC(4p-2h) and DEA-EOMCC(4p-2h) $\{N_u\}$, respectively, [92, 93] which represent state-of-the-art methodologies within the DEA-EOMCC framework and which are particularly well-suited to describe the electronic structure and spectra of diradical systems and single bond breaking in closed-shell molecules leading to doublet radical fragments, can be made considerably more economical when the corresponding 3p-1h contributions are treated using active orbitals. The resulting DEA-EOMCC(3p-1h,4p-2h) $\{N_u\}$ approach, developed and implemented in this work, replaces the expensive \mathcal{N}^6 -like $n_o n_u^5$ steps associated with 3p-1h excitations by the much less time consuming \mathcal{N}^5 -like $N_u n_o n_u^4$ operations, where N_u is the number of active unoccupied orbitals in the underlying (N-2)-electron closed-shell core, in addition to downscaling the prohibitively expensive \mathcal{N}^8 -like $n_o^2 n_u^6$ steps associated with 4p-2h contributions to a manageable \mathcal{N}^6 -like $N_u^2 n_o^2 n_u^4$ level.

The performance of the DEA-EOMCC(3p-1h,4p-2h){ N_u } scheme and its lower-order DEA-EOMCC(3p-1h){ N_u } counterpart examined through benchmark calculations for the low-lying singlet and triplet states of methylene, trimethylenemethane, cyclobutadiene and its derivatives, and cyclopentadienyl cation and bond breaking in F₂. We have demonstrated that the DEA-EOMCC(3p-1h,4p-2h){ N_u } method is practically as accurate as its parent DEA-EOMCC(4p-2h){ N_u } and DEA-EOMCC(4p-2h) models at the fraction of their computational cost involved in the DEA-EOMCC(4p-2h){ N_u } and DEA-EOMCC(4p-2h) and DEA-EOMCC methodology, such as rigorous spin and symmetry adaptation, which are difficult to achieve within the standard particle-conserving CC/EOMCC framework. We have also demonstrated that the DEA-EOMCC(3p-1h,4p-2h){ N_u } scheme is almost as insensitive to the choice of the underlying

MO basis used in the calculations as the considerably more expensive DEA-EOMCC $(4p-2h)\{N_u\}$ and DEA-EOMCC(4p-2h) approaches.

In addition to the above work and more testing, an important development that would be useful in the context of the active-space DEA-EOMCC methodologies discussed in this dissertation would be an extension of the recently proposed CC(P;Q) formalism of Refs. [129, 211, 212, 249], which enables one to correct the results of the active-space CC and EOMCC calculations for the missing correlation effects of interest (e.g., CC/EOMCC calculations with singles, doubles, and active-space triples for the remaining triple excitations), to the DEA-EOMCC case. We could, for example, contemplate the enhanced and still economical DEA-EOMCC(3p-1h) $\{N_u\}$ and DEA-EOMCC(3p-1h,4p-2h) $\{N_u\}$ models, where one would use the CC(P;Q) framework to design the inexpensive non-iterative corrections to the DEA-EOMCC(3p-1h) $\{N_u\}$ and DEA-EOMCC(3p-1h,4p-2h) $\{N_u\}$ energies that capture the missing 3p-1h or 3p-1h and 4p-2h correlation effects outside those that are already included in the active-space DEA-EOMCC(3p-1h){ N_u } and DEA-EOMCC(3p-1h,4p-2h){ N_u } approximate approximate N_u mations. As in the past [108, 109, 111, 115, 129], it might also be interesting to examine various other ways of selecting 3p-1h and 4p-2h excitations to further reduce computer costs by using more active spin-orbital indices in the definitions of 3p-1h and 4p-2h amplitudes. Considering active-space DEA-EOMCC schemes and their DIP-EOMCC counterparts with higher-than-4p-2h/4h-2p excitations would be useful too. Finally, it would be very interesting to extend the active-space DEA-EOMCC methods developed in this thesis project to other multiply electron-attached and multiply ionized EOMCC methods, such as the higherlevel variants of the recently examined triply electron-attached theories [209] and their triply ionized counterparts, which can be used to describe open-shell species with three electrons outside the corresponding closed-shell cores. In this case, we would use active orbitals to select 4p-1h/4h-1p and 5p-2h/5h-2p components of the relevant electron attaching or ionizing $R_{\mu}^{(\pm 3)}$ operators.

APPENDICES

APPENDIX A

Derivation of the Non-Iterative

Energy Correction Defining the

Biorthogonal MMCC Theory

In this appendix, we present the derivation of the biorthogonal MMCC formula [128] for the non-iterative energy correction $\delta_{\mu}^{(A)}$ that when added to the CC/EOMCC energy $E_{\mu}^{(A)}$ generates the full CI energy E_{μ} . We begin the derivation by replacing the generic function Ψ given by the expression

$$\Lambda[\Psi] = \frac{\langle \Psi | H R_{\mu}^{(A)} e^{T^{(A)}} | \Phi \rangle}{\langle \Psi | R_{\mu}^{(A)} e^{T^{(A)}} | \Phi \rangle}.$$
(A.1)

with the exact full CI wave function Ψ_{μ} , which gives rise to the following expression for the full CI energy E_{μ} :

$$E_{\mu} = \frac{\langle \Psi_{\mu} | H R_{\mu}^{(A)} e^{T^{(A)}} | \Phi \rangle}{\langle \Psi_{\mu} | R_{\mu}^{(A)} e^{T^{(A)}} | \Phi \rangle}.$$
 (A.2)

We should recall that $T^{(A)}$ and $R^{(A)}_{\mu}$ are the cluster and linear excitation operators that define the wave function in the truncated CC/EOMCC method A. We replace the exact bra state $\langle \Psi_{\mu}|$ in Eq. (A.2) by the ansatz given by

$$\langle \Psi_{\mu} | = \langle \Phi | \mathcal{L}_{\mu} e^{-T(A)}, \tag{A.3}$$

where

$$\mathcal{L}_{\mu} = \sum_{n=0}^{N} \mathcal{L}_{\mu,n}, \quad \mathcal{L}_{\mu,n} = \left(\frac{1}{n!}\right)^{2} \ell_{\mu,i_{1}...i_{n}}^{a_{1}...a_{n}} a^{i_{1}} \cdots a^{i_{n}} a_{a_{n}} \cdots a_{a_{1}}, \tag{A.4}$$

where N represents the number of correlated electrons. The $\mathcal{L}_{\mu,n}$ are the n-body components of the deexcitation operator \mathcal{L}_{μ} while $\ell^{a_1...a_n}_{\mu,i_1...i_n}$ are the corresponding amplitudes. Using the fact that $T^{(A)}$ and $R^{(A)}_{\mu}$ commute, we obtain,

$$E_{\mu} = \frac{\langle \Phi | \mathcal{L}_{\mu} \, \bar{H}^{(A)} R_{\mu}^{(A)} | \Phi \rangle}{\langle \Phi | \mathcal{L}_{\mu} \, R_{\mu}^{(A)} | \Phi \rangle},\tag{A.5}$$

where $\bar{H}^{(A)}$ is the similarity-transformed Hamiltonian of CC method A defined by

$$\bar{H}_{\text{open}} = (He^T)_{C,\text{open}} = e^{-T}He^T - (He^T)_{C,\text{closed}}.$$
(A.6)

By imposing the normalization condition given by

$$\langle \Phi | \mathcal{L}_{\mu} R_{\mu}^{(A)} | \Phi \rangle = 1, \tag{A.7}$$

the denominator in Eq. (A.5) goes to one, leaving the following expression for the full CI energy of state μ :

$$E_{\mu} = \langle \Phi | \mathcal{L}_{\mu} \,\bar{H}^{(A)} R_{\mu}^{(A)} | \Phi \rangle. \tag{A.8}$$

At this point, we insert the resolution of the identity in the N-electron Hilbert space,

$$P + Q^{(A)} + Q^{(R)} = \mathbf{1},\tag{A.9}$$

where

$$P = |\Phi\rangle\langle\Phi|,\tag{A.10}$$

$$Q^{(A)} = \sum_{n=1}^{m_A} \sum_{\substack{i_1 < \dots < i_n \\ a_1 < \dots < a_n}} |\Phi_{i_1 \dots i_n}^{a_1 \dots a_n}\rangle \langle \Phi_{i_1 \dots i_n}^{a_1 \dots a_n}|, \tag{A.11}$$

and

$$Q^{(R)} = \sum_{n=m_A+1}^{N} \sum_{\substack{i_1 < \dots < i_n \\ a_1 < \dots < a_n}} |\Phi_{i_1\dots i_n}^{a_1\dots a_n}\rangle \langle \Phi_{i_1\dots i_n}^{a_1\dots a_n}|, \qquad (A.12)$$

in between \mathscr{L}_{μ} and $\bar{H}^{(A)}$, and use the decomposition of \mathscr{L}_{μ} defined by

$$\mathscr{L}_{\mu} = \mathscr{L}_{\mu}^{(A)} + \delta \mathscr{L}_{\mu}^{(A)}, \tag{A.13}$$

where

$$\mathscr{L}_{\mu}^{(A)} = \sum_{n=0}^{m_A} \mathscr{L}_{\mu,n},\tag{A.14}$$

and

$$\delta \mathcal{L}_{\mu}^{(A)} = \sum_{n=m_A+1}^{N} \mathcal{L}_{\mu,n}, \tag{A.15}$$

while utilizing the property that $\langle \Phi | \mathscr{L}_{\mu}^{(A)} Q^{(R)} = 0$. This gives

$$E_{\mu} = \langle \Phi | \mathcal{L}_{\mu}^{(A)}(P + Q^{(A)})\bar{H}^{(A)}R_{\mu}^{(A)}|\Phi\rangle + \langle \Phi | \delta \mathcal{L}_{\mu}^{(A)}Q^{(R)}\bar{H}^{(A)}R_{\mu}^{(A)}|\Phi\rangle. \tag{A.16}$$

Since the EOMCC eigenvalue problem [48–50],

$$\langle \Phi_{i_1...i_n}^{a_1...a_n} | (\bar{H}_{\text{open}}^{(A)} R_{\mu,\text{open}}^{(A)})_C | \Phi \rangle = \omega_{\mu}^{(A)} r_{\mu,a_1...a_n}^{i_1...i_n}, \tag{A.17}$$

with

$$r_{\mu,0} = \langle \Phi | (\bar{H}_{\text{open}}^{(A)} R_{\mu,\text{open}}^{(A)})_C | \Phi \rangle / \omega_{\mu}^{(A)}, \tag{A.18}$$

can be written as

$$(P + Q^{(A)})\bar{H}^{(A)}R_{\mu}^{(A)}|\Phi\rangle = E_{\mu}^{(A)}R_{\mu}^{(A)}|\Phi\rangle, \tag{A.19}$$

we can simplify Eq. (A.16) to

$$E_{\mu} = E_{\mu}^{(A)} \langle \Phi | \mathcal{L}_{\mu}^{(A)} R_{\mu}^{(A)} | \Phi \rangle + \langle \Phi | \delta \mathcal{L}_{\mu}^{(A)} Q^{(R)} \bar{H}^{(A)} R_{\mu}^{(A)} | \Phi \rangle. \tag{A.20}$$

Substituting the normalization condition given by Eq. (A.7) and the explicit form of $Q^{(R)}$ given by Eq. (A.12) into Eq. (A.20) yields

$$E_{\mu} = E_{\mu}^{(A)} + \sum_{n=m_A+1}^{N} \sum_{\substack{i_1 < \dots < i_n \\ a_1 < \dots < a_n}} \langle \Phi | \delta \mathcal{L}_{\mu}^{(A)} | \Phi_{i_1 \dots i_n}^{a_1 \dots a_n} \rangle \langle \Phi_{i_1 \dots i_n}^{a_1 \dots a_n} | \bar{H}^{(A)} R_{\mu}^{(A)} | \Phi \rangle. \tag{A.21}$$

We know that the $\langle \Phi | \delta \mathscr{L}_{\mu}^{(A)} | \Phi_{i_1...i_n}^{a_1...a_n} \rangle$ term that enters Eq. (A.21) simply represents the amplitudes defining the \mathscr{L}_{μ} deexcitation operator, $\ell_{\mu,i_1...i_n}^{a_1...a_n}$, with $n > m_A$. Furthermore, comparison of Eq. (A.21) with Eq. (3.4) reveals the presence of the generalized moments of the CC/EOMCC equations $\mathfrak{M}_{\mu,a_1...a_n}^{i_1...i_n}(m_A) = \langle \Phi_{i_1...i_n}^{a_1...a_n} | \bar{H}^{(A)} R_{\mu}^{(A)} | \Phi \rangle$. It should be noted that for a given CC/EOMCC method A, not all of the moments $\mathfrak{M}_{\mu,a_1...a_n}^{i_1...i_n}(m_A)$ with $n > m_A$ are non-zero. Indeed, for a given approximation, there is generally a value of n above which

all moments $\mathfrak{M}^{i_1...i_n}_{\mu,a_1...a_n}(m_A)$ are zero. For instance, in the case of CCSD (the $m_A=2$ case), only the triply, quadruply, pentuply, and hextuply excited moments, i.e. moments with n=3-6, are nonzero when the Hamiltonian contains pairwise interactions only, and thus $N_{0,A}=6$ (the CCSD equations are solved by zeroing the singly and doubly excited moments, $\mathfrak{M}^i_{0,a}(2)$ and $\mathfrak{M}^{ij}_{0,ab}(2)$, respectively, hence the triply excited moments are the first to be nonzero). Similarly, in the EOMCCSD case with $\mu>0$, $N_{\mu,A}=8$. Taking advantage of these observations, along with the fact that the moments are zero for $n>N_{\mu,A}$, Eq. (A.21) can be rewritten as

$$\delta_{\mu}^{(A)} \equiv E_{\mu} - E_{\mu}^{(A)} = \sum_{n=m_A+1}^{N_{\mu,A}} \sum_{\substack{i_1 < \dots < i_n \\ a_1 < \dots < a_n}} \ell_{\mu,i_1\dots i_n}^{a_1\dots a_n} \mathfrak{M}_{\mu,a_1\dots a_n}^{i_1\dots i_n} (m_A)$$
(A.22)

which completes the derivation.

APPENDIX B

Factorized Form of the

DEA-EOMCC(4p-2h) Equations Based on CCSD Reference Wave Functions

In this appendix, we present the fully factorized form of the equations defining the DEA-EOMCC(4p-2h) eigenvalue problems, exploited in this study, in terms of the one- and two-electron molecular integrals, $f_p^q = \langle p|f|q \rangle$ (f is the Fock operator) and $v_{pq}^{rs} = \langle pq|v|rs \rangle$ – $\langle pq|v|sr \rangle$, respectively, defining the Hamiltonian, T_1 and T_2 cluster amplitudes defining the underlying (N-2)-electron ground-state CCSD problem, and the $R_{\mu,2p}$, $R_{\mu,3p-1h}$, and $R_{\mu,4p-2h}$ amplitudes defining the electron attaching operator, $R_{\mu}^{(+2)}$. In presenting these equations, we use the Einstein summation over repeated upper and lower indices, and symbol μ at the relevant $r_{abc_1...c_n}^{k_1...k_n}(\mu)$ amplitudes defining $R_{\mu}^{(+2)}$ is dropped.

The DEA-EOMCC(4p-2h) equations can be given the following form:

$$\langle \Phi^{ab} | (\bar{H}_{N,\text{open}}^{(\text{CCSD})} R_{\mu}^{(+2)})_{C} | \Phi \rangle = \mathscr{A}_{ab} [-\bar{h}_{a}^{e} r_{be} + \frac{1}{4} \bar{h}_{ab}^{ef} r_{ef} + \frac{1}{2} \bar{h}_{m}^{e} r_{abe}^{m} - \frac{1}{2} \bar{h}_{am}^{ef} r_{bef}^{m} + \frac{1}{8} v_{mn}^{ef} r_{abef}^{mn}]$$

$$= \omega_{\mu}^{(N)} r_{ab}, \tag{B.1}$$

$$\langle \Phi^{abc}_{k} | (\bar{H}_{N,\text{open}}^{(\text{CCSD})} R_{\mu}^{(+2)})_{C} | \Phi \rangle = \mathscr{A}_{a/bc} [-\bar{h}_{ab}^{ke} r_{ce} - \frac{1}{3} \bar{h}_{m}^{k} r_{abc}^{m}$$

$$+ \bar{h}_{a}^{e} r_{bce}^{k} + \bar{h}_{am}^{ke} r_{bce}^{m} + \frac{1}{2} \bar{h}_{ab}^{ef} r_{cef}^{k} + \frac{1}{2} I_{am} t_{bc}^{km}$$

$$+ \frac{1}{3} \bar{h}_{m}^{e} r_{abce}^{km} - \frac{1}{6} \bar{h}_{mn}^{ke} r_{abce}^{mn} + \frac{1}{2} \bar{h}_{am}^{ef} r_{bcef}^{km}]$$

$$= \omega_{\mu}^{(N)} r_{abc}^{k}, \qquad (B.2)$$

$$\langle \Phi^{abcd}_{kl} | (\bar{H}_{N,\text{open}}^{(\text{CCSD})} R_{\mu}^{(+2)})_{C} | \Phi \rangle = \mathcal{A}_{a/bcd} \mathcal{A}_{b/cd} \mathcal{A}^{kl}
[-\frac{1}{6} \bar{h}_{am}^{kl} r_{bcd}^{\ m} + \frac{1}{2} \bar{h}_{ab}^{ke} r_{cde}^{\ l} + I_{abm}^{\ k} t_{cd}^{lm} + \frac{1}{2} I_{abc}^{\ e} t_{de}^{kl}
+ \frac{1}{12} \bar{h}_{m}^{k} r_{abcd}^{\ lm} - \frac{1}{6} \bar{h}_{a}^{e} r_{bcde}^{\ kl} + \frac{1}{48} \bar{h}_{mn}^{kl} r_{abcd}^{\ mn}
+ \frac{1}{3} \bar{h}_{am}^{ke} r_{bcde}^{\ lm} + \frac{1}{8} \bar{h}_{ab}^{ef} r_{cde}^{\ kl}]
= \omega_{\mu}^{(N)} r_{abcd}^{\ kl},$$
(B.3)

where, in addition to one- and two-body matrix elements of the similarity-transformed Hamiltonian $\bar{H}_{N,\text{open}}^{(\text{CCSD})}$ of the CCSD approach, \bar{h}_p^q and \bar{h}_{pq}^{rs} , respectively, which can be found elsewhere (cf., e.g., Refs. [66, 68]), we define the following intermediates:

$$I_{am} = \bar{h}_{am}^{ef} r_{ef} + v_{mn}^{ef} r_{aef}^{n}, \tag{B.4}$$

$$I_{abm}^{k} = \bar{h}_{am}^{ke} r_{be} + \frac{1}{8} I_{mn} t_{ab}^{kn} + \frac{1}{2} \bar{h}_{mn}^{ke} r_{abe}^{n} - \frac{1}{2} \bar{h}_{am}^{ef} r_{bef}^{k} + \frac{1}{4} v_{mn}^{ef} r_{abef}^{kn},$$
(B.5)

$$I_{abc}^{e} = \bar{h}_{ab}^{ef} r_{cf} - \bar{h}_{am}^{ef} r_{bcf}^{m} + \frac{1}{6} v_{mn}^{ef} r_{abcf}^{mn}, \tag{B.6}$$

$$I_{mn} = v_{mn}^{ef} r_{ef}. (B.7)$$

The antisymmetrizers $\mathscr{A}_{p/qrs} \equiv \mathscr{A}^{p/qrs}$, $\mathscr{A}_{p/qr} \equiv \mathscr{A}^{p/qr}$, and $\mathscr{A}_{pq} \equiv \mathscr{A}^{pq}$, which enter Eqs. (B.1)–(B.3), are defined in the usual way as

$$\mathscr{A}_{p/qrs} \equiv \mathscr{A}^{p/qrs} = 1 - (pq) - (pr) - (ps), \tag{B.8}$$

$$\mathscr{A}_{p/qr} \equiv \mathscr{A}^{p/qr} = 1 - (pq) - (pr), \tag{B.9}$$

and

$$\mathscr{A}_{pq} \equiv \mathscr{A}^{pq} = 1 - (pq), \tag{B.10}$$

respectively, with (pq) representing a transposition of two indices. The corresponding DEA-EOMCC $(4p-2h)\{N_u\}$ equations can be obtained by constraining the spin-orbital indices defining the projections on the $|\Phi^{abcd}_{kl}\rangle$ (the DEA-EOMCC $(4p-2h)\{N_u\}$) determinants and the indices defining the corresponding 4p-2h amplitudes, $r_{abcd}^{\ kl}(\mu)$ which enter the above DEA-EOMCC(4p-2h) equations, to the active-space logic of the $r_{\mu,4p-2h}$ operators, Eqs. (4.11).

BIBLIOGRAPHY

BIBLIOGRAPHY

- J. A. Pople, M. Head-Gordon, D. J. Fox, K. Raghavachari, and L. A. Curtiss, J. Chem. Phys. 90, 5622 (1989).
- [2] L. A. Curtiss, K. Raghavachari, G. W. Trucks, and J. A. Pople, J. Chem. Phys. 94, 7221 (1991).
- [3] L. A. Curtiss, K. Raghavachari, P. C. Redfern, and J. A. Pople, J. Chem. Phys. 106, 1063 (1997).
- [4] L. A. Curtiss, P. C. Redfern, K. Raghavachari, and J. A. Pople, J. Chem. Phys. 109, 42 (1998).
- [5] L. A. Curtiss, K. Raghavachari, P. C. Redfern, and J. A. Pople, J. Chem. Phys. 112, 7374 (2000).
- [6] L. A. Curtiss, P. C. Redfern, and K. Raghavachari, J. Chem. Phys. 123, 124107 (2005).
- [7] P. Jurecka, J. Sponer, J. Cerny, and P. Hobza, Phys. Chem. Chem. Phys. 8, 1985 (2006).
- [8] K. E. Riley and P. Hobza, J. Phys. Chem. A 111, 8257 (2007).
- [9] J. Rezac, K. E. Riley, and P. Hobza, J. Chem. Theory Comput. 7, 2427 (2011).
- [10] B. Ruscic, R. E. Pinzon, M. L. Morton, G. von Laszewski, S. Bittner, S. G. Nijsure, K. A. Amin, M. Minkoff, and A. F. Wagner, J. Phys. Chem. A 108, 9979 (2004).
- [11] B. Ruscic, in 2005 Yearbook of Science and Technology, annual update to McGraw-Hill Encyclopedia of Science and Technology (McGraw-Hill, New York, 2004) pp. 3–7.
- [12] B. Ruscic, R. E. Pinzon, G. von Laszewski, D. Kodeboyina, A. Burcat, D. Leahy, D. Montoya, and A. F. Wagner, J. Phys. Conf. Ser. 16, 561 (2005).
- [13] J. Zheng, Y. Zhao, and D. G. Truhlar, J. Chem. Theory Comput. 3, 569 (2007).
- [14] A. Karton, A. Tarnopolsky, J.-F. Lamere, G. C. Schatz, and J. M. L. Martin, J. Phys. Chem. A 112, 12868 (2008).
- [15] W. Zhang, D. G. Truhlar, and M. Tang, J. Chem. Theory Comput. 9, 3965 (2013).
- [16] M. Korth and S. Grimme, J. Chem. Theory Comput. 5, 993 (2009).
- [17] M. Schreiber, M. R. Silva-Junior, S. P. A. Sauer, and W. Thiel, J. Chem. Phys. 128, 134110 (2008).

- [18] M. R. Silva-Junior, M. Schreiber, S. P. A. Sauer, and W. Thiel, J. Chem. Phys. 129, 104103 (2008).
- [19] S. P. A. Sauer, M. Schreiber, M. R. Silva-Junior, and W. Thiel, J. Chem. Theory Comput. 5, 555 (2009).
- [20] M. R. Silva-Junior, S. P. Sauer, M. Schreiber, and W. Thiel, Mol. Phys. 108, 453 (2010).
- [21] M. R. Silva-Junior, M. Schreiber, S. P. A. Sauer, and W. Thiel, J. Chem. Phys. 133, 174318 (2010).
- [22] T. J. Watson, Jr., V. F. Lotrich, P. G. Szalay, A. Perera, and R. J. Bartlett, J. Phys. Chem. A 117, 2569 (2013).
- [23] I. Schapiro, K. Sivalingam, and F. Neese, J. Chem. Theory Comput. 9, 3567 (2013).
- [24] J. Sous, P. Goel, and M. Nooijen, Mol. Phys. 112, 616 (2014).
- [25] D. Kánnár and P. G. Szalay, J. Chem. Theory Comput. 10, 3757 (2014).
- [26] K. Ruedenberg, M. Schmidt, M. Gilbert, and S. Eliot, Chem. Phys. 71, 41 (1982).
- [27] B. O. Roos, in *Ab Initio Methods in Quantum Chemistry*, Vol. 2, edited by K. P. Lawley (Wiley, New York, 1987) pp. 399–445.
- [28] K. Anderson, P.-Å. Malmqvist, B. O. Roos, A. J. Sadlej, and K. Woliński, J. Phys. Chem. 94, 5483 (1990).
- [29] K. Anderson, P.-Å. Malmqvist, and B. O. Roos, J. Chem. Phys. **96**, 1218 (1992).
- [30] C. Angeli, R. Cimiraglia, S. Evangelisti, T. Leininger, and J.-P. Malrieu, J. Chem. Phys. **114**, 10252 (2001).
- [31] C. Angeli, R. Cimiraglia, and J.-P. Malrieu, Chem. Phys. Lett. **350**, 297 (2001).
- [32] C. Angeli and R. Cimiraglia, Theor. Chem. Acc. 107, 313 (2002).
- [33] C. Angeli, R. Cimiraglia, and J.-P. Malrieu, J. Chem. Phys. 117, 9138 (2002).
- [34] J. Čížek, J. Chem. Phys. 45, 4256 (1966).
- [35] J. Čížek, Adv. Chem. Phys. 14, 35 (1969).
- [36] J. Čížek and J. Paldus, Int. J. Quantum Chem. 5, 359 (1971).
- [37] J. Paldus, J. Čížek, and I. Shavitt, Phys. Rev. A 5, 50 (1972).
- [38] D. Mukherjee and P. K. Mukherjee, Chem. Phys. 39, 325 (1979).
- [39] E. Dalgaard and H. J. Monkhorst, Phys. Rev. A 28, 1217 (1983).

- [40] M. Takahashi and J. Paldus, J. Chem. Phys. 85, 1486 (1986).
- [41] H. Koch and P. Jørgensen, J. Chem. Phys. **93**, 3333 (1990).
- [42] H. Koch, H. J. A. Jensen, P. Jørgensen, and T. Helgaker, J. Chem. Phys. 93, 3345 (1990).
- [43] O. Christiansen, H. Koch, and P. Jørgensen, Chem. Phys. Lett. 243, 409 (1995).
- [44] H. Koch, O. Christiansen, P. Jørgensen, and J. Olsen, Chem. Phys. Lett. **244**, 75 (1995).
- [45] O. Christiansen, H. Koch, and P. Jørgensen, J. Chem. Phys. 103, 7429 (1995).
- [46] O. Christiansen, H. Koch, and P. Jørgensen, J. Chem. Phys. **105**, 1451 (1996).
- [47] O. Christiansen, H. Koch, P. Jørgensen, and J. Olsen, Chem. Phys. Lett. **256**, 185 (1996).
- [48] J. Geertsen, M. Rittby, and R. J. Bartlett, Chem. Phys. Lett. **164**, 57 (1989).
- [49] D. C. Comeau and R. J. Bartlett, Chem. Phys. Lett. **207**, 414 (1993).
- [50] J. F. Stanton and R. J. Bartlett, J. Chem. Phys. 98, 7029 (1993).
- [51] J. D. Watts and R. J. Bartlett, Chem. Phys. Lett. 233, 81 (1995).
- [52] J. D. Watts and R. J. Bartlett, Chem. Phys. Lett. **258**, 581 (1996).
- [53] M. Nooijen and R. J. Bartlett, J. Chem. Phys. **106**, 6441 (1997).
- [54] M. Nooijen and R. J. Bartlett, J. Chem. Phys. **107**, 6812 (1997).
- [55] E. Runge and E. K. U. Gross, Phys. Rev. Lett. **52**, 997 (1984).
- [56] M. E. Casida and M. Huix-Rotllant, Ann. Rev. Phys. Chem. **63**, 287 (2012).
- [57] S. Grimme and M. Waletzke, J. Chem. Phys. **111**, 5645 (1999).
- [58] A. K. Dutta, N. Vaval, and S. Pal, J. Chem. Theory Comput. 9, 4313 (2013).
- [59] M. Nooijen and J. G. Snijders, Int. J. Quantum Chem. Symp. 26, 55 (1992).
- [60] M. Nooijen and J. G. Snijders, Int. J. Quantum Chem. 48, 15 (1993).
- [61] J. F. Stanton and J. Gauss, J. Chem. Phys. **101**, 8938 (1994).
- [62] R. J. Bartlett and J. F. Stanton, in *Reviews in Computational Chemistry*, Vol. 5, edited by K. B. Lipkowitz and D. B. Boyd (VCH Publishers, New York, 1994) pp. 65–169.
- [63] K. Kowalski and P. Piecuch, J. Chem. Phys. **120**, 1715 (2004).

- [64] P. Piecuch, K. Kowalski, I. S. O. Pimienta, and M. J. McGuire, Int. Rev. Phys. Chem. 21, 527 (2002).
- [65] P. Piecuch, K. Kowalski, I. S. O. Pimienta, P.-D. Fan, M. Lodriguito, M. J. McGuire, S. A. Kucharski, T. Kuś, and M. Musiał, Theor. Chem. Acc. 112, 349 (2004).
- [66] M. Włoch, J. R. Gour, K. Kowalski, and P. Piecuch, J. Chem. Phys. 122, 214107 (2005).
- [67] M. Włoch, M. D. Lodriguito, P. Piecuch, and J. R. Gour, Mol. Phys. 104, 2149 (2006), 104 (2006) 2991 [Erratum].
- [68] P. Piecuch, J. R. Gour, and M. Włoch, Int. J. Quantum Chem. 109, 3268 (2009).
- [69] G. Fradelos, J. J. Lutz, T. A. Wesołowski, P. Piecuch, and M. Włoch, J. Chem. Theory Comput. 7, 1647 (2011).
- [70] P. Piecuch, J. A. Hansen, and A. O. Ajala, Mol. Phys. **113**, 3805 (2015).
- [71] K. Kowalski and P. Piecuch, J. Chem. Phys. **115**, 643 (2001).
- [72] K. Kowalski and P. Piecuch, Chem. Phys. Lett. **347**, 237 (2001).
- [73] S. A. Kucharski, M. Włoch, M. Musiał, and R. J. Bartlett, J. Chem. Phys. 115, 8263 (2001).
- [74] J. R. Gour, P. Piecuch, and M. Włoch, Mol. Phys. 108, 2633 (2010).
- [75] M. Nooijen and R. J. Bartlett, J. Chem. Phys. 102, 3629 (1995).
- [76] M. Nooijen and R. J. Bartlett, J. Chem. Phys. 102, 6735 (1995).
- [77] S. Hirata, M. Nooijen, and R. J. Bartlett, Chem. Phys. Lett. 328, 459 (2000).
- [78] M. Musiał and R. J. Bartlett, J. Chem. Phys. 119, 1901 (2003).
- [79] J. R. Gour, P. Piecuch, and M. Włoch, J. Chem. Phys. 123, 134113 (2005).
- [80] J. R. Gour, P. Piecuch, and M. Włoch, Int. J. Quantum Chem. 106, 2854 (2006).
- [81] J. R. Gour and P. Piecuch, J. Chem. Phys. **125**, 234107 (2006).
- [82] M. Musiał, S. A. Kucharski, and R. J. Bartlett, J. Chem. Phys. 118, 1128 (2003).
- [83] M. Musiał and R. J. Bartlett, Chem. Phys. Lett. 384, 210 (2004).
- [84] Y. J. Bomble, J. C. Saeh, J. F. Stanton, P. G. Szalay, M. Kállay, and J. Gauss, J. Chem. Phys. **122**, 154107 (2005).
- [85] M. Kamiya and S. Hirata, J. Chem. Phys. **125**, 074111 (2006).
- [86] M. Nooijen, Int. J. Mol. Sci. 3, 656 (2002).

- [87] K. W. Sattelmeyer, H. F. Schaefer, III, and J. F. Stanton, Chem. Phys. Lett. 378, 42 (2003).
- [88] M. Musiał, A. Perera, and R. J. Bartlett, J. Chem. Phys. **134**, 114108 (2011).
- [89] M. Musiał, S. A. Kucharski, and R. J. Bartlett, J. Chem. Theory Comput. 7, 3088 (2011).
- [90] T. Kuś and A. I. Krylov, J. Chem. Phys. **135**, 084109 (2011).
- [91] T. Kuś and A. I. Krylov, J. Chem. Phys. **136**, 244109 (2012).
- [92] J. Shen and P. Piecuch, J. Chem. Phys. **138**, 194102 (2013).
- [93] J. Shen and P. Piecuch, Mol. Phys. **112**, 868 (2014).
- [94] A. O. Ajala, J. Shen, and P. Piecuch, J. Phys. Chem. A **121**, 3469 (2017).
- [95] M. Ishida, K. Toyota, M. Ehara, H. Nakatsuji, and M. J. Frisch, J. Chem. Phys. 120, 2593 (2004).
- [96] Y. Ohtsuka, P. Piecuch, J. R. Gour, M. Ehara, and H. Nakatsuji, J. Chem. Phys. 126, 164111 (2007).
- [97] Y. G. Khait, W. Jiang, and M. Hoffmann, Int. J. Quantum Chem. 109, 1855 (2009).
- [98] N. Oliphant and L. Adamowicz, J. Chem. Phys. 94, 1229 (1991).
- [99] N. Oliphant and L. Adamowicz, J. Chem. Phys. 96, 3739 (1992).
- [100] P. Piecuch, N. Oliphant, and L. Adamowicz, J. Chem. Phys. 99, 1875 (1993).
- [101] P. Piecuch and L. Adamowicz, Chem. Phys. Lett. 221, 121 (1994).
- [102] P. Piecuch and L. Adamowicz, J. Chem. Phys. 100, 5792 (1994).
- [103] P. Piecuch and L. Adamowicz, J. Chem. Phys. 102, 898 (1995).
- [104] K. B. Ghose, P. Piecuch, and L. Adamowicz, J. Chem. Phys. 103, 9331 (1995).
- [105] K. B. Ghose and L. Adamowicz, J. Chem. Phys. 103, 9324 (1995).
- [106] K. B. Ghose, P. Piecuch, S. Pal, and L. Adamowicz, J. Chem. Phys. 104, 6582 (1996).
- [107] L. Adamowicz, P. Piecuch, and K. B. Ghose, Mol. Phys. 94, 225 (1998).
- [108] P. Piecuch, S. A. Kucharski, and R. J. Bartlett, J. Chem. Phys. 110, 6103 (1999).
- [109] P. Piecuch, S. A. Kucharski, and V. Špirko, J. Chem. Phys. 111, 6679 (1999).
- $[110]\,$ K. Kowalski and P. Piecuch, J. Chem. Phys. ${\bf 113},\,8490$ (2000).

- [111] K. Kowalski, S. Hirata, M. Włoch, P. Piecuch, and T. L. Windus, J. Chem. Phys. 123, 074319 (2005).
- [112] P. Piecuch, S. Hirata, K. Kowalski, P.-D. Fan, and T. L. Windus, Int. J. Quantum Chem. 106, 79 (2006).
- [113] G. Hagen, T. Papenbrock, D. J. Dean, A. Shwenk, A. Nogga, M. Włoch, and P. Piecuch, Phys. Rev. C 76, 034302 (2007).
- [114] P.-D. Fan and S. Hirata, J. Chem. Phys. **124**, 104108 (2006).
- [115] P. Piecuch, Mol. Phys. **108**, 2987 (2010).
- [116] J. A. Hansen, P. Piecuch, J. J. Lutz, and J. R. Gour, Phys. Scr. 84, 028110 (2011).
- [117] S. J. Stoneburner, J. Shen, A. O. Ajala, P. Piecuch, D. G. Truhlar, and L. Gagliardi, J. Chem. Phys. 147, 164120 (2017).
- [118] K. Emrich, Nucl. Phys. A **351**, 379 (1981).
- [119] P. Piecuch and R. J. Bartlett, Adv. Quantum Chem. 34, 295 (1999).
- [120] A. E. Kondo, P. Piecuch, and J. Paldus, J. Chem. Phys. **102**, 6511 (1995).
- [121] A. E. Kondo, P. Piecuch, and J. Paldus, J. Chem. Phys. **104**, 8566 (1996).
- [122] P. Piecuch, M. Włoch, M. Lodriguito, and J. R. Gour, in *Recent Advances in the The-ory of Chemical and Physical Systems*, Progress in Theoretical Chemistry and Physics, Vol. 15, edited by S. Wilson, J.-P. Julien, J. Maruani, E. Brändas, and G. Delgado-Barrio (Springer, Dordrecht, 2006) pp. 45–106.
- [123] K. Kowalski and P. Piecuch, J. Chem. Phys. 115, 2966 (2001).
- [124] K. Kowalski and P. Piecuch, J. Chem. Phys. 116, 7411 (2002).
- [125] P. Piecuch and K. Kowalski, in *Computational Chemistry: Reviews of Current Trends*, Vol. 5, edited by J. Leszczyński (World Scientific, Singapore, 2000) pp. 1–104.
- [126] K. Kowalski and P. Piecuch, J. Chem. Phys. 113, 18 (2000).
- [127] P. Piecuch and M. Włoch, J. Chem. Phys. 123, 224105 (2005).
- [128] P. Piecuch, M. Włoch, J. R. Gour, and A. Kinal, Chem. Phys. Lett. 418, 467 (2006).
- [129] J. Shen and P. Piecuch, Chem. Phys. 401, 180 (2012).
- [130] L. Meissner and R. Bartlett, J. Chem. Phys. 102, 7490 (1995).
- [131] G. D. Purvis, III and R. J. Bartlett, J. Chem. Phys. 76, 1910 (1982).
- [132] J. M. Cullen and M. C. Zerner, J. Chem. Phys. 77, 4088 (1982).

- [133] G. E. Scuseria, A. C. Scheiner, T. J. Lee, J. E. Rice, and H. F. Schaefer, III, J. Chem. Phys. 86, 2881 (1987).
- [134] P. Piecuch and J. Paldus, Int. J. Quantum Chem. 36, 429 (1989).
- [135] S. Coussan, Y. Ferro, A. Trivella, M. Rajzmann, P. Roubin, R. Wieczorek, C. Manca, P. Piecuch, K. Kowalski, M. Włoch, S. A. Kucharski, and M. Musiał, J. Phys. Chem. A 110, 3920 (2006).
- [136] K. Kowalski, S. Krishnamoorthy, O. Villa, J. R. Hammond, and N. Govind, J. Chem. Phys. 132, 154103 (2010).
- [137] K. Kornobis, N. Kumar, P. Lodowski, M. Jaworska, P. Piecuch, J. J. Lutz, B. M. Wong, and P. M. Kozlowski, J. Comp. Chem. 34, 987 (2013).
- [138] M. Kállay and P. Surjan, J. Chem. Phys. **113**, 1359 (2000).
- [139] S. Hirata, M. Nooijen, and R. J. Bartlett, Chem. Phys. Lett. **326**, 255 (2000).
- [140] S. Hirata, J. Chem. Phys. **121**, 51 (2004).
- [141] M. Kállay and J. Gauss, J. Chem. Phys. **121**, 9257 (2004).
- [142] S. Hirata, M. Nooijen, I. Grabowski, and R. J. Bartlett, J. Chem. Phys. 114, 3919 (2001), 115, 3967 (2001) [Erratum].
- [143] T. Shiozaki, K. Hirao, and S. Hirata, J. Chem. Phys. **126**, 244106 (2007).
- [144] K. Kowalski, J. Chem. Phys. **130**, 194110 (2009).
- [145] A. I. Krylov, Chem. Phys. Lett. **338**, 375 (2001).
- [146] A. I. Krylov and C. D. Sherrill, J. Chem. Phys. 116, 3194 (2002).
- [147] L. V. Slipchenko and A. I. Krylov, J. Chem. Phys. **117**, 4694 (2002).
- [148] P. U. Manohar and A. I. Krylov, J. Chem. Phys. 129, 194105 (2008).
- [149] C. D. Sherrill and P. Piecuch, J. Chem. Phys. 122, 124104 (2005).
- [150] M. Z. Zgierski, S. Patchkovskii, and E. C. Lim, J. Chem. Phys. 123, 081101 (2005).
- [151] M. Z. Zgierski, S. Patchkovskii, T. Fujiwara, and E. C. Lim, J. Phys. Chem. A 109, 9384 (2005).
- [152] S. Nangia, D. G. Truhlar, M. J. McGuire, and P. Piecuch, J. Phys. Chem. A 109, 11643 (2005).
- [153] M. Valiev and K. Kowalski, J. Phys. Chem. A 110, 13106 (2006).
- [154] M. Valiev and K. Kowalski, J. Chem. Phys. 125, 211101 (2006).

- [155] D. M. Chipman, J. Chem. Phys. **124**, 044305 (2006).
- [156] M. Z. Zgierski, S. Patchkovskii, and E. C. Lim, Can. J. Chem. 85, 124 (2007).
- [157] S. Tokura, K. Yagi, T. Tsuneda, and K. Hirao, Chem. Phys. Lett. 436, 30 (2007).
- [158] B. Ginovska, D. M. Camaioni, and M. Dupuis, J. Chem. Phys. 127, 084309 (2007).
- [159] P.-D. Fan, M. Valiev, and K. Kowalski, Chem. Phys. Lett. 458, 205 (2008).
- [160] D. M. Chipman, J. Phys. Chem. A **112**, 13372 (2008).
- [161] Á. Kvaran, H. Wang, K. Matthiasson, A. Bodi, and E. Jónsson, J. Chem. Phys. 129, 164313 (2008).
- [162] D. I. Lyakh, V. V. Ivanov, and L. Adamowicz, J. Chem. Phys. **128**, 074101 (2008).
- [163] J. R. Hammond, W. A. de Jong, and K. Kowalski, J. Chem. Phys. 128, 224102 (2008).
- [164] N. Govind, P. V. Sushko, W. P. Hess, M. Valiev, and K. Kowalski, Chem. Phys. Lett. 470, 353 (2009).
- [165] L. A. Burns, D. Murdock, and P. H. Vaccaro, J. Chem. Phys. **130**, 144304 (2009).
- [166] S. I. Bokarev, E. K. Dolgov, V. A. Bataev, and I. A. Godunov, Int. J. Quantum Chem. 109, 569 (2009).
- [167] K. R. Glaesemann, N. Govind, S. Krishnamoorthy, and K. Kowalski, J. Phys. Chem. A 114, 8764 (2010).
- [168] P. N. Day, K. A. Nguyen, and R. Pachter, J. Chem. Theory Comput. 6, 2809 (2010).
- [169] K. Lopata, R. Reslan, M. Kowalska, D. Neuhauser, N. Govind, and K. Kowalski, J. Chem. Theor. Comput. 7, 3686 (2011).
- [170] K. Kowalski, R. M. Olson, S. Krishnamoorthy, V. Tipparaju, and E. Aprá, J. Chem. Theor. Comput. 7, 2200 (2011).
- [171] P. D. Dau, J. Su, H.-T. Liu, J.-B. Liu, D.-L. Huang, J. Li, and L.-S. Wang, Chem. Sci. 3, 1137 (2012).
- [172] G. Murdachaew, M. Valiev, S. M. Kathmann, and X.-B. Wang, J. Phys. Chem. A 116, 2055 (2012).
- [173] P. D. Dau, J. Su, H.-T. Liu, D.-L. Huang, J. Li, and L.-S. Wang, J. Chem. Phys. 137, 064315 (2012).
- [174] N. De Silva, S. Y. Willow, and M. S. Gordon, J. Phys. Chem. A 117, 11847 (2013).
- [175] J. Su, P. D. Dau, C.-F. Xu, D.-L. Huang, H.-T. Liu, F. Wei, L.-S. Wang, and J. Li, Chem. Asian J. 8, 2489 (2013).

- [176] J. Su, W.-H. Xu, C.-F. Xu, W. H. E. Schwarz, and J. Li, Inorg. Chem. 52, 9867 (2013).
- [177] E. Berardo, H.-S. Hu, K. Kowalski, and M. A. Zwijnenburg, J. Chem. Phys. 139, 064313 (2013).
- [178] P. Tecmer, N. Govind, K. Kowalski, W. A. de Jong, and L. Visscher, J. Chem. Phys. 139, 034301 (2013).
- [179] P. Piecuch, J. A. Hansen, D. Staedter, S. Faure, and V. Blanchet, J. Chem. Phys. 138, 201102 (2013).
- [180] J. Su, P. D. Dau, Y.-H. Qiu, H.-T. Liu, C.-F. Xu, D.-L. Huang, L.-S. Wang, and J. Li, Inorg. Chem. 52, 6617 (2013).
- [181] F. Trinter, J. B. Williams, M. Weller, M. Waitz, M. Pitzer, J. Voigtsberger, C. Schober, G. Kastirke, C. Müller, C. Goihl, P. Burzynski, F. Wiegandt, R. Wallauer, A. Kalinin, L. P. H. Schmidt, M. S. Schöffler, Y.-C. Chiang, K. Gokhberg, T. Jahnke, and R. Dörner, Phys. Rev. Lett. 111, 233004 (2013).
- [182] J. J. Lutz and P. Piecuch, Comput. Theor. Chem. 1040-1041, 20 (2014).
- [183] P. Zhou, J. Liu, K. Han, and G. He, J. Comput. Chem. 35, 109 (2014).
- [184] G. Schoendorff and A. K. Wilson, J. Chem. Phys. **140**, 224314 (2014).
- [185] H.-S. Hu, K. Bhaskaran-Nair, E. Aprà, N. Govind, and K. Kowalski, J. Phys. Chem. A 118, 9087 (2014).
- [186] J. Su, P. D. Dau, H.-T. Liu, D.-L. Huang, F. Wei, W. H. E. Schwarz, J. Li, and L.-S. Wang, J. Chem. Phys. 142, 134308 (2015).
- [187] W. J. Hehre, R. Ditchfield, and J. A. Pople, J. Chem. Phys. 56, 2257 (1972).
- [188] A. Schäfer, H. Horn, and R. Ahlrichs, J. Chem. Phys. 97, 2571 (1992).
- [189] B. G. Levine, C. Ko, J. Quenneville, and T. J. Martínez, Mol. Phys. 104, 1039 (2006).
- [190] B. G. Levine, J. D. Coe, and T. J. Martínez, J. Phys. Chem. B 112, 405 (2008).
- [191] M. Włoch, J. R. Gour, and P. Piecuch, J. Phys. Chem. A 111, 11359 (2007).
- [192] M. W. Schmidt, K. K. Baldridge, J. A. Boatz, S. T. Elbert, M. S. Gordon, J. H. Jensen, S. Koseki, N. Matsunaga, K. A. Nguyen, S. J. Su, T. L. Windus, M. Dupuis, and J. A. Montgomery, J. Comput. Chem. 14, 1347 (1993).
- [193] M. S. Gordon and M. W. Schmidt, in *Theory and Applications of Computational Chemistry: The First Forty Years*, edited by C. E. Dykstra, G. Frenking, K. S. Kim, and G. E. Scuseria (Elsevier, Amsterdam, 2005) pp. 1167–1190.

- [194] P. Piecuch, S. A. Kucharski, K. Kowalski, and M. Musiał, Comp. Phys. Commun. 149, 71 (2002).
- [195] A. Öhrn and O. Christiansen, Phys. Chem. Chem. Phys. 3, 730 (2001).
- [196] H. Köppel, W. Domcke, and L. S. Cederbaum, Adv. Chem. Phys. 57, 59 (1984).
- [197] Y. J. Bomble, K. W. Sattelmeyer, J. F. Stanton, and J. Gauss, J. Chem. Phys. 121, 5236 (2004).
- [198] J. Hubbard, Proc. R. Soc. Lond., Ser. A 240, 539 (1957).
- [199] N. M. Hugenholtz, Physica **23**, 481 (1957).
- [200] F. Coester, Nucl. Phys. 7, 421 (1958).
- [201] F. Coester and H. Kümmel, Nucl. Phys. 17, 477 (1960).
- [202] H. Monkhorst, Int. J. Quantum Chem. Symp. 11, 421 (1977).
- [203] J. Paldus and X. Li, Adv. Chem. Phys. 110, 1 (1999).
- [204] R. J. Bartlett and M. Musiał, Rev. Mod. Phys. 79, 291 (2007).
- [205] S. Ghosh, D. Mukherjee, and S. Bhattacharya, Mol. Phys. 43, 173 (1981).
- [206] H. Nakatsuji and K. Hirao, Int. J. Quantum Chem. 20, 1301 (1981).
- [207] H. Nakatsuji, K. Ohta, and T. Yonezawa, J. Phys. Chem. 87, 3068 (1983).
- [208] H. Nakatsuji, Chem. Phys. Lett. **177**, 331 (1991).
- [209] M. Musiał, M. Olszówka, D. I. Lyakh, and R. J. Bartlett, J. Chem. Phys. 137, 174102 (2012).
- [210] J. Gauss, in *Encyclopedia of Computational Chemistry*, Vol. 1, edited by P. v. R. Schleyer, N. L. Allinger, T. Clark, J. Gasteiger, P. A. Kollman, H. F. Schaefer, III, and P. R. Schreiner (Wiley, Chichester, 1998) pp. 615–636.
- [211] J. Shen and P. Piecuch, J. Chem. Phys. 136, 144104 (2012).
- [212] J. Shen and P. Piecuch, J. Chem. Theory Comput. 8, 4968 (2012).
- [213] K. Hirao and H. Nakatsuji, J. Comput. Phys. 45, 246 (1982).
- [214] E. R. Davidson, J. Comput. Phys. 17, 87 (1975).
- [215] T. H. Dunning, Jr., J. Chem. Phys. 90, 1007 (1989).
- [216] T. H. Dunning, Jr., J. Chem. Phys. 55, 716 (1971).

- [217] C. D. Sherrill, M. L. Leininger, T. J. van Huis, and H. F. Schaefer, III, J. Chem. Phys. 108, 1040 (1998).
- [218] P. G. Wenthold, J. Hu, R. R. Squires, and W. C. Lineberger, J. Am. Chem. Soc. 118, 475 (1996).
- [219] T. Saito, S. Nishikara, S. Yamanaka, Y. Kitagawa, T. Kawakami, S. Yamada, H. Isobe, M. Okumura, and K. Yamaguchi, Theor. Chem. Acc. 130, 749 (2011).
- [220] T. H. Dunning, Jr., J. Chem. Phys. **53**, 2823 (1970).
- [221] X. Li and J. Paldus, J. Chem. Phys. **125**, 164107 (2006).
- [222] J. F. Harrison, Acc. Chem. Res. 7, 378 (1974).
- [223] I. Shavitt, Tetrahedron 41, 1531 (1985).
- [224] W. A. Goddard, III, Science **227**, 917 (1985).
- [225] H. F. Schaefer, III, Science **231**, 1100 (1986).
- [226] P. R. Bunker, in Comparison of Ab Initio Quantum Chemistry with Experiment for Small Molecules, edited by R. J. Bartlett (Reidel, Dordrecht, 1985) pp. 141–170.
- [227] J. F. Harrison, in Advances in the Theory of Atomic and Molecular Systems: Conceptual and Computational Advances in Quantum Chemistry, Progress in Theoretical Chemistry and Physics, Vol. 19, edited by P. Piecuch, J. Maruani, G. Delgado-Barrio, and S. Wilson (Springer, Dordrecht, 2009) pp. 33–43.
- [228] D. E. Woon and T. H. Dunning, Jr., J. Chem. Phys. 103, 4572 (1995).
- [229] R. A. Kendall, T. H. Dunning, Jr., and R. J. Harrison, J. Chem. Phys. 96, 67696 (1992).
- [230] T. Helgaker, W. Klopper, H. Koch, and J. Noga, J. Chem. Phys. **106**, 9639 (1997).
- [231] A. Halkier, T. Helgaker, P. Jørgensen, W. Klopper, H. Koch, J. Olsen, and A. K. Wilson, Chem. Phys. Lett. 286, 243 (1998).
- [232] W. M. C. Foulkes, L. Mitas, R. J. Needs, and G. Rajagopal, Rev. Mod. Phys. 73, 33 (2001).
- [233] M. P. Nightingale and C. J. Umrigar, eds., Quantum Monte Carlo Methods in Physics and Chemistry, NATO ASI Ser. C, Vol. 525 (Kluwer, Dordrecht, 1999).
- [234] S. Zhang and H. Krakauer, Phys. Rev. Lett. 90, 136401 (2003).
- [235] P. M. Zimmerman, J. Toulouse, Z. Zhang, C. B. Musgrave, and C. J. Umrigar, J. Chem. Phys. 131, 124103 (2009).
- [236] P. Jensen and P. R. Bunker, J. Chem. Phys. 89, 1327 (1988).

- [237] E. R. Davidson, D. Feller, and P. Phillips, Chem. Phys. Lett. 76, 416 (1980).
- [238] N. C. Handy, Y. Yamaguchi, and H. F. Schaefer, III, J. Chem. Phys. 84, 4481 (1986).
- [239] P. Piecuch, X. Li, and J. Paldus, Chem. Phys. Lett. 230, 377 (1994).
- [240] A. Alijah and G. Duxbury, Mol. Phys. **70**, 605 (1990).
- [241] C. J. Cramer and B. A. Smith, J. Phys. Chem. 100, 9664 (1996).
- [242] L. V. Slipchenko and A. I. Krylov, J. Chem. Phys. 118, 6874 (2003).
- [243] L. V. Slipchenko and A. I. Krylov, J. Chem. Phys. **123**, 084107 (2005).
- [244] R. J. Baseman, D. W. Pratt, M. Chow, and P. Dowd, J. Am. Chem. Soc. 98, 5726 (1976).
- [245] E. Papajak and D. G. Truhlar, J. Chem. Theory Comput. 6, 597 (2010).
- [246] A. Raghavachari, J. A. Pople, E. S. Replogle, M. Head-Gordon, and N. C. Handy, Chem. Phys. Lett. 167, 115 (1990).
- [247] U. S. Mahapatra, B. Datta, and D. Mukherjee, J. Chem. Phys. 110, 6171 (1999).
- [248] P. G. Szalay and R. J. Bartlett, Chem. Phys. Lett. **214**, 481 (1993).
- [249] N. P. Bauman, J. Shen, and P. Piecuch, Mol. Phys. **115**, 2860 (2017).